Dartmouth College
Dartmouth Digital Commons

Dartmouth College Ph.D Dissertations | Theses and Dissertations

Summer 7-6-2022

Novel functions for Arp2/3 complex-mediated actin networks discovered in Chlamydomonas reinhardtii

Brae M. Bigge
Dartmouth College, brae.m.bigge.gr@dartmouth.edu

Follow this and additional works at: https://digitalcommons.dartmouth.edu/dissertations

 Part of the Cell Biology Commons

Recommended Citation

Bigge, Brae M., "Novel functions for Arp2/3 complex-mediated actin networks discovered in Chlamydomonas reinhardtii" (2022). *Dartmouth College Ph.D Dissertations*. 109.
https://digitalcommons.dartmouth.edu/dissertations/109

This Thesis (Ph.D.) is brought to you for free and open access by the Theses and Dissertations at Dartmouth Digital Commons. It has been accepted for inclusion in Dartmouth College Ph.D Dissertations by an authorized administrator of Dartmouth Digital Commons. For more information, please contact dartmouthdigitalcommons@groups.dartmouth.edu.

“Novel functions for Arp2/3 complex-mediated actin networks discovered in *Chlamydomonas reinhardtii*”

A Thesis
Submitted to the Faculty
in partial fulfillment of the requirements for the
degree of

Doctor of Philosophy

in
Biochemistry and Cell Biology

by Brae M. Bigge

Guarini School of Graduate and Advanced Studies
Dartmouth College
Hanover, New Hampshire

July 2022

Examining Committee:

(chair) ***Prachee Avasthi, PhD***

Charles Barlowe, PhD

James Moseley, PhD

Mira Krendel, PhD

F. Jon Kull, Ph.D.
Dean of the Guarini School of Graduate and Advanced Studies

ABSTRACT

Chlamydomonas reinhardtii, a unicellular member of the *Chlorophyta* or Green Algae phylum, has been used for decades as a model for ciliary studies. Using this tool, previous work from our lab found a role for actin in ciliary assembly and maintenance. However, while the microtubule-based, membrane-ensheathed cilia of *Chlamydomonas* are highly conserved in relation to mammalian cells, the actin cytoskeleton is not as simple. *Chlamydomonas* contains two actin genes: IDA5, a conventional actin, and NAP1, a divergent actin. Here, we find that despite the divergence of NAP1, it is still able to interact with the actin nucleator, the Arp2/3 complex. We take advantage of this interaction to further dissect the role of actin in ciliary assembly and maintenance, as focusing on actin networks nucleated by a single actin nucleator allows us to look at a subset of the filamentous actin in this cell instead. By doing this, we are able to uncover a novel trafficking pathway for ciliary material where proteins and membranes are reclaimed from a pool in the cell body plasma membrane through Arp2/3 complex-dependent endocytosis. This trafficking pathway is important for ciliary assembly from zero length, ciliary maintenance, and ciliary elongation in the presence of lithium.

ACKNOWLEDGEMENTS

To *my mentor, Prachee*: I will be forever grateful I did that fourth rotation! This would not have been possible without your guidance and support. You taught me to be excited about science and the things I believe in, because anyone who knows you knows that your excitement is contagious. You taught me to be confident in myself and in my work and passionate about fixing the things in science (and the world) that don't serve me or others well. Because of you, I know that I'm a better scientist and person, and I know I'll do great things in my next steps.

To the *faculty and staff at Dartmouth*: Thank you so much to the entire MCB program at Dartmouth for being so kind and welcoming when our lab joined in 2020. In particular, the BCB faculty, staff, and students have really made me feel at home here in the department.

To my *committee*: I'd like to extend a special thank you to my advisory committee members here at Dartmouth: James B Moseley and Charles K Barlowe, who have been extra welcoming and extra helpful. Thanks for checking in on us and making sure we have everything we need. Thank you also to my outside committee member, Mira Krendel for agreeing to be on my committee and for your helpful advice on my work.

To the *faculty and staff at KUMC:* Thank you to my committee from KUMC (Bret Freudenthal, Brenda Rongish, Andras Czirok, and Sue Jasperson) for helping me through my comprehensive exam, and thank you to the Self Graduate Fellowship at the University of Kansas. The professional development and network of my peers that I gained from even my short time as a Self Graduate Fellow are invaluable.

To my *collaborators*: Thank you to David Sept and Courtney Schroeder, who contributed to Chapter 2 of this text; Nicholas Rosenthal, who helped with Chapter 3 of this text; Evan Craig, David Mueller, Miroslava Schaffer, and Ben Engel who were instrumental for Appendix I; and Ningning Zhang, Ru Zhang, and everyone else who contributed to the work in Appendix II.

To the *current and past members of the Avasthi lab*: I'm so grateful for every person I got to work with during my time in the Avasthi lab. I would especially like to thank Brittany Jack, who was my "lab twin" and who helped me find a home in the lab.

I'd also like to thank Nicholas Rosenthal and Larissa Dougherty, who moved from Kansas to Dartmouth alongside me and have been my little community here. And a particular thank you to Larissa: you've become one of my best friends and have made these last few years not just possible, but enjoyable.

To my *family*: Thank you for your unconditional support and for pushing me to be a better version of myself even when it meant packing me up and shipping me across the country. Mom and dad (Pamela and Michael Bigge), you have played a vital role in making me into who I am today, and I will forever be grateful for the sacrifices you both made so that I could succeed. Grandma and grandpa (Elaine and Dean Bigge), your love and support mean the world to me now and always. And Lane, thank you for being a wonderful brother and making me smile even on the tough days. To the Hatfields, thank you for welcoming me into your family and supporting me as if I were one of your own. And finally, thank you, Scott Hatfield. You encourage me, help me with all the difficult decisions and hard days, follow me around the country without complaint, and celebrate the good days with me. You make every day better, and I'm so thankful for your support, your love, your patience, etc. And last but not least, thank you to my soul dog, Amy.

Table of Contents

List of tables

List of figures

List of Abbreviations

6-BIO ..... 6-bromoindirubin-3'-oxime
ABP ..... Actin Binding Protein
ARP ..... Actin Related Protein
BFA ..... Brefeldin A
CHX ..... Cycloheximide
CoIP ..... Co-Immunoprecipitation
CrPRF ..... *Chlamydomonas* Profilin
CytoD ..... Cytochalasin D
db-cAMP ..... dibutyryl cyclic AMP
DIC ..... Differential Interference Contrast
DRP ..... Dynamin Related Protein
FOR1-4 ..... *Chlamydomonas* Formin1-4
GSK3 ..... Glycogen Synthase Kinase 3
IBMX 3-isobutyl-1-methylxanthine
IDA5 ..... Inner Arm Dynein 5 (Conventional actin)
IFT ..... Intraflagellar Transport
LatB ..... Latrunculin B
LiCl ..... Lithium Chloride
MYO1-3 ..... *Chlamydomonas* Myosin1-3
M-N ..... Minimal media without nitrogen
NAP1 ..... Novel Actin-like Protein 1 (Divergent actin)
NaPPi ..... Sodium pyrophosphate
TAP ..... Tris Acetate Phosphate Media

CHAPTER 1:
INTRODUCTION

Chlamydomonas reinhardtii:

This work utilizes the organism *Chlamydomonas reinhardtii,* a unicellular green alga that is uniquely situated to tell us about both plant and animal systems and how they evolved. *Chlamydomonas* is an established model for several cellular structures and processes, including cilia and photosynthesis, but *Chlamydomonas* is also emerging as a model for cytoskeletal research. Here, we use this system to study the unique features of its actin cytoskeleton and how it influences cilia.

Chlamydomonas *Taxonomy:*

The unicellular *Chlamydomonas reinhardtii* is part of the Plantae kingdom and belongs to the Chlorophyta, or green algae, phylum (**Fig. 1.1**). Within the phylum it belongs to the Chlorophyceae class and the Chlamydomonadales order (**Fig. 1.1)**. The identifying features of *Chlamydomonas* are its two persistent, apical flagella or cilia, its cell wall, and its single chloroplast (Harris et al., 2009a) (**Fig. 1.2)**. *Chlamydomonas* are sometimes referred to as a "plan-imal", a nod to its taxonomic location between land plants and animals. As one might suspect based on this taxonomic location, the organism contains genes and features specific to both plants and animals (Merchant et al., 2007). For example, the persistent eukaryotic flagella or cilia were retained during evolution and are more like those of mammalian cells, while the large chloroplast is a plant-like feature (Merchant et al., 2007). This makes this organism uniquely situated to provide evolutionary information about both plants and animals.

The genome of *Chlamydomonas* is about 121 mega-bases (compared to 140 Mb in *Arabidopsis,* 2851 Mb in humans, 12 Mb in *S. Cerevisiae,* and 5 Mb in *e. Coli*) and has high GC content of 64% (Merchant et al., 2007). *Chlamydomonas reinhardtii* has a fully sequenced and well-annotated genome (Merchant et al., 2007), and there is an extensive library of mutated strains available that covers 83% of the *Chlamydomonas* nuclear genes (Cheng et al., 2017; Li et al., 2019), making it a very useful and powerful model to study many cellular processes.

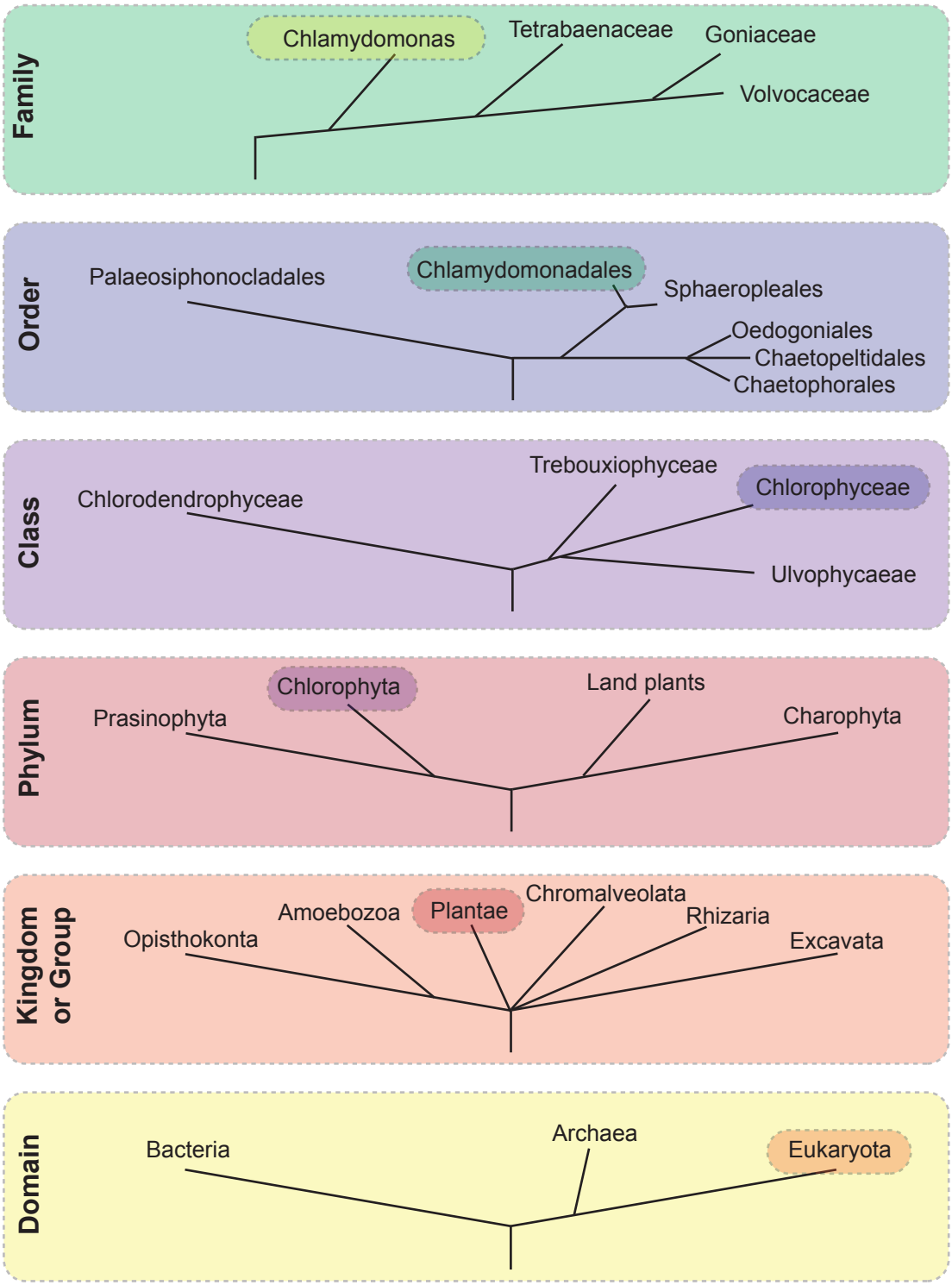

Fig. 1.1. *Chlamydomonas* taxonomy. *Chlamydomonas* is a eukaryotic member of the plant group. It is a Chlorophyte, or green algae cell. Within that phylum is it a member of the Chlorophyceae class and the Chlamydomonadales order. Trees are not simplified, and the length of the lines is not representative of distance. Highlighted word in each tree is the phylogenetic group that is then dissected in the next tree up in the fig. .

Chlamydomonas *anatomy:*

The *Chlamydomonas* cell is a single polarized ellipsoid-shaped cell contained in a cell wall composed of hydroxyproline-rich glycoproteins (Harris et al., 2009b) (**Fig. 1.2)**. At the apical edge of the cell are two persistent and symmetrical cilia extending from the basal bodies (Harris et al., 2009b) (**Fig. 1.2)**. The cilia are used for motility and for sensing the environment. They are highly conserved in relation to mammalian cilia, making them an ideal model for ciliary studies (Pazour and Witman, 2009). Near the base of the cilia are 2 contractile vacuoles used to respond to osmotic pressure changes (Komsic-Buchmann et al., 2014). The nucleus is located posterior to the vacuoles and has a nucleolus visible in electron microscopy (Harris et al., 2009b) (**Fig. 1.2)**. The cell also contains several mitochondria, a few Golgi apparatus, and an endoplasmic reticulum (**Fig. 1.2**). Otherwise, the majority (roughly 40%) of the cytoplasm is taken up by a large cup-shaped chloroplast situated on the basal edge of the cell (Harris et al., 2009b) (**Fig. 1.2)**. This is conserved in relation to higher plants, making *Chlamydomonas* chloroplasts a great model for studying photosynthesis. This combined with the ease of growing these cells has also made *Chlamydomonas* a popular choice for biofuel studies.

In this work, we take advantage of some of the conserved properties of *Chlamydomonas,* mainly the cilia, but we also take advantage of some less conserved properties of *Chlamydomonas*.

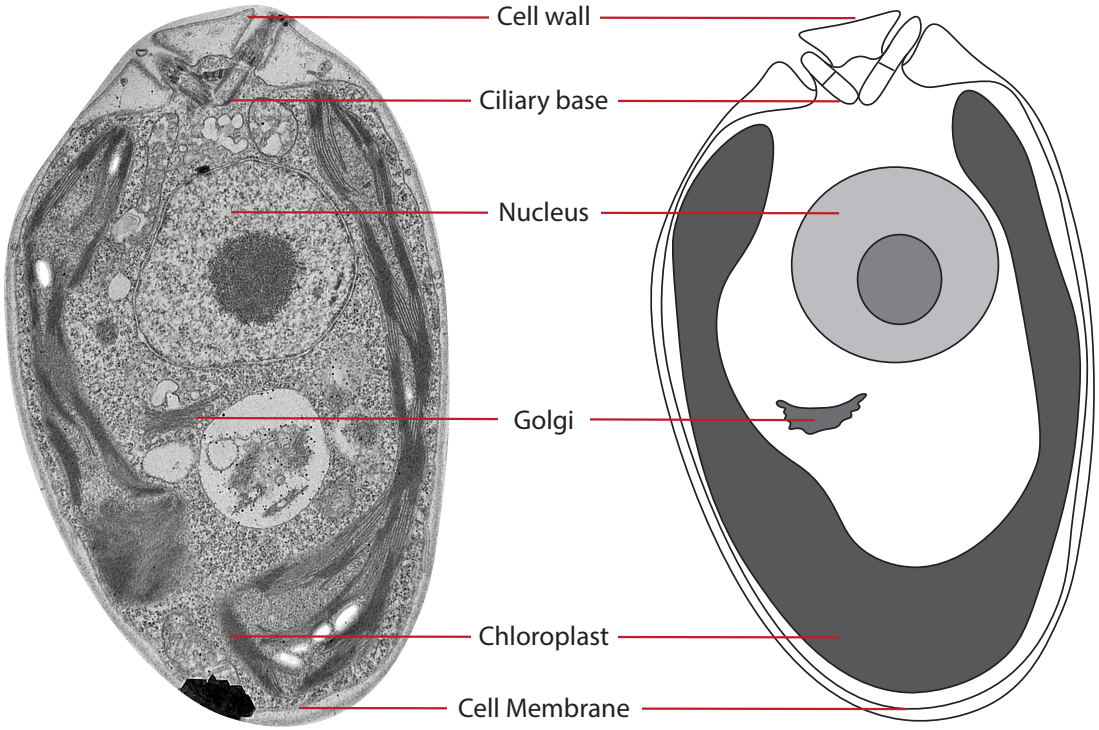

Fig. 1.2. *Chlamydomonas* cellular architecture. An electron micrograph of a *Chlamydomonas* cell and a cartoon drawing of the same cell. The cell wall, ciliary base, nucleus, Golgi, chloroplast, and cell membrane are labelled. The grey region in the middle of the nucleus is the prominent nucleolus visible on the micrograph.

***Chlamydomonas* as an established ciliary model system:**

Specialized organelles important for sensing the environment and for motility, cilia or flagella (used interchangeably in the context of this work) are widely conserved and exist on nearly every cell in the human body, as well as in organisms ranging from complex mammals to single-celled protists. Because of the wide presence of cilia and because of their important functions, defects in the maintenance or assembly of cilia can result in a wide range of diseases termed ciliopathies (Reiter and Leroux, 2017). However, the complexity of mammalian organisms and cells can make it difficult to study cilia. In culture, cilia grow on mammalian cells only under specific conditions, like nutrient starvation. However, the two cilia of *Chlamydomonas* are present for a much larger window due to *Chlamydomonas'* prolonged G1 phase and are conserved in relation to mammalian cilia. Further, the simplicity of *Chlamydomonas* makes it a powerful model to study the complexity surrounding the mammalian cilia (**Fig. 1.3)** (Pazour and Witman, 2009). Much of what is known about ciliary regulation and assembly comes from studies done in *Chlamydomonas*.

Cilia extend from a basal body apparatus, or a centrosome docked to the surface of the cell during interphase (Dutcher, 2009), and are composed of a microtubule core, called an axoneme. In motile cilia, this microtubule core contains 9 microtubule doublets arranged in a cylinder surrounding a central pair of microtubules (**Fig. 1.3)** (Pazour and Witman, 2009). In primary cilia, where the main goal is sensing the environment, the microtubule core still contains 9 microtubule doublets, but the central pair is not present (**Fig. 1.3)** (Berbari et al., 2009). The axoneme is ensheathed by a plasma membrane that is contiguous with the cell body plasma membrane. However, the ciliary membrane is separated from the cell body plasma membrane by a septin-composed structure called the diffusion barrier (Hu Qicong et al., 2010). For cilia to properly function they must undergo ciliogenesis, or the assembly of cilia, and then they must maintain a specified length.

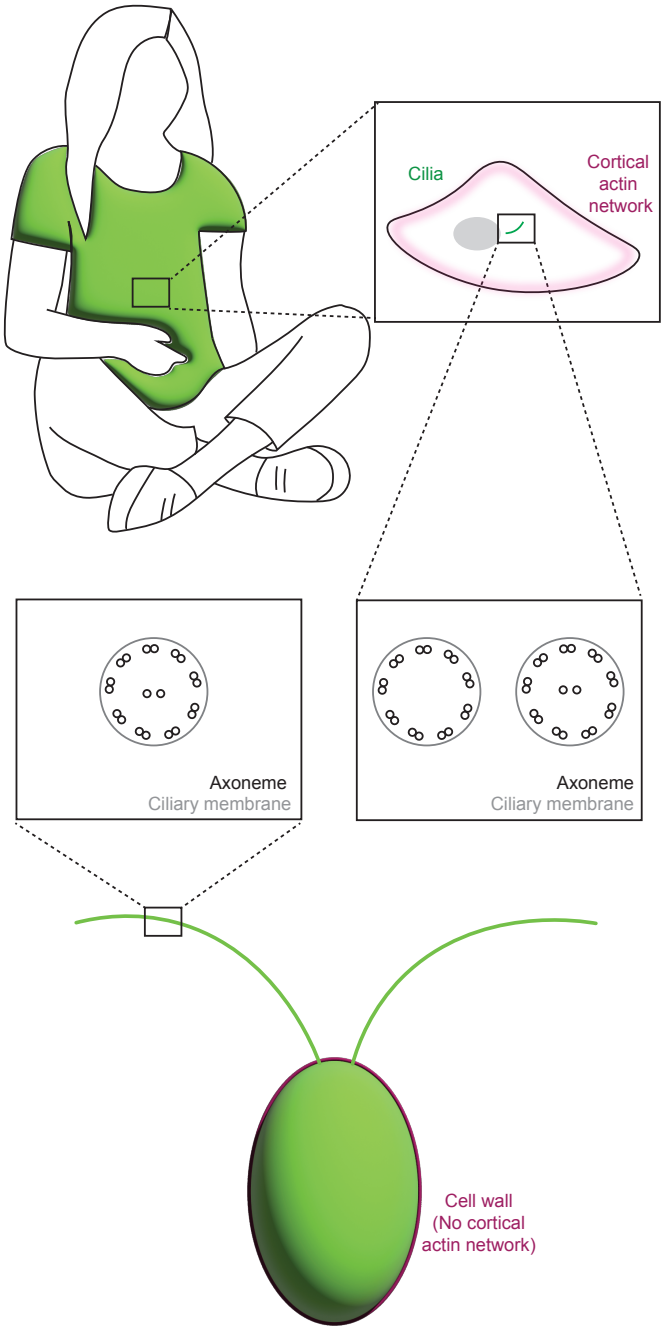

Fig. 1.3. *Chlamydomonas* cilia are highly conserved in relation to mammalian cilia. Cilia from *Chlamydomonas* have a similar structure to mammalian motile cilia, while mammalian primary cilia lack central pairs. One important difference between the two cells that results in differences in ciliary assembly and regulation is the presence or absence of the cortical actin network (magenta).

Ciliary assembly:

Chlamydomonas presents an ideal model for studying ciliary assembly for several reasons including the conservation and simplicity discussed previously. There are ciliary mutants available that allow mechanistic studies of the processes involved in assembly and maintenance of cilia. For example, there are several short flagella mutants (Kuchka and Jarvik, 1987), long flagella mutants (Asleson and Lefebvre, 1998; Barsel et al., 1988; McVittie, 1972), paralyzed flagella mutants (Huang et al., 1979), and even variable flagella mutants (Adams et al., 1985; Kuchka and Jarvik, 1982; Marshall et al., 2005), all of which are useful to understanding the cellular functions involved in assembly and regulating cilia. Additionally, in mammalian cells, ciliogenesis must be induced by nutrient starvation which can take days, but in *Chlamydomonas* the cilia are persistently present when cells are in liquid culture due to the prolonged G1 phase of the organism. Further, the cilia can be easily removed with low pH shock and then allowed to synchronously regenerate over the course of about 2 hours (**Fig. 1.4)** (Jack and Avasthi, 2018; Lefebvre, 1995; Rosenbaum et al., 1969; Rosenbaum and Child, 1967). The stages of assembly can be dissected using assays where some perturbation is introduced in these synchronously regenerating cells that is designed to allow for evaluation of new protein synthesis, new protein incorporation, and existing protein incorporation (Jack and Avasthi, 2018; Lefebvre, 1995; Rosenbaum et al., 1969) (**Fig. 1.5**).

Using these assays and others, it has been discovered that cilia assemble through several distinct steps in *Chlamydomonas*. First, the centrosome, or basal body, docks to the edge of the cell where the cilia will grow creating a template for the axoneme and a place for proteins entering the cilia to dock (Dutcher, 2009). This differs from intracellular ciliogenesis where a pre-ciliary vesicle forms on one end of the centrosome where the cilium will form. This vesicle grows as the budding cilium grows, and eventually fuses with the plasma membrane (Sorokin, 1968). In *Chlamydomonas,* after basal body docking, protein and membrane are required for assembly. Existing membrane and protein are incorporated into cilia through the gating region at the base of the cilia, called the transition zone, and that new protein synthesis is also required for assembly, because cilia can grow to half-length in the presence of the protein synthesis inhibitor, cycloheximide (Rosenbaum et al., 1969) (**Fig. 1.5**). So, the protein for the first

half of cilia is already present in the cell, but the protein for the remainder of cilia must be synthesized. The new protein must also be trafficked to the cilia as there are no ribosomes in the ciliary region (Diener et al., 2015) and finally incorporated into cilia (Jack et al., 2019; Jack and Avasthi, 2018; Lefebvre, 1995; Rosenbaum et al., 1969) (**Fig. 1.5**). Membrane and membrane proteins incorporated into cilia can come from the Golgi (Dentler, 2013; Nachury et al., 2010; Rohatgi and Snell, 2010), and soluble proteins have been found to be trafficked on Golgi-derived vesicles in a "piggy-back" fashion (Wood and Rosenbaum, 2014). However, these ciliary materials can also come from the plasma membrane (Dentler, 2013) potentially through some endocytic mechanism or lateral diffusion.

Once proteins arrive at the cilia, they are trafficked to the tip of the cilia where the axoneme assembles (Johnson and Rosenbaum, 1992) through a process called intraflagellar transport (IFT) (Cole, 2009). IFT is a bi-directional movement of particles, or trains, from the base of cilia to the tip (anterograde) and from the tip of cilia to the base (retrograde) (Kozminski et al., 1993). The anterograde transport and retrograde transport are driven by kinesin (Adams et al., 1982; Huang et al., 1977; Walther et al., 1994) and dynein motors respectively (Pazour et al., 1999, 1998; Porter et al., 1999). The trains themselves are composed of IFT complexes, termed IFT complex A and IFT complex B, which link the cargo to the appropriate motors (Cole et al., 1998; Pazour et al., 2000; Piperno et al., 1998). This process is highly regulated to allow cilia to grow to the appropriate length through a mechanism that is not well understood.

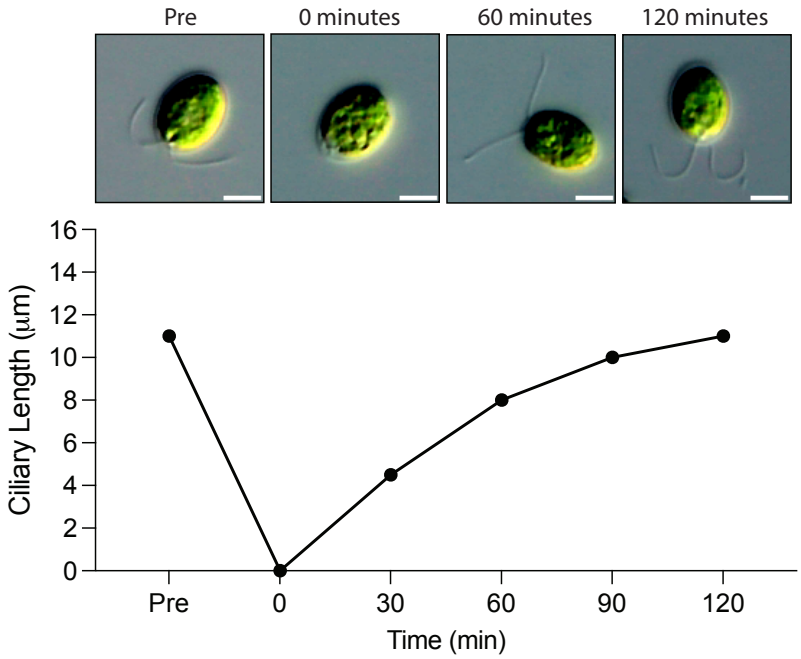

Fig. 1.4. Ciliary regeneration in *Chlamydomonas*. *Chlamydomonas* cells are deflagellated with low pH shock, then returned to normal pH media to regenerate cilia. Samples are taken every 30 minutes and imaged on a DIC microscope. The cilia can then be measured in ImageJ/FIJI and plotted. Scale bar in the images represents 5 μm.

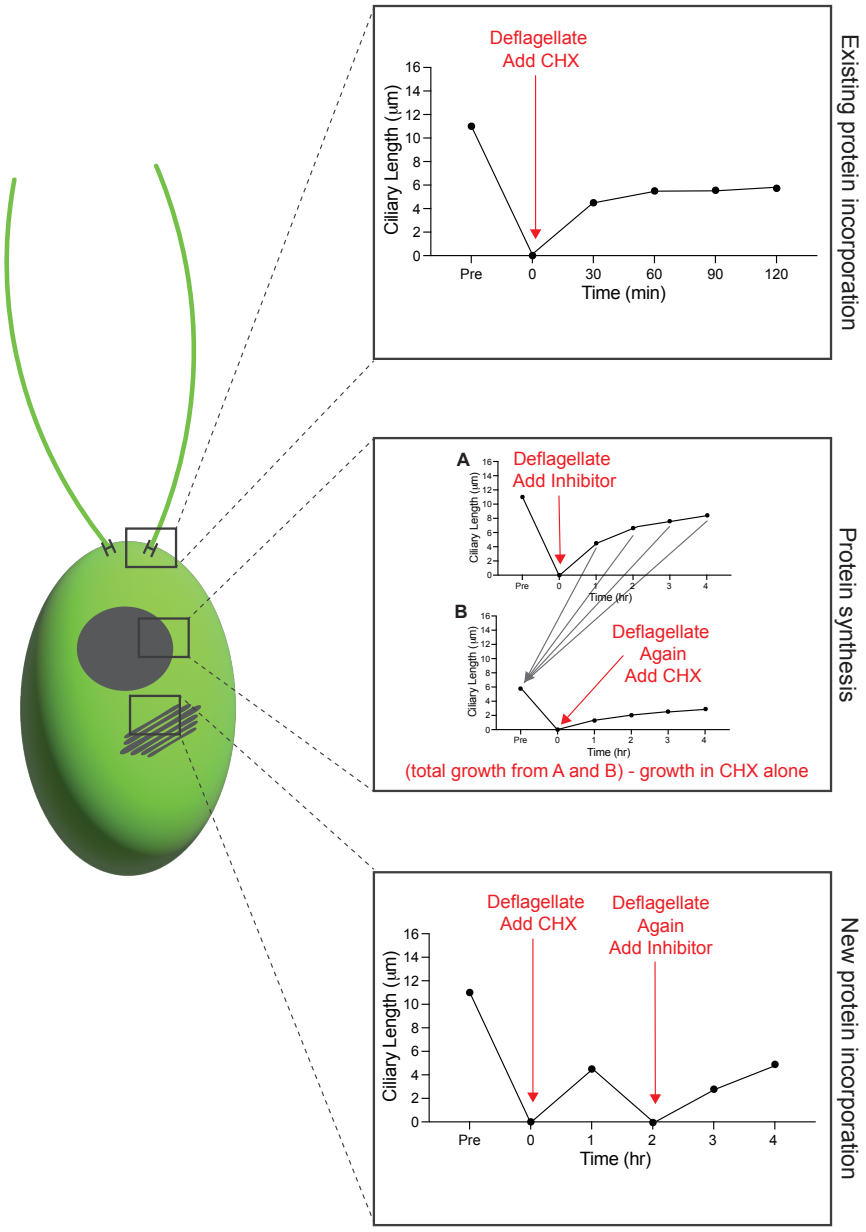

Fig. 1.5. Dissection of ciliary assembly in *Chlamydomonas*. Using the inhibitor cycloheximide (CHX) and any inhibitor of interest, one can determine the effect of inhibition on the stages of ciliary assembly by performing these assays. In the first assay, protein synthesis is blocked, meaning any assembly must be due to incorporation of ciliary material already existing in the cell. In the second assay, cells are deflagellated and grown in the inhibitor of interest for a predetermined time. Cells are then deciliated and grown in cycloheximide. The total growth during these two periods of assembly are added together, then the growth in cycloheximide alone, which represents the size of the existing protein pool, is subtracted to give you the total amount of protein synthesized for growth. Finally, to measure the trafficking and incorporation of new protein, the last assay is done. In this assay, cells are grown in cycloheximide to remove all existing protein in the cell. Then cells are deciliated again and grown in the inhibitor of choice. Any ciliary growth must come from protein being newly synthesized, trafficked, and incorporated.

Ciliary length regulation:

One of the big questions in ciliary biology is how cilia know their optimal length and know to grow to that length specifically. Several models of ciliary length regulation have been proposed using data from *Chlamydomonas* (Avasthi and Marshall, 2012; Ishikawa and Marshall, 2017a; Ludington et al., 2015; Marshall, 2015). Despite subsequent findings that either support or refute various models, each model gives rise to key implications regarding ciliary length regulation.

The limiting-precursor model suggests that cells make exactly enough ciliary precursor proteins to form cilia of a certain length. This cannot be the case because even without new protein synthesis cilia are able to grow to half length, suggesting cells contain enough extra or pre-cursor protein to at least grow half of a cilium (Rosenbaum et al., 1969).

A few diffusion-based models have been proposed. The first depends on the diffusion of free tubulin (Levy, 1974). This model was thought to be unlikely because tubulin was thought to be carried primarily by IFT machinery. However, recently it was found that tubulin is transported via diffusion (Craft Van De Weghe et al., 2020). The other diffusion-based models depend on the diffusion of some signal molecule from the cilia (Ludington et al., 2015) or the diffusion of the motor protein, kinesin (Hendel et al., 2018).

The molecular ruler model suggests there is some protein with a specified length that corresponds to the desired length of the cilia, but no protein has been identified in eukaryotic cilia that could serve as a molecular ruler (Marshall, 2015).

The time-of-flight model proposes that there is a degradable signal, like phosphorylation, that is incorporated into IFT trains that move into the cilia. The longer the IFT trains with the signal are in the cilia, the more time for the signal to be degraded, thus providing a readout of ciliary length. However, no active length measurer has been identified (Ishikawa and Marshall, 2017b).

Another model suggests that mechanosensitive ion channels in the ciliary membrane regulate ciliary length because the longer the cilia is the more ion channels can be present in the membrane and the more ions can be imported into the cell (Beck and Uhl, 1994; Besschetnova et al., 2010).

The swim speed feedback model proposes that the cilia grow to an optimal length for swimming and that the length therefore depends on fluid forces upon the cilia (Osterman and Vilfan, 2011; Tam and Hosoi, 2011). Support for this model comes from the fact that cells with very short or very long cilia have trouble swimming efficiently.

Finally, the balance point model considers the constant turnover of tubulin at ciliary tips and the fact that ciliary assembly is not a linear process, but instead slows as cilia lengthen. This model suggests that there is a point where the decreasing assembly rate and the constant disassembly rate where cilia reach and then maintain a steady state length (Marshall et al., 2005; Marshall and Rosenbaum, 2001).

Thus, protein availability, signaling, protein synthesis, protein trafficking, gating at the base of the cilia, and IFT itself may be responsible for maintaining ciliary length. Work from our lab, including work in this thesis, provides some information that might help researchers uncover the mystery of ciliary length regulation and how the actin and actin-based processes might be involved.

***Chlamydomonas* as an emerging model to study the actin cytoskeleton:**

The simplicity of the single celled algae and the powerful tools available in this organism make it a useful model to study the conserved cilia, but it is also an interesting and useful model to study the actin cytoskeleton. Typically, a complicated system with gene redundancy, tissue specificity, and a vast array of interactors, the actin cytoskeleton of *Chlamydomonas* is relatively simple, yet interesting, because the actin cytoskeleton of *Chlamydomonas* has 2 actin genes: IDA5 (inner dynein arm 5), a conventional actin with 91% sequence identity compared to human ß-actin; and NAP1 (novel actin-like protein 1), a divergent actin that shares only about 63% of its sequence with human ß-actin (**Fig. 1.6)** (Hirono et al., 2003; Kato-Minoura et al., 1997; Onishi et al., 2016). This secondary actin NAP1 is classified as an actin-like protein as opposed to an actin related protein (ARP) because it can polymerize (Bigge et al., 2020, p. 20; Kato-Minoura, 2011), it is more closely related to actin than it is to any ARPs, and because it can functionally compensate for the conventional actin IDA5 (Jack et al., 2019). Further, while the sequence of NAP1 is divergent, the structure of the monomer is relatively well conserved in relation to IDA5 (**Fig. 1.7).** NAP1 proteins are unique to *Chlamydomonas* and its closest relatives including *Volvox* and *Gonium* **(Fig. 1.6**). However, what we can learn from studying proteins like NAP1 extends beyond this small corner of the tree of life.

Chlamydomonas provides a unique opportunity to study divergent actin phenotypes as it contains a built-in comparison to conventional actins. Further, these two actins are easily separable. IDA5, the conventional actin, is the primary actin expressed in normal vegetative cells. However, when cells are treated with Latrunculin B (LatB), a drug that sequesters actin monomers leading to eventual filament depolymerization, the conventional IDA5 is depolymerized, but the divergent NAP1 is insensitive to LatB; in fact, NAP1 is upregulated with LatB treatment (Kato-Minoura et al., 1998; Onishi et al., 2018, 2016). Additionally, genetic mutants of both IDA5 and NAP1 exist allowing for more study of individual contributions of the two actins. The *ida5* mutant has a point mutation that causes a frameshift and produces an early stop codon that eliminates actin function (Kato et al., 1993, p. 5). The *nap1* mutant introduces a new splice site that causes a 157 nucleotide deletion that causes a deletion of the last 120 amino acids eliminating actin function (Onishi et al., 2016). And finally, to get rid of all of the

filamentous actin in the cell, the *nap1* mutant that contains only IDA5 can be treated with LatB (Jack et al., 2019; Onishi et al., 2016).

However, despite the benefits of studying this system in this organism, *Chlamydomonas* has not historically been used as a model to study actin. In fact, many were hesitant regarding the importance of actin in these cells. This is because the actin cytoskeleton of *Chlamydomonas* has been notoriously difficult to visualize and because the loss of the primary actin did not result in any major phenotypic differences (Avasthi et al., 2014; Kato et al., 1993, p. 5; Kato-Minoura et al., 1997, p. 5; Ohara et al., 1998). Full loss of the primary actin IDA5 led to only small differences in ciliary assembly (Avasthi et al., 2014), some minor swimming defects due to the presence of IDA5 in the ciliary dynein (Ohara et al., 1998), and defects in fertilization tubule formation for mating (Ohara et al., 1998). The convergence of work from our lab to visualize actin in these cells with new bright and stable fluorophores and better imaging technology and the finding that a secondary actin can functionally compensate for the primary actin using a newly available *nap1* mutant has led to the emergence of *Chlamydomonas* as a model for actin as well as cilia (Craig et al., 2019; Craig and Avasthi, 2019; Jack et al., 2019; Onishi et al., 2016).

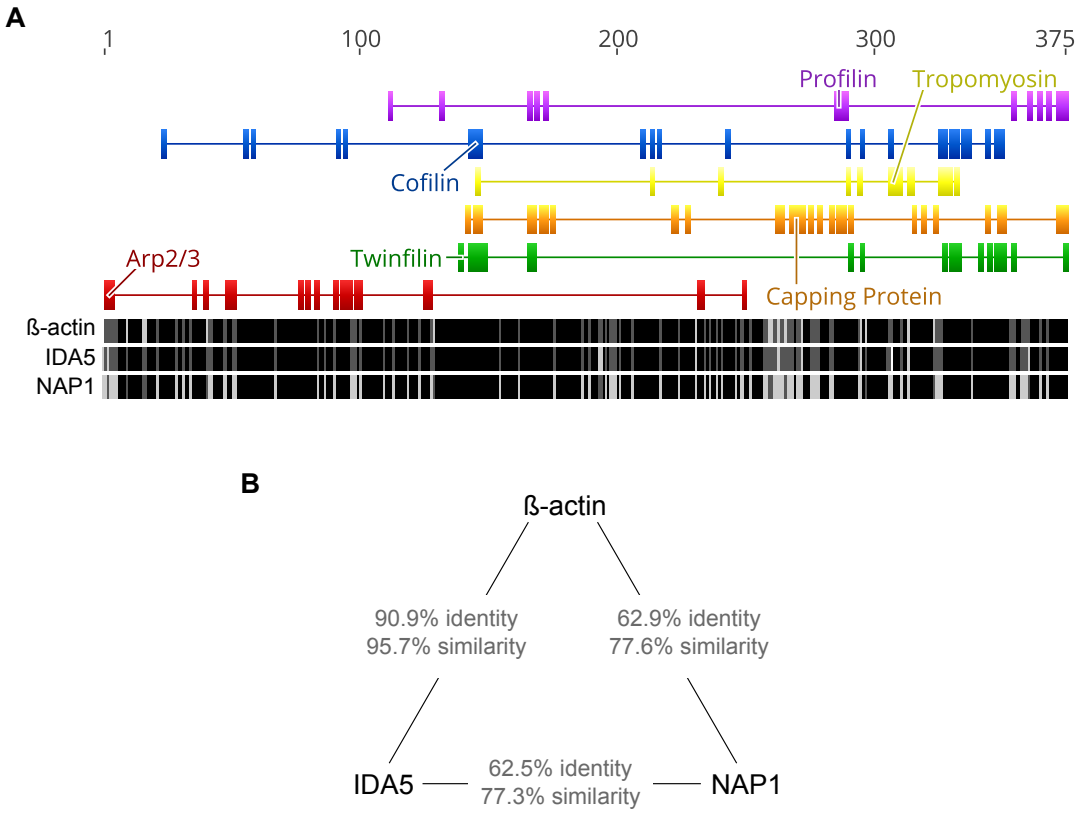

Fig. 1.6. IDA5 is similar to conventional actin, while NAP1 is divergent. A) MUSCLE sequence alignment created in Geneious between bovine ß-actin, IDA5 and NAP1. Black residues are conserved, dark grey residues are similar, and light grey residues are divergent. Boxes above the sequence correspond to the regions of actin expected to bind the noted actin binding proteins. **B)** Percent identity and percent similarity between bovine ß-actin, IDA5, and NAP1 based on the alignment in A.

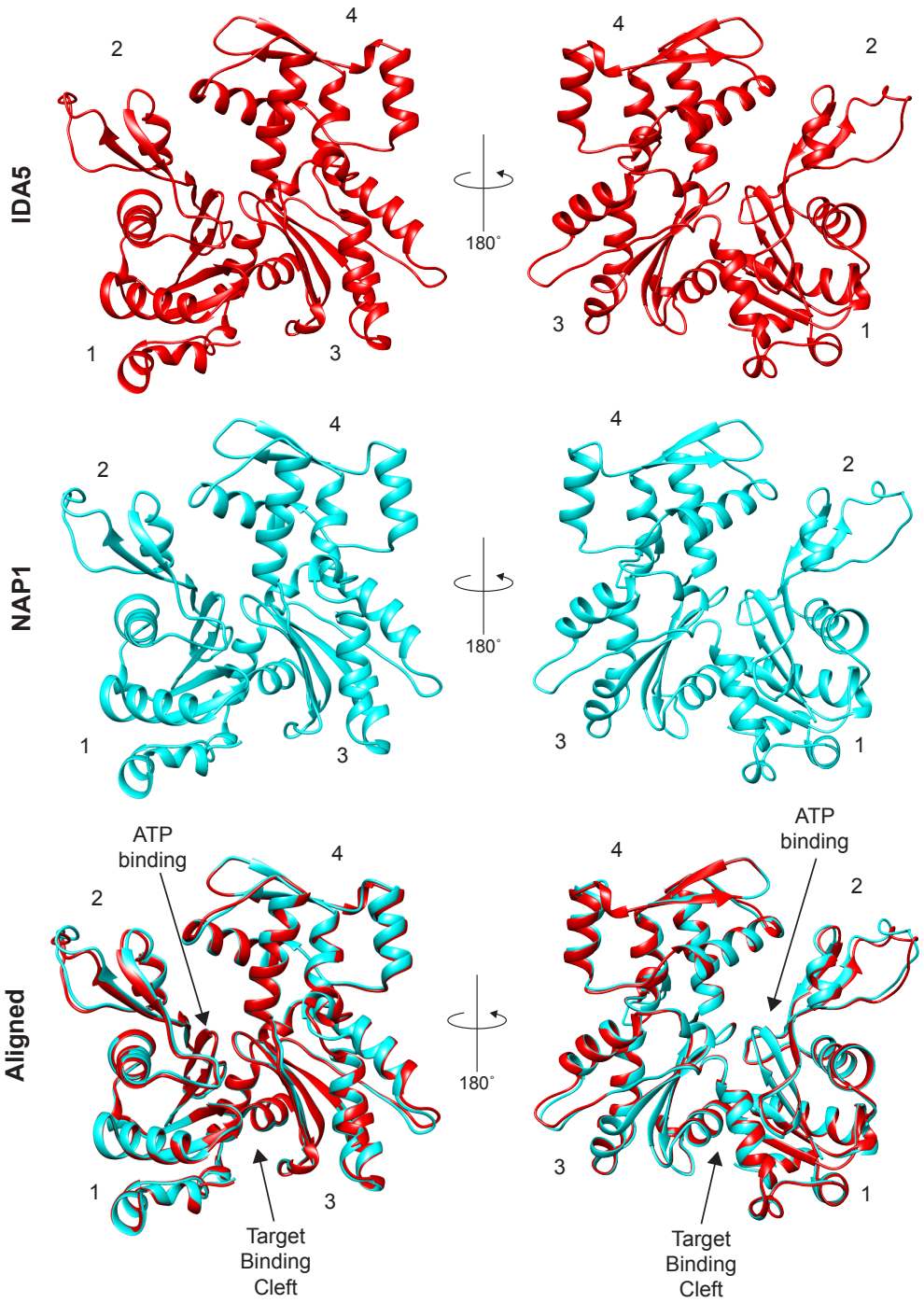

Fig. 1.7. IDA5 and NAP1 share structural features despite sequence divergence. Homology models of IDA5 and NAP1 created using Alphafold. Subdomains are labelled 1-4. The last row contains aligned structures highlighting the structural similarity between IDA5 and NAP1 despite their sequence divergence.

Visualizing actin in Chlamydomonas*:*

The visualization of the actin cytoskeleton has been notoriously difficult in *Chlamydomonas*. Actin antibodies do not discriminate between filamentous and monomeric actin creating diffuse signal throughout the cell. This is further complicated by the presence of the two actins. Further, traditional methods of actin labeling using phallotoxins and SiR-actin have not traditionally been successful. For years, the only structure really visible using any method of actin labeling was the fertilization tubule, a very bright and highly concentrated actin structure that extends from the apex of mating type plus cells during mating (Detmers et al., 1985).

Our first real glimpse into the actin cytoskeleton in these organisms came with the use of a fluorescently-labelled actin binding peptide, LifeAct-Venus, which could be used to not only visualize actin in cells, but also to visualize actin dynamics (Avasthi et al., 2014; Onishi et al., 2016). Using this method, a filamentous actin structure present in normal vegetative cells was identified. An accumulation of filamentous actin was found posterior to the nucleus, termed the midcell actin signal, and occasionally apical actin puncta were observed (Avasthi et al., 2014; Onishi et al., 2016).

In 2019 (**Appendix I**), a protocol was optimized for reliable visualization of the *Chlamydomonas* actin cytoskeleton using fluorescent phalloidin (**Fig. 1.8)** (Craig et al., 2019; Craig and Avasthi, 2019). This protocol provided higher resolution than the LifeAct peptide and opened the door for more studies of the actin cytoskeleton in this organism. Briefly, to optimize phalloidin labeling, we used the bright and photostable Atto fluorophores conjugated to phalloidin. We also limited background fluorescence by reducing incubation time to 16 minutes and deconvolving microscopy images to remove out-of-focus light. We found that the previously identified midcell actin signal that was seen with LifeAct was also present with this new phalloidin staining protocol (**Fig. 1.7**), as well as apical puncta that will be important in this thesis (Craig et al., 2019).

This protocol has been further improved by employing spinning disk confocal microscopy or airyscan confocal microscopy to obtain higher resolution with less background (**Fig. 1.8)**. These advances in filamentous actin visualization in *Chlamydomonas* have paved the way for further exploration of the cytoskeleton in these cells and helped them to become an emerging model for the study of actin.

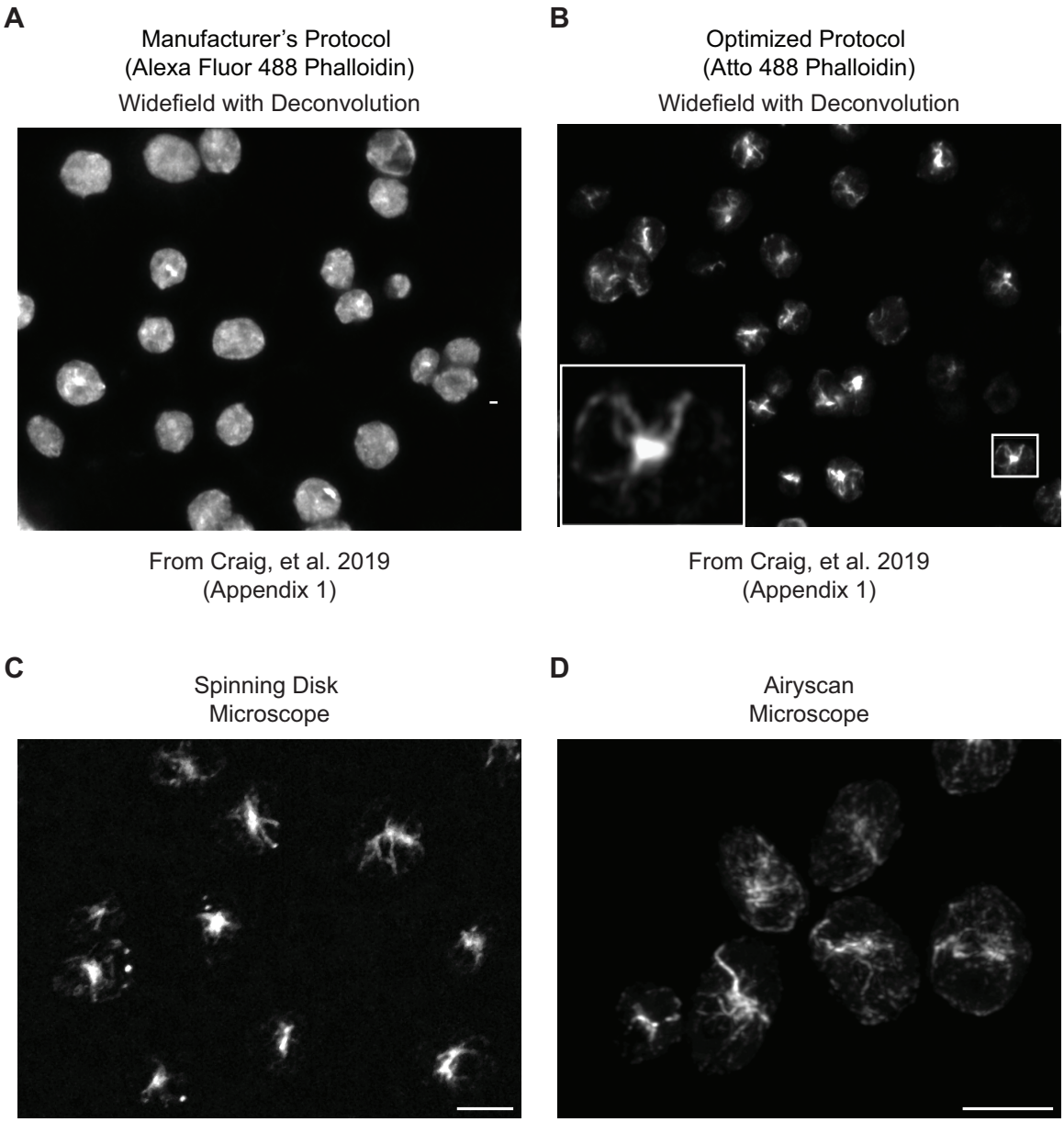

Fig. 1.8. Improved actin visualization has sparked new discovery in the *Chlamydomonas* actin field. A) *Chlamydomonas* cells with actin visualized with the manufacturer's protocol for AlexaFluor488 Phalloidin on a widefield fluorescent microscope followed by deconvolution. **B)** Cells with actin visualized with the optimized protocol from Craig, et al. 2019 using Atto488 Phalloidin. These were visualized with a widefield microscope followed by deconvolution. **C)** Cells with actin visualized with the optimized protocol from Craig, et al. 2019 but imaged using spinning disk microscopy without deconvolution. Scale bar is 5 μm. **D)** Cells with actin visualized with the optimized protocol but imaged using airyscan microscopy. Scale bar is 5 μm.

Actin binding proteins in Chlamydomonas:

Like other organisms, in *Chlamydomonas* the actin cytoskeleton is regulated by a group of proteins called actin binding proteins (ABPs) (Pollard, 2016). *Chlamydomonas* contains several proteins that are closely related to conventional actin binding proteins (**Table 1.1**). These proteins were identified primarily based on sequence searches, so there are likely other actin binding proteins present in *Chlamydomonas* that have less sequence conservation. Further, there are likely actin binding proteins that are unique to *Chlamydomonas* and related organisms that have yet to be identified. Of the proteins identified so far only a handful have been investigated, including profilin, the formins, the myosins, and, in this thesis, the Arp2/3 complex.

The *Chlamydomonas* profilin, CrPRF, binds actin monomers, like conventional profilins. However, unlike conventional profilins, CrPRF inhibits exchange of nucleotides on G-actin and seems to primarily function to sequester monomers and inhibit actin nucleation and elongation (Christensen et al., 2019; Kovar et al., 2001). The *Chlamydomonas* formin, FOR1, can overcome this inhibition and rapidly assemble actin filaments from PRF1-bound actin monomers (Christensen et al., 2019). CrPRF is found in the cilia and in the cell body, where it is particularly enriched in the apical region of the cell near the base of the cilia, or the fertilization tubule in mating cells (Kovar et al., 2001). CrPRF appears to play a role in the formation of the fertilization tubule in *Chlamydomonas* (Christensen et al., 2019), and it seems to be important for protection of IDA5 monomers from degradation as *prf1-1* mutants contain significantly decreased levels of IDA5 and PRF1 is overexpressed when cells are treated with Latrunculin B to depolymerize IDA5 filaments (Onishi et al., 2018).

Chlamydomonas contains at least 4 formin genes encoding 4 formin proteins: FOR1, FOR2, FOR3, and FOR4, each containing FH2 domains required for the ability of formins to nucleate linear actin filaments (Christensen et al., 2019). However, FOR1 is the only *Chlamydomonas* formin that has been extensively studied. FOR1 nucleates actin polymerization but elongates filaments weakly in the absence of CrPRF1; FOR1 nucleates and elongates actin filaments rapidly in the presence of CrPRF1 (Christensen et al., 2019). FOR1 also seems to be required for fertilization tubule formation (Christensen et al., 2019), but its role outside of mating has not been investigated.

The myosins, molecular motors often involved in contractile functions and vesicle transport, are the most well-characterized actin binding proteins in *Chlamydomonas*. There are 3 myosins present in *Chlamydomonas:* MYO1, MYO2, and MYO3. MYO1 and MYO3 are most similar to plant type XI myosins, which are similar to mammalian myosin V (Avasthi et al., 2014). Myosin V is often involved in transport of proteins from the Golgi throughout the cell (Deretic, 2013; Hsiao et al., 2012; Jin et al., 2011; Mazelova et al., 2009; Nachury et al., 2007; Pedersen et al., 2008; Reiter and Mostov, 2006; Schott et al., 2002). MYO2 is a type VIII myosin, which are myosins often expressed in plants that have been found to be involved in endocytosis (Avasthi et al., 2014; Avisar et al., 2008, 2008; Golomb et al., 2008; Reichelt et al., 1999; Sattarzadeh et al., 2008; Volkmann et al., 2003). The *Chlamydomonas* myosins are involved in ciliary assembly, and MYO2 has been found to localize near the base of cilia (Avasthi et al., 2014). Type II myosins are typically involved in cleavage furrow formation, but none of the *Chlamydomonas* myosins localize to the cleavage furrow, suggesting they are not involved in cleavage furrow formation (Onishi et al., 2019).

Finally, the *Chlamydomonas* Arp2/3 complex is investigated in detail in this work. The Arp2/3 complex nucleates branched actin networks and is often involved in membrane remodeling functions, like the formation of lamellipodia for cell motility and endocytosis (Goley and Welch, 2006, p. 3). The complex, composed of Arp2, Arp3, and ARPC1-5 is almost completely present in *Chlamydomonas*. The core of the complex ARPC2 and ARPC4, the first subunits of the resulting daughter filament Arp2 and Arp3, and the regulatory subunits ARPC1 and ARPC3 are present in *Chlamydomonas* with varying degrees of sequence conservation. However, and ARPC5 has not yet been identified. This suggests the Arp2/3 complex of *Chlamydomonas* is ether a six-membered complex or it contains a highly divergent ARPC5 subunit. The complex is involved in ciliary assembly and maintenance (Bigge et al., 2020), in dysfunctional ciliary elongation in the presence of lithium (Bigge and Avasthi, 2022), in a potential endocytic process (Bigge et al., 2020), and in the formation and maintenance of actin structures throughout the cell (Bigge et al., 2020; Bigge and Avasthi, 2022).

Table 1.1: Actin binding proteins in *Chlamydomonas*

Class	Name	*Chlamydomonas* gene
Actin folding	TCP-1/CCT	Cre10.g439100
	Prefoldin	Cre06.g261650 Cre07.g342250 Cre09.g405400 Cre16.g671750 Cre12.g523150 Cre12.g502750
Actin/microtubule cross-linker	Coronin	Cre08.g382620 Cre12.g512750
	p53	Cre12.g550500
adhesion protein	Presenilin	Cre02.g078858
Bundler/cross-linker	α-actinin	Cre11.g468450
	Spectrin	Cre07.g340450
	Filamin	Cre12.g521550
	Villin	Cre.12g524400
	Epsin	Cre16.g664450
	Fimbrin/Plastin	Cre16.g664450
Capping protein	Tensin	Cre06.g308400
	Fragmin	Cre08.g375000
	Gelsolin/Severin/Brevin	Cre12.g555550
Filament Stabilizer	Tropomyosin	Cre06.g278257 Cre03.g155100 Cre07.g339050 Cre12.g514550 Cre17.g704950 Cre06.g294700 Cre05.g236050 Cre12.g547651 Cre03.g145487 Cre02.g091900 Cre01.g048000
Membrane Binding/Linking	Annexin/Calpactin	Cre01.g025650
	Ezrin/Radixin/Moesin	Cre02.g097300
	Talin/Merlin	Cre06.g278125
Monomer binding	Profilin	Cre10.g427250
	Actobindin	Cre16.g683200
MYosin Family Motor Protein	Class VIII Myosin	Cre09.g416250 (MYO2)
	Class XI Myosin	Cre13.g563900 (MYO3) Cre16.g658650 (MYO1)
Nucleation Promoting Factor	Verprolin/WIP	Cre05.g244701
	Sra-1	Cre12.g522450
Nucleator	Arp2/3 Complex	Cre16.g687500 (Arp2) Cre16.g676050 (Arp3) Cre16.g648100 (ARPC1) Cre17.g747197 (ARPC2) Cre09.g397950 (ARPC3) Cre06.g260800 (ARPC4)
	Formin	Cre03.g166700 (FOR1) Cre05.g232900 (FOR2) Cre06.g311250 (FOR3)

		Cre04.g229163 (FOR4)
Regulator	Calmodulin	Cre03.g178150 Cre03.g178350 Cre03.g150300 Cre11.g468450 Cre03.g210177 Cre07.g328900 Cre01.g051250 Cre17.g705000 Cre02.g114750 Cre19.g750597 Cre13.g571700
	YpkA	Cre12.g549800
	TOR2	Cre09.g400553
	IQGAP	Cre06.g281200
	Neurocalcin	Cre08.g363750
	Troponin	Cre06.g308000
Severing protein	ADF/Cofilin	Cre07.g339050

Actin function in Chlamydomonas:

Actin is involved in the cell cycle in most cells. In *Chlamydomonas,* where cells can undergo sexual or asexual reproduction, this is no different. During the sexual lifecycle, cells differentiate into plus gametes or minus gametes depending on cell line (Harris et al., 2009c). Each cell type develops a mating structure composed of actin (Cavalier-Smith, 1975; Detmers et al., 1985, 1983; Friedmann et al., 1968; Goodenough and Weiss, 1975). The mating type plus gametes form a fertilization tubule at the apex of the cell between the cilia. The tubule is primarily composed of filamentous actin, and the primary actin, IDA5 is essential for the formation of normal fertilization tubules (Detmers et al., 1985; Ohara et al., 1998). We also know that profilin and formin are involved in the formation of this structure (Christensen et al., 2019). In mating type minus gametes, an actin cap forms at the apex of the cell where the cilia are located. This is also composed of filamentous actin. During mating, the mating type plus and minus gametes undergo an agglutination stage where proteins on the cilia of each (SAG1 in mating type plus cells and SAD1 in mating type minus cells) bind to each other bringing the cells and their mating type structures into proximity (Adair et al., 1983; Ferris et al., 2005; Snell and Goodenough, 2009). The cells eventually fuse when the fertilization tubule of the mating type plus cell enters the mating type minus cell (Harris et al., 2009c).

Asexual reproduction, while not requiring actin to form mating structures, still involves actin. *Chlamydomonas* cells undergo multiple fission, meaning that they spend an extended period in G1 phase and replicate all cell contents and grow much larger before dividing several times in a row (Cross, 2020; Onishi et al., 2019). During this cycle cells undergo mitosis. In interphase, actin is diffusely localized in the perinuclear region (Craig et al., 2019; Harper et al., 1992). In preprophase, actin localization becomes more angular, and during prophase and metaphase, actin bands curve over the surface of the nuclear envelope (Craig et al., 2019; Harper et al., 1992). During anaphase, actin is a diffuse band extending along the anterior to the elongating nucleus (Craig et al., 2019; Harper et al., 1992). In telophase and cytokinesis, actin localizes along the site of the cleavage furrow (Craig et al., 2019; Harper et al., 1992; Onishi et al., 2019). Typically, actin is thought to be primarily involved in the final stage of mitosis, cytokinesis, where the cells physically split into two, and specifically for the formation of the cleavage

furrow during this stage. In fact, it is widely thought that the formation of the cleavage furrow is driven by the contraction of a ring of actin and myosin, termed the contractile ring. However, in *Chlamydomonas,* actin was dispensable for the formation of the cleavage furrow and even for cell division itself, although division did occur less efficiently without filamentous actin present, and it was discovered that actin might be involved in the division of the chloroplast (Onishi et al., 2019).

Outside of cell division and mating, actin functions in *Chlamydomonas* have not been extensively studied. However, we also know that cells lacking the primary actin, IDA5, have defective swimming, likely because of the role of monomeric IDA5 as a member of the inner dynein arm of the *Chlamydomonas* cilia (Ohara et al., 1998). More recent work by our lab has found additional roles for actin in maintaining and assembling cilia in *Chlamydomonas* (Avasthi et al., 2014; Jack et al., 2019).

Actin and cilia:

The regulation of the microtubule-based cilium extends to other cytoskeletal components, namely actin. Roles for actin have been found in the assembly and maintenance of *Chlamydomonas* cilia as well as mammalian cilia. However, importantly, mammalian cells lack a cell wall meaning they have a cortical actin network to help maintain cell shape. This cortical actin network is not present in *Chlamydomonas,* meaning using this organism, researchers can get at the underlying functions of actin in ciliary assembly.

Mammalian actin in ciliary assembly and regulation:

Typically, in mammalian cells, actin disruption causes increases in ciliary length and percentage of ciliated cells (Kohli et al., 2017; Sharma et al., 2011). The effect of actin on cilia in mammalian cells is complicated by the presence of a cortical actin network located just inside the membrane that may block centrosome access to the membrane. Outside of this, there are many potential reasons for the increase ciliary length and number induced by loss of actin, including roles for actin in basal body docking and stabilization (Kim et al., 2010; Pan et al., 2007; Park et al., 2008; Tu et al., 2017; Yeyati et al., 2017). In fact, the centrosome, which becomes the basal bodies during ciliogensis, also functions as an actin organizer (Farina et al., 2016; Inoue et al., 2019).

More recent work has shown evidence for actin in trafficking of cilia-bound vesicles from various locations in the cell to growing cilia. In intracellular ciliogenesis, where preciliary vesicles are trafficked to the ciliary base where they fuse to form a ciliary vesicle around the budding cilium, actin networks are needed. Specifically, the Arp2/3 complex and myosin-Va are required for proper vesicle fusion of the preciliary vesicles at the centriole (Wu et al., 2018). Vesicle budding in the endocytic pathway, which may be involved in ciliary assembly, also requires actin (Girao et al., 2008). Endocytic compartments are connected to a vesicular network that may be involved in ciliary assembly via a trafficking pathway requiring actin (Kim et al., 2010). Further, actin-dependent membrane remodeling is required for ciliary exocytosis (Nager et al., 2017) and ciliary resorption (Saito et al., 2017).

Finally, actin itself has recently been found within the axoneme of cilia, suggesting that actin is a key protein in cilia (Kiesel et al., 2020). Overall, we know that actin is involved in a number of processes that influence ciliogenesis based on work in mammalian cells. However, *Chlamydomonas* allows for further dissection of the requirement for actin at each distinct step of ciliary assembly (**Figs. 1.4-5)**.

Chlamydomonas *actin in ciliary assembly regulation:*

In *Chlamydomonas,* where cilia are persistently present and where assembly and regulation are not complicated by the presence of a cortical actin network, loss of filamentous actin results in shortened cilia and defective assembly. When cells were treated with Cytochalasin D (CytoD), which disrupts the actin cytoskeleton, steady-state cilia shortened significantly, but cilia were able to assemble to normal length following treatment (Dentler and Adams, 1992). Similarly, when cells were treated with Latrunculin B (LatB), which sequesters actin monomers leading to eventual filament depolymerization, ciliary assembly rate was only slightly decreased with cells eventually reaching normal length (Avasthi et al., 2014). For some time, these results puzzled researchers who expected loss of actin to have a more dramatic effect on cilia.

The answer came with the creation of *nap1* null mutant which was used to discover that the divergent NAP1 could compensate for the primary actin IDA5 (Jack et al., 2019; Onishi et al., 2016). This opened the door to the discovery that at least one functional actin is required for several steps of ciliary assembly including incorporation of existing protein, new protein synthesis, trafficking of new protein through the Golgi, and organization of the transition zone (Jack et al., 2019) (**Fig. 1.9)**. We also know that loss of actin causes problems with the injection of IFT trains for assembly (Avasthi et al., 2014) (**Fig. 1.9**).

In this thesis, we build on the knowledge found by taking a broad brush and getting rid of all filamentous actin by focusing instead on a subset of filamentous actin nucleated by a single actin binding protein.

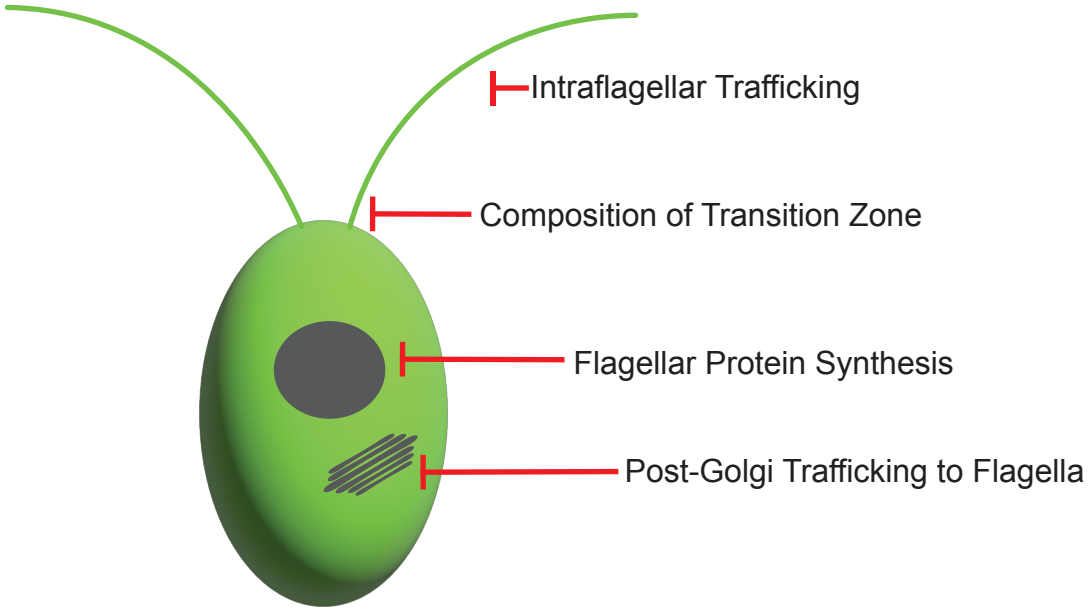

Fig. 1.9. Actin's function in cilia in *Chlamydomonas*. Using cells that acutely have no filamentous actin (IDA5 or NAP1), it was discovered that actin has roles in ciliary protein synthesis, post-Golgi trafficking to cilia, and composition of the transition zone (Jack et al., 2019). We also know that cells lacking IDA5 have effects in IFT regulation (Avasthi et al., 2014). Fig. adapted from Jack et al., 2019.

Research Objectives:

In this work, the ciliary model organism *Chlamydomonas* is deployed to help answer questions about actin regulation and function. Because *Chlamydomonas* has two actins: one conventional and one divergent, it offers a unique opportunity to study actin regulation with a built-in control and to understand segregation and functions of actin binding proteins that interact with one or both actins. Using this system, we questioned whether we could determine if binding proteins would interact with the two actins based on conservation. Specifically, we asked if the Arp2/3 complex could interact with both the conventional and divergent actin as the region of the divergent actin expected to bind the Arp2/3 complex was less than 50% conserved.

Next, we aimed to characterize the cellular functions of the Arp2/3 complex in this organism, as the complex has not been studied in this organism yet. Previous work from our lab established a role for actin in ciliary maintenance and assembly by broadly inhibiting filamentous actin in the cell (Avasthi et al., 2014; Jack et al., 2019), and initial work showed defects in ciliary maintenance and assembly when the Arp2/3 complex was inhibited as well. This allows us to further dissect some of these broad roles for filamentous actin in ciliary assembly. By focusing on the Arp2/3 complex, we can learn more about the functions of the Arp2/3 complex in the cell, but we can also learn more about ciliary length maintenance and ciliary assembly. We also took this one step further and examine the role of the Arp2/3 complex and actin networks mediated by this complex in a ciliary defect that occurs across cell types and organisms, lengthening induced by lithium treatment.

In order to characterize the role of the Arp2/3 complex in these functions, we also investigated other Arp2/3 complex functions in the cell. Primarily, we characterized an endocytic pathway in these cells that has not previously been investigated. We also learned more about actin organization in the cell and what specific actin networks might be doing. Overall, we characterize the interactions of the conventional IDA5 and the divergent NAP1 with the Arp2/3 complex, we investigate the roles of the Arp2/3 complex in the cell, and ultimately to integrate these findings, we propose a novel mechanism for ciliary regulation, assembly, and defective lengthening that relies on Arp2/3 complex-mediated actin networks and endocytosis.

References:

Adair, W.S., Hwang, C., Goodenough, U.W., 1983. Identification and visualization of the sexual agglutinin from the mating-type plus flagellar membrane of Chlamydomonas. Cell 33, 183–193. https://doi.org/10.1016/0092-8674(83)90347-1

Adams, G.M., Huang, B., Luck, D.J., 1982. Temperature-Sensitive, Assembly-Defective Flagella Mutants of CHLAMYDOMONAS REINHARDTII. Genetics 100, 579–586. https://doi.org/10.1093/genetics/100.4.579

Adams, G.M., Wright, R.L., Jarvik, J.W., 1985. Defective temporal and spatial control of flagellar assembly in a mutant of Chlamydomonas reinhardtii with variable flagellar number. J. Cell Biol. 100, 955–964. https://doi.org/10.1083/jcb.100.3.955

Asleson, C.M., Lefebvre, P.A., 1998. Genetic analysis of flagellar length control in Chlamydomonas reinhardtii: a new long-flagella locus and extragenic suppressor mutations. Genetics 148, 693–702. https://doi.org/10.1093/genetics/148.2.693

Avasthi, P., Marshall, W.F., 2012. Stages of ciliogenesis and regulation of ciliary length. Differ. Res. Biol. Divers. 83, S30–S42. https://doi.org/10.1016/j.diff.2011.11.015

Avasthi, P., Onishi, M., Karpiak, J., Yamamoto, R., Mackinder, L., Jonikas, M.C., Sale, W.S., Shoichet, B., Pringle, J.R., Marshall, W.F., 2014. Actin Is Required for IFT Regulation in Chlamydomonas reinhardtii. Curr. Biol. 24, 2025–2032. https://doi.org/10.1016/j.cub.2014.07.038

Avisar, D., Prokhnevsky, A.I., Dolja, V.V., 2008. Class VIII Myosins Are Required for Plasmodesmatal Localization of a Closterovirus Hsp70 Homolog. J. Virol. 82, 2836. https://doi.org/10.1128/JVI.02246-07

Barsel, S.E., Wexler, D.E., Lefebvre, P.A., 1988. Genetic analysis of long-flagella mutants of Chlamydomonas reinhardtii. Genetics 118, 637–648. https://doi.org/10.1093/genetics/118.4.637

Beck, C., Uhl, R., 1994. On the localization of voltage-sensitive calcium channels in the flagella of Chlamydomonas reinhardtii. J. Cell Biol. 125, 1119–1125.

Berbari, N.F., O'Connor, A.K., Haycraft, C.J., Yoder, B.K., 2009. The Primary Cilium as a Complex Signaling Center. Curr. Biol. 19, R526–R535. https://doi.org/10.1016/j.cub.2009.05.025

Besschetnova, T.Y., Kolpakova-Hart, E., Guan, Y., Zhou, J., Olsen, B.R., Shah, J.V., 2010. Identification of signaling pathways regulating primary cilium length and flow-mediated adaptation. Curr. Biol. 20, 182–187.

Bigge, B.M., Avasthi, P., 2022. Lithium-induced ciliary lengthening sparks Arp2/3 complex-dependent endocytosis. bioRxiv 2022.04.18.488674. https://doi.org/10.1101/2022.04.18.488674

Bigge, B.M., Rosenthal, N.E., Sept, D., Schroeder, C.M., Avasthi, P., 2020. Initial ciliary assembly in Chlamydomonas requires Arp2/3-dependent recruitment from a ciliary protein reservoir in the plasma membrane. bioRxiv 2020.11.24.396002. https://doi.org/10.1101/2020.11.24.396002

Cavalier-Smith, T., 1975. Electron and light microscopy of gametogenesis and gamete fusion in Chlamydomonas reinhardii. Protoplasma 86, 1–18. https://doi.org/10.1007/BF01275619

Cheng, X., Liu, G., Ke, W., Zhao, L., Lv, B., Ma, X., Xu, N., Xia, X., Deng, X., Zheng, C., Huang, K., 2017. Building a multipurpose insertional mutant library for forward and reverse genetics in Chlamydomonas. Plant Methods 13, 36. https://doi.org/10.1186/s13007-017-0183-5

Christensen, J.R., Craig, E.W., Glista, M.J., Mueller, D.M., Li, Y., Sees, J.A., Huang, S., Suarez, C., Mets, L.J., Kovar, D.R., Avasthi, P., 2019. Chlamydomonas reinhardtii formin FOR1 and profilin PRF1 are optimized for acute rapid actin filament assembly. Mol. Biol. Cell 30, 3123–3135. https://doi.org/10.1091/mbc.E19-08-0463

Cole, D.G., 2009. Chapter 4 - Intraflagellar Transport, in: Harris, E.H., Stern, D.B., Witman, G.B. (Eds.), The Chlamydomonas Sourcebook (Second Edition). Academic Press, London, pp. 71–113. https://doi.org/10.1016/B978-0-12-370873-1.00041-1

Cole, D.G., Diener, D.R., Himelblau, A.L., Beech, P.L., Fuster, J.C., Rosenbaum, J.L., 1998. Chlamydomonas kinesin-II-dependent intraflagellar transport (IFT): IFT particles contain proteins required for ciliary assembly in Caenorhabditis elegans sensory neurons. J. Cell Biol. 141, 993–1008. https://doi.org/10.1083/jcb.141.4.993

Craft Van De Weghe, J., Harris, J.A., Kubo, T., Witman, G.B., Lechtreck, K.F., 2020. Diffusion rather than intraflagellar transport likely provides most of the tubulin required for axonemal assembly in Chlamydomonas. J. Cell Sci. 133. https://doi.org/10.1242/jcs.249805

Craig, E.W., Avasthi, P., 2019. Visualizing Filamentous Actin Using Phalloidin in Chlamydomonas reinhardtii. Bio-Protoc. 9. https://doi.org/10.21769/BioProtoc.3274

Craig, E.W., Mueller, D.M., Bigge, B.M., Schaffer, M., Engel, B.D., Avasthi, P., 2019. The elusive actin cytoskeleton of a green alga expressing both conventional and divergent actins. Mol. Biol. Cell mbc.E19-03-0141. https://doi.org/10.1091/mbc.E19-03-0141

Cross, F.R., 2020. Regulation of Multiple Fission and Cell-Cycle-Dependent Gene Expression by CDKA1 and the Rb-E2F Pathway in Chlamydomonas. Curr. Biol. CB 30, 1855-1865.e4. https://doi.org/10.1016/j.cub.2020.03.019

Dentler, W., 2013. A Role for the Membrane in Regulating Chlamydomonas Flagellar Length. PLOS ONE 8, e53366. https://doi.org/10.1371/journal.pone.0053366

Dentler, W.L., Adams, C., 1992. Flagellar microtubule dynamics in Chlamydomonas: cytochalasin D induces periods of microtubule shortening and elongation; and colchicine induces disassembly of the distal, but not proximal, half of the flagellum. J. Cell Biol. 117, 1289–1298. https://doi.org/10.1083/jcb.117.6.1289

Deretic, D., 2013. Crosstalk of Arf and Rab GTPases en route to cilia. Small GTPases 4, 70–77. https://doi.org/10.4161/sgtp.24396

Detmers, P.A., Carboni, J.M., Condeelis, J., 1985. Localization of actin in Chlamydomonas using antiactin and NBD-phallacidin. Cell Motil. 5, 415–430. https://doi.org/10.1002/cm.970050505

Detmers, P.A., Goodenough, U.W., Condeelis, J., 1983. Elongation of the fertilization tubule in Chlamydomonas: new observations on the core microfilaments and the effect of transient intracellular signals on their structural integrity. J. Cell Biol. 97, 522–532. https://doi.org/10.1083/jcb.97.2.522

Diener, D.R., Lupetti, P., Rosenbaum, J.L., 2015. Proteomic analysis of isolated ciliary transition zones reveals the presence of ESCRT proteins. Curr. Biol. CB 25, 379–384. https://doi.org/10.1016/j.cub.2014.11.066

Dutcher, S.K., 2009. Chapter 2 - Basal Bodies and Associated Structures, in: Harris, E.H., Stern, D.B., Witman, G.B. (Eds.), The Chlamydomonas Sourcebook (Second Edition). Academic Press, London, pp. 15–42. https://doi.org/10.1016/B978-0-12-370873-1.00039-3

Farina, F., Gaillard, J., Guérin, C., Couté, Y., Sillibourne, J., Blanchoin, L., Théry, M., 2016. The centrosome is an actin-organizing centre. Nat. Cell Biol. 18, 65–75. https://doi.org/10.1038/ncb3285

Ferris, P.J., Waffenschmidt, S., Umen, J.G., Lin, H., Lee, J.-H., Ishida, K., Kubo, T., Lau, J., Goodenough, U.W., 2005. Plus and minus sexual agglutinins from Chlamydomonas reinhardtii. Plant Cell 17, 597–615. https://doi.org/10.1105/tpc.104.028035

Friedmann, I., Colwin, A.L., Colwin, L.H., 1968. Fine-structural aspects of fertilization in Chlamydomonas reinhardi. J. Cell Sci. 3, 115–128.

Goley, E.D., Welch, M.D., 2006. The ARP2/3 complex: an actin nucleator comes of age. Nat. Rev. Mol. Cell Biol. 7, 713–726. https://doi.org/10.1038/nrm2026

Golomb, L., Abu-Abied, M., Belausov, E., Sadot, E., 2008. Different subcellular localizations and functions of Arabidopsis myosin VIII. BMC Plant Biol. 8, 3. https://doi.org/10.1186/1471-2229-8-3

Goodenough, U.W., Weiss, R.L., 1975. Gametic differentiation in Chlamydomonas reinhardtii. III. Cell wall lysis and microfilament-associated mating structure activation in wild-type and mutant strains. J. Cell Biol. 67, 623–637.

Harper, J.D., McCurdy, D.W., Sanders, M.A., Salisbury, J.L., John, P.C., 1992. Actin dynamics during the cell cycle in Chlamydomonas reinhardtii. Cell Motil. Cytoskeleton 22, 117–126. https://doi.org/10.1002/cm.970220205

Harris, E.H., Stern, D.B., Witman, G.B. (Eds.), 2009a. Chapter 1 - The Genus Chlamydomonas, in: The Chlamydomonas Sourcebook (Second Edition). Academic Press, London, pp. 1–24. https://doi.org/10.1016/B978-0-12-370873-1.00001-0

Harris, E.H., Stern, D.B., Witman, G.B. (Eds.), 2009b. Chapter 2 - Cell Architecture, in: The Chlamydomonas Sourcebook (Second Edition). Academic Press, London, pp. 25–64. https://doi.org/10.1016/B978-0-12-370873-1.00002-2

Harris, E.H., Stern, D.B., Witman, G.B. (Eds.), 2009c. Chapter 5 - The Sexual Cycle, in: The Chlamydomonas Sourcebook (Second Edition). Academic Press, London, pp. 119–157. https://doi.org/10.1016/B978-0-12-370873-1.00005-8

Hendel, N.L., Thomson, M., Marshall, W.F., 2018. Diffusion as a Ruler: Modeling Kinesin Diffusion as a Length Sensor for Intraflagellar Transport. Biophys. J. 114, 663–674. https://doi.org/10.1016/j.bpj.2017.11.3784

Hirono, M., Uryu, S., Ohara, A., Kato-Minoura, T., Kamiya, R., 2003. Expression of conventional and unconventional actins in Chlamydomonas reinhardtii upon deflagellation and sexual adhesion. Eukaryot. Cell 2, 486–493. https://doi.org/10.1128/ec.2.3.486-493.2003

Hsiao, Y.-C., Tuz, K., Ferland, R.J., 2012. Trafficking in and to the primary cilium. Cilia 1, 4. https://doi.org/10.1186/2046-2530-1-4

Hu Qicong, Milenkovic Ljiljana, Jin Hua, Scott Matthew P., Nachury Maxence V., Spiliotis Elias T., Nelson W. James, 2010. A Septin Diffusion Barrier at the Base of the Primary Cilium Maintains Ciliary Membrane Protein Distribution. Science 329, 436–439. https://doi.org/10.1126/science.1191054

Huang, B., Piperno, G., Luck, D.J., 1979. Paralyzed flagella mutants of Chlamydomonas reinhardtii. Defective for axonemal doublet microtubule arms. J. Biol. Chem. 254, 3091–3099.

Huang, B., Rifkin, M.R., Luck, D.J., 1977. Temperature-sensitive mutations affecting flagellar assembly and function in Chlamydomonas reinhardtii. J. Cell Biol. 72, 67–85.

Inoue, D., Obino, D., Pineau, J., Farina, F., Gaillard, J., Guerin, C., Blanchoin, L., Lennon-Duménil, A.-M., Théry, M., 2019. Actin filaments regulate microtubule growth at the centrosome. EMBO J. 38. https://doi.org/10.15252/embj.201899630

Ishikawa, H., Marshall, W.F., 2017a. Intraflagellar Transport and Ciliary Dynamics. Cold Spring Harb. Perspect. Biol. 9. https://doi.org/10.1101/cshperspect.a021998

Ishikawa, H., Marshall, W.F., 2017b. Testing the time-of-flight model for flagellar length sensing. Mol. Biol. Cell 28, 3447–3456. https://doi.org/10.1091/mbc.e17-06-0384

Jack, B., Avasthi, P., 2018. Erratum to: Chemical Screening for Flagella-Associated Phenotypes in Chlamydomonas reinhardtii. Methods Mol. Biol. Clifton NJ 1795, E1. https://doi.org/10.1007/978-1-4939-7874-8_19

Jack, B., Mueller, D.M., Fee, A.C., Tetlow, A.L., Avasthi, P., 2019. Partially Redundant Actin Genes in Chlamydomonas Control Transition Zone Organization and Flagellum-Directed Traffic. Cell Rep. 27, 2459-2467.e3. https://doi.org/10.1016/j.celrep.2019.04.087

Jin, Y., Sultana, A., Gandhi, P., Franklin, E., Hamamoto, S., Khan, A.R., Munson, M., Schekman, R., Weisman, L.S., 2011. Myosin V Transports Secretory Vesicles via a Rab GTPase Cascade and Interaction with the Exocyst Complex. Dev. Cell 21, 1156–1170. https://doi.org/10.1016/j.devcel.2011.10.009

Johnson, K.A., Rosenbaum, J.L., 1992. Polarity of flagellar assembly in Chlamydomonas. J. Cell Biol. 119, 1605–1611. https://doi.org/10.1083/jcb.119.6.1605

Kato, T., Kagami, O., Yagi, T., Kamiya, R., 1993. Isolation of two species of Chlamydomonas reinhardtii flagellar mutants, ida5 and ida6, that lack a newly identified

heavy chain of the inner dynein arm. Cell Struct. Funct. 18, 371–377. https://doi.org/10.1247/csf.18.371

Kato-Minoura, T., 2011. Extremely low polymerizability of a highly-divergent Chlamydomonas actin (NAP). Biochem. Biophys. Res. Commun. 412, 723–727. https://doi.org/10.1016/j.bbrc.2011.08.040

Kato-Minoura, T., Hirono, M., Kamiya, R., 1997. Chlamydomonas Inner-Arm Dynein Mutant, ida5, Has a Mutation in an Actin-encoding Gene. J. Cell Biol. 137, 649–656. https://doi.org/10.1083/jcb.137.3.649

Kato-Minoura, T., Uryu, S., Hirono, M., Kamiya, R., 1998. Highly divergent actin expressed in a Chlamydomonas mutant lacking the conventional actin gene. Biochem. Biophys. Res. Commun. 251, 71–76. https://doi.org/10.1006/bbrc.1998.9373

Kiesel, P., Alvarez Viar, G., Tsoy, N., Maraspini, R., Gorilak, P., Varga, V., Honigmann, A., Pigino, G., 2020. The molecular structure of mammalian primary cilia revealed by cryo-electron tomography. Nat. Struct. Mol. Biol. https://doi.org/10.1038/s41594-020-0507-4

Komsic-Buchmann, K., Wöstehoff, L., Becker, B., 2014. The contractile vacuole as a key regulator of cellular water flow in Chlamydomonas reinhardtii. Eukaryot. Cell 13, 1421–1430. https://doi.org/10.1128/EC.00163-14

Kovar, D.R., Yang, P., Sale, W.S., Drobak, B.K., Staiger, C.J., 2001. Chlamydomonas reinhardtii produces a profilin with unusual biochemical properties. J. Cell Sci. 114, 4293–4305.

Kozminski, K.G., Johnson, K.A., Forscher, P., Rosenbaum, J.L., 1993. A motility in the eukaryotic flagellum unrelated to flagellar beating. Proc. Natl. Acad. Sci. U. S. A. 90, 5519–5523. https://doi.org/10.1073/pnas.90.12.5519

Kuchka, M.R., Jarvik, J.W., 1987. Short-Flagella Mutants of Chlamydomonas reinhardtii. Genetics 115, 685–691. https://doi.org/10.1093/genetics/115.4.685

Kuchka, M.R., Jarvik, J.W., 1982. Analysis of flagellar size control using a mutant of Chlamydomonas reinhardtii with a variable number of flagella. J. Cell Biol. 92, 170–175. https://doi.org/10.1083/jcb.92.1.170

Lefebvre, P.A., 1995. Flagellar amputation and regeneration in Chlamydomonas, in: Methods in Cell Biology. Elsevier, pp. 3–7.

Levy, E.M., 1974. Flagellar elongation as a moving boundary problem. Bull. Math. Biol. 36, 265–273.

Li, X., Patena, W., Fauser, F., Jinkerson, R.E., Saroussi, S., Meyer, M.T., Ivanova, N., Robertson, J.M., Yue, R., Zhang, R., Vilarrasa-Blasi, J., Wittkopp, T.M., Ramundo, S., Blum, S.R., Goh, A., Laudon, M., Srikumar, T., Lefebvre, P.A., Grossman, A.R., Jonikas, M.C., 2019. A genome-wide algal mutant library and functional screen identifies genes required for eukaryotic photosynthesis. Nat. Genet. 51, 627–635. https://doi.org/10.1038/s41588-019-0370-6

Ludington, W.B., Ishikawa, H., Serebrenik, Y.V., Ritter, A., Hernandez-Lopez, R.A., Gunzenhauser, J., Kannegaard, E., Marshall, W.F., 2015. A Systematic Comparison of

Mathematical Models for Inherent Measurement of Ciliary Length: How a Cell Can Measure Length and Volume. Biophys. J. 108, 1361–1379. https://doi.org/10.1016/j.bpj.2014.12.051

Marshall, W.F., 2015. How Cells Measure Length on Subcellular Scales. Spec. Issue Quant. Cell Biol. 25, 760–768. https://doi.org/10.1016/j.tcb.2015.08.008

Marshall, W.F., Qin, H., Rodrigo Brenni, M., Rosenbaum, J.L., 2005. Flagellar length control system: testing a simple model based on intraflagellar transport and turnover. Mol. Biol. Cell 16, 270–278. https://doi.org/10.1091/mbc.e04-07-0586

Marshall, W.F., Rosenbaum, J.L., 2001. Intraflagellar transport balances continuous turnover of outer doublet microtubules: implications for flagellar length control. J. Cell Biol. 155, 405–414.

Mazelova, J., Astuto-Gribble, L., Inoue, H., Tam, B.M., Schonteich, E., Prekeris, R., Moritz, O.L., Randazzo, P.A., Deretic, D., 2009. Ciliary targeting motif VxPx directs assembly of a trafficking module through Arf4. EMBO J. 28, 183–192. https://doi.org/10.1038/emboj.2008.267

McVittie, A., 1972. Flagellum mutants of Chlamydomonas reinhardii. J. Gen. Microbiol. 71, 525–540. https://doi.org/10.1099/00221287-71-3-525

Merchant, S.S., Prochnik, S.E., Vallon, O., Harris, E.H., Karpowicz, S.J., Witman, G.B., Terry, A., Salamov, A., Fritz-Laylin, L.K., Marechal-Drouard, L., Marshall, W.F., Qu, L.-H., Nelson, D.R., Sanderfoot, A.A., Spalding, M.H., Kapitonov, V.V., Ren, Q., Ferris, P., Lindquist, E., Shapiro, H., Lucas, S.M., Grimwood, J., Schmutz, J., Cardol, P., Cerutti, H., Chanfreau, G., Chen, C.-L., Cognat, V., Croft, M.T., Dent, R., Dutcher, S., Fernandez, E., Fukuzawa, H., Gonzalez-Ballester, D., Gonzalez-Halphen, D., Hallmann, A., Hanikenne, M., Hippler, M., Inwood, W., Jabbari, K., Kalanon, M., Kuras, R., Lefebvre, P.A., Lemaire, S.D., Lobanov, A.V., Lohr, M., Manuell, A., Meier, I., Mets, L., Mittag, M., Mittelmeier, T., Moroney, J.V., Moseley, J., Napoli, C., Nedelcu, A.M., Niyogi, K., Novoselov, S.V., Paulsen, I.T., Pazour, G., Purton, S., Ral, J.-P., Riano-Pachon, D.M., Riekhof, W., Rymarquis, L., Schroda, M., Stern, D., Umen, J., Willows, R., Wilson, N., Zimmer, S.L., Allmer, J., Balk, J., Bisova, K., Chen, C.-J., Elias, M., Gendler, K., Hauser, C., Lamb, M.R., Ledford, H., Long, J.C., Minagawa, J., Page, M.D., Pan, J., Pootakham, W., Roje, S., Rose, A., Stahlberg, E., Terauchi, A.M., Yang, P., Ball, S., Bowler, C., Dieckmann, C.L., Gladyshev, V.N., Green, P., Jorgensen, R., Mayfield, S., Mueller-Roeber, B., Rajamani, S., Sayre, R.T., Brokstein, P., Dubchak, I., Goodstein, D., Hornick, L., Huang, Y.W., Jhaveri, J., Luo, Y., Martinez, D., Ngau, W.C.A., Otillar, B., Poliakov, A., Porter, A., Szajkowski, L., Werner, G., Zhou, K., Grigoriev, I.V., Rokhsar, D.S., Grossman, A.R., 2007. The Chlamydomonas genome reveals the evolution of key animal and plant functions. Science 318, 245–250. https://doi.org/10.1126/science.1143609

Nachury, M.V., Loktev, A.V., Zhang, Q., Westlake, C.J., Peränen, J., Merdes, A., Slusarski, D.C., Scheller, R.H., Bazan, J.F., Sheffield, V.C., Jackson, P.K., 2007. A Core Complex of BBS Proteins Cooperates with the GTPase Rab8 to Promote Ciliary Membrane Biogenesis. Cell 129, 1201–1213. https://doi.org/10.1016/j.cell.2007.03.053

Nachury, M.V., Seeley, E.S., Jin, H., 2010. Trafficking to the ciliary membrane: how to get across the periciliary diffusion barrier? Annu. Rev. Cell Dev. Biol. 26, 59–87. https://doi.org/10.1146/annurev.cellbio.042308.113337

Ohara, A., Kato-Minoura, T., Kamiya, R., Hirono, M., 1998. Recovery of flagellar inner-arm dynein and the fertilization tubule in Chlamydomonas ida5 mutant by transformation with actin genes. Cell Struct. Funct. 23, 273–281. https://doi.org/10.1247/csf.23.273

Onishi, M., Pecani, K., Jones, T., Pringle, J.R., Cross, F.R., 2018. F-actin homeostasis through transcriptional regulation and proteasome-mediated proteolysis. Proc. Natl. Acad. Sci. 115, E6487. https://doi.org/10.1073/pnas.1721935115

Onishi, M., Pringle, J.R., Cross, F.R., 2016. Evidence That an Unconventional Actin Can Provide Essential F-Actin Function and That a Surveillance System Monitors F-Actin Integrity in Chlamydomonas. Genetics 202, 977–96. https://doi.org/10.1534/genetics.115.184663

Onishi, M., Umen, J.G., Cross, F.R., Pringle, J.R., 2019. Cleavage-furrow formation without F-actin in Chlamydomonas. bioRxiv 789016. https://doi.org/10.1101/789016

Osterman, N., Vilfan, A., 2011. Finding the ciliary beating pattern with optimal efficiency. Proc. Natl. Acad. Sci. 108, 15727–15732.

Pazour, G.J., Dickert, B.L., Vucica, Y., Seeley, E.S., Rosenbaum, J.L., Witman, G.B., Cole, D.G., 2000. Chlamydomonas IFT88 and its mouse homologue, polycystic kidney disease gene tg737, are required for assembly of cilia and flagella. J. Cell Biol. 151, 709–718. https://doi.org/10.1083/jcb.151.3.709

Pazour, G.J., Dickert, B.L., Witman, G.B., 1999. The DHC1b (DHC2) isoform of cytoplasmic dynein is required for flagellar assembly. J. Cell Biol. 144, 473–481. https://doi.org/10.1083/jcb.144.3.473

Pazour, G.J., Wilkerson, C.G., Witman, G.B., 1998. A dynein light chain is essential for the retrograde particle movement of intraflagellar transport (IFT). J. Cell Biol. 141, 979–992. https://doi.org/10.1083/jcb.141.4.979

Pazour, G.J., Witman, G.B., 2009. Chapter 15 - The Chlamydomonas Flagellum as a Model for Human Ciliary Disease, in: Harris, E.H., Stern, D.B., Witman, G.B. (Eds.), The Chlamydomonas Sourcebook (Second Edition). Academic Press, London, pp. 445–478. https://doi.org/10.1016/B978-0-12-370873-1.00052-6

Pedersen, L.B., Veland, I.R., Schrøder, J.M., Christensen, S.T., 2008. Assembly of primary cilia. Dev. Dyn. 237, 1993–2006. https://doi.org/10.1002/dvdy.21521

Piperno, G., Siuda, E., Henderson, S., Segil, M., Vaananen, H., Sassaroli, M., 1998. Distinct mutants of retrograde intraflagellar transport (IFT) share similar morphological and molecular defects. J. Cell Biol. 143, 1591–1601. https://doi.org/10.1083/jcb.143.6.1591

Pollard, T.D., 2016. Actin and Actin-Binding Proteins. Cold Spring Harb Perspect Biol 8. https://doi.org/10.1101/cshperspect.a018226

Porter, M.E., Bower, R., Knott, J.A., Byrd, P., Dentler, W., 1999. Cytoplasmic dynein heavy chain 1b is required for flagellar assembly in Chlamydomonas. Mol. Biol. Cell 10, 693–712. https://doi.org/10.1091/mbc.10.3.693

Reichelt, S., Knight, A.E., Hodge, T.P., Baluska, F., Samaj, J., Volkmann, D., Kendrick-Jones, J., 1999. Characterization of the unconventional myosin VIII in plant cells and its localization at the post-cytokinetic cell wall. Plant J. 19, 555–567. https://doi.org/10.1046/j.1365-313X.1999.00553.x

Reiter, J.F., Leroux, M.R., 2017. Genes and molecular pathways underpinning ciliopathies. Nat. Rev. Mol. Cell Biol. 18, 533–547. https://doi.org/10.1038/nrm.2017.60

Reiter, J.F., Mostov, K., 2006. Vesicle transport, cilium formation, and membrane specialization: The origins of a sensory organelle. Proc. Natl. Acad. Sci. 103, 18383. https://doi.org/10.1073/pnas.0609324103

Rohatgi, R., Snell, W.J., 2010. The ciliary membrane. Curr. Opin. Cell Biol. 22, 541–546. https://doi.org/10.1016/j.ceb.2010.03.010

Rosenbaum, J.L., Child, F.M., 1967. Flagellar regeneration in protozoan flagellates. J. Cell Biol. 34, 345–364. https://doi.org/10.1083/jcb.34.1.345

Rosenbaum, J.L., Moulder, J.E., Ringo, D.L., 1969. Flagellar elongation and shortening in Chlamydomonas. The use of cycloheximide and colchicine to study the synthesis and assembly of flagellar proteins. J. Cell Biol. 41, 600–619. https://doi.org/10.1083/jcb.41.2.600

Sattarzadeh, A., Franzen, R., Schmelzer, E., 2008. The Arabidopsis class VIII myosin ATM2 is involved in endocytosis. Cell Motil. Cytoskeleton 65, 457–468. https://doi.org/10.1002/cm.20271

Schott, D.H., Collins, R.N., Bretscher, A., 2002. Secretory vesicle transport velocity in living cells depends on the myosin-V lever arm length. J. Cell Biol. 156, 35–40. https://doi.org/10.1083/jcb.200110086

Snell, W.J., Goodenough, U.W., 2009. Chapter 12 - Flagellar Adhesion, Flagellar-Generated Signaling, and Gamete Fusion during Mating, in: Harris, E.H., Stern, D.B., Witman, G.B. (Eds.), The Chlamydomonas Sourcebook (Second Edition). Academic Press, London, pp. 369–394. https://doi.org/10.1016/B978-0-12-370873-1.00049-6

Sorokin, S.P., 1968. Reconstructions of centriole formation and ciliogenesis in mammalian lungs. J. Cell Sci. 3, 207–230.

Tam, D., Hosoi, A., 2011. Optimal feeding and swimming gaits of biflagellated organisms. Proc. Natl. Acad. Sci. 108, 1001–1006.

Volkmann, D., Mori, T., Tirlapur, U.K., König, K., Fujiwara, T., Kendrick-Jones, J., Baluska, F., 2003. Unconventional myosins of the plant-specific class VIII: endocytosis, cytokinesis, plasmodesmata/pit-fields, and cell-to-cell coupling. Cell Biol. Int. 27, 289–291. https://doi.org/10.1016/s1065-6995(02)00330-x

Walther, Z., Vashishtha, M., Hall, J.L., 1994. The Chlamydomonas FLA10 gene encodes a novel kinesin-homologous protein. J. Cell Biol. 126, 175–188. https://doi.org/10.1083/jcb.126.1.175

Wood, C.R., Rosenbaum, J.L., 2014. Proteins of the Ciliary Axoneme Are Found on Cytoplasmic Membrane Vesicles during Growth of Cilia. Curr. Biol. 24, 1114–1120. https://doi.org/10.1016/j.cub.2014.03.047

Wu, C.-T., Chen, H.-Y., Tang, T.K., 2018. Myosin-Va is required for preciliary vesicle transportation to the mother centriole during ciliogenesis. Nat. Cell Biol. 20, 175–185. https://doi.org/10.1038/s41556-017-0018-7

CHAPTER 2:

The Arp2/3 complex of *Chlamydomonas reinhardtii* interacts with both the conventional and the divergent actin

This chapter has not been published but will be posted on BioRxiv. This work was a collaboration with David Sept and Courtney Schroeder.

ABSTRACT

The unicellular green algae *Chlamydomonas reinhardtii* has been used for years to study the microtubule-based cilium, which is used to sense the environment and to move. However, the organism could also be useful for the study of the actin cytoskeleton because *Chlamydomonas* has 2 actin genes: *IDA5*, a conventional actin which shares 91% of its sequence with human actin, and *NAP1*, a divergent actin that shares only 63% of its sequence with human actin and is only present in a handful of organisms. Here, we look at a single actin binding protein, the Arp2/3 complex, which helps create actin networks for specific functions .We chose this protein because a comparison between the conventional IDA5 and the divergent NAP1 shows a large amount of variation in the region expected to bind the Arp2/3 complex. We hypothesized that the Arp2/3 complex would interact with IDA5 but not NAP1. Instead, we found that the Arp2/3 complex mediates both IDA5 and NAP1 networks to form actin-dependent structures and carry out actin-dependent functions despite the divergence of the secondary actin. This suggests that there is promiscuity of actin binding proteins that may affect their ability to tolerate mutations or modifications, their sorting within the cell, and their competition with other actin binding proteins.

INTRODUCTION

The actin cytoskeleton of Chlamydomonas has two actin genes. The first, IDA5 (inner dynein arm 5), is a conventional actin that shares over 90% of its peptide sequence with human ß-actin (Hirono et al., 2003; Kato-Minoura et al., 1998). The second actin gene, NAP1 (novel actin-like protein 1), is a more divergent actin that shares only 63% of its peptide sequence with human ß-actin (Hirono et al., 2003; Kato-Minoura et al., 1998) (**Fig. 2.1**). However, NAP1 is considered to be an actin-like protein because it is able to polymerize, it is more similar to actin than it is to actin related proteins, and it is able to compensate for the conventional IDA5 (Jack et al., 2019; Kato-Minoura, 2011; Onishi et al., 2016; M. Onishi et al., 2018). The presence of both a conventional and a divergent actin allow us to ask questions about actin divergence while directly comparing to a more conventional actin.

Despite these promising features, Chlamydomonas has not been traditionally used as a model to study the actin cytoskeleton. For years, people were unconvinced of the utility of studying actin in this organism for two reasons: it was difficult to visualize, and it really did not seem to be playing many important roles in the cell. This is because null mutants of the primary actin IDA5 had very few phenotypes, showing only a mild swimming defect (Kato et al., 1993, p. 5; Kato-Minoura et al., 1997, p. 5; Ohara et al., 1998, p. 5), a relatively mild ciliary assembly defect (Avasthi et al., 2014), and defects in fertilization tubule assembly (Detmers et al., 1983; Ohara et al., 1998). However, recent work using a new nap1 mutant strain has found that this is because the divergent actin NAP1 is able to functionally compensate for the loss of the conventional actin (Jack et al., 2019; Onishi et al., 2016), suggesting that the two actins are capable of interacting with common actin regulators. The convergence of these discoveries about the functional overlap of the two actins and the development of new technology for visualization of this protein by our lab (Craig et al., 2019; Craig and Avasthi, 2019) have made way for Chlamydomonas to begin emerging as an ideal system for studies of the actin cytoskeleton.

One important characteristic of the Chlamydomonas actins is that their functions are separable. The conventional IDA5 is primary actin expressed in vegetative cells, but treatment with Latrunculin B (LatB) results in depolymerization of all filamentous IDA5.

Meanwhile, the divergent NAP1, normally expressed at negligible levels, is insensitive to LatB and is in fact upregulated during LatB treatment (Hirono et al., 2003; Onishi et al., 2016; M. Onishi et al., 2018). Additionally, genetic mutants of both IDA5 and NAP1 exist to allow for further dissection of the actin network (Kato-Minoura et al., 1998, p. 1, 1997, p. 1; Onishi et al., 2016, p. 1). Altogether, this makes Chlamydomonas uniquely situated to answer some long-standing questions about the actin cytoskeleton.

Here, we harness the divergent and unusual aspects of Chlamydomonas biology to ask questions about the actin cytoskeleton. The two actin genes of this organism allow us to make hypotheses about the capabilities of actin binding proteins. We specifically ask whether the Arp2/3 complex can interact with both a conventional and a divergent actin. We find that despite a large amount of sequence variance in the Arp2/3 binding site of the divergent actin, the Arp2/3 complex can mediate actin networks to fulfil actin functions in the cell and to form actin structures. Through these findings, we contribute to our basic understanding of the interactions between actin and its binding partners and how those interactions function within the cell.

RESULTS

The regions of IDA5 and NAP1 that bind the Arp2/3 complex are not well-conserved:

Previous work from our lab began to characterize the Arp2/3 complex of *Chlamydomonas reinhardtii* (Bigge et al., 2020). The complex, which is typically seven-membered, contains almost all subunits, which have varying degrees of importance in the function of the complex and have varying sequence conservation between mammalian and *Chlamydomonas* cells. *Chlamydomonas* ARPC2 and ARPC4, which form the complex core, are 29.1% and 68% similar to mammalian subunits respectively; Arp2 and Arp3, which serve as the first subunits of the new filament, are 75.1% and 61.5% similar to mammalian subunits respectively; and ARPC1 and ARPC3, which play a role in nucleation regulation, are 44.1% and 52.6% similar to mammalian subunits respectively (Bigge et al., 2020; Gournier et al., 2001; Robinson et al., 2001). The only potentially missing subunit is ARPC5, though a very divergent ARCP5 could exist and Arp2/3 complexes lacking an ARPC5 subunit are still able to create branches (Gournier et al., 2001). However, work from our lab has established that the Arp2/3 complex is able to function to maintain ciliary length and assembly, aid in the formation of actin structures, and likely participate in endocytosis (Bigge et al., 2020). This leads us to questions regarding the interaction between the Arp2/3 complex and the actin cytoskeleton in this organism.

As mentioned previously, the actin cytoskeleton of *Chlamydomonas* has 2 very different actins genes: *IDA5*, a conventional actin, and *NAP1*, a divergent actin (Hirono et al., 2003; Kato-Minoura et al., 1998; Onishi et al., 2016). The region of actin on the mother filament that binds ARPC2 and ARPC4 (Goley et al., 2010), the core of the Arp2/3 complex, is well-conserved in IDA5 (**Fig. 2.1A-B**). However, this region in NAP1 is quite divergent with only 43% of the 30 residues thought to bind ARPC2 and ARPC4 conserved in NAP1 (**Fig. 2.1A-B**). Thus, we hypothesize that the Arp2/3 complex can interact with IDA5 normally but not with NAP1.

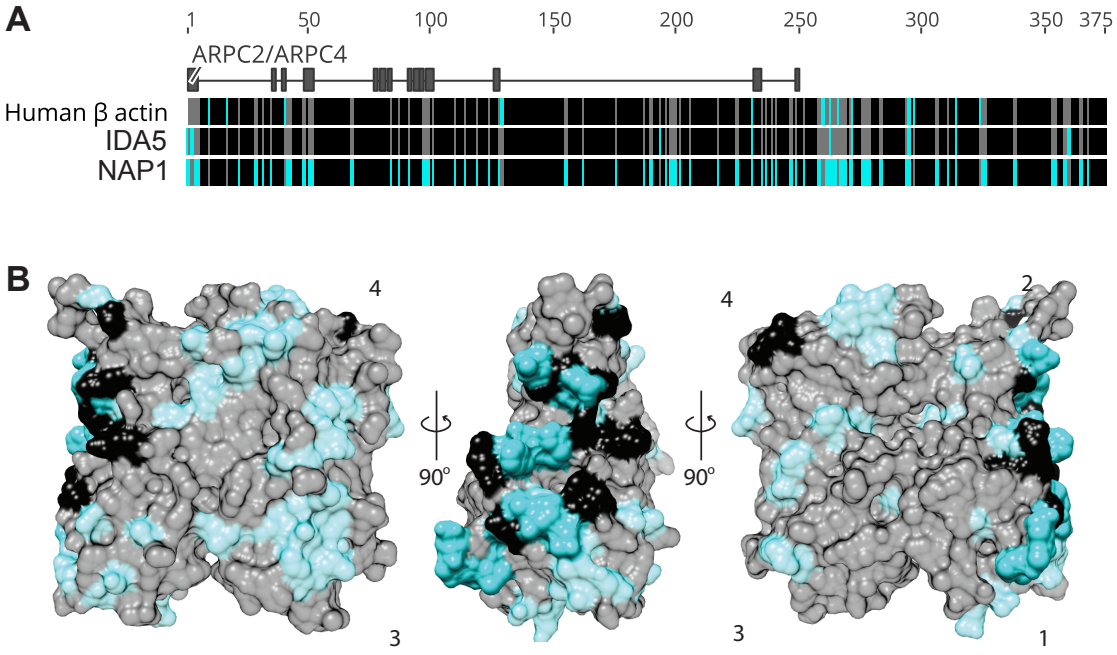

Fig. 2.1. The ARPC2/ARPC4 binding region of NAP1 is not well-conserved. A) Conservation map based on the sequence alignment between IDA5, NAP1, and human actin generated in Geneious using MUSCLE alignment. Black residues are conserved, grey residues are similar, and cyan residues are divergent. The regions of actin that bind ARPC2/ARPC4 are annotated above the alignment, with grey bars connected by lines. 43% of residues that interact with Arp2/3 are conserved in NAP1. The full alignment containing IDA5 and NAP1 with human actin and actin related proteins can be found in Supplemental Fig. 1. **B)** Homology model of IDA5 based on the structure PDB 2ZWH with conservation of NAP1 mapped on the surface. Grey (transparent) residues are conserved between IDA5 and NAP1, while cyan residues are divergent. The darker cyan and black regions (non-transparent) interact with ARPC2/ARPC3, while the more transparent regions do not.

The Arp2/3 complex can mediate networks of IDA5 and NAP1 to form actin structures:

We first wondered whether the Arp2/3 complex could regulate the formation of actin structures specific to either IDA5 or NAP1. Under normal conditions, IDA5, the conventional actin, is the primary actin expressed with NAP1 being expressed at negligible levels (Onishi et al., 2018). When IDA5 is the primary actin expressed, we see two main actin structures: a mid-cell actin network and apical actin dots (**Fig. 2.2A and A'**). To determine if the Arp2/3 complex is involved in regulating networks composed of the conventional IDA5, we looked at these two filamentous actin structures in wild-type cells and in *arpc4* mutant cells that are lacking a functional Arp2/3 complex. Using a phalloidin staining protocol optimized for *Chlamydomonas* (Craig et al., 2019; Craig and Avasthi, 2019), we found that the *arpc4* mutant cells have a quite different filamentous actin distribution compared to wild-type cells.

The *arpc4* mutant cells have a more condensed actin distribution in the middle of the cell with occasional bundles leading toward the base of the cilium (**Fig. 2.2B-B'**). This was quantified two ways. First, line scans were taken through each cell from the apex between cilia to the farthest point on the basal surface (**Fig. 2.2C-D**). Line scans show increased consistency and a more condensed nature of the actin signal in the arpc4 mutants (**Fig. 2.2C-D**). We further quantified this by fitting each line scan with a curve and uniformly measuring the width of the curves at half the maximum to show the width of the signal in the apical to basal plane (**Fig. 2.2E**). This quantification shows that the *arpc4* mutants do indeed have a more condensed mid-cell actin in the axis measured (**Fig. 2.2F**). We also quantified the ratio of the mid-cell actin area to the total cell area to determine if the actin signal of the *arpc4* mutant cells was more compact in all planes (**Fig. 2.2G-H**). Mid-cell actin area was determined by uniformly thresholding all images so that only the actin signal in the mid-cell is visible. This quantification confirms *arpc4* mutant cells have a more compact mid-cell actin structure (**Fig. 2.2H**). Furthermore, the actual intensity of the signal was found to be increased in the *arpc4* mutant cells (**Fig. 2.2I**), while the fluorescence of the total cell, which was corrected for background fluorescence, is increased in the wild-type cells (**Fig. 2.2J**).

Besides the actin signal seen in the mid-cell region of wild-type cells, apical dots are also typically seen near the base of cilia (**Fig. 2.2A**). Previous work from our lab established that the *arpc4* mutant cells have barely any dots compared to wild-type cells with about 75% of wild-type cells containing dots and less than 5% of *arpc4* mutant cells having dots (Bigge et al., 2020). These results suggest that the Arp2/3 complex is involved in regulation of both filamentous-IDA5 structures, the mid cell actin and the apical actin dots.

Next, we wanted to investigate whether the Arp2/3 complex could regulate a NAP1 structure. NAP1, which is normally expressed at negligible levels, is upregulated when cells are treated with Latrunculin B (LatB) (Craig et al., 2019; Onishi et al., 2018, 2016). LatB sequesters monomers eventually leading to depolymerization of conventional actin filaments, like IDA5 (Spector et al., 1989). During the period following LatB treatment, when IDA5 is depolymerized and NAP1 is upregulated, a ring or cage of filamentous actin forms around the nucleus (**Fig. 2.2K**) (Craig et al., 2019). This structure is likely composed of NAP1 as it forms when IDA5 is depolymerized and NAP1 is upregulated. Additionally, previous work shows that this ring can form in *ida5* mutants when only NAP1 is present, but that it cannot form in *nap1* mutants when only IDA5 is present (Craig et al., 2019), lending further support to the idea that these rings are composed of NAP1. So, we questioned whether the Arp2/3 complex could regulate the formation of this NAP1 ring. While wild-type cells formed rings, the *arpc4* mutant did not form LatB-induced rings (**Fig. 2.2K**). Altogether, this suggests, that the Arp2/3 complex is involved in the formation of this NAP1 structure as well as for the formation of the IDA5 structures. This was confirmed using the chemical inhibitor CK-666, as simultaneous treatment with CK-666 and LatB resulted in significantly reduced ring formation (**Fig. 2.2L**).

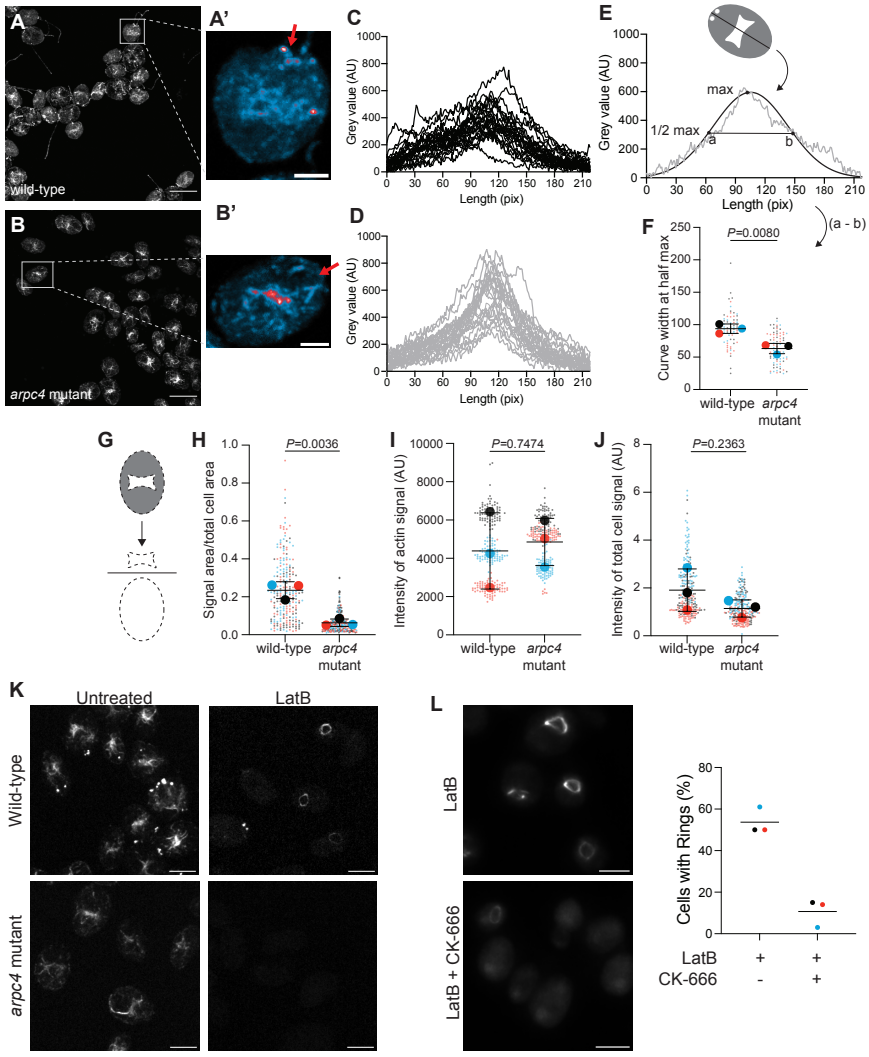

Fig. 2.2. Loss of a functional Arp2/3 complex results in changes in actin distribution. A-B) Wild-type (A) and *arpc4* mutant cells (B) stained with phalloidin. Images were taken as a z-stack and are shown as a maximum intensity projection. Scale bar represents 10µm. **A'-B'** shows the mid-cell actin network of the wild-type cells (A') or *arpc4* mutant cells (B'). Red arrow is pointing to the apex of the cell. Scale bar represents 2µm. **C-D)** For wild-type cells (C) and *arpc4* mutant cells (D), line scans were taken through the cell from apical to basal. Background was subtracted and the length was normalized, then each line scan was plotted. n=25 for 3 separate experiments. **E)** Example of a line scan (grey) and fitted Gaussian curve (black) showing how to calculate the full width at half max shown in F. **F)** The full width at half max shown with a superplot using 3 separate biological replicates where n=25. Large dots show the mean for each replicate. Mean and standard deviation of the means are represented by line and error bars. P value found using a two-tailed t-test. **G)** Diagram showing how the mid-cell actin/total cell signal was calculated. **H)** The ratio of mid-cell actin to total cell signal shown with a superplot where each large dot is the mean of 1 of 3 separate biological replicates where n=75. Large dots show the mean for each replicate. Mean and standard deviation of the 3 means are represented by line and error bars. P value found using a two-tailed t-test. **I)** The background-subtracted intensity of the mid-cell actin networks shown with a superplot where each large dot represents a mean from 1 of 3 separate biological replicates where n-75. Large dots show the mean for each replicate. Mean and standard deviation of the 3 means are represented by line and error bars. P value found using a two-tailed t-test. **J)** Corrected total cell fluorescence shown with a superplot where large dots represent the means from each of 3 biological replicates where n=75. Large dots show the mean for each replicate. Mean and standard deviation of the 3 means are represented by line and error bars. P value found using a two-tailed t-test. **K)** Wild-type and *arpc4* mutant cells were treated with 10 μM LatB for 3 hours to induce rings. Scale bar represents 5 μm. **L)** Wild-type cells were treated with 10 μM LatB to induce ring formation. One sample was simultaneously treated with 100 μM CK-666 to block Arp2/3 complex function. Cells treated with both CK-666 and LatB formed significantly less rings (P<0.0001) as determined by Chi-square analysis.

The Arp2/3 complex can mediate networks of IDA5 and NAP1 to maintain ciliary length:

Despite the sequence divergence, previous work from our lab has found that the two actins function redundantly in ciliary assembly (Jack et al., 2019). This led us to question whether the two actins could interact with the Arp2/3 complex for actin-dependent ciliary maintenance and assembly functions. We answer this question using the *nap1* null mutant that only contains IDA5 and the *ida5* null mutant that only contains NAP1 (Kato et al., 1993; Kato-Minoura et al., 1997; Onishi et al., 2016). In this assay, cells are treated with an inhibitor, and because intact actin filaments are required to maintain cilia, the ciliary length can be used as a readout of actin network integrity. This is illustrated in the case of LatB originally shown in Avasthi et al., 2014 and confirmed here. When wild-type cells containing both IDA5 and NAP1 are treated with LatB, cilia shorten but can restore their length. This is because NAP1 is upregulated and resistant to LatB, and therefore, can compensate for the lost IDA5 (Onishi et al., 2016). When *nap1* mutant cells containing only IDA5 are treated with LatB, cilia shorten because NAP1 is not present to compensate for depolymerized IDA5. When *ida5* cells containing only NAP1 are treated with LatB, there is no effect as NAP1 is insensitive to LatB (**Fig. 2.3A**).

We modified this assay by treating wild-type cells, *nap1* mutants, and *ida5* mutants with the Arp2/3 complex inhibitor CK-666, which binds at the interface between Arp2 and Arp3 and prevents a confirmational change that is required for nucleation, or the inactive CK-689 (Hetrick et al., 2013). Unlike what was seen with LatB, which affects NAP1 and IDA5 differently, we found that in all three strains, cilia of cells treated with CK-666 shorten. Thus, inhibiting the Arp2/3 complex affects cells that express either actin alone (**Fig. 2.3B**), suggesting the Arp2/3 complex may interact with both IDA5 and NAP1 to maintain ciliary length despite the sequence divergence of NAP1 in the Arp2/3 complex binding region.

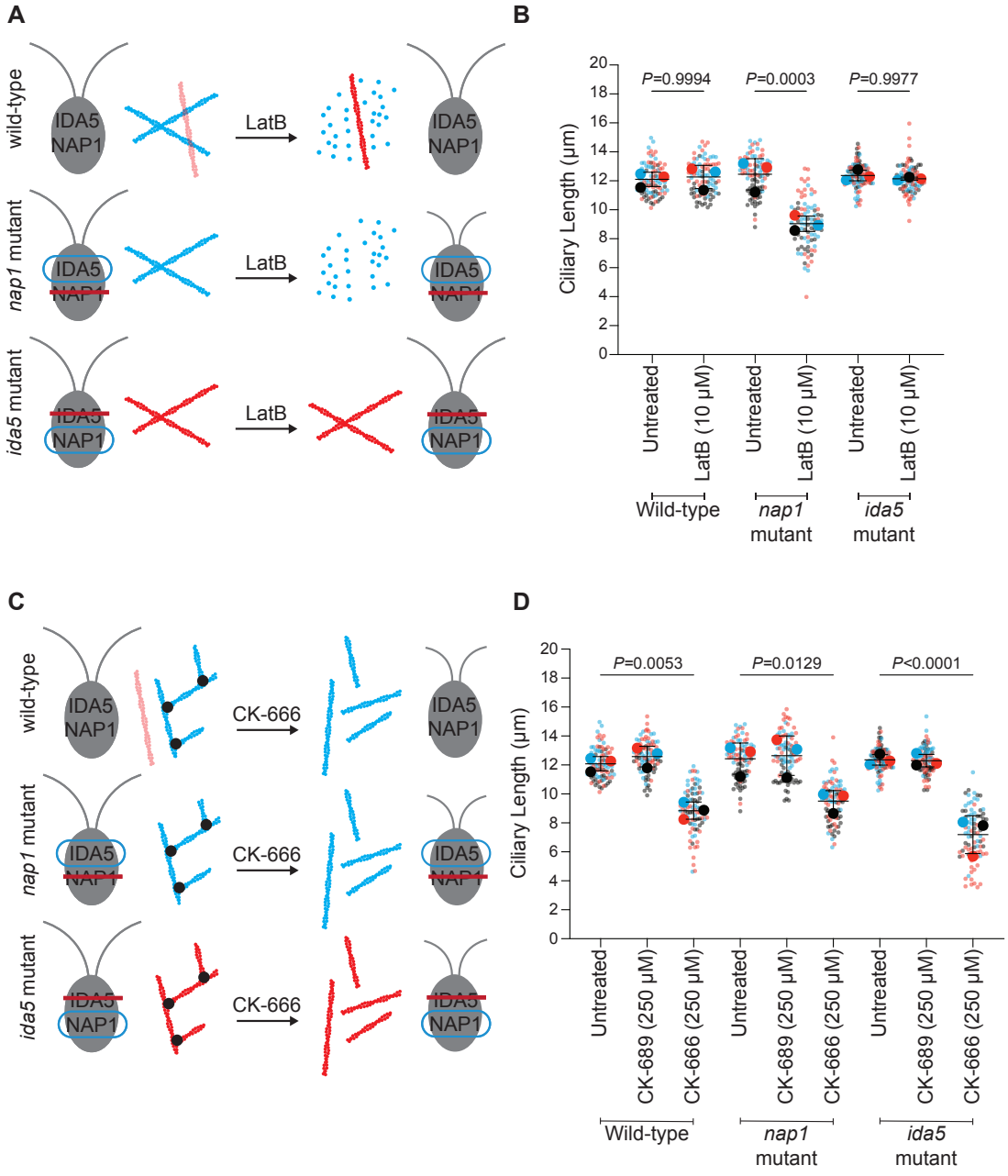

Fig. 2.3. The Arp2/3 complex mediates networks of both IDA5 and NAP1 for ciliary length maintenance. A) Diagram of experiment in B. **B)** Wild-type cells, *nap1* mutant cells, and *ida5* mutant cells were treated with LatB for 2 hours and then cilia were measured. Superplot shows the ciliary lengths from 3 separate biological replicates where n=30 in each replicate. Large dots show the means from each replicate, small dots represent individual points. The mean and standard deviation of the means from each replicate are shown as the line and error bars. P values determined with one-way ANOVA and Tukey's multiple comparisons analysis. **C)** Diagram of experiment in D. **D)** Wild-type, *nap1* mutant cells, and *ida5* mutant cells were treated with either CK-666 or the inactive CK-689 for 2 hours and then cilia were measured. Superplot shows the ciliary lengths from 3 separate biological replicates where n=30 in each replicate. Large dots show the means from each replicate, small dots represent individual points. The mean and standard deviation of the means from each replicate are shown as the line and error bars. P values determined with one-way ANOVA and Tukey's multiple comparisons analysis.

DISCUSSION

Here, we leverage the unique actin cytoskeleton of *Chlamydomonas* to answer questions about the interactions of actin binding proteins with actins of varying sequence divergence. Stepping outside the traditional systems allowed us to broaden our understanding of the functions and abilities of the Arp2/3 complex. We find that despite a large amount of sequence variance in the region of NAP1 that is expected to bind the Arp2/3 complex, the Arp2/3 complex is still able to mediate networks of NAP1 to carry out actin-dependent functions and to form actin structures. This is evidenced through functional studies of IDA5 and NAP1 in the absence of Arp2/3 complex function (**Fig. 2.2-3**).

It is also possible that the divergence of the *Chlamydomonas* Arp2/3 complex and the nucleating machinery itself helps overcome the sequence differences between IDA5 and NAP1. The conventional Arp2/3 complex is a seven membered complex containing Arp2, Arp3, and ARPC1-5. We have identified the more important subunits Arp2, Arp3, and ARPC1-4 in *Chlamydomonas,* but have not yet found an ARPC5 subunit, which is thought to mediate the association of ARPC1 with the complex but whose absence does not fully prevent nucleation or cross-linking. This could mean that the *Chlamydomonas* Arp2/3 complex is six-membered, but it could also mean that the ARPC5 subunit is so highly divergent that it is not able to be found with typical sequence searches. These could be discriminated between by doing a pulldown of the full Arp2/3 complex, which could yield a potential ARPC5 subunit. Of the subunits that do exist in *Chlamydomonas,* the similarity to mammalian subunits varies quite a bit with Arp2 (75.1% sequence similarity, 55.7% sequence identity), Arp3 (61.5% similarity, 45.7% identity), and ARPC4 (68% similarity, 50% identity) being more highly conserved, while ARPC1 (44.1% similarity, 28.9% identity), ARPC2 (29.1% similarity, 16.7% identity), and ARPC3 (52.6% similarity, 29.4% identity) are less conserved (Bigge et al., 2020). This divergence could account for the ability of *Chlamydomonas* Arp2/3 complex to bind the divergent NAP1.

The Arp2/3 complex of *Chlamydomonas* could have undergone co-evolution with actin in order to be able to ineract with both IDA5 and NAP1. To test this hypothesis, we aligned the ARPC4 protein from mammalian cells, from *Chlamydomonas,* and from a

close relative of *Chlamdyomonas* that does not contain NAP1, *Coccomyxa* **(Fig. 2.4**). Overall, *Coccomyxa* ARPC4 seems to be less conserved than *Chlamydomonas* ARPC4 (**Fig. 2.4**). However, the local regions expected to bind the mother filament might be more conserved in *Coccomyxa* **(Fig. 2.4).** Additional work would need to be done to further test this hypothesis.

We also cannot claim based on this work that the Arp2/3 complex of this organism is nucleating branched or dendritic actin networks, especially considering the divergence of the Arp2/3 complex, though this would be an interesting future direction. Further, the Arp2/3 complex conventionally acts by binding to the side of an existing filament or mother filament and nucleating a new daughter filament off the side of that mother filament with the help of a nucleation promoting factor. Interestingly, most of the conventional nucleation promoting factors found throughout eukaryotes have not yet been identified in this organism. However, other work from our lab has identified roles for the Arp2/3 complex in ciliary assembly and length regulation, in the formation of actin structures, and in a potential endocytic mechanism in *Chlamydomonas,* suggesting that this divergent system is functioning in some capacity (Bigge et al., 2020; Bigge and Avasthi, 2022).

Another interesting future direction would be to investigate if these two actins are able to co-polymerize forming heterogenous filaments. The ability of the Arp2/3 complex to bind filaments of both IDA5 and NAP1 lead to questions about whether the Arp2/3 complex could cross-link filaments of IDA5 with filaments of NAP1. It would also be useful to learn if any other actin binding proteins might interact with one actin or the other.

Altogether, we find that this single actin nucleator, the Arp2/3 complex, can mediate networks of a conventional actin, IDA5, and a divergent actin, NAP1, suggesting that the actin nucleating ability of the Arp2/3 complex is quite robust. This work can contribute to our overall knowledge of actin biology and inform hypotheses regarding many characteristics of the actin cytoskeleton, including the promiscuity of actin binding proteins and their ability to tolerate mutations and the sorting of actin by actin binding proteins within the cell.

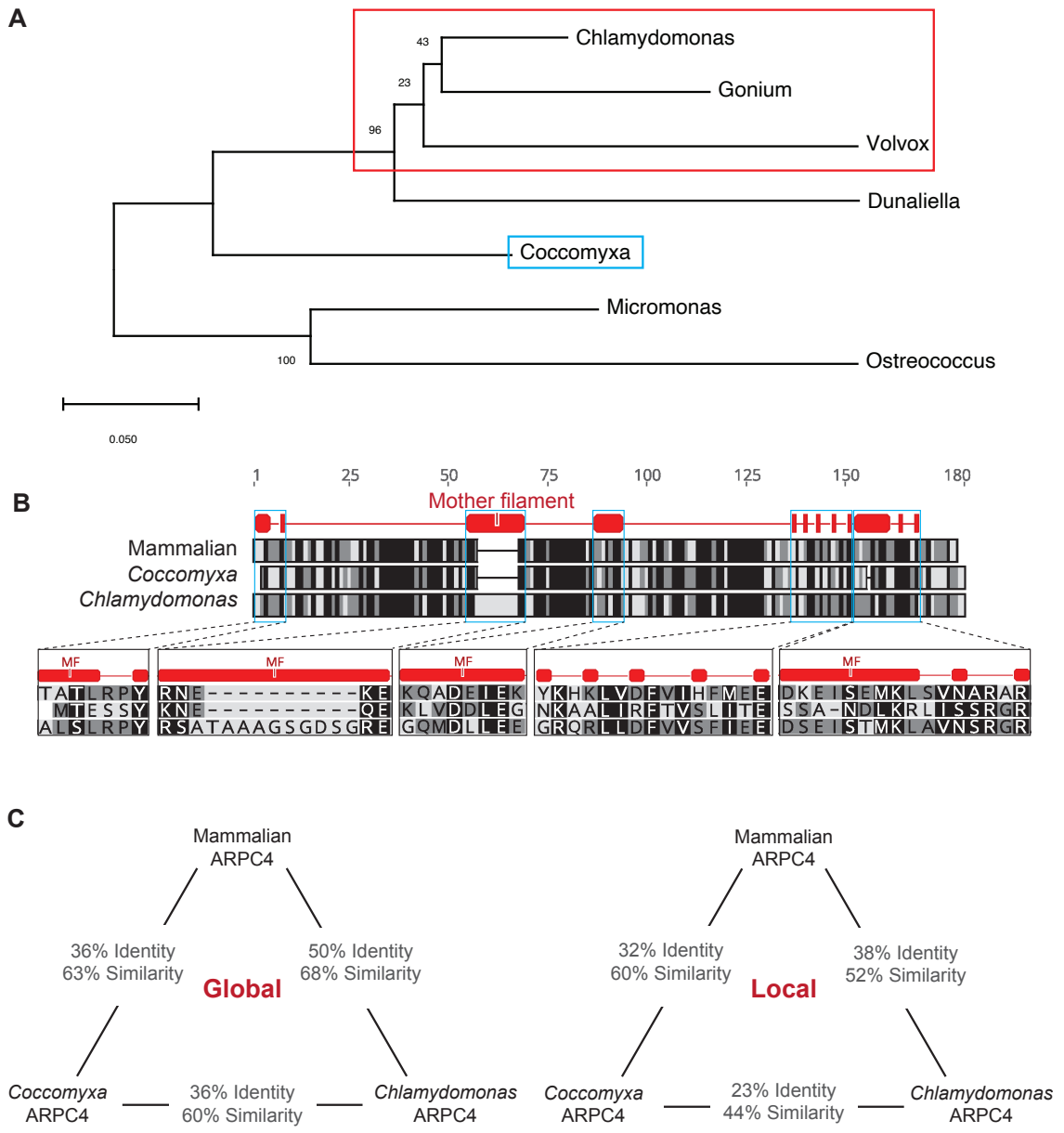

Fig. 2.4. ARPC4 conservation in *Chlamydomonas* neighbors lacking NAP1. A) Phylogenetic tree created in Geneious showing *Chlamydomonas* and its neighbors. The red box shows organisms that contain NAP1. *Coccomyxa* is boxed in cyan because it is used for the following comparisons. **B)** Alignment of mammalian (bovine) ARPC4, *Coccomyxa* ARPC4, and *Chlamydomonas* ARPC4 protein sequences. Black residues are conserved, medium grey residues are similar, and light grey residues are divergent. The regions below show zoomed in versions of the regions of the ARPC4 protein sequences thought to bind the mother filament. **C)** Diagram showing similarity and identity between the ARPC4 proteins from the three organisms. Global refers to the entire protein sequence, while local refers just to the regions that are thought to bind the mother filament (MF).

MATERIALS AND METHODS

Strains:

The wild-type *Chlamydomonas* strain (CC-5325) and the *ida5* mutant (CC-3420). The *arpc4* mutant was obtained from the *Chlamydomonas* mutant library (Cheng et al., 2017; Li et al., 2019) and was previously characterized in depth (Bigge et al., 2020). The *nap1* mutant was a gift from Fred Cross, Masayuki Onishi, and John Pringle. 1.5% Tris-Acetate Phosphate Agar (TAP) plates were used to grow and maintain strains. Liquid TAP media was used to grow cultures for experiments under constant blue (450- 475 nm) and red light (625-660 nm) and with agitation. Typically liquid cultures were allowed to incubate overnight before experiments.

Homology modeling and sequence studies:

Arp2/3 homology model was created using the Modeller plugin in UCSF Chimera. The template used was 1U2Z (Nolen et al., 2004; Pettersen et al., 2004; Sali and Blundell, 1993). Percent identity and similarity is calculated in relation to the human Arp2/3 complex members. Conservation map of the Chlamydomonas actins is based on the sequence alignment between IDA5, NAP1, and human actin generated in Geneious using MUSCLE. The regions of actin that bind ARPC2/ARPC4 were determined previously (Goley et al., 2010). Swiss-model was used to generate a homology model of IDA5 based on the structure PDB 2ZWH (Oda et al., 2009; Waterhouse et al., 2018). The homology model was visualized, and conservation was mapped on the protein surface using Chimera (Pettersen et al., 2004).

Ciliary studies:

Cells treated with drugs (either 250 μM CK-666, 250 μM CK-689, or 10 μM LatB) were incubated with constant agitation and under light for 2 hours. Samples were diluted to a final concentration of 1% glutaraldehyde after the specified time period and incubated at 4 degrees to allow cells to settle. Samples of settled cells were then imaged using a Zeiss Axioscope 5 DIC microscope with a 40X objective (0.75 numerical aperture). In ImageJ, ciliary length was quantified. One cilium per cell was measured using the segmented line

and fit spline function. Generally, 30 cilia were measured per sample unless otherwise specified.

Phalloidin staining and quantification:

Procedure adapted from Craig and Avasthi, 2019. Cells from each sample were adhered to poly-lysine coated coverslips and then fixed with fresh 4% paraformaldehyde in 1X HEPES in PBS. Samples were permeabilized with 80% acetone followed by 100% acetone and allowed to dry fully. Samples were rehydrated with PBS, stained with atto-phalloidin-488, and finally washed with PBS again and allowed to dry before mounting with Fluoromount-G. Cells were then imaged using a Nikon Eclipse Ti-E microscope with a Yokogawa, two-camera, CSU0W1 spinning disk system with a Nikon LU-N4 laser launch at room temperature with a 100X oil-immersion objective (1.45 numerical aperture). Images were acquired using Nikon Elements as z-stacks and analyzed using ImageJ as follows.

Z-stacks were obtained, and in ImageJ, sum projections were created for quantification purposes, while maximum intensity projections were created for viewing. Using sum slices in ImageJ, lines were drawn for line scans from the apex of the cell between cilia to furthest away basal position. Line scans were then normalized to each other, and background was subtracted. A gaussian curve was fit to each scan for full width at half max quantification. Next, images in ImageJ were thresholded to the point to where either the whole cell was visible or just the mid-cell actin was visible. From these thresholded images, the area of the particle was obtained as well as the mean intensity and integrated density. The area of the mid-cell actin signal was divided by the area of the full cell to give a ratio. The mid-cell intensity was taken by using the mean signal and subtracting the background. The background corrected total cell fluorescence was calculated by taking the integrated density and subtracting the sum of the area and the background mean intensity.

ACKNOWLEDGEMENTS

Our most sincere gratitude to Masayuki Onishi for the *nap1* mutant, Ann Lavanway for assistance with microscopy, and the Avasthi lab for all their help throughout the project.

We also thank our funding sources including the Madison and Lila Self Graduate Fellowship at the University of Kansas Medical Center and the MIRA (R35GM128702). Finally, we thank the BioMT core at Dartmouth College (NIH/NIGMS COBRE award P20-GM113132), the Genomics and Molecular Biology Shared Resources Core (NCI Cancer Center Support Grant 5P30CA023108-37), and the KIDDRC NIH U54 HD 090216 at the University of Kansas Medical Center, Kansas City, KS 66160.

REFERENCES

Avasthi, P., Onishi, M., Karpiak, J., Yamamoto, R., Mackinder, L., Jonikas, M.C., Sale, W.S., Shoichet, B., Pringle, J.R., Marshall, W.F., 2014. Actin Is Required for IFT Regulation in Chlamydomonas reinhardtii. Curr. Biol. 24, 2025–2032. https://doi.org/10.1016/j.cub.2014.07.038

Bigge, B.M., Avasthi, P., 2022. Lithium-induced ciliary lengthening sparks Arp2/3 complex-dependent endocytosis. bioRxiv 2022.04.18.488674. https://doi.org/10.1101/2022.04.18.488674

Bigge, B.M., Rosenthal, N.E., Sept, D., Schroeder, C.M., Avasthi, P., 2020. Initial ciliary assembly in Chlamydomonas requires Arp2/3-dependent recruitment from a ciliary protein reservoir in the plasma membrane. bioRxiv 2020.11.24.396002. https://doi.org/10.1101/2020.11.24.396002

Campellone, K., Welch, M., 2010. A nucleator arms race: cellular control of actin assembly. Nat. Rev. Mol. Cell Biol. 11, 237–251.

Cheng, X., Liu, G., Ke, W., Zhao, L., Lv, B., Ma, X., Xu, N., Xia, X., Deng, X., Zheng, C., Huang, K., 2017. Building a multipurpose insertional mutant library for forward and reverse genetics in Chlamydomonas. Plant Methods 13, 36. https://doi.org/10.1186/s13007-017-0183-5

Craig, E.W., Avasthi, P., 2019. Visualizing Filamentous Actin Using Phalloidin in Chlamydomonas reinhardtii. Bio-Protoc. 9. https://doi.org/10.21769/BioProtoc.3274

Craig, E.W., Mueller, D.M., Bigge, B.M., Schaffer, M., Engel, B.D., Avasthi, P., 2019. The elusive actin cytoskeleton of a green alga expressing both conventional and divergent actins. Mol. Biol. Cell mbc.E19-03-0141. https://doi.org/10.1091/mbc.E19-03-0141

Detmers, P.A., Goodenough, U.W., Condeelis, J., 1983. Elongation of the fertilization tubule in Chlamydomonas: new observations on the core microfilaments and the effect of transient intracellular signals on their structural integrity. J. Cell Biol. 97, 522–532. https://doi.org/10.1083/jcb.97.2.522

Goley, E.D., Rammohan, A., Znameroski, E.A., Firat-Karalar, E.N., Sept, D., Welch, M.D., 2010. An actin-filament-binding interface on the Arp2/3 complex is critical for nucleation and branch stability. Proc. Natl. Acad. Sci. 107, 8159. https://doi.org/10.1073/pnas.0911668107

Goley, E.D., Welch, M.D., 2006. The ARP2/3 complex: an actin nucleator comes of age. Nat. Rev. Mol. Cell Biol. 7, 713–726. https://doi.org/10.1038/nrm2026

Gournier, H., Goley, E.D., Niederstrasser, H., Trinh, T., Welch, M.D., 2001. Reconstitution of Human Arp2/3 Complex Reveals Critical Roles of Individual Subunits in Complex Structure and Activity. Mol. Cell 8, 1041–1052. https://doi.org/10.1016/S1097-2765(01)00393-8

Hetrick, B., Han, M.S., Helgeson, L.A., Nolen, B.J., 2013. Small Molecules CK-666 and CK-869 Inhibit Actin-Related Protein 2/3 Complex by Blocking an Activating Conformational Change. Chem. Biol. 20, 701–712. https://doi.org/10.1016/j.chembiol.2013.03.019

Hirono, M., Uryu, S., Ohara, A., Kato-Minoura, T., Kamiya, R., 2003. Expression of conventional and unconventional actins in Chlamydomonas reinhardtii upon deflagellation and sexual adhesion. Eukaryot. Cell 2, 486–493. https://doi.org/10.1128/ec.2.3.486-493.2003

Jack, B., Mueller, D.M., Fee, A.C., Tetlow, A.L., Avasthi, P., 2019. Partially Redundant Actin Genes in Chlamydomonas Control Transition Zone Organization and Flagellum-Directed Traffic. Cell Rep. 27, 2459-2467.e3. https://doi.org/10.1016/j.celrep.2019.04.087

Kato, T., Kagami, O., Yagi, T., Kamiya, R., 1993. Isolation of two species of Chlamydomonas reinhardtii flagellar mutants, ida5 and ida6, that lack a newly identified heavy chain of the inner dynein arm. Cell Struct. Funct. 18, 371–377. https://doi.org/10.1247/csf.18.371

Kato-Minoura, T., 2011. Extremely low polymerizability of a highly-divergent Chlamydomonas actin (NAP). Biochem. Biophys. Res. Commun. 412, 723–727. https://doi.org/10.1016/j.bbrc.2011.08.040

Kato-Minoura, T., Hirono, M., Kamiya, R., 1997. Chlamydomonas Inner-Arm Dynein Mutant, ida5, Has a Mutation in an Actin-encoding Gene. J. Cell Biol. 137, 649–656. https://doi.org/10.1083/jcb.137.3.649

Kato-Minoura, T., Uryu, S., Hirono, M., Kamiya, R., 1998. Highly divergent actin expressed in a Chlamydomonas mutant lacking the conventional actin gene. Biochem. Biophys. Res. Commun. 251, 71–76. https://doi.org/10.1006/bbrc.1998.9373

Li, X., Patena, W., Fauser, F., Jinkerson, R.E., Saroussi, S., Meyer, M.T., Ivanova, N., Robertson, J.M., Yue, R., Zhang, R., Vilarrasa-Blasi, J., Wittkopp, T.M., Ramundo, S., Blum, S.R., Goh, A., Laudon, M., Srikumar, T., Lefebvre, P.A., Grossman, A.R., Jonikas, M.C., 2019. A genome-wide algal mutant library and functional screen identifies genes required for eukaryotic photosynthesis. Nat. Genet. 51, 627–635. https://doi.org/10.1038/s41588-019-0370-6

Nolen, B.J., Littlefield, R.S., Pollard, T.D., 2004. Crystal structures of actin-related protein 2/3 complex with bound ATP or ADP. Proc. Natl. Acad. Sci. U. S. A. 101, 15627. https://doi.org/10.1073/pnas.0407149101

Oda, T., Iwasa, M., Aihara, T., Maéda, Y., Narita, A., 2009. The nature of the globular- to fibrous-actin transition. Nature 457, 441–445. https://doi.org/10.1038/nature07685

Ohara, A., Kato-Minoura, T., Kamiya, R., Hirono, M., 1998. Recovery of flagellar inner-arm dynein and the fertilization tubule in Chlamydomonas ida5 mutant by transformation with actin genes. Cell Struct. Funct. 23, 273–281. https://doi.org/10.1247/csf.23.273

Onishi, M., Pecani, K., Jones, T. th, Pringle, J.R., Cross, F.R., 2018. F-actin homeostasis through transcriptional regulation and proteasome-mediated proteolysis. Proc Natl Acad Sci U A 115, E6487-e6496. https://doi.org/10.1073/pnas.1721935115

Onishi, M., Pringle, J.R., Cross, F.R., 2016. Evidence That an Unconventional Actin Can Provide Essential F-Actin Function and That a Surveillance System Monitors F-Actin

Integrity in Chlamydomonas. Genetics 202, 977–96. https://doi.org/10.1534/genetics.115.184663

Pettersen, E.F., Goddard, T.D., Huang, C.C., Couch, G.S., Greenblatt, D.M., Meng, E.C., Ferrin, T.E., 2004. UCSF Chimera--a visualization system for exploratory research and analysis. J. Comput. Chem. 25, 1605–1612. https://doi.org/10.1002/jcc.20084

Robinson, R.C., Turbedsky, K., Kaiser, D.A., Marchand, J.-B., Higgs, H.N., Choe, S., Pollard, T.D., 2001. Crystal Structure of Arp2/3 Complex. Science 294, 1679. https://doi.org/10.1126/science.1066333

Sali, A., Blundell, T.L., 1993. Comparative protein modelling by satisfaction of spatial restraints. J. Mol. Biol. 234, 779–815. https://doi.org/10.1006/jmbi.1993.1626

Spector, I., Shochet, N.R., Blasberger, D., Kashman, Y., 1989. Latrunculins—novel marine macrolides that disrupt microfilament organization and affect cell growth: I. Comparison with cytochalasin D. Cell Motil. 13, 127–144. https://doi.org/10.1002/cm.970130302

Waterhouse, A., Bertoni, M., Bienert, S., Studer, G., Tauriello, G., Gumienny, R., Heer, F.T., de Beer, T.A.P., Rempfer, C., Bordoli, L., Lepore, R., Schwede, T., 2018. SWISS-MODEL: homology modelling of protein structures and complexes. Nucleic Acids Res. 46, W296–W303. https://doi.org/10.1093/nar/gky427

CHAPTER 3:

Initial ciliary assembly in *Chlamydomonas* requires Arp2/3 complex-dependent endocytosis

Published as:

Initial ciliary assembly in *Chlamydomonas* requires Arp2/3 complex-dependent endocytosis

Brae M Bigge[1,2], Nicholas E Rosenthal[1,2], Prachee Avasthi[1,2]

[1]Biochemistry and Cell Biology Department, Geisel School of Medicine at Dartmouth College, Hanover, New Hampshire

[2]Anatomy and Cell Biology Department, University of Kansas Medical Center, Kansas City, Kansas

doi: https://doi.org/10.1101/2020.11.24.396002

SUMMARY

Using the ciliary model system *Chlamydomonas*, we find Arp2/3 complex-mediated endocytosis is needed to reclaim cell body plasma membrane for early ciliary assembly.

ABSTRACT

Ciliary assembly, trafficking, and regulation are dependent on microtubules, but the mechanisms of ciliary assembly also require the actin cytoskeleton. Here, we dissect subcellular roles of actin in ciliogenesis by focusing on actin networks nucleated by the Arp2/3 complex in the powerful ciliary model, *Chlamydomonas*. We find the Arp2/3 complex is required for the initial stages of ciliary assembly when protein and membrane are in high demand but cannot yet be supplied from the Golgi complex. We provide evidence for Arp2/3 complex-dependent endocytosis of ciliary proteins, an increase in endocytic activity upon induction of ciliary growth, and relocalization of plasma membrane proteins to newly formed cilia. Our data support a new model of ciliary protein and membrane trafficking during early ciliogenesis whereby proteins previously targeted to the plasma membrane are reclaimed by Arp2/3 complex-dependent endocytosis for initial ciliary assembly.

INTRODUCTION

The cilium of the unicellular, green alga *Chlamydomonas reinhardtii* has long been used as a model due to its structural and mechanistic conservation relative to mammalian cilia. Cilia consist of microtubules that extend from the cell surface and are ensheathed in plasma membrane. Their assembly relies on microtubule dynamics and trafficking of protein and membrane (Nachury et al., 2010), as well as intraflagellar transport (IFT), a motor-based transport system that moves tubulin and other cargo through the cilium (Pedersen and Rosenbaum, 2008).

Although cilia are composed of microtubules and depend on them for assembly, the mechanisms governing ciliary maintenance and assembly extend to other cytoskeletal proteins, like actin. The microtubule organizing center, the centrosome, from which cilia are nucleated functions as an actin organizer (Farina et al., 2016; Inoue et al., 2019). In mammalian cells, cortical actin disruption results in increased ciliary length and percentage of ciliated cells (Kim et al., 2010; Park et al., 2008), and when ciliogenesis is triggered by serum starvation, preciliary vesicles are trafficked to the centriole where they fuse to form a ciliary vesicle around the budding cilium. In intracellular ciliogenesis, when Arp2/3 complex-branched actin is lost, vesicle fusion defects lead to depletion of preciliary vesicles at the centriole, suggesting a role for branched actin in intracellular ciliogenesis (Wu et al., 2018). Further, actin itself has been found within cilia, suggesting that actin is a key protein in ciliary maintenance and assembly (Kiesel et al., 2020).

Chlamydomonas cells are ideal for tackling the question of actin-dependent ciliary trafficking due to their lack of a cortical actin network and their ability to undergo consistent and robust ciliogenesis without requiring serum starvation. In *Chlamydomonas*, disruption of actin networks with Cytochalasin D resulted in short cilia (Dentler and Adams, 1992) and disruption with Latrunculin B (LatB), which sequesters monomers leading to filament depolymerization, resulted in short cilia and impaired regeneration (Avasthi et al., 2014; Jack et al., 2019). *Chlamydomonas* actin networks are required for accumulation of IFT machinery at the base of cilia and for entry of IFT material into cilia (Avasthi et al., 2014), as well as for trafficking of post-Golgi vesicles to cilia, synthesis of ciliary proteins, and organization of the ciliary gating region (Jack et

al., 2019). Many advances in our understanding of the relationship between cilia and actin were discovered using *Chlamydomonas*.

The actin cytoskeleton of *Chlamydomonas* contains two actin genes: *IDA5*, a conventional actin with 91% sequence identity to human β-actin; and *NAP1*, a divergent actin that shares only 63% of its sequence with human β-actin (Hirono et al., 2003; Kato-Minoura et al., 1998). We consider NAP1 to be an actin-like protein as opposed to an actin related protein (ARP) because it has a higher sequency identity to actin than to conventional ARPs and because it is able to functionally compensate for the conventional IDA5 (Jack et al., 2019; Onishi et al., 2019, 2018, 2016). Under normal, vegetative conditions, IDA5 is the primary actin expressed, but when cells are treated with LatB, the LatB-insensitive NAP1 is upregulated (Hirono et al., 2003; Onishi et al., 2018, 2016). This separability of the two actins led to the discovery that they can compensate for each other in ciliary maintenance and assembly (Jack et al., 2019). Studies of actin's role in ciliary assembly used global disruption, knocking out either one of the filamentous actins or acutely knocking out both, yet actin networks have diverse compositions and topologies that lead to specific subfunctions within cells.

Actin networks rely on actin binding proteins that contribute to the formation, arrangement, and function of the networks. One such actin binding protein is the Arp2/3 complex, which nucleates branched or dendritic networks. These networks are often involved in membrane remodeling functions, like lamellipodia and endocytosis (Campellone and Welch, 2010). The Arp2/3 complex consists of 7 subunits: Arp2, Arp3, and ARPC1-5 (**Fig. 3.1**). Each subunit plays a specific role of varying importance in the nucleation process. ARPC2 and ARPC4 form the complex core and the primary contacts with the mother filament, Arp2 and Arp3 serve as the first subunits of the daughter filament, and ARPC1 and ARPC3 play a role in nucleation but are not critical for branch formation (Gournier et al., 2001; Robinson et al., 2001). Each of these subunits is found in *Chlamydomonas,* but they have a range of sequence homologies compared to conventional Arp2/3 complexes (**Fig. 3.1**). The ARPC5 subunit has yet to be found in *Chlamydomonas*. ARPC5 is thought to be important for the association of ARPC1 to the complex, but a mammalian complex lacking ARPC5 and ARPC1 maintains some nucleating and branching activity and is able to cross-link actin (Gournier et al., 2001).

Here, using the chemical inhibitor CK-666 to inhibit the nucleating function of the Arp2/3 complex (Hetrick et al., 2013) and a genetic mutant of a critical Arp2/3 complex member, ARPC4 (Cheng et al., 2017; Li et al., 2019), we take a more delicate approach to investigating the actin's in ciliary assembly by separating different actin networks into their subfunctions based on topology. Specifically, we probe the involvement of actin networks nucleated by the Arp2/3 complex in ciliary maintenance and assembly. This approach in these cells has allowed us to propose a new model implicating a subset of filamentous actin in redistribution of membrane and proteins for the initial stages of ciliogenesis.

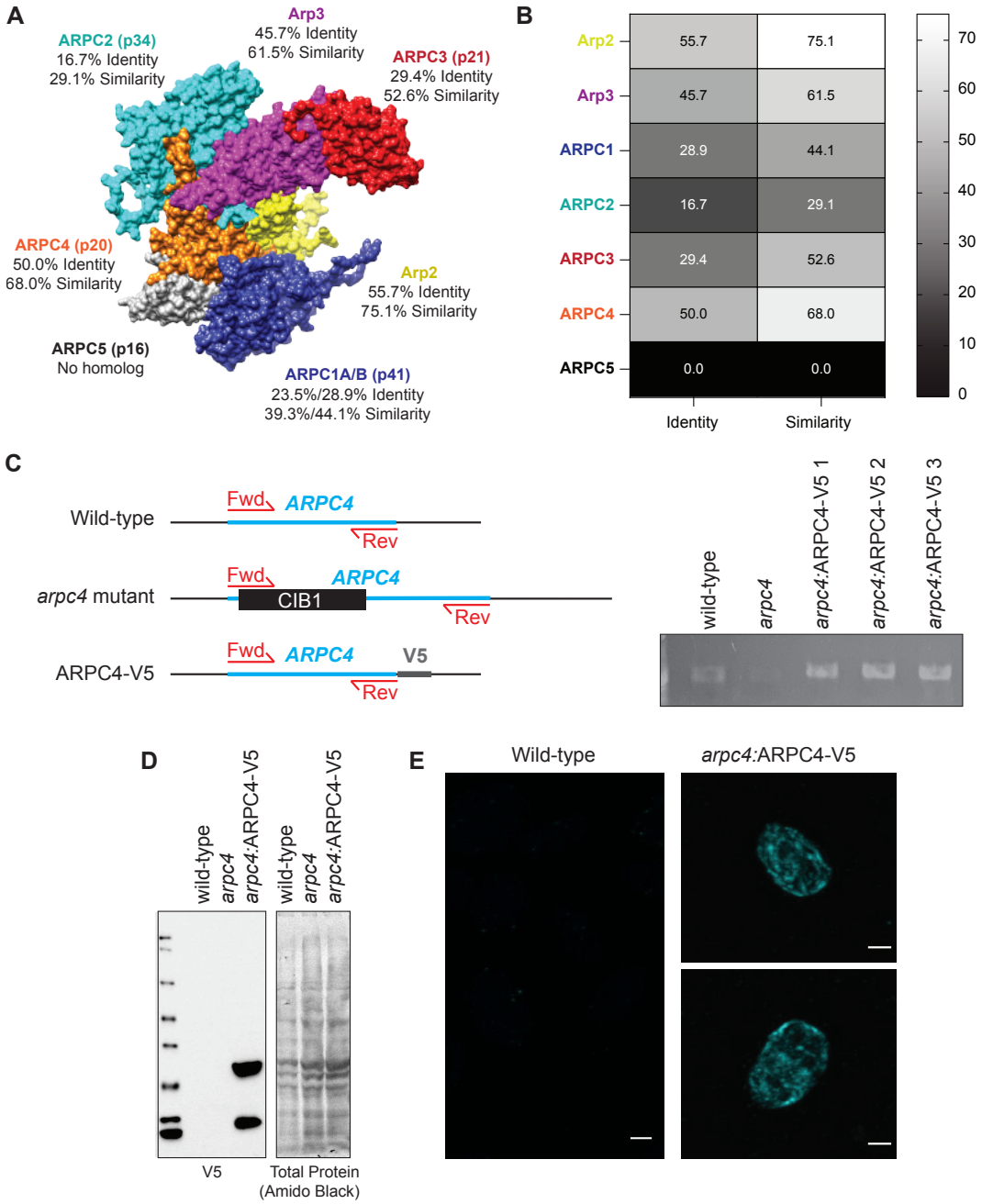

Fig. 3.1. Arp2/3 complex conservation in *Chlamydomonas*. A) Homology model of the *Chlamydomonas* Arp2/3 complex based on the bovine Arp2/3 complex (PDB:1K8K). Percent identity and similarity for the protein sequences of the Arp2/3 complex of *Chlamydomonas* compared to the bovine Arp2/3 complex. **B)** Heatmap of sequence identity and similarity of the Arp2/3 complex members of *Chlamydomonas* compared to those of the bovine complex. The ARPC1 isoform used for comparison was ARPC1B as it was more highly conserved to the *Chlamydomonas* ARPC1. Percentages were determined based on a MUSCLE alignment in Geneious. **C)** Diagram of wild-type ARPC4, mutated ARPC4, and ARPC4-V5 with primer position. PCR gel showing presences of the *ARPC4* gene in wild-type and rescue colonies, but not in the *arpc4* mutant. **D)** Western blot using V5 antibody (Thermo) showing protein expression of V5 in rescues containing *ARPC4-V5*. Total protein was probed using amido black. **E)** Immunofluorescence using the V5 antibody (Thermo). Wild-type cells show little to no signal, while cells expressing *ARPC4-V5* on the *arpc4* mutant background (colony 3) do show signal. Scale bar represents 2 μm.

RESULTS

Loss of Arp2/3 complex function inhibits normal regeneration and maintenance of cilia:

To investigate the role of Arp2/3 complex-mediated actin networks in ciliary assembly, we used two tools. First, we used the chemical inhibitor CK-666 which blocks the nucleating ability of the Arp2/3 complex by binding the interface between Arp2 and Arp3 and locking the complex in an inactive state (Hetrick et al., 2013). The Arp2 and Arp3 subunits of the *Chlamydomonas* Arp2/3 complex are 75.1% and 61.5% similar to mammalian Arp2/3 complex respectively (**Fig. 3.1**). This, along with the ability of CK-666 to recapitulate the effects of a genetic mutant of the Arp2/3 complex, suggest that CK-666 can target *Chlamydomonas* Arp2/3 complex. Second, we obtained a loss of function mutant of the critical Arp2/3 complex member, ARPC4 from the *Chlamydomonas* Resource Center (Cheng et al., 2017; Li et al., 2019). The *arpc4* mutant was confirmed via PCR and further evaluated using a genetic rescue where a V5-tagged ARPC4 construct is expressed in *arpc4* mutant cells, *arpc4:*ARPC4-V5. This was confirmed via PCR, western blot, and immunofluorescence (**Fig. 3.1C-E**). While we can confirm the presence of ARPC4-V5 with immunofluorescence, the actual localization of ARPC4-V5 is not discernable due to diffuse signal (**Fig. 3.1E**). This could be because all ARPC4-V5 in the cell is not being incorporated into active Arp2/3 complexes.

We probed the requirement for the Arp2/3 complex in maintenance of cilia by treating cells with CK-666 or the inactive control CK-689 for 2 hours until cilia reached a new steady state length. Consistent with previous results (Avasthi et al., 2014), CK-666 decreased ciliary length (**Fig. 3.2A**), while not affecting overall cell health (**Figure 3.3**). We saw no changes with the inactive CK-689 (**Fig. 3.2A**) or when *arpc4* mutant cells lacking a functional Arp2/3 complex were treated with CK-666 (**Fig. 3.2A**). Untreated *arpc4* mutant cells recapitulate the CK-666 result, showing decreased ciliary length when compared to wild-type cells (**Fig. 3.2B**). This defect in ciliary length was rescuable with ARPC4-V5 (**Fig. 3.2B**). Overall, this suggests the Arp2/3 complex is required for normal ciliary maintenance.

Next, we explored the involvement of the Arp2/3 complex in ciliary assembly where protein and membrane both from existing pools and from synthesis are in high

demand (Diener et al., 2015; Jack et al., 2019; Nachury et al., 2010; Rohatgi and Snell, 2010; Wingfield et al., 2017). Cells were deciliated by low pH shock and allowed to synchronously regenerate cilia at normal pH (Lefebvre, 1995). *arpc4* mutant cells were slow to regenerate cilia, and roughly 60% of cells did not regrow cilia (**Fig. 3.2C-D**). This phenotype was rescued by with ARPC4-V5 (**Fig. 3.2C-D**). Importantly, the most severe defect in assembly is in initial steps when existing protein and membrane are being incorporated into cilia.

The striking decrease in ciliary assembly is puzzling because loss of the Arp2/3 complex, and therefore only a subset of actin filaments, results in a more dramatic phenotype than *nap1* mutants treated with LatB, which lack all filamentous actins (Jack et al., 2019). However, in *arpc4* mutant cells, a functional Arp2/3 complex never exists. In *nap1* mutant cells treated with LatB, treatment begins shortly after deciliation resulting in an acute perturbation. Further, LatB functions by sequestering actin monomers to promote filament disassembly, and the effects may not be immediate (Spector et al., 1989). Thus, there is likely a brief window where actin filaments can assert their initial role in ciliary regeneration before being depolymerized. To avoid this, we began LatB treatment in *nap1* mutants 30 minutes before deciliation, which allowed us to observe what happens when actin is not present immediately after deciliation. We see slightly decreased ciliary length consistent with the acute treatment but dramatically decreased percent ciliation, which is consistent with the *arpc4* mutant results (**Fig. 3.2E-F**).

Treatment with CK-666, an Arp2/3 complex inhibitor, gives a similar result. In cells treated with CK-666 immediately following deciliation, the Arp2/3 complex may assert its role in assembly before being inhibited by CK-666. By pre-treating cells with CK-666 for 1 hour before deciliation, we can observe what happens when Arp2/3 complex function is lost immediately following deciliation. When we do so, we see a more dramatic defect in ciliary length and percent ciliation than we do with just acute CK-666 treatment (**Fig. 3.2G-H**), suggesting the Arp2/3 complex is required for a very early initial step of assembly that occurs before we have a chance to treat the cells.

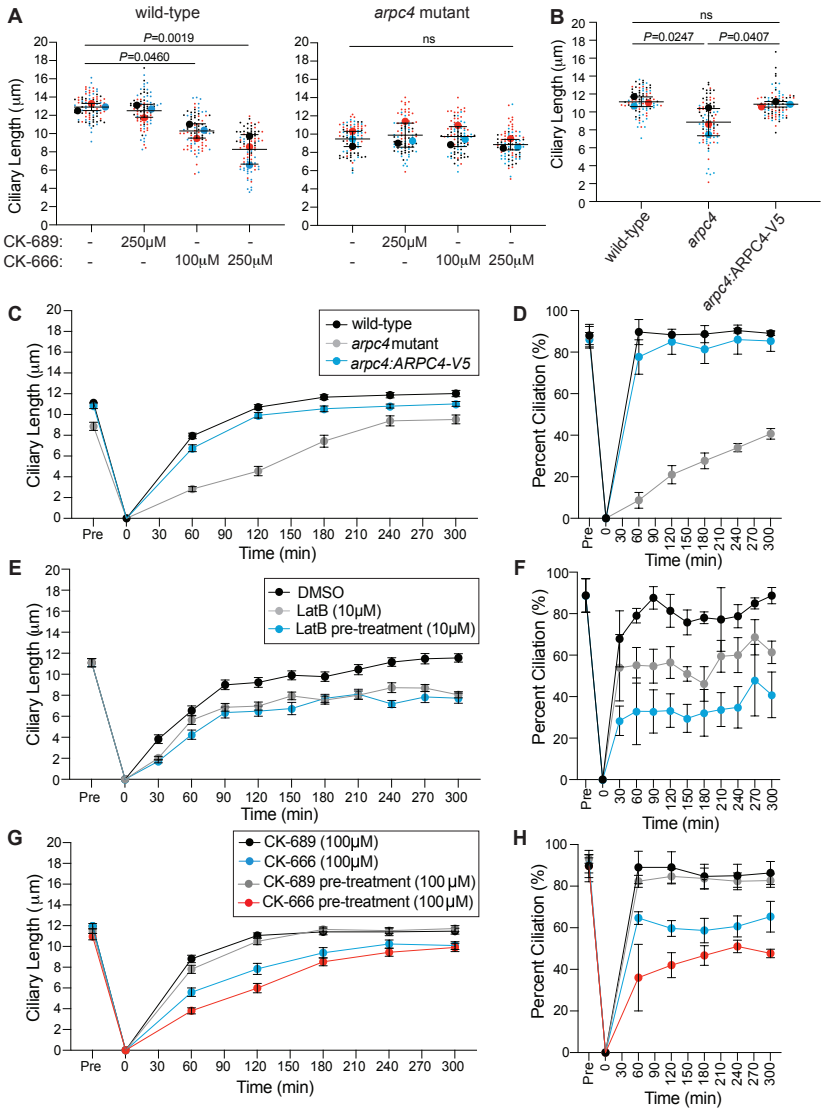

Fig. 3.2. The Arp2/3 complex is required for normal ciliary maintenance and assembly. A) Wild-type and *arpc4* mutant cells were treated with 100µM or 250µM CK-666 or the inactive CK-689 for 2 hours. Superplots show the mean ciliary lengths from 3 separate biological replicates with error bars representing standard deviation. n=30 for each treatment in each biological replicate. **B)** Wild-type cells, *arpc4* mutant cells, and *arpc4:ARPC4-V5* cells steady state cilia were also measured with no treatment. Superplots show the mean of 3 biological replicates with error bars representing standard deviation. n=30 for each strain in each biological replicate. **C-D)** Wild-type cells and *arpc4* mutant cells were deciliated using a pH shock, cilia were allowed to regrow and ciliary length (C) and percent ciliation (D) were determined. Means are displayed with error bars representing 95% confidence interval (C) or standard deviation (D). n=30 (C) or n=100 (D) for each strain and each time-point in 3 separate biological replicates. For every time point except 0 min, P<0.0001 for both length and percent ciliation. **E-F)** *nap1* mutant cells were pre-treated with 10µM LatB for 30 minutes before deciliation or treated with LatB upon the return to neutral pH following deciliation. Ciliary length (E) and percent ciliation (F) were determined for each time point. Error bars represent 95% confidence interval (E) or standard deviation (F). n=30 (E) or n=100 (F) for 3 separate experiments. For every time point P>0.0001 between DMSO and treated samples, except 30min (10μM LatB) which is ns. **G-H)** Wild-type cells were pre-treated with CK-666 or the inactive CK-689 (100μM) for 1 hour before deciliation of treated with CK-666 or the inactive CK-689 (100μM) following deciliation. Ciliary length (G) and percent ciliation were measured (H). Error bars represent 95% confidence interval (G) or standard deviation (H). n=30 (G) or n=100 (H) for 3 separate experiments.

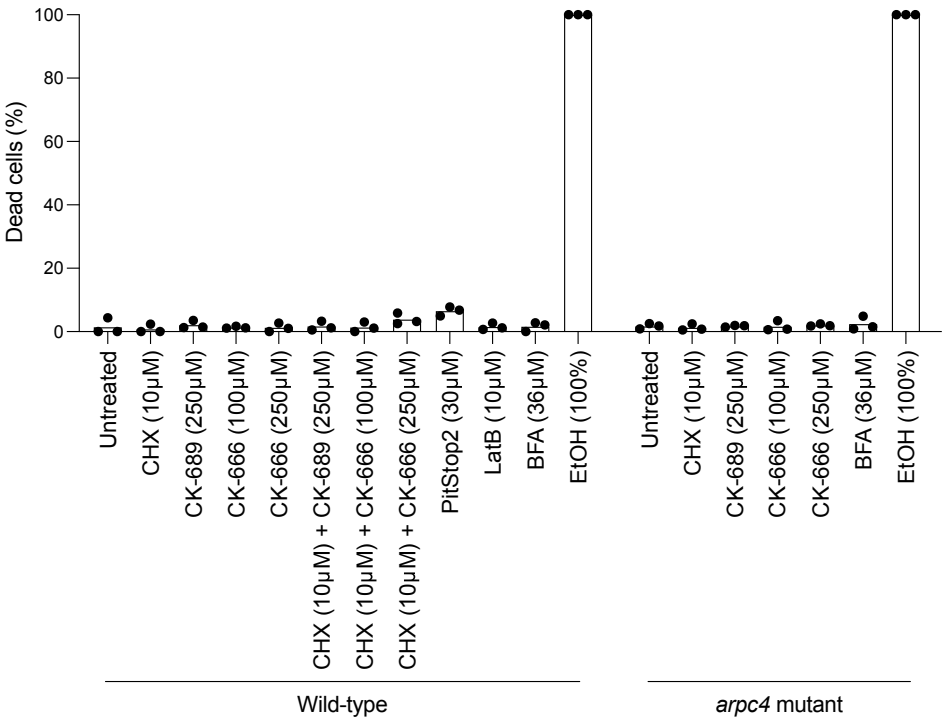

Fig. 3.3. Health of cells treated with chemical inhibitors. For each chemical inhibitor throughout the paper cells were stained with sytox to determine health of the cells. Ethanol (EtOH) is used as a positive control as it kills the cells. Cells were treated with LatB or PitStop2 for 1 hour consistent with what was used in the paper. Cells treated with any concentrations of CK-666, CK-689, or CHX were treated for 2 hours consistent with what was used in the paper and when ciliary growth should be complete. Cells treated with BFA were treated for 3 hours consistent with what was used in the paper. n > 70 cells in 3 separate experiments.

The Arp2/3 complex is required for the incorporation of existing membrane and proteins for ciliary assembly:

There are several actin-dependent steps of ciliary assembly, including incorporation of existing protein and membrane and synthesis and trafficking of new protein for cilia. Using a method to label nascent peptides, we found that loss of ARPC4 did not prevent upregulation of translation following deciliation (**Fig. 3.4**). In this experiment, we halt translation and fluorescently label newly translated polypeptides. Wild-type and *arpc4* mutant cells were tested using this reaction either before deciliation, following deciliation and one hour of regrowth, or following deciliation and one hour of regrowth in cycloheximide (CHX), which inhibits protein synthesis by blocking the elongation step of protein translation. Wild-type and *arpc4* mutant cells displayed an increase in cell fluorescence following deciliation, especially around the nucleus, indicating an increase in protein synthesis following deciliation (**Fig. 3.4**). Importantly, this increase in cell fluorescence was not significantly different between wild-type and *arpc4* mutant cells, suggesting loss of Arp2/3 complex function does not prevent upregulation of protein synthesis following deciliation. This also indicates *arpc4* mutant cells are aware their cilia were lost, as they respond with increased protein synthesis.

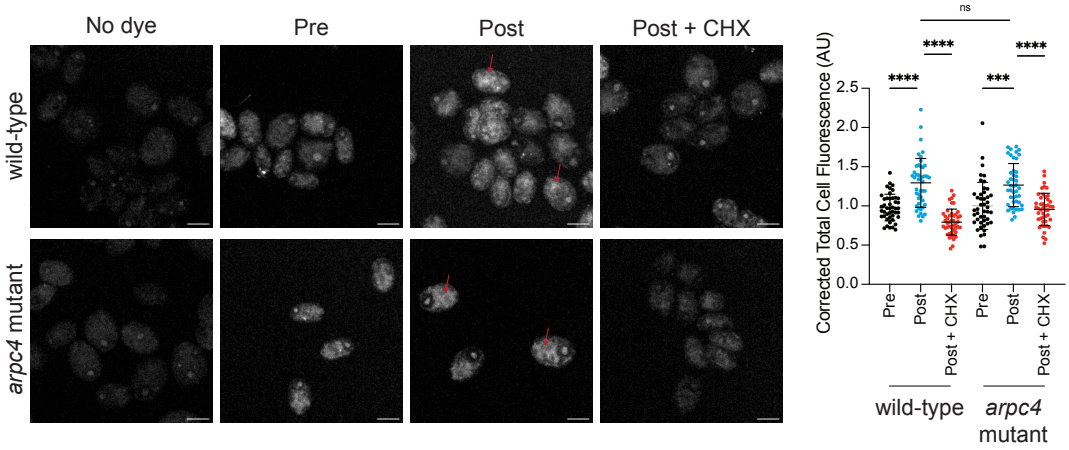

Fig. 3.4. Protein synthesis following deciliation is not defective in *arpc4* mutants. Wild-type and *arpc4* mutant cells were treated with Click-iT OPP either before deciliation, after deciliation and one hour of regrowth, or after deciliation and one hour of regrowth in 10μM CHX which blocks protein translation. Following deciliation there was an increase in fluorescence in cells, particularly around the nucleus (red arrows). The total cell fluorescence was measured and corrected to background then quantified in the graph. n=30 cells per treatment group in 3 separate experiments. **** means P<0.0001. Scale bar represents 5μm .

Given that *arpc4* mutant cells respond to deciliation with protein synthesis, another possible role of the Arp2/3 complex in ciliary assembly is the incorporation of a pool of existing proteins and membrane, which is actin-dependent (Jack et al., 2019). Further, disruption of Arp2/3 complex-mediated actin networks results in slow initial ciliary assembly, when it is likely that existing protein is being incorporated. We tested this by treating cells with cycloheximide (**Figs. 3.5A, 3.3**) (Rosenbaum et al., 1969). Without protein synthesis, there is no trafficking or incorporation of new proteins. So, any ciliary growth we see is due to incorporation of existing protein alone. Normally, cells that are deciliated and treated with cycloheximide grow cilia to about half-length within 2 hours (**Fig. 3.5B**). In *arpc4* mutant cells treated with cycloheximide, cilia display minimal growth; throughout a 5-hour period, only 6% of cells grew cilia (**Fig. 3.5B**). This suggests the Arp2/3 complex is indispensable for incorporation of existing protein and membrane during ciliary assembly.

We suspected *arpc4* mutant cells either lacked the normal pool of ciliary precursor proteins or were unable to incorporate it. However, the inability of the genetic mutants to regenerate in cycloheximide prevents us from doing the typical studies testing new protein synthesis, precursor pool size, and new protein incorporation outlined in Jack et al. 2018 as they require regeneration in cycloheximide. To get around this, we used an acute perturbation, chemical inhibition in wild-type cells that have a normal ciliary precursor pool (as evidenced by their ability to grow to half-length in cycloheximide). Cells were deciliated and then CK-666 was added (in addition to cycloheximide) only for regrowth. Thus, the CK-666 could not affect precursor pool size. Cells treated with CK-666 and cycloheximide could not incorporate the precursor pool we know exists in these wild-type cells into cilia, while cilia of cells treated with only cycloheximide or cycloheximide and the inactive control, CK-689 grew to half length (**Figs. 3.5C-D**). This suggests the problem with incorporation in cells lacking a functional Arp2/3 complex lies outside of availability of the precursor pool.

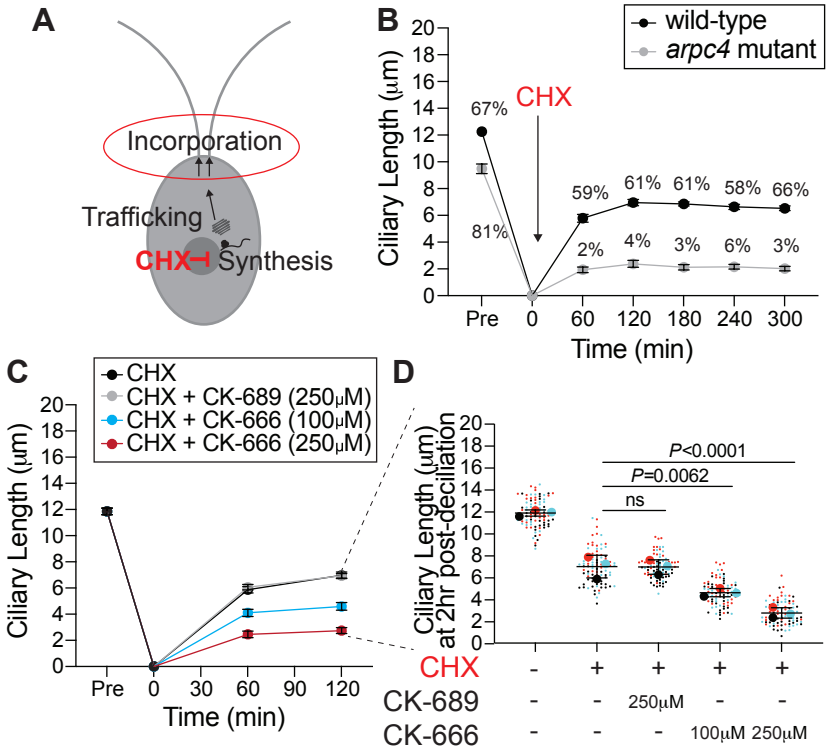

Fig. 3.5. The Arp2/3 complex is required for incorporation of existing protein during ciliary assembly. **A)** Treating cells with cycloheximide inhibits protein synthesis, which means only incorporation of existing protein into the cilia is observed**. B)** Wild-type cells and *arpc4* mutants were deciliated and allowed to regrow in 10μM CHX. The percentages above the lines represent the percent of cells with cilia at the indicated time points. The mean is shown with error bars representing 95% confidence interval. n=30 for each strain and each time point in 3 separate experiments. For every time point besides 0 min, P<0.0001 for both length and percent ciliation. **C**) Wild-type cells were deciliated and then treated with a combination of 10μM cycloheximide (CHX) and CK-666 (100μM or 250μM) or CK-689 (the inactive control, 250μM) at the same concentration during regrowth. The mean is shown with error bars representing 95% confidence interval. n=30 for each strain and each time point in 3 separate experiments. At both 1- and 2-hour time points P<0.0001 for cells treated with CK-666 compared to wild-type cells, and ns for cells treated with CK-689 compared to wild-type cells. **D)** The length of cilia after 2 hours of treatment and regrowth. Superplot shows the mean of 3 separate experiments with error bars representing standard deviation. n=30 for each treatment group 3 separate experiments.

Cilia of *arpc4* mutant cells resorb faster in the absence of the Golgi:

Because we see defects in ciliary assembly and maintenance when cells are likely incorporating existing protein, and we know the protein needed for assembly is in excess due to our acute perturbations with CK-666, we next investigated membrane delivery to cilia. This is of particular interest as the Arp2/3 complex is often involved in membrane remodeling. Typically, the Golgi is thought to be the main source of membrane for cilia (Nachury et al., 2010; Rohatgi and Snell, 2010), and ciliary membrane, membrane proteins, and some axonemal proteins are transported in or attached to vesicles in cytosol (Wood and Rosenbaum, 2014). In *Chlamydomonas*, this has been demonstrated by the ciliary shortening of cells treated with Brefeldin A (BFA), a drug that causes Golgi collapse by interfering with ER to Golgi transport (Dentler, 2013). To determine if the Arp2/3 complex is involved in trafficking of new protein from the Golgi to cilia, we examined the Golgi following deciliation using transmission electron microscopy in *arpc4* mutants (**Fig. 3.6A**). The Golgi appeared grossly normal, had the same number of cisternae, and did not show an accumulation of post-Golgi membrane as previously reported when perturbing filamentous actin (Jack et al., 2019) (**Figs. 3.6A-B**).

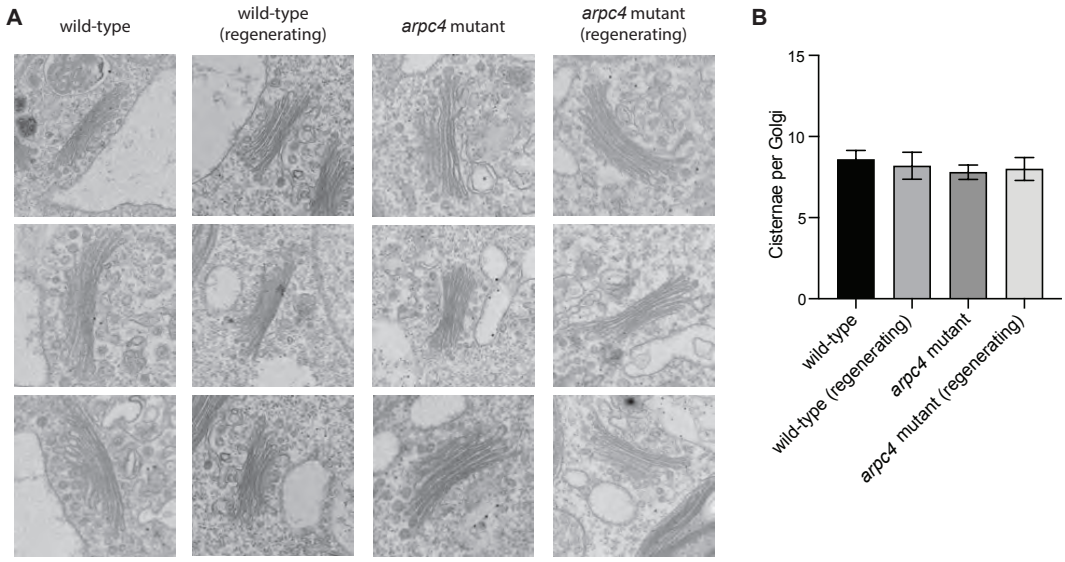

Fig. 3.6. The Arp2/3 complex is not required for Golgi organization. A) Transmission electron micrographs of Golgi found in wild-type or *arpc4* cells. **B)** Number of cisternae per Golgi for each condition. n=5. Error bars represent standard deviation.

Alternative pathways for delivery of ciliary material have also been found in *Chlamydomonas*. In one experiment, surface proteins were biotinylated and then cells were deciliated, so the membrane and proteins within cilia were lost. When cilia were allowed to regrow, biotinylated proteins were found within the new cilia suggesting they came from the plasma membrane (Dentler, 2013). Therefore, we hypothesized that due to its role in membrane remodeling in other organisms, the Arp2/3 complex may be part of an endocytic pathway that provides membrane to cilia (**Fig. 3.7A**). To test if membrane could be coming from an endocytic source, we treated cells with BFA to collapse the Golgi and block exocytosis forcing cells to utilize other sources of ciliary membrane. Wild-type cilia treated with BFA resorb, but *arpc4* mutant cells resorb faster (**Figs. 3.7B and D, 3.3**), and the number of cells with cilia in *arpc4* mutant cells dramatically decreased with BFA treatment (**Fig. 3.7C**). Meanwhile, cells treated with other known ciliary resorption-inducing drugs that do not specifically target Golgi traffic, 3-isobutyl-1-methylxanthine (IBMX) (Pasquale and Goodenough, 1987) or sodium pyrophosphate (NaPPi) (Lefebvre et al., 1978) show an increased velocity of resorption in wild-type cells compared to *arpc4* mutant cells (**Fig. 3.8**), suggesting the faster resorption of *arpc4* mutant cells in BFA is specific to the effects of BFA. Thus, wild-type cells are more capable of maintaining cilia without membrane supply from the Golgi, suggesting there must be another source for membrane that is dependent upon the Arp2/3 complex.

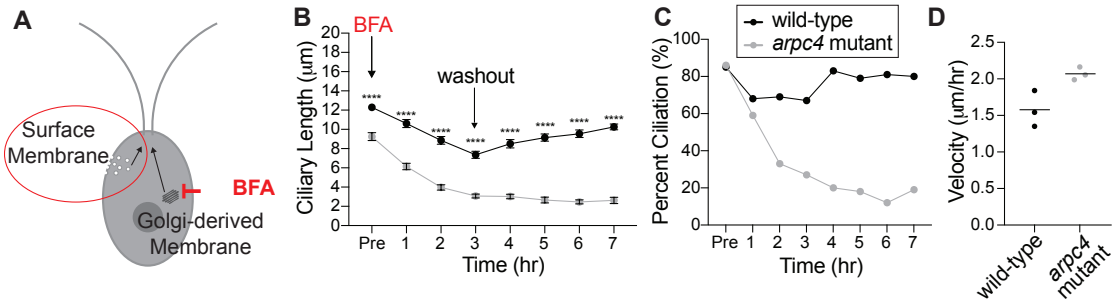

Fig. 3.7. The Arp2/3 complex is required for ciliary maintenance in the absence of intact Golgi. A) Treating cells with Brefeldin A (BFA) causes the Golgi to collapse meaning any membranes and proteins used to maintain the cilia must come from other sources. **B)** Cells were treated with 36μM BFA for 3 hours at which time the drug was washed out. Wild-type is represented by black, while *arpc4* mutants are grey. The mean is shown with error bars representing 95% confidence interval. Error bars represent 95% confidence interval of the mean. n=30 for each time point and each strain in 3 separate experiments. **** represents P<0.0001. **C)** Percent ciliation of the cells in B. n=100. **D)** Resorption speed for wild-type cells and *arpc4* mutant cells as determined by fitting a line to the first 4 time points before washout and determining the slope of the line. Line represents the mean of 3 separate experiments. N=3. P=0.0314

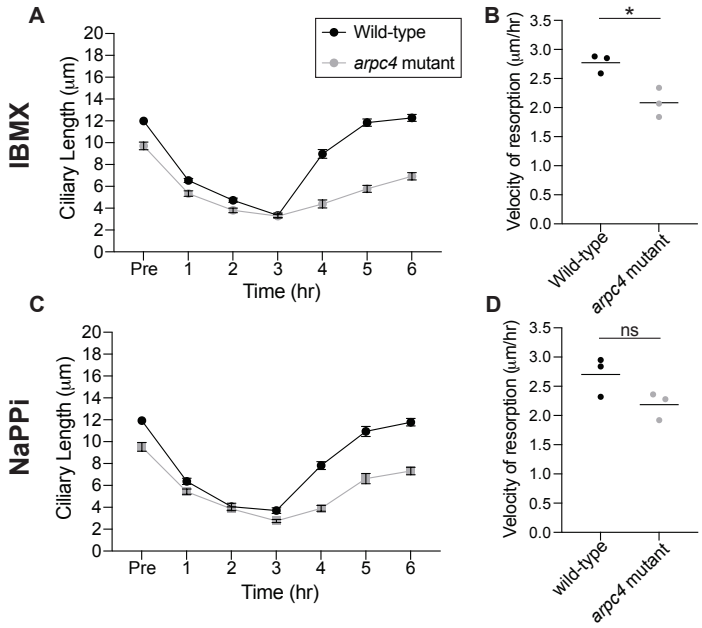

Fig. 3.8. Resorption of cilia with NaPPi and IBMX is not increased in the *arpc4* mutant as it is with BFA. A) Cells were treated with 1mM IBMX and allowed to resorb their cilia. After 3 hours, IBMX was washed out and cells were allowed to regrow cilia. n=30 in 3 separate experiments**. B)** The velocity of IBMX resorption was determined by fitting a line to the first 4 points during regeneration and determining the slope in 3 separate experiments. P=0.0158. **C)** Cells were treated with 20mM NaPPi and allowed to resorb their cilia. After 3 hours, NaPPi was washed out and cilia were allowed to regrow. n=30 in 3 separate experiments. **D)** The velocity of NaPPi resorption was determined by fitting a line to the first 4 points of resorption and determining the slope in 3 separate experiments. P=0.0945. The slightly slower velocities of resorption in the *arpc4* mutant may be due to the fact that these cells start with shorter cilia and therefore have less to resorb or it may be due to problems in endocytosis that is thought to be required for resorption of cilia (Saito et al., 2017).

Ciliary membrane proteins follow different paths from the plasma membrane to the cilia:

To determine if ciliary membrane and therefore membrane proteins could be coming from a pool in the plasma membrane we did an experiment first described in W. Dentler 2013. Surface proteins were biotinylated, then cells were deciliated. After the cilia regrew for 5 hours, they were isolated and probed for biotinylated protein (**Fig. 3.9A**). Any biotinylated protein present in newly grown and isolated cilia must have come from a pool in the plasma membrane. First, we noticed differences in the biotinylated proteins found in wild-type cilia and *arpc4* mutant cilia before deciliation, suggesting there are overall differences in the composition of wild-type and *arpc4* mutant cilia (**Figs. 3.9B-C**). If ciliary membrane proteins are coming from the cell body plasma membrane in an Arp2/3 complex-dependent manner as we hypothesize, this must be the case, as this would mean wild-type and *arpc4* mutant cells have differences in the trafficking pathways that bring ciliary material to cilia. More specifically, there are biotinylated proteins present in wild-type cells that are never present in *arpc4* mutant cells, so there is a mechanism for delivery of proteins to the cilia from the plasma membrane that absolutely requires the Arp2/3 complex (**Figs. 3.9B-C**). There are also some proteins that are present to a higher degree in our arpc4 mutants. We suspect this could be due to compensation by other pathways or defects in turnover of proteins in the cilia, perhaps through an exocytic mechanism. Next, looking at the cilia post-deciliation. Cilia were harvested 5 hours following deciliation because the arpc4 mutant cilia regrow quite slowly. This means that cells might have time to employee other trafficking methods for getting material to cilia, but we still see striking differences. We found that while some proteins returned in both wild-type and arpc4 mutant (**Figs. 3.9B-E, black arrow and black bars**) and some returned to a higher degree in *arpc4* mutant cells (**Figs. 3.9B-E, grey arrow and grey bars**). This suggests there are multiple paths to the ciliary membrane, some of which are Arp2/3 complex-independent and some that are Arp2/3 complex-dependent. This may represent lateral diffusion and endocytosis respectively. Importantly, this assay tells us that membrane proteins can and do come to the cilia from the cell body plasma membrane.

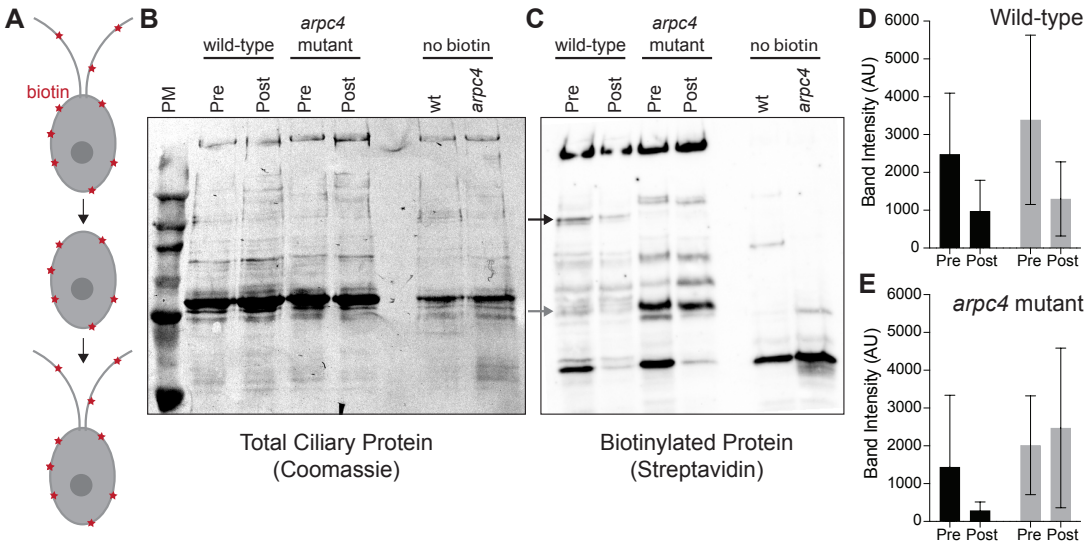

Fig. 3.9. Ciliary membrane proteins have multiple paths from the plasma membrane. A) Cells were biotinylated, deciliated, and allowed to regrow before cilia were isolated and probed for biotinylated protein**. B)** Total protein in wild-type and *arpc4* mutant ciliary isolate investigated by western blot and Coomassie. **C)** Wild-type and *arpc4* mutant cells ciliary isolate was investigated by western blot and probed using streptavidin. Black arrow shows ciliary protein present to a higher degree in wild-type cells than *arpc4* mutant cells. Grey arrows show ciliary protein that is present to a higher degree in *arpc4* mutant cells than in wild-type cells. **D)** Bands represented by black and grey arrows are quantified for the wild-type cells. Data acquired from 3 separate experiments. **E)** Bands represented by black and grey arrows are quantified for the *arpc4* mutant cells. Data represented as the mean from 3 separate experiments. Error bars represent standard deviation.

The Arp2/3 complex is required for the internalization and relocalization of a membrane protein from the periphery of the cell to cilia:

Upon finding that Arp2/3 complex-dependent endocytosis occurs in *Chlamydomonas*, we next asked if this endocytosis could be responsible for relocalization and internalization of a known ciliary protein. SAG1 is a membrane protein important for mating in *Chlamydomonas* cells (Belzile et al., 2013; Ranjan et al., 2019). When cells are induced for mating with dibutyryl-cAMP (db-cAMP), SAG1 relocalizes from the cell periphery to cilia, where it facilitates ciliary adhesion between mating cells. This relocalizaiton of SAG1 is thought to occur through internalization and internal trafficking on microtubules (Belzile et al., 2013; Ranjan et al., 2019).

We examined whether actin and the Arp2/3 complex were required for transport of HA-tagged SAG1 to the cell apex and cilia during mating (**Fig. 3.10A**). We observed cells treated with either LatB to depolymerize IDA5 or CK-666 to perturb the Arp2/3 complex (**Figs. 3.10**). Before induction, SAG1-HA localized to the cell periphery (**Fig. 3.10B, top**). 30 minutes after induction with db-cAMP, SAG1-HA relocalized to the cell apex and to cilia in untreated cells (**Fig. 3.10B, left**). In both LatB and CK-666 treated cells, this apical enrichment decreased (**Fig. 3.10B, middle and right**). We took line scans through the cell from the apex to the basal region (**Figs. 3.10C-D**) and calculated the percentage of cells with apical enrichment. Untreated cells had a higher percent of apical enrichment when compared with LatB or CK-666 treated cells (**Fig. 3.10E**). Thus, cells with perturbed Arp2/3 complex or filamentous actin show decreased efficiency of SAG1-HA relocalization.

We asked if this decrease in relocalization in cells with actin and Arp2/3 complex inhibition could be due to a decrease in internalization of SAG1-HA through a process that seems to require endocytosis. We used a method first described by Belzile et al. 2013, where cells were induced and treated with a low percentage (0.01%) of trypsin, which hydrolyzes exterior proteins but cannot enter the cell. In untreated cells, we see an increase in SAG1-HA protein levels following induction because SAG1-HA is internalized and becomes protected from trypsin (**Fig. 3.10F**). In cells treated with either LatB or CK-666 we see a decrease in this trypsin protection (**Fig. 3.10F**). We quantified this by subtracting the amount of protein before induction from the amount of protein

present after induction, which gives a value representing the amount of SAG1-HA protected from trypsin due to internalization (**Fig. 3.10G**). We confirmed that with genetic perturbation of the Arp2/3 complex we see similar results, although the overall expression of SAG1-HA seems to be decreased in this case (**Fig. 3.10H-J**).The decrease in SAG1-HA following induction in LatB or CK-666 treated cells indicates a role for Arp2/3 complex and actin in internalization of this specific ciliary membrane protein.

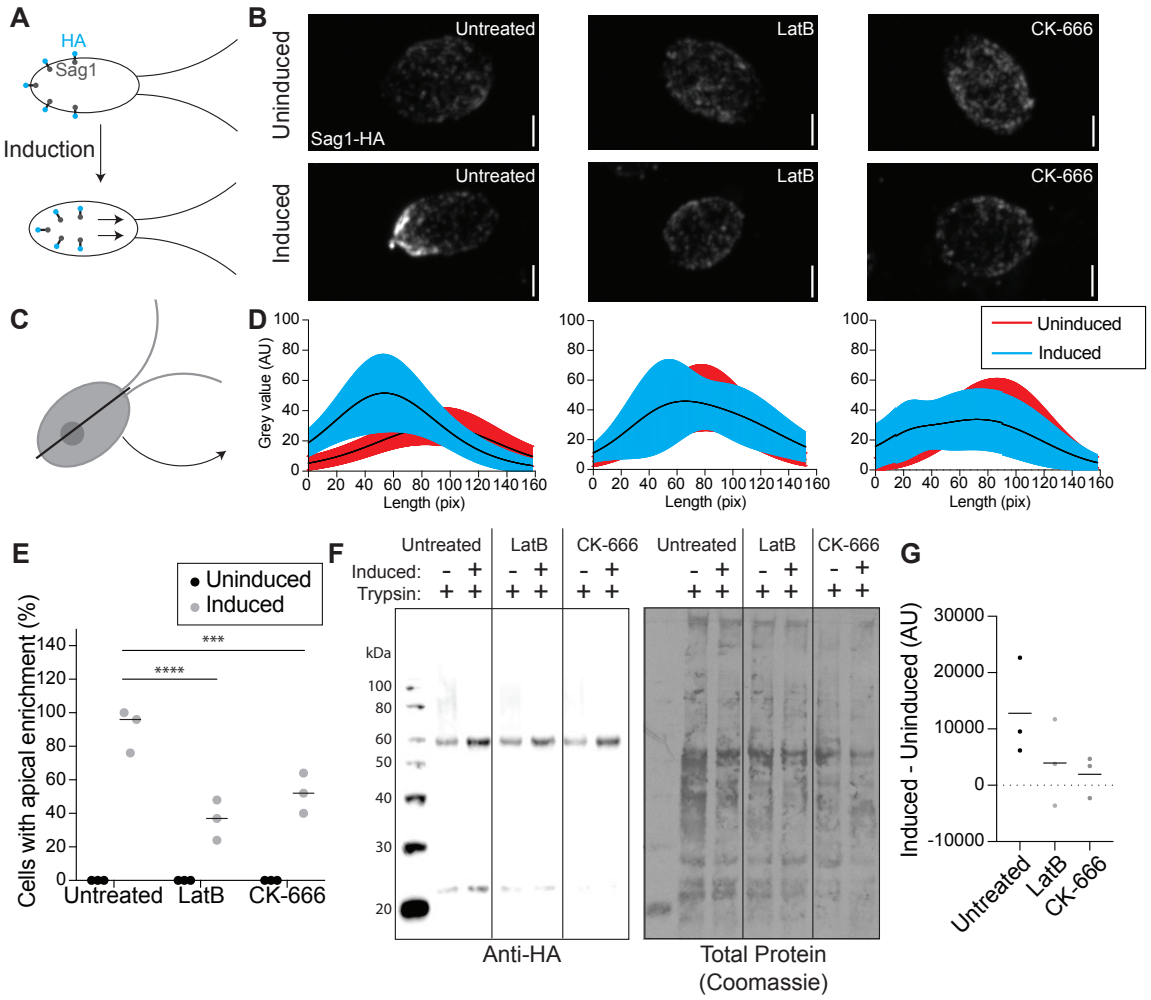

Fig. 3.10. The Arp2/3 complex is required for the relocalization and internalization of the ciliary protein SAG1 for mating. A) When mating is induced SAG1-HA is internalized and relocalized to the apex of the cells and cilia. **B)** Maximum intensity projections of z-stacks showing SAG1-HA. Scale bar represents 2µm. **C)** Line scans were taken through the cells in z-stack sum images. **D)** Line scans in untreated cells (left), LatB treated cells (middle), and CK-666 (right) were normalized and fit with a gaussian curve. The curves were averaged. Black lines represent mean and shaded regions represent standard deviation. Red shows uninduced samples, cyan shows induced samples. 0 on the y-axis represents the apex of the cell. n=30 from a single representative experiment. **E)** Percentage of cells with apical enrichment for uninduced (black) and induced (grey) cells for each treatment group. The mean is shown with the solid line. N=30 for 3 separate experiments for each treatment. **F)** Western blot showing amount of SAG1-HA in uninduced and induced cells in each treatment group all treated with 0.01% trypsin. **G)** Intensity of the bands in F were normalized to the total protein as determined by Coomassie staining. Uninduced was subtracted from induced to give a representation of the amount of SAG1-HA internalized. Line represents mean of 3 separate experiments. **H)** SAG1-HA cells and *arpc4* mutant cells were mated.

Apical actin dots are dependent on the Arp2/3 complex:

Since ciliary membrane proteins can come from the Golgi or the plasma membrane and *arpc4* mutant cells have a more severe defect in incorporating ciliary proteins from non-Golgi sources, we asked if Arp2/3 complex-mediated actin networks might be responsible for plasma membrane remodeling in *Chlamydomonas* as it is in other organisms. Thus, we looked at the effects of loss of Arp2/3 complex function on actin structures. Using new protocols for visualizing actin in *Chlamydomonas* (Craig et al., 2019), we stained wild-type cells and *arpc4* mutant cells with fluorescent phalloidin. In wild-type cells, apical dots reminiscent of endocytic actin patches in yeast are seen near the base of cilia (**Fig. 3.11A**). We quantified the presence of dots in the wild-type cells compared to *arpc4* mutant cells (**Fig. 3.11A-B**). While about 70% of wild-type cells contain the dots, less than 5% of *arpc4* mutant cells had dots (**Fig. 3.11B**), suggesting the Arp2/3 complex is required for formation of this structure. Expression of the ARPC4-V5 construct in *arpc4* mutant cells rescued the dots (**Fig. 3.11C**). The reliance of this structure on the Arp2/3 complex led us to question whether these dots could represent endocytic membrane remodeling.

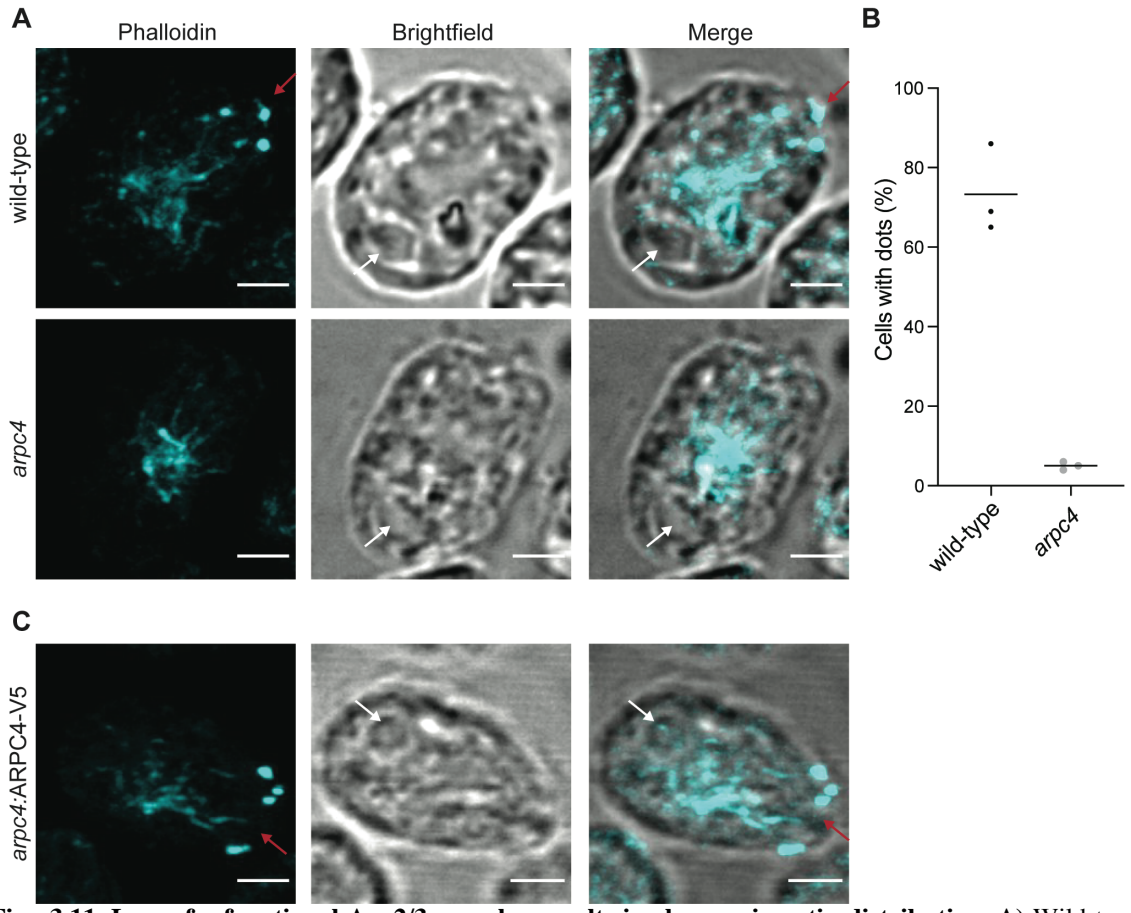

Fig. 3.11. Loss of a functional Arp2/3 complex results in changes in actin distribution. A) Wild-type and *arpc4* mutant cells stained with phalloidin to visualize the actin network along with brightfield to show cell orientation. Images were taken as a z-stack using airsycan imaging and are shown as a maximum intensity projection. Red arrow is pointing to dots at the apex of the cell, and white arrow is pointing to the pyrenoid near the basal end of the cell. Scale bars represent 2μm. **B)** Percentage of cells with apical dots as shown in A. Percentages taken from 3 separate experiments where n=100. Line represents the mean. P<0.0001. **C)** Presence of apical dots in the *arpc4* mutant rescue expressing ARPC4-V5. Images were taken as a z-stack using airsycan imaging and are shown as a maximum intensity projection. Red arrow is pointing to dots at the apex of the cell, and white arrow is pointing to the pyrenoid near the basal end of the cell. Scale bars represent 2μm.

Endocytosis occurs in Chlamydomonas:

The Arp2/3 complex is thought to be involved in endocytosis in cell-walled yeast to overcome turgor pressure (Aghamohammadzadeh and Ayscough, 2009; Basu et al., 2014; Carlsson and Bayly, 2014). Chlamydomonas cells also have a cell wall and since the actin dots resemble yeast endocytic pits (Adams and Pringle, 1984; Ayscough et al., 1997; Goode et al., 2015), we hypothesized that Arp2/3 complex-dependent endocytosis might be occurring in Chlamydomonas though this process has not yet been directly demonstrated in this organism. To determine what kind of endocytosis likely occurs in these cells, we compared the endocytosis-related proteins found in mammals and plants to those in Chlamydomonas (**Figure 3.12A**). Chlamydomonas lacks much of the important machinery for almost all typical endocytosis processes, including caveolin for caveolin-mediated endocytosis, flotillin for flotillin-dependent endocytosis, and endophilin for endophilin-dependent endocytosis (**Figure 3.12A**). However, clathrin-mediated endocytosis is conserved to a higher extent than other endocytic mechanisms.

We aimed to probe the likelihood of endocytosis occurring in Chlamydomonas, but a mutant for the proteins involved in clathrin-mediated endocytosis does not currently exist and methods of targeted mutagenesis in Chlamydomonas are not yet reliable. So, we turned to our best alternative PitStop2, which inhibits the interaction of adaptor proteins with clathrin, halting clathrin endocytosis, despite reported off-target effects on global endocytosis in mammalian cells (Willox et al., 2014). We also used the dynamin inhibitor Dynasore, which is thought to block endocytosis by inhibiting the GTPase activity of dynamin (Macia et al., 2006), although this inhibitor has also been found to affect actin in some mammalian cells (Mooren Olivia L. and Schafer Dorothy A., 2009; Park et al., 2013; Yamada et al., 2009). Although both PitStop2 and Dynasore are reported to have off-target effects in different pathways, their intended target is in the same pathway. Therefore, by using both we hope to reduce concerns of off-target effects. To further minimize off-target effects, this experiment was done in a fast time scale and at the lowest concentration possible. For this experiment, we used the fixable lipophilic dye FM 4-64FX (Cochilla et al., 1999; Gachet and Hyams, 2005), which is impermeable to the plasma membrane but is endocytosed into cells showing bright foci where dye is enriched in endocytic compartments. We incubated the dye for 1 minute to allow enough time for

internalization into endosomes but not enough for incorporation into various cellular membrane structures. The ability of cells to internalize membrane was measured by calculating the total cell fluorescence inside the cell after dye internalization (**Figure 3.12B**). Cells treated with PitStop2 or Dynasore internalized significantly less membrane dye (**Figure 3.12C**), which supports the idea that endocytosis is occurring in these cells and that it is likely clathrin-mediated.

Next, we tested whether endocytosis is Arp2/3 complex-dependent by using this membrane internalization assay on arpc4 mutant cells compared to wild-type cells and CK-666 treated cells compared to CK-689 treated cells. arpc4 mutant cells and cells treated with CK-666 have decreased total cell fluorescence (**Figure 3.12D-F**) suggesting endocytosis in Chlamydomonas is Arp2/3 complex-dependent.

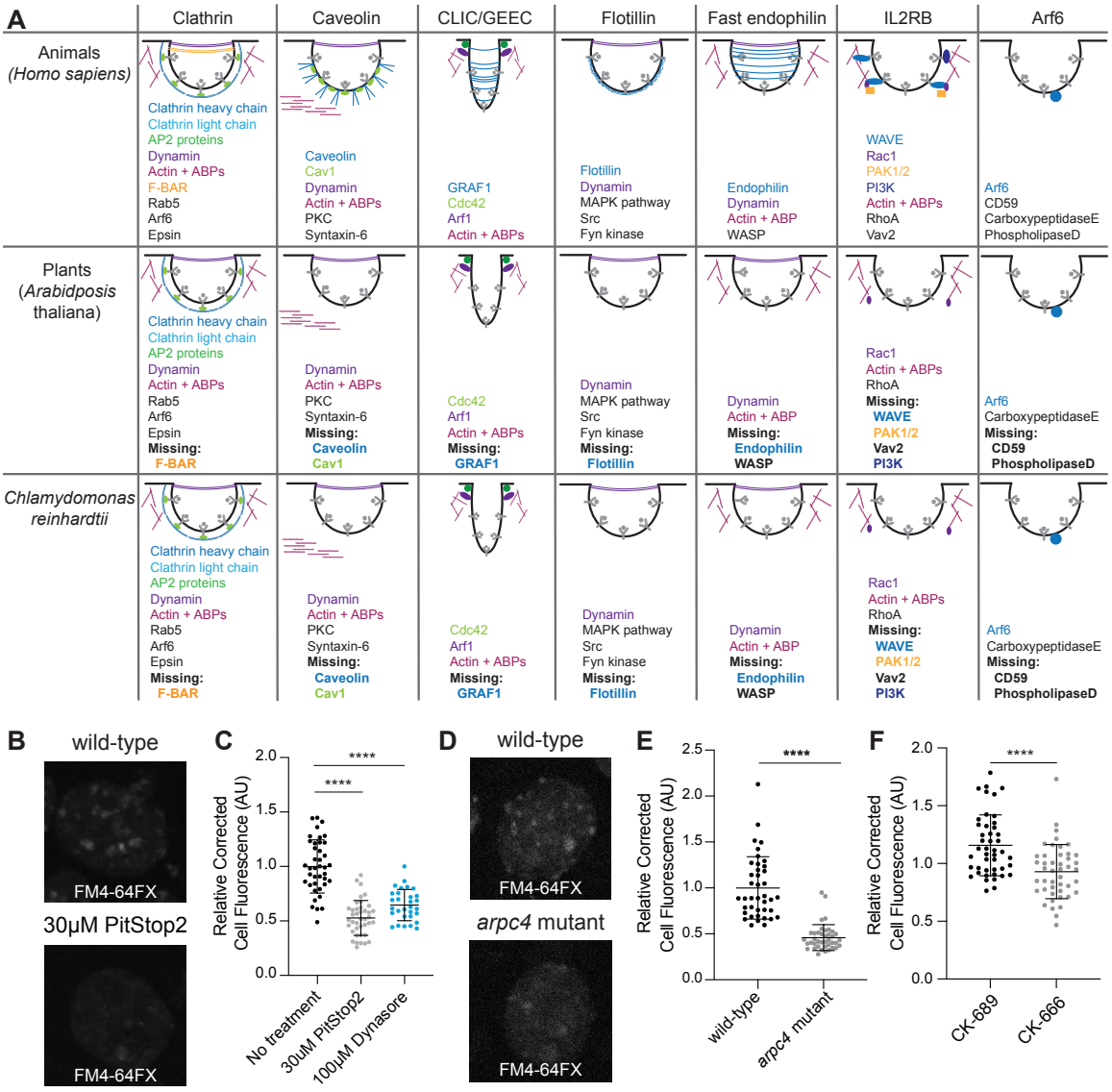

Figure 3.12. Arp2/3 complex-dependent endocytosis is conserved in Chlamydomonas. A) Gene presence was determined using BLAST. Word colors correspond to diagram colors. **B)** Cells treated with 30μM PitStop2 were incubated with FM4-64FX and imaged on a spinning disk confocal. Max intensity projections of z-stacks are shown. Scale bars are 2μm. **C)** The background corrected fluorescence for each sample, including cells treated with 100μM Dynasore. The mean is shown with error bars showing standard deviation. n=30 in 3 separate experiments. P<0.0001. **D)** Wild-type and arpc4 mutant cells treated with FM4-64FX and imaged on a spinning disk confocal. Max intensity projections of z-stacks are shown. Scale bars are 2μm. **E)** The background corrected fluorescence for each sample. The mean is shown with error bars representing standard deviation. n=30 in 3 separate experiments. P<0.0001. **F)** The background corrected fluorescence for cells treated with CK-666 or CK-689. The mean is shown with error bars representing standard deviation. n=30 in 3 separate experiments. P<0.0001.

Actin dots increase in an Arp2/3 complex and endocytosis-dependent manner following deciliation:

Having established that the Arp2/3 complex is required for ciliary assembly, membrane dye internalization, and endocytosis of a known ciliary protein, we wondered if these functions could be connected given that *arpc4* mutant cells have defects in maintaining cilia from non-Golgi sources. We returned to the Arp2/3 complex-dependent actin dots that are reminiscent of endocytic pits in yeast. Because ciliary membrane and proteins can come from the plasma membrane (Dentler, 2013), we suspected there would be an increase in actin dots following deciliation. We used phalloidin to visualize the actin cytoskeleton of wild-type cells before and immediately following deciliation, as well as 10 minutes later (**Fig. 3.13A**). We saw an increase in both the percentage of cells with dots and the number of dots per cell immediately following deciliation that returned to normal by 10 minutes (**Figs. 3.13A, D**). This is consistent with the results in **Figs. 3.3E-F** and confirms that the defect in ciliary assembly is due to an event occurring very early in ciliary assembly, within the first few minutes after deciliation.

In the *arpc4* mutant cells dots were never observed, before or after deciliation (**Figs. 3.13B, D**), confirming these dots are Arp2/3 complex dependent. Next, we investigated if the dots were due to endocytosis by treating cells with PitStop2 and looking for this same increase in dots. This treatment almost fully blocked the appearance of dots following deciliation and eliminated the presence of cells with 3 or more dots (**Figs. 3.13C-D**), suggesting an Arp2/3 complex-dependent endocytic mechanism is related to these dots.

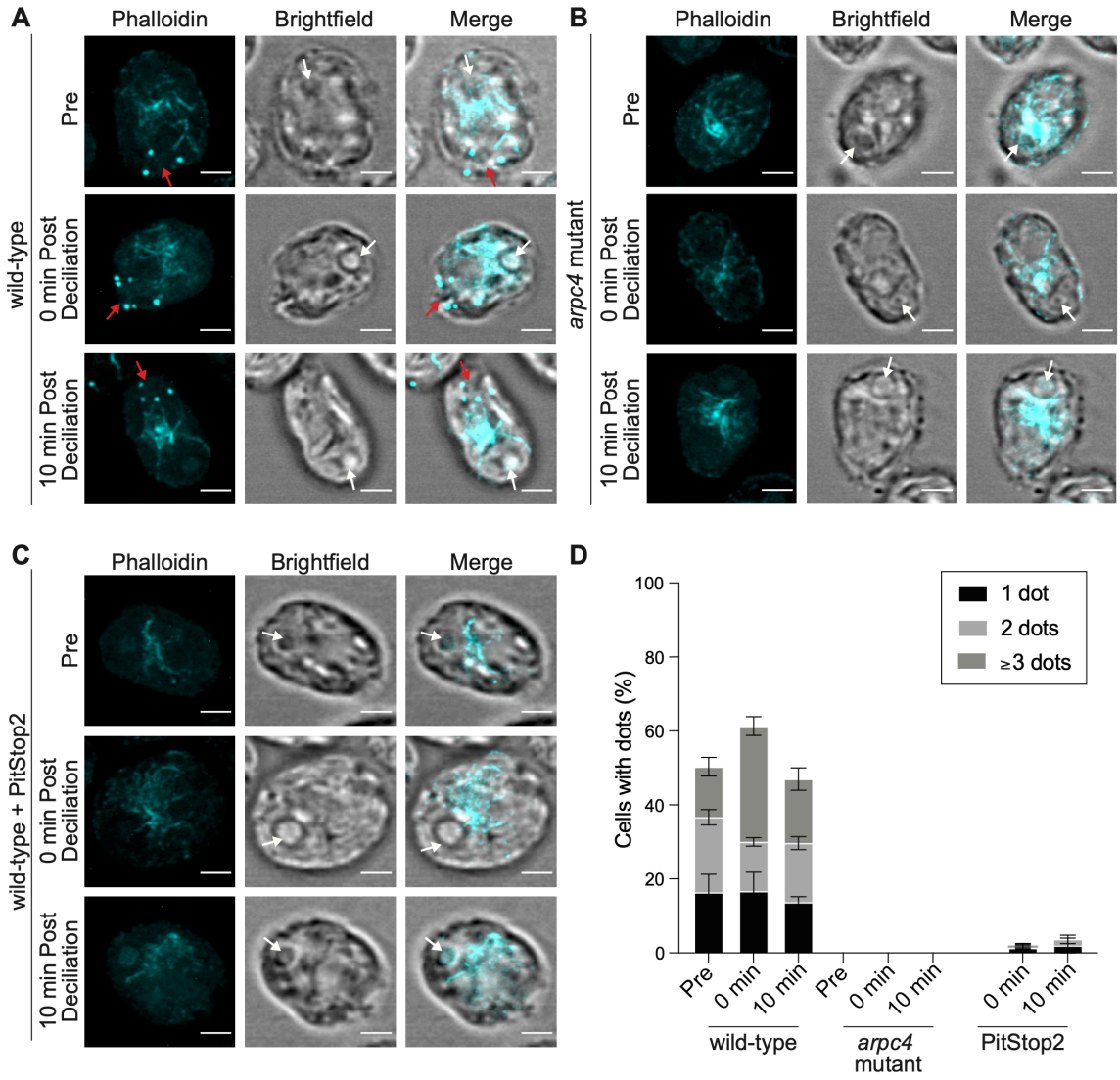

Fig. 3.13. Actin dots require the Arp2/3 complex and endocytosis. A-C) Wild-type cells **(A)**, *arpc4* mutant cells **(B)**, and wild-type cells treated with 30 μM PitStop2 **(C)** stained with phalloidin to visualize the actin network before deciliation, immediately following deciliation, and 10 minutes following deciliation. Brightfield images are to visualize cell orientation. Images were taken as a z-stack and are shown as a maximum intensity projections. Scale bar represents 2µm. Red arrows point to dots at the apex of the cell, and white arrows point to the pyrenoid at the opposite end of the cell. **D)** The percentage of cells with 1 dot, 2 dot, or 3 dots in each condition. Quantification based on sum slices of z-stacks taken using a spinning disk confocal. n=100 in 3 separate experiments. For wild-type, the total number of cells with dots is significantly different for the 0 min time point (**) and the number of dotted cells with 3 or more dots is significantly different for the 0-time point (****).

DISCUSSION

In this study, we investigate the Arp2/3 complex of *Chlamydomonas reinhardtii* that functions to maintain and assemble cilia. This complex potentially lacks the ARPC5 subunit, although it is possible that a divergent ARPC5 exists. In yeast, deletion of any of the genes encoding Arp2/3 complex members causes severe defects, but these defects differ in severity depending on the complex members deleted, suggesting complex members have varying degrees of importance in Arp2/3 complex function (Winter et al., 1999). The role of ARPC5 in actin nucleation is being investigated, but some groups have found it unnecessary for function of the complex (Gournier et al., 2001; von Loeffelholz et al., 2020). Furthermore, our data show that knocking out function of the ARPC5-less *Chlamydomonas* Arp2/3 complex results in various phenotypes, suggesting the wild-type complex is active. In this paper, we study the Arp2/3 complex using 2 main perturbations: genetic inhibition of the ARPC4 member of the complex and chemical inhibition with the inhibitor CK-666. CK-666 is designed for mammalian cells, but we believe that CK-666 is functional in *Chlamydomonas* because it can recapitulate the effects of the genetic mutant. Additionally, if we treat the *arpc4* mutant with CK-666 we do not see these same phenotypes, again suggesting that CK-666 is acting to block the same functions as the genetic *arcp4* mutant (**Fig. 3.3A**). Because the Arp2/3 complex has known functions in membrane dynamics, this led us to pursue models of Arp2/3 complex-dependent membrane trafficking to cilia.

Previously, three models of membrane protein trafficking to cilia have been proposed regarding where ciliary vesicles fuse relative to a diffusion barrier composed of septins (Hu Qicong et al., 2010), which delineates ciliary membrane and cell body plasma membrane (Nachury et al., 2010). The first is that Golgi vesicles containing ciliary proteins fuse with the ciliary membrane inside the cilium. Proteins, both membrane and soluble, have been found to travel from the Golgi to the cilia on or in cytoplasmic vesicles (Wood and Rosenbaum, 2014). Second, Golgi vesicles containing ciliary proteins fuse outside but near the cilium still within the diffusion barrier (Nachury et al., 2007; Papermaster et al., 1985; Zuo et al., 2009). In *Chlamydomonas*, mastigoneme proteins travel from the Golgi and are exocytosed for use on the exterior of the cell (Bouck, 1971). In the third model, Golgi vesicles containing proteins fuse with the

plasma membrane outside the diffusion barrier where they move in the plane of the plasma membrane across this barrier, perhaps through lateral diffusion that requires remodeling or passing through the diffusion barrier. Evidence for this path was shown using Hedgehog signaling protein Smoothened, which relocalizes in a dynamin-independent manner from the plasma membrane to the cilia immediately after stimulation in pulse labeling studies (Milenkovic et al., 2009).

Our data all together support a fourth model, likely occurring in concert with other models, in which membrane and membrane proteins are recruited to the cilium from a reservoir in the cell body plasma membrane. We show that the Arp2/3 complex is required for ciliary assembly from zero-length (**Fig. 3.3**); we show that ciliary membrane proteins can and do come from the cell body plasma membrane, both generally (**Fig. 3.9**) and for a specific protein (**Fig. 3.10**); we show that the Arp2/3 complex is required for endocytosis (**Fig. 3.12**) and for the formation of actin dots reminiscent of endocytic pits or patches (**Figs. 3.11, 3.13**); and finally we show an endocytosis-dependent increase in Arp2/3 complex-mediated actin dots immediately following deciliation (**Fig. 3.13**). Thus, we hypothesize that ciliary membrane proteins and membrane targeted to the plasma membrane of the cell outside the diffusion barrier can be endocytosed and trafficked to cilia, either within or outside of the diffusion barrier in an actin and Arp2/3 complex-dependent manner.

Although our data do not eliminate the possibility of Arp2/3 complex function in supply of ciliary membrane and protein stored in other endosomal compartments, ciliary localization of proteins initially labeled on the cell surface with biotin (**Fig. 3.9**) suggests some ciliary membrane proteins incorporated during assembly are coming from the plasma membrane itself. One limitation to this study is the time frame. We isolated cilia following 5 hours of regrowth to get a measurable amount of *arpc4* mutant cilia, which have very defective growth. This means that compensatory mechanisms such as synthesis and slower trafficking may be involved. An endocytic mechanism of trafficking in intracellular ciliogenesis has been investigated in mammalian RPE1 cells. The ciliary pocket found at the base of primary and motile cilia formed intracellularly has been found to be an endocytically active region (Molla-Herman et al., 2010) but clathrin-mediated endocytosis was not required for ciliogenesis in those cells. The Bardet Biedl Syndrome

complex (BBsome), which is involved in regulation of ciliary membrane protein composition, has been shown to interact with clathrin directly at the ciliary pocket to facilitate membrane sorting in trypanosomes (Langousis et al., 2016). Further, some BBsome complex members resemble coat proteins such as clathrin (Jin et al., 2010) suggesting a direct role for the this cilium regulatory complex in membrane functions. It has also been found that disruption of recycling endosomes reduces the localization of polycystin-2 to cilia, suggesting a role for recyclying endosomes in the localization of proteins to the cilia (Monis et al., 2017). In *Chlamydomonas*, clathrin heavy chain has been found to localize at the base of cilia (Kaplan et al., 2012). While the mechanism was unknown, it has been shown that plasma membrane surface-exposed proteins are relocalized to cilia during ciliary regeneration (Dentler, 2013), a result we recapitulated and demonstrated depends, in part, upon the Arp2/3 complex.

Altogether, this leads us to hypothesize that the role of the Arp2/3 complex in ciliary assembly is through endocytic recruitment from a ciliary protein reservoir in the plasma membrane before newly synthesized protein and Golgi-derived membrane can supply additional materials (**Fig. 3.14B**). While this model provides a possible route that some ciliary proteins and membranes take to the cilia, we believe this is one of several paths that can be taken to the cilia. This could be further investigated by determining specific proteins that may take these different paths to the cilia. Trafficking to cilia is likely cargo- and time-dependent, and which path proteins take may tell us the order and speed in which they populate the cilium for subsequent function.

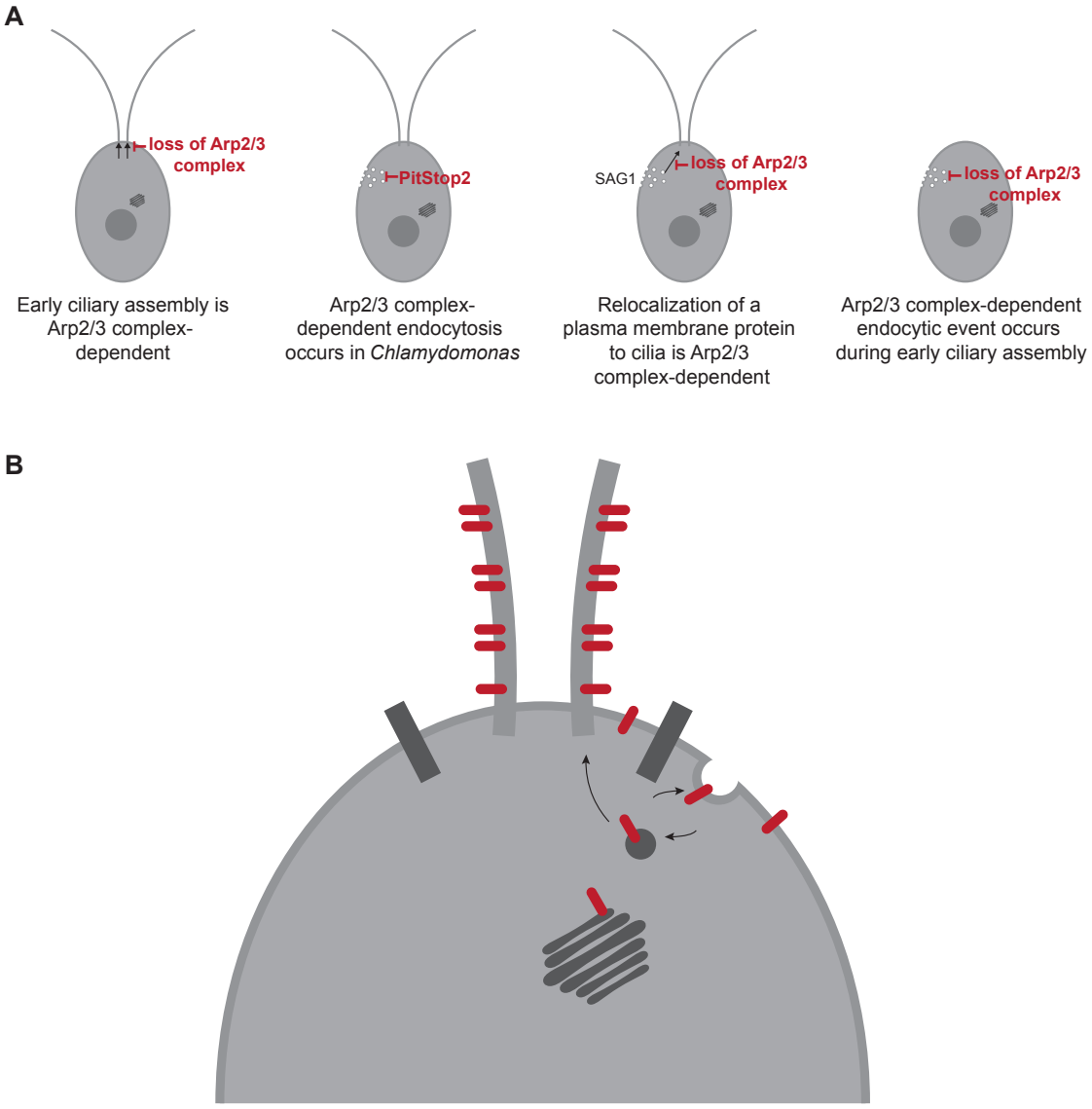

Fig. 3.14. The Arp2/3 complex is required for membrane and protein delivery via a Golgi-independent, endocytosis-like process. A) Arp2/3-mediated actin networks are required for ciliary assembly in *Chlamydomonas* particularly during the initial stages. These actin networks are also required for endocytosis, and for the endocytosis-like relocalization of a ciliary protein from the plasma membrane to the cilia. Finally, a large endocytic event occurs immediately following deciliation that is Arp2/3 complex-mediated. **B)** Proposed model of membrane protein and membrane transport from the plasma membrane to the cilia through endocytosis.

METHODS

Strains:

The wild-type *Chlamydomonas* strain (CC-5325) and the *arpc4* mutant (LMJ.RY0402.232713) are from the *Chlamydomonas* resource center. The *arpc4:*ARPC4-V5 strain was made by cloning the gene into pChlamy4 (*Chlamydomonas* resource center). Colonies were screened for the absence (in the case of the mutant) or presence (in the case of the rescue) by PCR using the primers AAAAGAATTCATGGCGCTCTCACTCAGGCCATA and AAAATCTAGACAGAAGGCAAGGGAGCGCAGGAA. The SAG1-HA strain was a gift from William Snell. Cells were grown and maintained on 1.5% Tris-Acetate Phosphate Agar (TAP) plates (*Chlamydomonas* resource center) under constant blue (450-475 nm) and red light (625-660 nm). For experiments, cells were grown in liquid TAP media (*Chlamydomonas* resource center) overnight under constant red and blue light with agitation from a rotator. To induce gametes for mating for the SAG1-HA experiments, cells were grown in liquid M-N media (*Chlamydomonas* resource center) overnight with constant red and blue light and agitation.

Ciliary studies:

For steady state experiments, cells were treated with specified drugs [either 100μM CK-666, 250μM CK-666 (Sigma, 182515) 250μM CK-689 (CalBiochem, 182517), 10μM LatB (Sigma, L5288), 10μM CHX (Sigma, C1988), or 36μM BFA (Sigma, B7651) all diluted in DMSO (Sigma, D2650)] and incubated with agitation for the allotted times. Following any incubation (as well as a pre sample), cells were diluted in an equal volume of 2% glutaraldehyde (EMS, 16220) and incubated at 4º Celsius until they sediment (within 24hrs). Following sedimentation, cells were imaged using a Zeiss Axioscope 5 DIC microscope with a 40X objective (0.75 numerical aperture) at room temperature with no immersion media or imaging media. Images were acquired using Zeiss Zen 3.1 (blue edition). Cilia were then measured using the segmented line function in ImageJ. One cilium per cell was measured and 30 cilia total were measured.

For regeneration experiments, a pre sample was taken by adding cells to an equal volume of 2% glutaraldehyde. Then cells were deciliated with 115µL of 0.5N acetic acid for 45 seconds. After this short incubation, the pH was returned to normal by adding 120µL of 0.5N KOH. A 0-minute sample was again taken by adding cells to an equal volume of 2% glutaraldehyde. Then cells were incubated with agitation and allowed to regrow cilia for the allotted time period with samples taken at the indicated time points by adding cells to an equal volume of 2% glutaraldehyde. Cells in glutaraldehyde were allowed to incubate at 4º Celsius until sedimentation (within 24hrs). Then, cells were imaged using the same Zeiss DIC microscope with a 40X objective and the same software. Cilia were then measured using the segmented line function in ImageJ. One cilium per cell was measured and 30 cilia total were measured.

ARPC4 Rescue:

The ARPC4 genetic sequence was isolated from Chlamydomonas cDNA using PCR with the Q5 DNA Polymerase (NEB, M0491L). The resulting fragment and the pChlamy4 plasmid (Thermofisher, A24231) were digested with EcoRI (NEB, R0101S) and XhoI (NEB, R0146S) for 1 hour followed by heat inactivation. Then, the fragment and vector were mixed in a 5:1 ratio and ligated with T4 DNA Ligase (NEB, M0202L) overnight at 16˚C. The vector was then transformed into One Shot TOP10 chemically competent cells (Invitrogen, C404003) following the product protocol. The transformed competent cells were plated on LB plates with 100 µg/mL ampicillin (IBI Scientific, IB02040) and grown overnight at 37˚C. The following morning colonies were screened using DreamTaq DNA Polymerase (Thermo, EP0702) and the forward primer AAAAGAATTCATGGCGCTCTCACTCAGGCCATA and the reverse primer AAAATCTAGACAGAAGGCAAGGGAGCGCAGGAA. Positive colonies were grown in liquid LB with 100 µg/mL ampicillin overnight at 37˚C. Plasmid DNA was isolated from bacterial cells and sequenced.

Plasmids containing the ARPC4 DNA were then transformed into *Chlamydomonas* cells. First, a 5 mL liquid culture of *arpc4* mutant cells was grown overnight with agitation and constant light in TAP. The following day 25 mL of TAP was brought to an OD_{730} of 0.1

using the 5 mL culture. This was incubated with agitation and under constant light overnight. The culture reached an OD_{730} of 0.3-0.4 for the transformation. Once this occurred, the plasmid was linearized using ScaI (NEB, R3122L). Meanwhile, the 25 mL culture was centrifuged at 500xg to pellet the cells. The TAP was removed and replaced with 5 mL of Max Efficiency Transformation Reagent for Algae (Invitrogen, 100021485). This was repeated 2 times. After the final centrifugation, the cells were resuspended in 250 μL of Max Efficiency Transformation Reagent. This was then split in two. 1000 μg of linearized plasmid was added to each. This was then electroporated using a BioRad Electroporator at 500V, 50 μF, and 800 Ω in a 4 mm cuvette. The cells were removed from the cuvette following electroporation, suspended in 7 mL of TAP + 40 mM sucrose, and incubated overnight in the dark. The following day the cells were pelleted and streaked on TAP + Zeocin (10 μg/mL) plates, then incubated in constant light for approximately 1 week or until colonies formed.

Colonies were screened using DreamTaq DNA Polymerase (Thermo, EP0702) and the same primers as above. Positive colonies were streaked onto new plates and allowed to grow up. Expression of ARPC4-V5 was confirmed with a western blot. Liquid cultures of cells were grown overnight, then pelleted at 500 xg for 1 minute. Cells were resuspended in lysis buffer [5% glycerol (), 1% NP-40 (), 1mM DTT (), 1X protease inhibitors (Thermo, 1861281)] and lysed using bead beating. Cell debris was spun down at 14000xg for 15 minutes. An equal amount of protein was loaded to a NuPAGE 10% Bis-Tris gel (Invitrogen, NP0316). The resulting gel was transferred to PVDF membrane (Millipore, IPVH00010) which was then blocked with 5% milk in PBST. The blot was incubated with rabbit anti-V5 primary antibody (Cell Signaling, D3H8Q) diluted to 1:1000 in 1% BSA, 1% milk overnight at 4˚C to probe for V5. The following day blots were washed 3 times in 1X PBST, then incubated with HRP-conjugated goat anti-rabbit secondary (Thermo, G-21234) diluted to 1:5000 in 1% milk 1% BSA for 1 hour at room temperature. The blot was washed again 3 times with 1X PBST. Then the blot was probed with West Pico Chemiluminescent Pico Substrate (Invitrogen, 34580). The membrane was stripped of antibody and total protein was determined with Coomassie

(Sigma, B0149) staining. Band intensity was measured in ImageJ and normalized to total protein.

Click-iT OPP Protein Synthesis Assay (Invitrogen, C10457):
Cells were grown overnight in TAP. The following day cells were deciliated as described above and allowed to regrow either with or without cycloheximide (10μM) to block protein synthesis. 1 hour following deciliation, cells were mounted onto poly-lysine (EMS, 19321-B) coverslips. Cells on coverslips were incubated with Click-iT OPP reagent containing the O-propargyl-puromycin (OPP) which is incorporated into nascent polypeptides for 30 minutes. OPP was removed and cells were washed once in PBS. Cells were then fixed with 4% PFA (EMS, 15710) in 1X HEPES (Sigma, 391338) for 15 minutes, then permeabilized with 0.5% Triton-X 100 in PBS for 15 minutes. Cells were washed twice with PBS. Detection was performed by incubating coverslips with 1X Click-iT OPP Reaction Cocktail that includes 1X Click-iT OPP Reaction Buffer, 1X Copper Protectant, 1X Alexafluor picolyl azide, and 1X Click-iT Reaction Buffer Additive for 30 minutes protected from light. This was removed and Reaction Rinse Buffer was added for 5 minutes. This was removed, coverslips were washed twice with PBS, allowed to dry fully, and mounted with Fluormount-G (Invitrogen, 00-4958-02).

Cells were then imaged on a Nikon Eclipse Ti-E microscope with a Yokogawa, two-camera, CSU0W1 spinning disk system with a Nikon LU-N4 laser launch at room temperature with a 100X oil-immersion objective (1.45 numerical aperture). Images were acquired using Nikon Elements and analyzed using ImageJ as follows. Z-stacks were obtained then combined into sum slices for quantification of maximum intensity projections for viewing. In the summed images, the integrated density and area of individual cells was obtained, as well as the background fluorescence. These were then used to calculate CTCF, which was then normalized to the “Pre” sample for each cell.

Phalloidin staining and quantification:
Procedure adapted from (Craig et al., 2019). Cells were mounted onto poly-lysine coverslips and fixed with fresh 4% paraformaldehyde in 1X HEPES. Coverslips with

cells were then permeabilized with acetone and allowed to dry. Cells were rehydrated with PBS, stained with Phalloidin-Atto 488 (Sigma, 49409-10NMOL), and finally washed with PBS and allowed to dry before mounting with Fluoromount-G (Craig et al., 2019). Cells were imaged using the Nikon Spinning Disk Confocal discussed above. Z-stacks were obtained in Nikon Elements, and in ImageJ, maximum intensity projections were created for viewing. Publication quality images were acquired using a Zeiss LSM880 with Airyscan with two photomultiplier tubes, a GaAsP detector, and a transmitted light detector. Images were taken at room temperature using a 100x (1.46 numerical aperture) oil-immersion lens. Images were acquired using Zeiss Zen (black edition) and prepared for publication using ImageJ.

Electron microscopy:

Cells (1mL of each strain) were deciliated via pH shock by adding 115µL of 0.5N acetic acid for 45 seconds followed by 120µL of 0.5N KOH to bring cells back to neutral pH. Cells were allowed to regrow cilia for 30 minutes. A pre sample and a 30-minute post-deciliation sample were fixed in an equal volume of 2% glutaraldehyde for 20 minutes at room temperature. Samples were then pelleted using gentle centrifugation for 10 minutes. The supernatant was removed, and cells were resuspended in 1% glutaraldehyde, 20mM sodium cacodylate. Cells were incubated for 1 hour at room temperature and then overnight at 4º Celsius. This protocol was first reported in (Dentler and Adams, 1992). A JEOL JEM-1400 Transmission Electron Microscope equipped with a Lab6 gun was used to acquire images. Images were quantified in ImageJ.

SAG1-HA Immunofluorescence:

Procedure adapted from (Belzile et al., 2013). SAG1-HA cells were grown overnight in M-N media to induce gametes. These cells were then treated with either 10µM LatB for 1 hour or 250µM CK-666 for 2 hours. Following treatment, mating was induced by adding db-cAMP (ChemCruz, Santa Cruz, CA) to a final concentration of 13.5mM and incubating for 30 minutes. Cells were adhered to coverslips and fixed with methanol. Cells were then dried and rehydrated with PBS and incubated with 100% block (5% BSA, 1% fish gelatin) for 30 minutes. The 100% block was replaced with new 100%

block containing 10% normal goat serum for another 30-minute incubation. The rabbit anti-HA primary antibody (Cell Signaling, C29F4) was diluted 1:1000 in 20% block in PBS. Coverslips were incubated at 4º Celsius in a humidified chamber overnight. The primary antibody was removed and washed away with 3 10-minute PBS washes. The Alexafluor 488-conjugated goat anti-rabbit secondary (Invitrogen, A-10088) was added, and coverslips were incubated at room temperature for 1 hour. This was followed by 3 more 10-minute PBS washes and finally mounting with Fluoromount-G. Cells were imaged using the Nikon Spinning Disk Confocal microscope, lens, and software discussed previously. Z-stacks were obtained, and maximum intensity projections were created for visualization and sum slices were created for quantification using ImageJ.

Images were quantified by using line scans from the apex of the cells to the basal region of the cells farthest away from the apex. Line scans were then normalized, and background subtracted before being combined into single graphs. Using the line scans, the intensity of signal at the basal region of the cells was subtracted from the signal at the apical region. Finally, cells with a difference over 30 were considered to be apically enriched and this was quantified as percentage of cells with apical staining.

SAG1-HA western blot:

Procedure adapted from (Belzile et al., 2013). SAG1-HA cells were grown overnight in M-N media to induce gametes. These cells were then treated with either 10μM LatB for 1 hour or 250μM CK-666 for 2 hours. Following treatment, mating induction was done by adding db-cAMP (ChemCruz, SC-201567B) to a final concentration of 13.5mM and incubating for 10 minutes. Cells were then treated with 0.01% trypsin (Sigma, T8003) for 5 minutes, pelleted (at 500xg for 2 minutes), resuspended in lysis buffer (5% glycerol, 1% NP-40, 1mM DTT, 1X protease inhibitors), and then lysed with bead beating. A western blot was carried out as described above using rabbit anti-HA primary antibody (Cell Signaling, C29F4) diluted to 1:1000 in 1% BSA, 1% milk and HRP-conjugated goat anti-rabbit secondary (Thermo, G-21234) diluted to 1:5000 in 1% milk 1% BSA.

Chlamydomonas mating:

SAG1-HA (mating type plus) and *arpc4* mutants (mating type minus) were incubated in M-N media (minimal media without nitrogen) for 8 hours to induce gamete formation. The two liquid cultures were then mixed and allowed to incubate under white light without agitation overnight. The next day the pellicle was transferred to a 4% TAP plate. This was incubated under white light overnight, then covered in foil and placed in a dark drawer for 5-7 days. After 5-7 days, the zygospores were transferred individually and manually from the 4% TAP plate to a 1.5% TAP plate using a dissecting microscope (Zeiss). This plate was incubated in white light overnight. The following day the zygospores that had split into tetrads were dissected. These were then allowed to grow before being screened via PCR for a colony containing the *arpc4* mutant and SAG1-HA.

Membrane stain:

Cells were treated with either PitStop2 (Sigma, SML1169) or Dynasore hydrate (Sigma, D7693) for 1 hour. Meanwhile, FM 4-64FX membrane stain (Invitrogen, F34653) was diluted to a stock concentration of 200μg/mL. Cells were adhered to poly-lysine coverslips. After a 5-minute incubation, cells were tilted off and 5μg/mL of ice-cold stain in Hank's Buffered Salt Solution (HBSS) without magnesium or calcium was added for 1 minute. The stain was tilted off and cells were fixed with ice cold 4% paraformaldehyde in HBSS without magnesium or calcium for 15 minutes. Coverslips were then rinsed 3 times for 10 minutes each in ice cold HBSS without magnesium or calcium. Finally, cells were mounted with Fluoromount-G and imaged using the Nikon Spinning Disk Confocal microscope, lens, and software discussed previously. Z-stacks were taken and combined into sum projections using ImageJ. The background corrected total cell fluorescence was then calculated by taking the integrated density and subtracting the sum of the area and the mean background intensity.

Biotin ciliary isolation:

Procedure adapted from (Dentler, 2013). 100mL of cells were grown in TAP for each condition until they reached an OD_{730} of 1.6 or above. Cells were then spun down and resuspended in M1 media and allowed to grow overnight. The next day cells were spun

down at 1800rpm for 3 minutes and resuspended in HM Media (10mM HEPES, 5mM MgSO4, pH 7.2). Solid biotin (Thermo, 21335) was added to 20μg/mL for each strain and incubated for 5 minutes with agitation. Cells were diluted with 10 volumes of fresh M1 media before being spun down at 1800rpm for 3 minutes. After all cells were pelleted, they were washed with fresh M1 media three times. A pre sample was set aside (100mL) and the remainder of the cells were resuspended in 4.5 pH M1 media for 45 seconds before being spun down again at 1800rpm for 3 minutes. Cells were then resuspended in pH 7.0 media and allowed to regrow their cilia for 4 hours. A sample was taken pre-biotinylation to use as a control for non-specific streptavidin binding.

Meanwhile, the cilia were isolated from the pre sample. The samples were centrifuged for 3 minutes at 1800rpm. Supernatant was drained and each pellet was resuspended in 2 mL of 10mM HEPES (pH 7.4). This was repeated 2 times. Then each pellet was resuspended in 1 mL of fresh ice-cold 4% HMDS (10mM HEPES pH 7.4, 5mM MgSO4, 1mM DTT, 4% w/v sucrose). Cells were deciliated by incubating with 25mM dibucaine for 2 minutes. Then ice cold HMDS with 0.5mM EGTA was added (1mL per 1.5mL of cells). This was then centrifuged for 3 minutes at 1800rpm. Supernatant was collected for each sample. Then HMDS with 25% sucrose was layered beneath the supernatant (2 mL of 25% HMDS for 1mL of supernatant) to create an interface. This was centrifuged at 4º Celsius for 10 min at 2400rpm with no brake to avoid disrupting interface where cilia should now be located. Cilia were removed, pelleted at 21130xg for 30 minutes, then resuspended in lysis buffer (5% glycerol, 1% NP-40, 1mM DTT, 1X protease inhibitors). This was repeated with the post samples 4 hours following deciliation. Protein gel electrophoresis and blotting was performed as described as above using an HRP-conjugated streptavidin (Thermo, S911).

Homology modeling and sequence studies:

Arp2/3 homology model was created using the Modeller plugin in UCSF Chimera. The template used was 1U2Z (Nolen et al., 2004; Pettersen et al., 2004; Sali and Blundell, 1993). Percent identity and similarity is calculated in relation to the human Arp2/3 complex members using a MUSCLE alignment in Geneious. The homology model was

visualized and conservation was mapped on the protein surface using Chimera (Pettersen et al., 2004).

Statistical analysis:

Statistical analyses were done if GraphPad Prism Version 9. Superplots were created using the method in (Lord et al., 2020). For any experiments comparing 2 groups (**Fig. 3.3D, 3.5C, and 3.5E**) an unpaired student's t-test comparing the means of the 3 biological replicates was used to determine P value. For experiments comparing multiple samples (**Fig. 3.1A, 3.1B, 3.1C, 3.1D, 3.2B, 3.2C, 3.3B, and 3.6E**), an ANOVA was used comparing the means of the 3 biological replicates. This was followed by a multiple comparisons test (Tukey's)**.** For any percentages shown (**Fig. 3.7D**), Chi-squared analysis was performed. For all experiments **** $P<0.0001$, *** $P<0.001$, ** $P<0.01$, * $P<0.1$ with p values listed in the fig. legends.

ACKNOWLEDGEMENTS:

Our gratitude to William Dentler for providing expertise especially in looking at the electron microscopy images and helpful advice, William Snell for providing the SAG1-HA strain, Henry Higgs for his feedback on version 1 of the manuscript, Ann Lavanway for assistance with microscopy, and the Avasthi lab for their help throughout the project. We also thank David Sept and Courtney M Schroeder for the help with the original version of this paper and for providing helpful comments.

We thank our funding sources including the Madison and Lila Self Graduate Fellowship at the University of Kansas Medical Center and the MIRA (R35GM128702). Finally, we thank the BioMT core at Dartmouth College (NIH/NIGMS COBRE award P20-GM113132), the Genomics and Molecular Biology Shared Resources Core (NCI Cancer Center Support Grant 5P30CA023108-37), and the KIDDRC NIH U54 HD 090216 at the University of Kansas Medical Center, Kansas City, KS 66160.

The authors have no additional competing financial interests.

AUTHOR CONTRIBUTIONS:

Brae M Bigge: Conceptualization, data curation, formal analysis, investigation, methodology, visualization, writing (original draft), writing (review & editing)
Nicholas E Rosenthal: Data curation, formal analysis, writing (review & editing)
Prachee Avasthi: Conceptualization, funding acquisition, project administration, resources, supervision

REFERENCES:

Adams, A.E., Pringle, J.R., 1984. Relationship of actin and tubulin distribution to bud growth in wild-type and morphogenetic-mutant Saccharomyces cerevisiae. J. Cell Biol. 98, 934–945. https://doi.org/10.1083/jcb.98.3.934

Aghamohammadzadeh, S., Ayscough, K.R., 2009. Differential requirements for actin during yeast and mammalian endocytosis. Nat. Cell Biol. 11, 1039–1042. https://doi.org/10.1038/ncb1918

Avasthi, P., Onishi, M., Karpiak, J., Yamamoto, R., Mackinder, L., Jonikas, M.C., Sale, W.S., Shoichet, B., Pringle, J.R., Marshall, W.F., 2014. Actin Is Required for IFT Regulation in Chlamydomonas reinhardtii. Curr. Biol. 24, 2025–2032. https://doi.org/10.1016/j.cub.2014.07.038

Ayscough, K.R., Stryker, J., Pokala, N., Sanders, M., Crews, P., Drubin, D.G., 1997. High rates of actin filament turnover in budding yeast and roles for actin in establishment and maintenance of cell polarity revealed using the actin inhibitor latrunculin-A. J. Cell Biol. 137, 399–416. https://doi.org/10.1083/jcb.137.2.399

Basu, R., Munteanu, E.L., Chang, F., 2014. Role of turgor pressure in endocytosis in fission yeast. Mol. Biol. Cell 25, 679–687. https://doi.org/10.1091/mbc.E13-10-0618

Belzile, O., Hernandez-Lara, C.I., Wang, Q., Snell, W.J., 2013. Regulated membrane protein entry into flagella is facilitated by cytoplasmic microtubules and does not require IFT. Curr. Biol. CB 23, 1460–1465. https://doi.org/10.1016/j.cub.2013.06.025

Bouck, G.B., 1971. THE STRUCTURE, ORIGIN, ISOLATION, AND COMPOSITION OF THE TUBULAR MASTIGONEMES OF THE OCHROMONAS FLAGELLUM. J. Cell Biol. 50, 362–384. https://doi.org/10.1083/jcb.50.2.362

Campellone, K., Welch, M., 2010. A nucleator arms race: cellular control of actin assembly. Nat. Rev. Mol. Cell Biol. 11, 237–251.

Carlsson, A.E., Bayly, P.V., 2014. Force generation by endocytic actin patches in budding yeast. Biophys. J. 106, 1596–1606. https://doi.org/10.1016/j.bpj.2014.02.035

Cheng, X., Liu, G., Ke, W., Zhao, L., Lv, B., Ma, X., Xu, N., Xia, X., Deng, X., Zheng, C., Huang, K., 2017. Building a multipurpose insertional mutant library for forward and reverse genetics in Chlamydomonas. Plant Methods 13, 36. https://doi.org/10.1186/s13007-017-0183-5

Cochilla, A.J., Angleson, J.K., Betz, W.J., 1999. MONITORING SECRETORY MEMBRANE WITH FM1-43 FLUORESCENCE. Annu. Rev. Neurosci. 22, 1–10. https://doi.org/10.1146/annurev.neuro.22.1.1

Craig, E.W., Mueller, D.M., Bigge, B.M., Schaffer, M., Engel, B.D., Avasthi, P., 2019. The elusive actin cytoskeleton of a green alga expressing both conventional and divergent actins. Mol. Biol. Cell mbc.E19-03-0141. https://doi.org/10.1091/mbc.E19-03-0141

Dentler, W., 2013. A Role for the Membrane in Regulating Chlamydomonas Flagellar Length. PLOS ONE 8, e53366. https://doi.org/10.1371/journal.pone.0053366

Dentler, W.L., Adams, C., 1992. Flagellar microtubule dynamics in Chlamydomonas: cytochalasin D induces periods of microtubule shortening and elongation; and colchicine

induces disassembly of the distal, but not proximal, half of the flagellum. J. Cell Biol. 117, 1289–1298. https://doi.org/10.1083/jcb.117.6.1289

Diener, D.R., Lupetti, P., Rosenbaum, J.L., 2015. Proteomic analysis of isolated ciliary transition zones reveals the presence of ESCRT proteins. Curr. Biol. CB 25, 379–384. https://doi.org/10.1016/j.cub.2014.11.066

Farina, F., Gaillard, J., Guérin, C., Couté, Y., Sillibourne, J., Blanchoin, L., Théry, M., 2016. The centrosome is an actin-organizing centre. Nat. Cell Biol. 18, 65–75. https://doi.org/10.1038/ncb3285

Gachet, Y., Hyams, J.S., 2005. Endocytosis in fission yeast is spatially associated with the actin cytoskeleton during polarised cell growth and cytokinesis. J. Cell Sci. 118, 4231–4242. https://doi.org/10.1242/jcs.02530

Goode, B.L., Eskin, J.A., Wendland, B., 2015. Actin and endocytosis in budding yeast. Genetics 199, 315–358. https://doi.org/10.1534/genetics.112.145540

Gournier, H., Goley, E.D., Niederstrasser, H., Trinh, T., Welch, M.D., 2001. Reconstitution of Human Arp2/3 Complex Reveals Critical Roles of Individual Subunits in Complex Structure and Activity. Mol. Cell 8, 1041–1052. https://doi.org/10.1016/S1097-2765(01)00393-8

Hetrick, B., Han, M.S., Helgeson, L.A., Nolen, B.J., 2013. Small Molecules CK-666 and CK-869 Inhibit Actin-Related Protein 2/3 Complex by Blocking an Activating Conformational Change. Chem. Biol. 20, 701–712. https://doi.org/10.1016/j.chembiol.2013.03.019

Hirono, M., Uryu, S., Ohara, A., Kato-Minoura, T., Kamiya, R., 2003. Expression of conventional and unconventional actins in Chlamydomonas reinhardtii upon deflagellation and sexual adhesion. Eukaryot. Cell 2, 486–493. https://doi.org/10.1128/ec.2.3.486-493.2003

Hu Qicong, Milenkovic Ljiljana, Jin Hua, Scott Matthew P., Nachury Maxence V., Spiliotis Elias T., Nelson W. James, 2010. A Septin Diffusion Barrier at the Base of the Primary Cilium Maintains Ciliary Membrane Protein Distribution. Science 329, 436–439. https://doi.org/10.1126/science.1191054

Inoue, D., Obino, D., Pineau, J., Farina, F., Gaillard, J., Guerin, C., Blanchoin, L., Lennon-Duménil, A.-M., Théry, M., 2019. Actin filaments regulate microtubule growth at the centrosome. EMBO J. 38. https://doi.org/10.15252/embj.201899630

Jack, B., Avasthi, P., 2018. Erratum to: Chemical Screening for Flagella-Associated Phenotypes in Chlamydomonas reinhardtii. Methods Mol. Biol. Clifton NJ 1795, E1. https://doi.org/10.1007/978-1-4939-7874-8_19

Jack, B., Mueller, D.M., Fee, A.C., Tetlow, A.L., Avasthi, P., 2019. Partially Redundant Actin Genes in Chlamydomonas Control Transition Zone Organization and Flagellum-Directed Traffic. Cell Rep. 27, 2459-2467.e3. https://doi.org/10.1016/j.celrep.2019.04.087

Jin, H., White, S.R., Shida, T., Schulz, S., Aguiar, M., Gygi, S.P., Bazan, J.F., Nachury, M.V., 2010. The conserved Bardet-Biedl syndrome proteins assemble a coat that traffics

membrane proteins to cilia. Cell 141, 1208–1219. https://doi.org/10.1016/j.cell.2010.05.015

Kaplan, O.I., Doroquez, D.B., Cevik, S., Bowie, R.V., Clarke, L., Sanders, A.A.W.M., Kida, K., Rappoport, J.Z., Sengupta, P., Blacque, O.E., 2012. Endocytosis Genes Facilitate Protein and Membrane Transport in C. elegans Sensory Cilia. Curr. Biol. 22, 451–460. https://doi.org/10.1016/j.cub.2012.01.060

Kato-Minoura, T., Uryu, S., Hirono, M., Kamiya, R., 1998. Highly divergent actin expressed in a Chlamydomonas mutant lacking the conventional actin gene. Biochem. Biophys. Res. Commun. 251, 71–76. https://doi.org/10.1006/bbrc.1998.9373

Kiesel, P., Alvarez Viar, G., Tsoy, N., Maraspini, R., Gorilak, P., Varga, V., Honigmann, A., Pigino, G., 2020. The molecular structure of mammalian primary cilia revealed by cryo-electron tomography. Nat. Struct. Mol. Biol. https://doi.org/10.1038/s41594-020-0507-4

Kim, J., Lee, J.E., Heynen-Genel, S., Suyama, E., Ono, K., Lee, K., Ideker, T., Aza-Blanc, P., Gleeson, J.G., 2010. Functional genomic screen for modulators of ciliogenesis and cilium length. Nature 464, 1048–1051. https://doi.org/10.1038/nature08895

Langousis, G., Shimogawa, M.M., Saada, E.A., Vashisht, A.A., Spreafico, R., Nager, A.R., Barshop, W.D., Nachury, M.V., Wohlschlegel, J.A., Hill, K.L., 2016. Loss of the BBSome perturbs endocytic trafficking and disrupts virulence of Trypanosoma brucei. Proc. Natl. Acad. Sci. U. S. A. 113, 632–637. https://doi.org/10.1073/pnas.1518079113

Lefebvre, P.A., 1995. Flagellar amputation and regeneration in Chlamydomonas, in: Methods in Cell Biology. Elsevier, pp. 3–7.

Lefebvre, P.A., Nordstrom, S.A., Moulder, J.E., Rosenbaum, J.L., 1978. Flagellar elongation and shortening in Chlamydomonas. IV. Effects of flagellar detachment, regeneration, and resorption on the induction of flagellar protein synthesis. J. Cell Biol. 78, 8–27. https://doi.org/10.1083/jcb.78.1.8

Li, X., Patena, W., Fauser, F., Jinkerson, R.E., Saroussi, S., Meyer, M.T., Ivanova, N., Robertson, J.M., Yue, R., Zhang, R., Vilarrasa-Blasi, J., Wittkopp, T.M., Ramundo, S., Blum, S.R., Goh, A., Laudon, M., Srikumar, T., Lefebvre, P.A., Grossman, A.R., Jonikas, M.C., 2019. A genome-wide algal mutant library and functional screen identifies genes required for eukaryotic photosynthesis. Nat. Genet. 51, 627–635. https://doi.org/10.1038/s41588-019-0370-6

Lord, S.J., Velle, K.B., Mullins, R.D., Fritz-Laylin, L.K., 2020. SuperPlots: Communicating reproducibility and variability in cell biology. J. Cell Biol. 219. https://doi.org/10.1083/jcb.202001064

Macia, E., Ehrlich, M., Massol, R., Boucrot, E., Brunner, C., Kirchhausen, T., 2006. Dynasore, a cell-permeable inhibitor of dynamin. Dev. Cell 10, 839–850. https://doi.org/10.1016/j.devcel.2006.04.002

Milenkovic, L., Scott, M.P., Rohatgi, R., 2009. Lateral transport of Smoothened from the plasma membrane to the membrane of the cilium. J. Cell Biol. 187, 365–374. https://doi.org/10.1083/jcb.200907126

Molla-Herman, A., Ghossoub, R., Blisnick, T., Meunier, A., Serres, C., Silbermann, F., Emmerson, C., Romeo, K., Bourdoncle, P., Schmitt, A., Saunier, S., Spassky, N., Bastin, P., Benmerah, A., 2010. The ciliary pocket: an endocytic membrane domain at the base of primary and motile cilia. J. Cell Sci. 123, 1785–1795. https://doi.org/10.1242/jcs.059519

Monis, W.J., Faundez, V., Pazour, G.J., 2017. BLOC-1 is required for selective membrane protein trafficking from endosomes to primary cilia. J. Cell Biol. 216, 2131–2150. https://doi.org/10.1083/jcb.201611138

Mooren Olivia L., Schafer Dorothy A., 2009. Constricting membranes at the nano and micro scale. Proc. Natl. Acad. Sci. 106, 20559–20560. https://doi.org/10.1073/pnas.0911630106

Nachury, M.V., Loktev, A.V., Zhang, Q., Westlake, C.J., Peränen, J., Merdes, A., Slusarski, D.C., Scheller, R.H., Bazan, J.F., Sheffield, V.C., Jackson, P.K., 2007. A Core Complex of BBS Proteins Cooperates with the GTPase Rab8 to Promote Ciliary Membrane Biogenesis. Cell 129, 1201–1213. https://doi.org/10.1016/j.cell.2007.03.053

Nachury, M.V., Seeley, E.S., Jin, H., 2010. Trafficking to the ciliary membrane: how to get across the periciliary diffusion barrier? Annu. Rev. Cell Dev. Biol. 26, 59–87. https://doi.org/10.1146/annurev.cellbio.042308.113337

Nolen, B.J., Littlefield, R.S., Pollard, T.D., 2004. Crystal structures of actin-related protein 2/3 complex with bound ATP or ADP. Proc. Natl. Acad. Sci. U. S. A. 101, 15627. https://doi.org/10.1073/pnas.0407149101

Onishi, M., Pecani, K., Jones, T. th, Pringle, J.R., Cross, F.R., 2018. F-actin homeostasis through transcriptional regulation and proteasome-mediated proteolysis. Proc Natl Acad Sci U A 115, E6487-e6496. https://doi.org/10.1073/pnas.1721935115

Onishi, M., Pringle, J.R., Cross, F.R., 2016. Evidence That an Unconventional Actin Can Provide Essential F-Actin Function and That a Surveillance System Monitors F-Actin Integrity in Chlamydomonas. Genetics 202, 977–96. https://doi.org/10.1534/genetics.115.184663

Onishi, M., Umen, J.G., Cross, F.R., Pringle, J.R., 2019. Cleavage-furrow formation without F-actin in Chlamydomonas. bioRxiv 789016. https://doi.org/10.1101/789016

Papermaster, D.S., Schneider, B.G., Besharse, J.C., 1985. Vesicular transport of newly synthesized opsin from the Golgi apparatus toward the rod outer segment. Ultrastructural immunocytochemical and autoradiographic evidence in Xenopus retinas. Invest. Ophthalmol. Vis. Sci. 26, 1386–1404.

Park, R.J., Shen, H., Liu, L., Liu, X., Ferguson, S.M., De Camilli, P., 2013. Dynamin triple knockout cells reveal off target effects of commonly used dynamin inhibitors. J. Cell Sci. 126, 5305–5312. https://doi.org/10.1242/jcs.138578

Park, T.J., Mitchell, B.J., Abitua, P.B., Kintner, C., Wallingford, J.B., 2008. Dishevelled controls apical docking and planar polarization of basal bodies in ciliated epithelial cells. Nat. Genet. 40, 871–879. https://doi.org/10.1038/ng.104

Pasquale, S.M., Goodenough, U.W., 1987. Cyclic AMP functions as a primary sexual signal in gametes of Chlamydomonas reinhardtii. J. Cell Biol. 105, 2279–2292. https://doi.org/10.1083/jcb.105.5.2279

Pedersen, L.B., Rosenbaum, J.L., 2008. Intraflagellar transport (IFT) role in ciliary assembly, resorption and signalling. Curr. Top. Dev. Biol. 85, 23–61. https://doi.org/10.1016/S0070-2153(08)00802-8

Pettersen, E.F., Goddard, T.D., Huang, C.C., Couch, G.S., Greenblatt, D.M., Meng, E.C., Ferrin, T.E., 2004. UCSF Chimera--a visualization system for exploratory research and analysis. J. Comput. Chem. 25, 1605–1612. https://doi.org/10.1002/jcc.20084

Ranjan, P., Awasthi, M., Snell, W.J., 2019. Transient Internalization and Microtubule-Dependent Trafficking of a Ciliary Signaling Receptor from the Plasma Membrane to the Cilium. Curr. Biol. 29, 2942-2947.e2. https://doi.org/10.1016/j.cub.2019.07.022

Robinson, R.C., Turbedsky, K., Kaiser, D.A., Marchand, J.-B., Higgs, H.N., Choe, S., Pollard, T.D., 2001. Crystal Structure of Arp2/3 Complex. Science 294, 1679. https://doi.org/10.1126/science.1066333

Rohatgi, R., Snell, W.J., 2010. The ciliary membrane. Curr. Opin. Cell Biol. 22, 541–546. https://doi.org/10.1016/j.ceb.2010.03.010

Rosenbaum, J.L., Moulder, J.E., Ringo, D.L., 1969. Flagellar elongation and shortening in Chlamydomonas. The use of cycloheximide and colchicine to study the synthesis and assembly of flagellar proteins. J. Cell Biol. 41, 600–619. https://doi.org/10.1083/jcb.41.2.600

Saito, M., Otsu, W., Hsu, K.-S., Chuang, J.-Z., Yanagisawa, T., Shieh, V., Kaitsuka, T., Wei, F.-Y., Tomizawa, K., Sung, C.-H., 2017. Tctex-1 controls ciliary resorption by regulating branched actin polymerization and endocytosis. EMBO Rep. 18, 1460–1472. https://doi.org/10.15252/embr.201744204

Sali, A., Blundell, T.L., 1993. Comparative protein modelling by satisfaction of spatial restraints. J. Mol. Biol. 234, 779–815. https://doi.org/10.1006/jmbi.1993.1626

Spector, I., Shochet, N.R., Blasberger, D., Kashman, Y., 1989. Latrunculins—novel marine macrolides that disrupt microfilament organization and affect cell growth: I. Comparison with cytochalasin D. Cell Motil. 13, 127–144. https://doi.org/10.1002/cm.970130302

von Loeffelholz, O., Purkiss, A., Cao, L., Kjaer, S., Kogata, N., Romet-Lemonne, G., Way, M., Moores, C.A., 2020. Cryo-EM of human Arp2/3 complexes provides structural insights into actin nucleation modulation by ARPC5 isoforms. bioRxiv 2020.05.01.071704. https://doi.org/10.1101/2020.05.01.071704

Willox, A.K., Sahraoui, Y.M.E., Royle, S.J., 2014. Non-specificity of Pitstop 2 in clathrin-mediated endocytosis. Biol. Open 3, 326–331. https://doi.org/10.1242/bio.20147955

Wingfield, J.L., Mengoni, I., Bomberger, H., Jiang, Y.-Y., Walsh, J.D., Brown, J.M., Picariello, T., Cochran, D.A., Zhu, B., Pan, J., Eggenschwiler, J., Gaertig, J., Witman, G.B., Kner, P., Lechtreck, K., 2017. IFT trains in different stages of assembly queue at

the ciliary base for consecutive release into the cilium. eLife 6, e26609. https://doi.org/10.7554/eLife.26609

Winter, D.C., Choe, E.Y., Li, R., 1999. Genetic dissection of the budding yeast Arp2/3 complex: a comparison of the in vivo and structural roles of individual subunits. Proc. Natl. Acad. Sci. U. S. A. 96, 7288–7293. https://doi.org/10.1073/pnas.96.13.7288

Wood, C.R., Rosenbaum, J.L., 2014. Proteins of the Ciliary Axoneme Are Found on Cytoplasmic Membrane Vesicles during Growth of Cilia. Curr. Biol. 24, 1114–1120. https://doi.org/10.1016/j.cub.2014.03.047

Wu, C.-T., Chen, H.-Y., Tang, T.K., 2018. Myosin-Va is required for preciliary vesicle transportation to the mother centriole during ciliogenesis. Nat. Cell Biol. 20, 175–185. https://doi.org/10.1038/s41556-017-0018-7

Yamada, H., Abe, T., Li, S.-A., Masuoka, Y., Isoda, M., Watanabe, M., Nasu, Y., Kumon, H., Asai, A., Takei, K., 2009. Dynasore, a dynamin inhibitor, suppresses lamellipodia formation and cancer cell invasion by destabilizing actin filaments. Biochem. Biophys. Res. Commun. 390, 1142–1148. https://doi.org/10.1016/j.bbrc.2009.10.105

Zuo, X., Guo, W., Lipschutz, J.H., 2009. The Exocyst Protein Sec10 Is Necessary for Primary Ciliogenesis and Cystogenesis In Vitro. Mol. Biol. Cell 20, 2522–2529. https://doi.org/10.1091/mbc.e08-07-0772

CHAPTER 4:
Lithium-induced ciliary lengthening sparks Arp2/3 complex-dependent endocytosis

Published as:

Lithium-induced ciliary lengthening sparks Arp2/3 complex-dependent endocytosis

[1]Brae M Bigge, Prachee Avasthi*

[1]Biochemistry and Cell Biology, Geisel School of Medicine, Dartmouth College, Hanover, NH

doi: https://doi.org/10.1101/2022.04.18.488674

ABSTRACT

Ciliary length is highly regulated, but can be disrupted by lithium, which causes ciliary elongation across cell types and organisms. We used the algal system *Chlamydomonas reinhardtii* to investigate the mechanism behind lithium-induced ciliary elongation. Protein synthesis is not required for lengthening and the target of lithium, GSK3, has substrates that can influence membrane dynamics. Further, ciliary assembly requires a supply of ciliary membrane as well as protein. Lithium-treated cilia elongate normally with Brefeldin treatment, but Dynasore treatment produced defective lengthening suggesting a source of membrane from the cell surface rather than the Golgi. Genetic or chemical perturbation of the Arp2/3 complex or dynamin, required for endocytosis, blocks lithium-induced ciliary lengthening. Finally, we found an increase in Arp2/3 complex- and endocytosis-dependent actin filaments near the ciliary base upon lithium treatment. Our results identify a mechanism for lithium-mediated cilium lengthening and demonstrate the endocytic pathway for cilium membrane supply in algae is likely a conserved mechanism given lithium's conserved effects across organisms.

INTRODCUTION

The plasma membrane-ensheathed, microtubule-based cilium is important for signaling and motility, and defects in this organelle can lead to a large number of diseases termed ciliopathies (Reiter and Leroux 2017). Thus, ciliary length is tightly regulated across cell types. However, the mechanisms by which such regulation occurs are still being investigated. Many studies have focused on perturbations that result in shorter cilia, but the relatively infrequent examples of ciliary lengthening can hold the keys to uncovering regulatory mechanisms.

An example of a perturbation that increases ciliary length is lithium. The ciliary elongation elicited by lithium treatment is ubiquitous across cell types, occurring in *Chlamydomonas* (Nakamura, Takino, and Kojima 1987; Wilson and Lefebvre 2004) (**Fig. 4.1**), chondrocytes (Soave et al. 2022; Thompson et al. 2016), ependymal cells (Kong et al. 2015), human fibroblast-like synoviocytes (Ou et al. 2009), fibroblasts (Ou et al. 2012), mouse brains (Miyoshi et al. 2009), NIH3T3 cells (Miyoshi et al. 2009), human induced pluripotent stem cell-derived neurons (Miki et al. 2019), Sertoli cells from pig testes (Ou et al. 2014), and others. Lithium is thought to target GSK3 (Wilson and Lefebvre 2004), but the mechanism by which this causes ciliary elongation are relatively unknown.

Much of what we know about ciliary length regulation comes from studies in the unicellular green algae *Chlamydomonas reinhardtii*. *Chlamydomonas* serves as a powerful model for studying length regulation and assembly of cilia as it has two persistent and symmetric cilia that are structurally and mechanistically similar to the cilia of mammalian cells. The cilia of *Chlamydomonas* can be easily severed and regrown in a matter of hours which allows for dissection of the complex processes involved in ciliary assembly and regulation (Jack and Avasthi 2018; Rosenbaum, Moulder, and Ringo 1969; Paul A. Lefebvre 1995; P. A. Lefebvre et al. 1978). Additionally, unlike mammalian cells, *Chlamydomonas* lacks a cortical actin network which simplifies the relationship between cilia and actin and makes this an ideal model to study such interactions. Further, genetic mutants for *Chlamydomonas* exist for 83% of the nuclear genome (Li et al. 2019; Cheng et al. 2017). These mutants can be used to identify important genes required for ciliary length regulation. For example, short flagella mutants (Jarvik et al. 1984, 1) and

long flagella mutants (Barsel, Wexler, and Lefebvre 1988; Asleson and Lefebvre 1998; Nguyen, Tam, and Lefebvre 2005, 1; L.-W. Tam, Wilson, and Lefebvre 2007) have been used to help researchers better understand the mechanisms involved in maintaining ciliary length.

Using *Chlamydomonas* several models for ciliary length regulation have been proposed (Ludington et al. 2015; Avasthi and Marshall 2012; Ishikawa and Marshall 2017a; Marshall 2015), including the limiting-precursor model (Rosenbaum, Moulder, and Ringo 1969), a few diffusion-based models (Levy 1974; Ludington et al. 2015; Hendel, Thomson, and Marshall 2018), the molecular ruler model (Marshall 2015), the time-of-flight model (Ishikawa and Marshall 2017b), the mechanosensitive ion channel model (Besschetnova et al. 2010; Beck and Uhl 1994), the swim speed feedback model (D. Tam and Hosoi 2011; Osterman and Vilfan 2011), and the balance point model (Marshall and Rosenbaum 2001; Marshall et al. 2005). The bulk of what we know regarding ciliary length regulation is related to the availability or turnover of protein, generally tubulin, but cilia are not merely composed of proteins. They are also ensheathed in plasma membrane. This leads to questions about whether membrane could be limiting. In fact, when cells are treated with Brefeldin A to collapse the Golgi and prevent the delivery of Golgi-derived membrane, cilia shorten (Dentler 2013). Previous data from our lab suggest that the Arp2/3 complex and actin are involved in reclaiming material from the cell body plasma membrane that is required for normal ciliary assembly (Bigge et al. 2020). We show that the Arp2/3 complex is required for the normal assembly of cilia and for endocytosis of both plasma membrane and plasma membrane proteins in various contexts. Further, we find that deciliation triggers Arp2/3 complex-dependent endocytosis by observing an increase in actin puncta immediately following deciliation (Bigge et al. 2020).

Because lithium causes ciliary lengthening across a broad range of cells and organisms, we use it as a tool to investigate the mechanisms that result in ciliary elongation in *Chlamydomonas* and beyond. We investigate the trafficking mechanisms that deliver the excess membrane required for additional growth past steady state length and find that endocytosis is important for ciliary elongation induced by lithium. Further, using both chemical inhibitors and genetic mutants, we find a role for Arp2/3 complex-

mediated actin networks in ciliary lengthening induced by lithium. Altogether, we propose a new model where the additional membrane required for lithium-induced ciliary lengthening is supplied through an endocytic process that depends on the Arp2/3 complex.

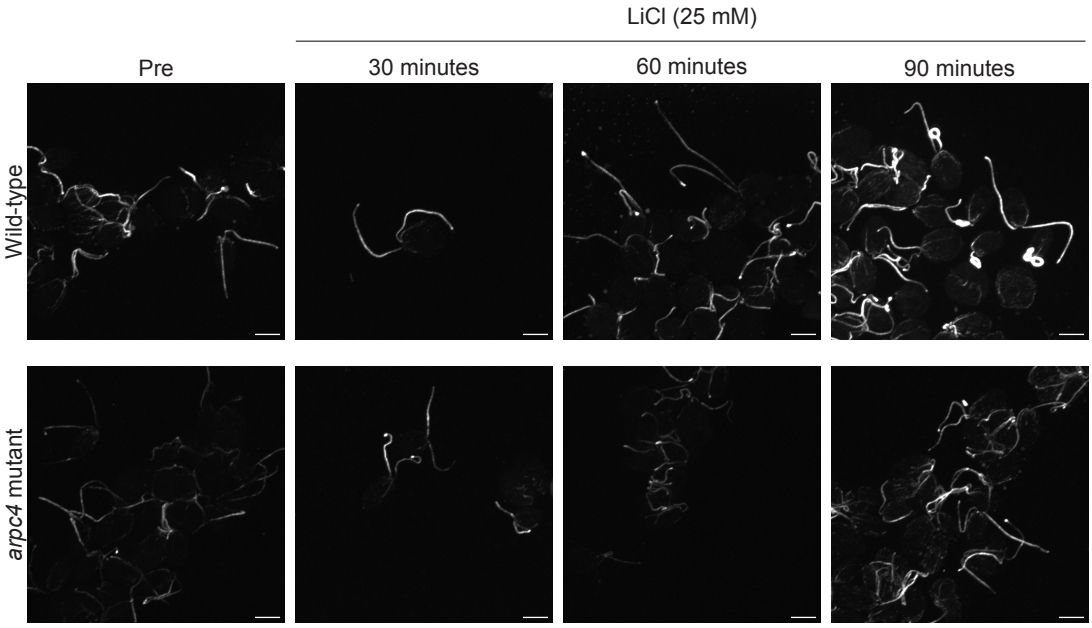

Fig. 4.1. Cilia elongate in lithium. Wild-type and *arpc4* mutant cells were treated with 25 mM LiCl and incubated for the specified time. They were then stained for acetylated tubulin to visualize the microtubule axoneme. Scale bar is 5 μm.

RESULTS

Inhibition of GSK3 by many mechanisms results in ciliary elongation

It has been proposed that lithium targets GSK3 in *Chlamydomonas* (Wilson and Lefebvre 2004), so we questioned whether inhibition of GSK3 was directly responsible for ciliary elongation seen with lithium. To answer this, we wanted to target GSK3 through other mechanisms. Genetic inhibition of GSK3 is not possible at the present time due to the lack of available null mutant. This could be due to GSK3 being essential for cell survival, or just because a mutant has not been successfully generated. However, three classes of GSK3 inhibitors exist: metal cations that interfere with ATP binding, ATP competitive inhibitors, and non-ATP competitive inhibitors. Lithium (LiCl) is thought to inhibit GSK3 by competing with magnesium ions required for ATP binding and by phosphorylation. To confirm that GSK3 inhibition is the cause of ciliary elongation caused by lithium, we employed inhibitors from each of the other two classes. We used CHIR99021 and (2'Z,3'E)-6-Bromoindirubin-3′-oxime (6-BIO) as ATP competitive inhibitors and Tideglusib as a non-ATP competitive inhibitor.

Consistent with previous results, treatment with LiCl induces ciliary elongation through either interference with ATP binding or through phosphorylation of GSK3 (**Fig. 4.2A**). The ATP competitive inhibitor CHIR99021 has been shown to modestly elongate cilia in foreskin fibroblasts (Ou et al. 2012). We confirmed that in *Chlamydomonas* 100 μM CHIR99021 also results in an increase in ciliary length (**Fig. 4.2B).** Next, we looked at the competitive inhibitor 6-BIO. Although 2 μM 6-BiO has been used in *Chlamydomonas* and caused ciliary shortening (Kong et al. 2015), when we treated cells with a much lower concentration of 100 nM 6-BIO, we observed ciliary elongation (**Fig. 4.2C**). Finally, we looked at a non-competitive inhibitor of GSK3, Tideglusib, for which the effects on cilia have not been previously observed. When cells were treated with 20 μM of Tideglusib, we saw an increase in ciliary length consistent with other methods of GSK3 inhibition (**Fig. 4.2D**). While each inhibitor may have its own set of off-target effects, they all share a unique on-target of GSK3, lending further support to GSK3 being the cilium length relevant target of GSK3. The minor variances between the drugs could be explained by the timeline in which we tested cilia (90 minutes) or the exact dosages we used. An example of this is 6-BIO where treatment with a low dose of 100 nM caused

ciliary lengthening, but treatment with a higher concentration of 2 μM reportedly caused ciliary shortening (Kong et al. 2015). Together, the data suggest that the mode of inhibition by chemical targets of GSK3 is not important for ciliary lengthening. Whether GSK3 was inhibited via competition for ATP binding or phosphorylation, cilia were able to elongate.

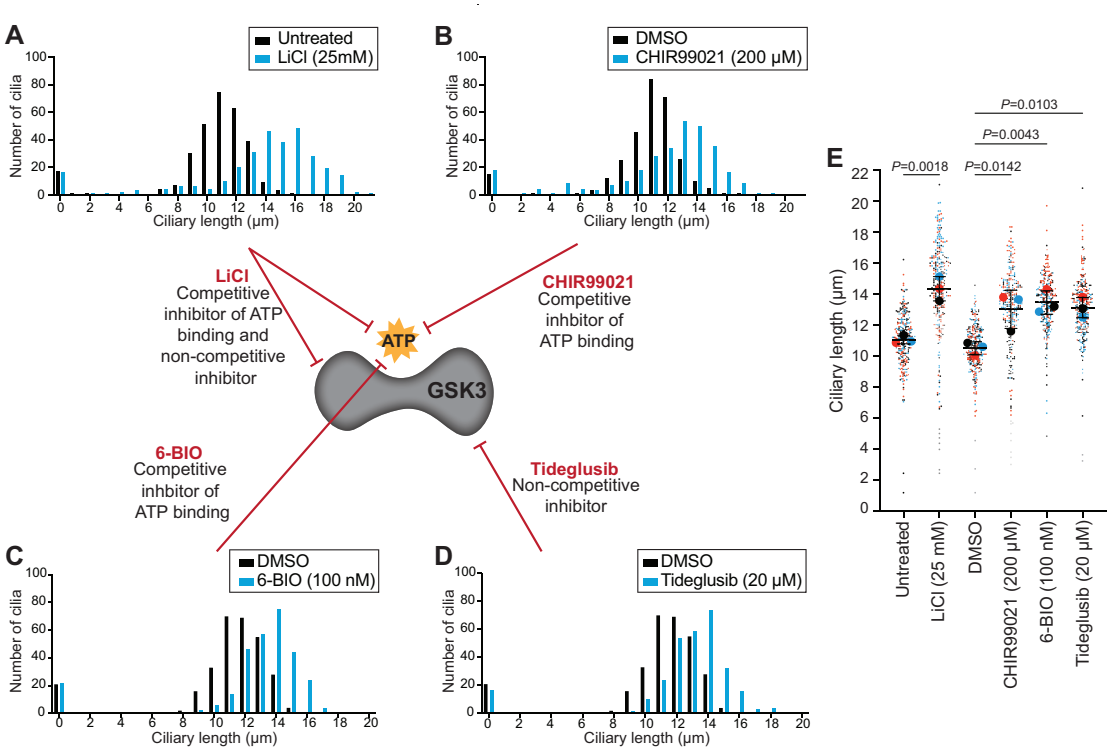

Fig. 4.2. Inhibition of GSK3 through multiple mechanisms results in ciliary elongation. A-D) Wild-type (CC-5325) cells were treated with GSK3 inhibitors including 25 mM LiCl (A), 200 μM CHIR99021 (B), 20 μM Tideglusib (C), or 100 nM BIO (D) for 90 minutes. Histograms show distribution of ciliary lengths. n=100 cells in 3 separate biological replicates. **E)** Dot plot representing the data in A-D excluding zero length cilia. Each color represents a separate biological replicate where n=100. The large dots represent means from each replicate and the mean (solid lines), standard deviation (error bars), and statistical analyses were calculated using those means. P values shown on the plot are the results of a one-way ANOVA followed by Tukey's multiple comparisons analysis.

Membrane for lithium-induced ciliary elongation comes from endocytosis

To better understand the mechanism behind ciliary elongation induced by GSK3 inhibition, we looked at the source of the ciliary material. The cilium is primarily composed of the microtubule-based axoneme and the membrane surrounding the organelle. Thus, for the rapid growth seen with lithium, the cell needs to deliver not only protein, but also membrane to the cilia during a relatively short time frame. Treatment of cells with lithium and cycloheximide, which blocks protein synthesis, resulted in ciliary elongation consistent with that of untreated cells, suggesting that new protein synthesis is not required for lithium-induced ciliary elongation and the protein required for assembly must come from a pool somewhere in the cell (Wilson and Lefebvre 2004) (**Fig. 4.3**).

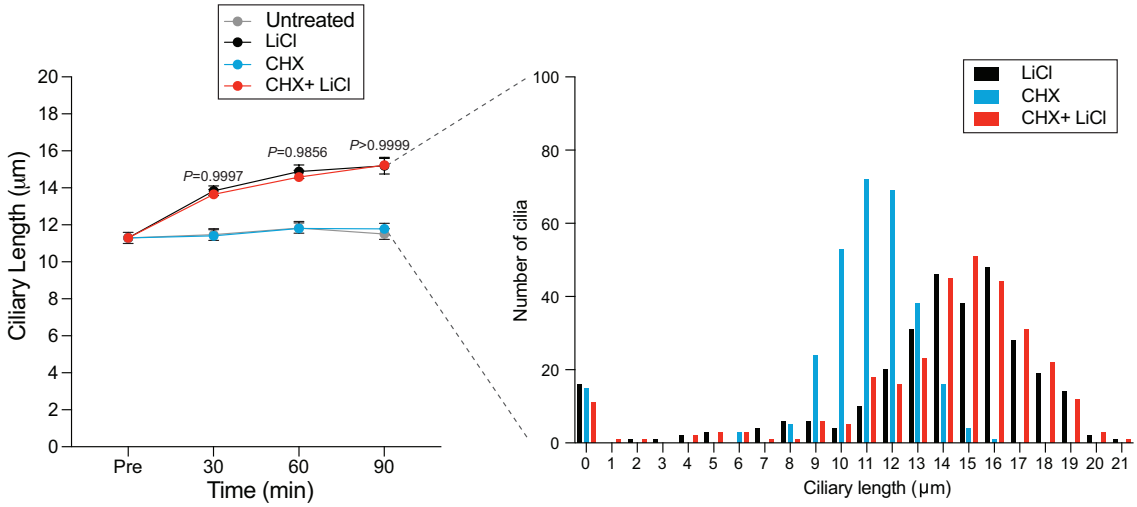

Fig. 4.3. New protein synthesis is not required for lithium-induced ciliary elongation. A) Wild-type cells were treated with either 25 mM LiCl, 10 μM Cycloheximide (CHX), or a combination of the two drugs. n=30 for each sample at each time point in 3 separate biological replicates. Significance was determined by one-way ANOVA and a Tukey's multiple comparisons test. The p values above the lines show the comparison between cells treated with LiCl alone or LiCl and CHX. In all cases, the comparison is not significant. **B)** A histogram representation of the 90-minute time point from (A). For this, n=100 for each sample in 3 separate biological replicates (300 total points).

The membrane required for ciliary elongation induced by lithium must come from one of two sources: the Golgi, which is generally thought to be the main source of ciliary membrane (Nachury, Seeley, and Jin 2010; Rohatgi and Snell 2010), or a pool in the cell body plasma membrane (Bigge et al. 2020). To differentiate between these two possibilities, we treated cells with either Brefeldin A (BFA), a drug that causes Golgi collapse, or Dynasore, a drug that interferes with dynamin-mediated endocytosis. When cells were treated with BFA to block membrane delivery from the Golgi, cilia were still able to elongate in LiCl (**Fig. 4.4A-B**). This suggests that membrane from the Golgi is not required for lithium-induced elongation.

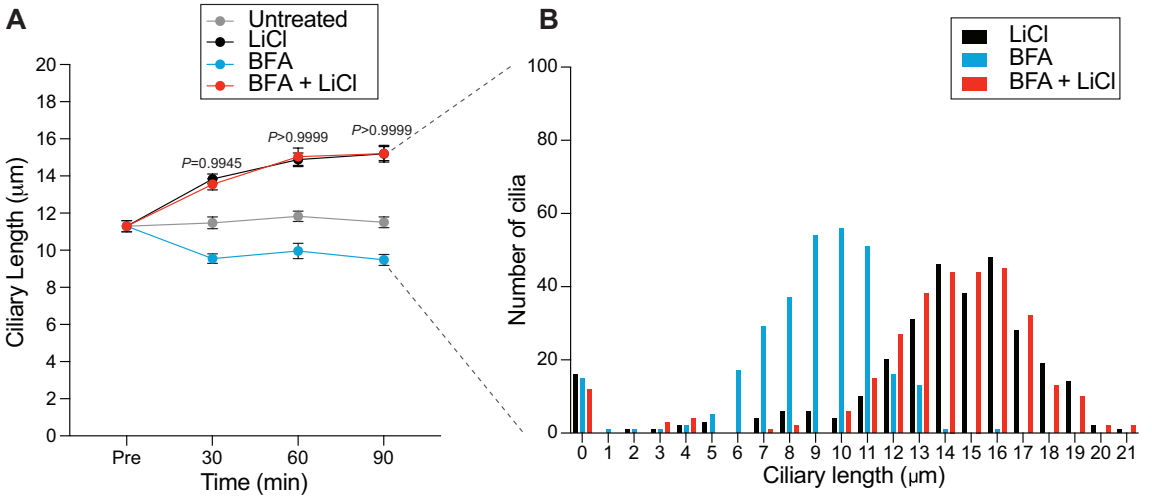

Fig. 4.4. Golgi-derived membrane is not required for lithium-induced ciliary elongation. A) Wild-type (CC-5325) cells were treated with 36 μM Brefeldin A or 36 μM Brefeldin A with 25 mM LiCl. n=30 cells per time point and sample in 3 separate biological replicates. Significance was determined using a two-way ANOVA with a Tukey's multiple comparisons test. Values above the lines show the comparison between LiCl and BFA with LiCl. Each time point is ns at the p-values listed on the graph. Additionally, cells treated with BFA alone have significantly ($p<0.0001$) shorter cilia than untreated cells, confirming function of BFA. **B)** The 90-minute time point from (A) was expanded to n=100 cells for each biological replicate. The histograms show distribution of ciliary lengths

Conversely, when treated with Dynasore to inhibit endocytosis, cilia could not elongate to the same degree as untreated cells (**Fig. 4.5A-B**), implying endocytosis is required for lithium-induced elongation and that endocytosis requires dynamin. This is consistent with results from our previous studies which show that ciliary membrane and membrane proteins are delivered from the cell body plasma membrane to the cilia. In an experiment first performed in Dentler 2013 and then later in Bigge et al. 2020, we biotinylated all cell surface proteins. Then, deciliated cells and allowed cilia to regrow. We then isolated cilia and probed for biotinylated proteins. Any biotinylated proteins present must have come from the cell body plasma membrane, and we found that indeed biotinylated proteins exist in the newly grown cilia, suggesting that ciliary membrane and membrane proteins can be recruited from the cell body plasma membrane (Dentler 2013; Bigge et al. 2020).

To further probe the involvement of endocytosis in ciliary elongation, we turned to the dynamin family. GSK3 has been previously shown to target the dynamin protein family. In neuronal and non-neuronal mammalian cells dynamin 1 is usually inactive due to phosphorylation by GSK3ß, but when cells are treated with CHIR99021 to inhibit GSK3, dynamin 1 is dephosphorylated and endocytosis rates increase significantly (Srinivasan et al. 2018; Smillie and Cousin 2012). Meanwhile, GSK3α has been found to phosphorylate mammalian Dynamin 2 (Laiman et al. 2021).

Canonical dynamins have not been identified in *Chlamydomonas,* but the genome contains many dynamin related proteins (DRPs). DRPs differ from dynamins in that they do not contain all 5 traditional dynamin domains: A GTPase domain, a middle domain, a pleckstrin homology domain, a guanine exchange domain, and a proline rich domain (Elde et al. 2005) (**Fig. 4.6A-B**). *Chlamydomonas* contains 9 DRPs with similarity to a canonical dynamin (DRP1-9). Despite lacking 2 of the canonical dynamin domains, the DRP with the highest sequence similarity and identity to canonical dynamin is DRP3 (**Fig. 4.6C-D**). To determine if GSK3 could be a potential kinase for this protein, we employed ScanSite4.0, which confirmed that of the 9 DRPs of *Chlamydomonas,* the only one with a traditional GSK3 target sequence was DRP3.

To investigate whether DRP3 might be involved in the ciliary elongation that results from lithium treatment, we obtained a mutant from the *Chlamydomonas* mutant

library (CLiP) (Cheng et al. 2017; Li et al. 2019). This mutant has a cassette inserted early in the gene. When we treated these cells with lithium, ciliary elongation was decreased (**Fig. 4.5C-E**), suggesting that this DRP3 is involved in the ciliary response to GSK3 inhibition. Elongation was not fully blocked by this mutation in DRP3, this is potentially due to the presence of other DRPs that might compensate for the lost function of DRP3.

Additionally, we showed that this DRP is required for internalization of a lipophilic membrane dye, FM4-46FX through endocytosis. This dye binds to the membrane but is unable to enter the cells on its own and must be endocytosed. In wild-type cells it is quickly endocytosed and visible as puncta within the cell (**Fig. 4.5F, H**) (Bigge et al. 2020). However, in *drp3* mutants the amount of dye endocytosed is significantly lower (**Fig. 4.5G-H**), suggesting that DRP3 is required for optimal endocytosis in these cells.

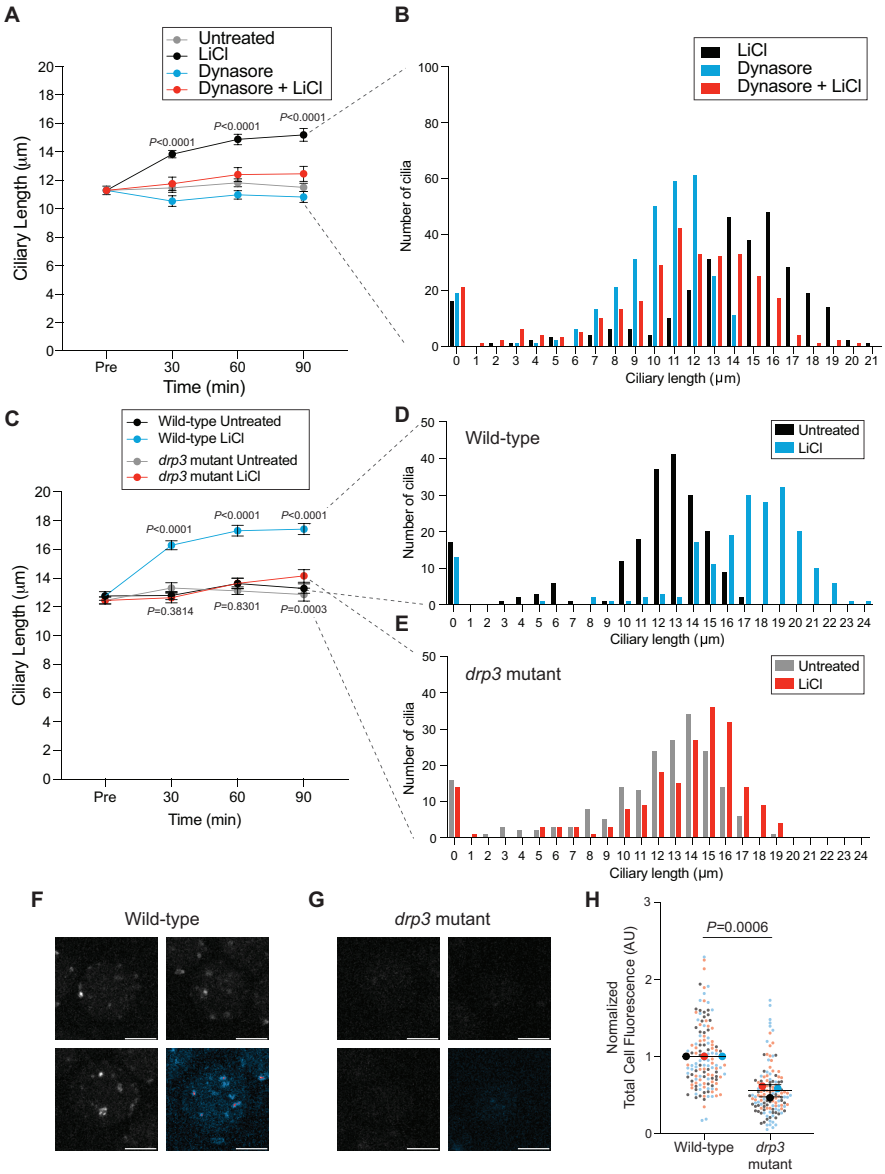

Fig. 4.5. Lithium-induced ciliary elongation requires endocytosis. A) Wild-type cells treated with 100 μM Dynasore or 100 μM Dynasore with 25 mM LiCl. n=30 cells per time point and sample in 3 separate biological replicates. Significance was determined by two-way ANOVA with a Tukey's multiple comparisons test. P values on the graph are comparing LiCl treated cells to cells treated with LiCl and Dynasore. Each time point is significantly different. **B)** The 90-minute time point from (A) was expanded to n=100 cells for each biological replicate. The histograms show distribution of ciliary lengths. **C)** Wild-type cells and *drp3* mutant cells treated with 25 mM LiCl. n=30 cells per time point and sample in 3 separate biological replicates. Significance was determined by two-way ANOVA with a Tukey's multiple comparisons test. P values on the graph are comparing wild-type cells to *drp3* mutant cells. The P values below the line compare untreated *drp3* mutant cells with LiCl-treated *drp3* mutant cells. **D-E)** The 90-minute time points from (D) were expanded to n=100 cells for each biological replicate. (D) represents wild-type cells and (E) represents *drp3* mutant cells. The histograms show distribution of ciliary lengths. **F-G)** Wild-type (F) and *drp3* mutant cells (G) were incubated with the membrane dye FM4-46FX and allowed to internalize for 1 minute. Z stacks were acquired and turned into maximum intensity projections for visualization. Scale bar represents 5 μM. **H)** Background corrected total cell fluorescence intensity of sum slices of stacks represented by F and G normalized to the wild-type cells. The small dots represent each data point n=45 in 3 separate experiments. The larger dots are the mean of each experiment. These were used to determine the center (mean), error (standard deviation), and significance (two-sided t-test).

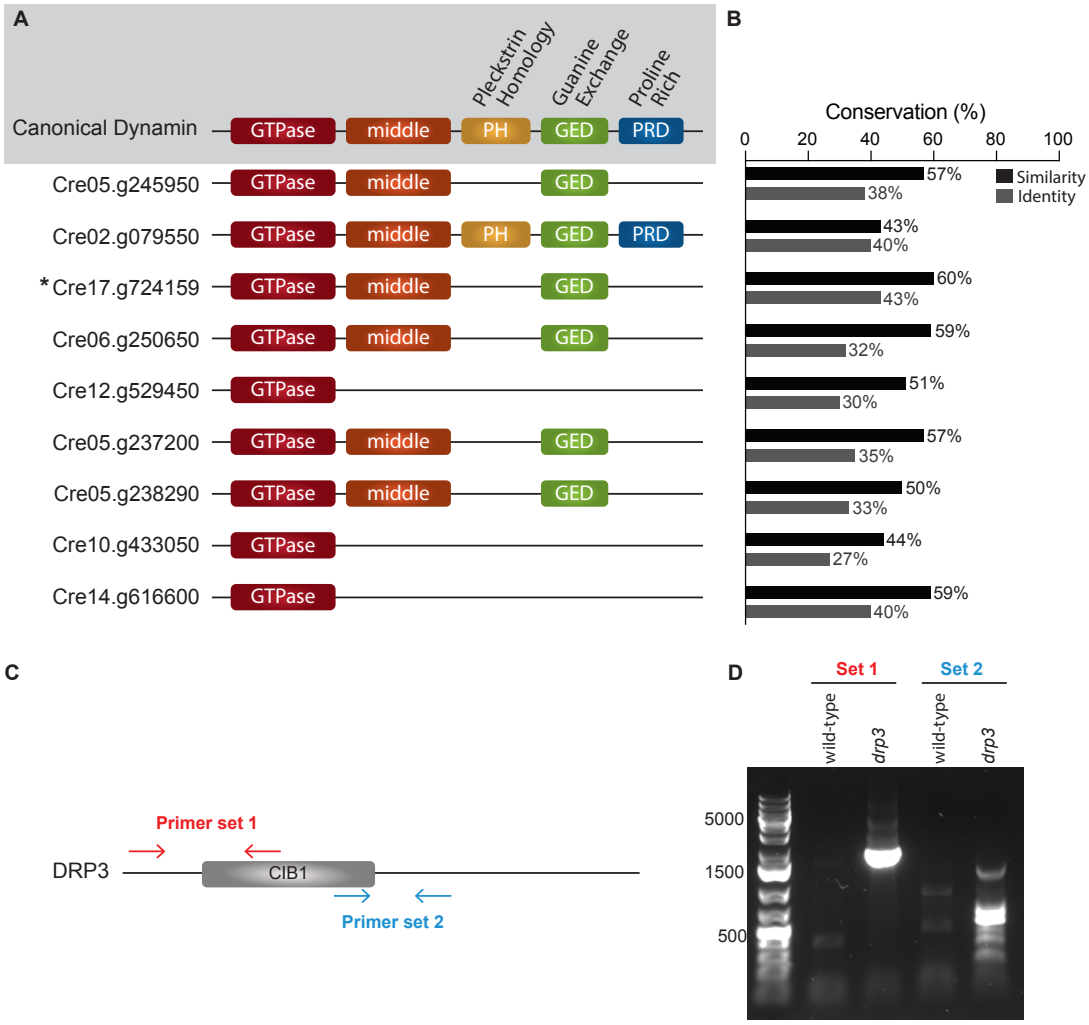

Fig. 4.6. *Chlamydomonas* contains several dynamin related proteins (DRPs) with the most similar to canonical dynamin being DRP3 (Cre17.g724159) A) The canonical dynamin contains 5 domains represented in different colors above. The *Chlamydomonas* genome contains no conventional dynamins but does contain 9 dynamin related proteins (DRPs) that have various similarities compared with canonical dynamin. The *Chlamydomonas* DRPs above are represented by the gene identifier and are ordered by DRP number (the first is DRP1, the second is DRP2, etc). **B)** The graph on the right shows the similarity and identity of each DRP compared to canonical mammalian dynamin as determined by MUSCLE alignment. The DRP that is the most closely related to canonical dynamin is DRP3, Cre17.g724159. **C)** Schematic of the DRP3 genomic sequence with the primers used to confirm mutation represented by arrows. **D)** DNA gel electrophoresis showing resulting DNA sequences from the PCR using the primer sets shown in C.

We performed a similar experiment to test for increased internalization during LiCl treatment when we expect membrane is being rapidly internalized. We found that there is a trend towards increased internalization within the first 30 minutes following lithium treatment suggesting that membrane is being internalized at a faster rate (**Fig. 4.7A-B**).

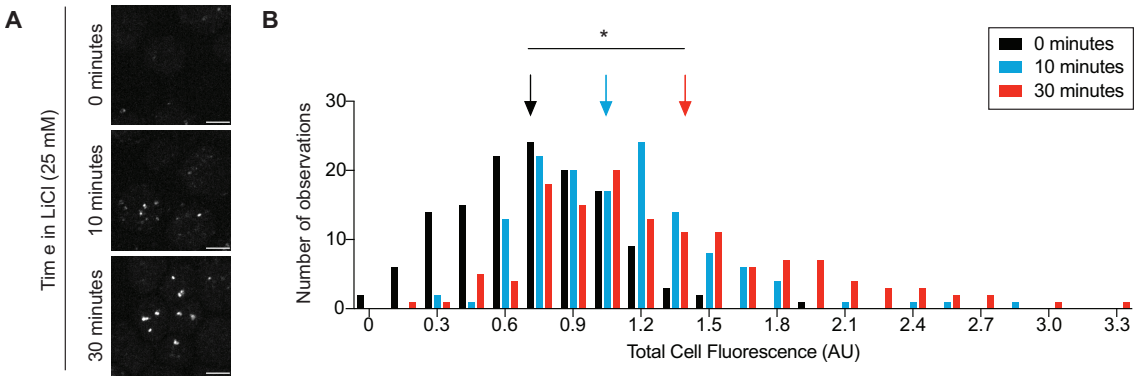

Fig. 4.7. Lithium-induced ciliary elongation increases membrane internalization. A) Wild-type cells treated with 25 mM LiCl for the appointed time were incubated with the membrane dye FM4-46FX and allowed to internalize membrane for 1 minute. Resulting images were acquired on a spinning disk microscope and turned into maximum intensity projections for visualization. Scale bar represents 5 μM. **B)** Background corrected total cell fluorescence intensity of sum slices of stacks. 3 separate experiments were performed where n=45 in each experiment. Each point was used to create the histogram. The means of each separate experiment were determined, and these were then used to determine the mean (represented by arrows with colors corresponding to each time point) and significance (one-way ANOVA with Tukey's multiple comparisons test). * represents P=0.0261.

Lithium-induced ciliary elongation promotes formation of filamentous actin puncta

The high demand for new membrane and protein during ciliary elongation led us to hypothesize that treatment with GSK3 inhibitors would lead to an increase in actin dynamics. Previously, we found that upon deciliation and rapid initial ciliary assembly, filamentous actin puncta visualized with phalloidin form at the apex of the cell near the cell body plasma membrane (Bigge et al. 2020). These puncta are reminiscent of endocytic pits seen in yeast and require the Arp2/3 complex, which is known to be involved in endocytosis in cells with cell walls, like yeast and *Chlamydomonas* (Bigge et al. 2020; Basu, Munteanu, and Chang 2014; Aghamohammadzadeh and Ayscough 2009; Carlsson and Bayly 2014). Further, they rely on proteins typically thought to be involved in endocytosis including the Arp2/3 complex and clathrin, and they form at times when it makes sense for endocytosis to be occurring, like immediately following deciliation when membrane and protein must be recruited to cilia in a timeframe too short for new protein and membrane synthesis, sorting, and trafficking (Bigge et al. 2020). To provide additional evidence that these are endocytic puncta, we also showed that a corresponding increase in membrane internalization occurs during this same timeframe using a fluorescent membrane dye that is endocytosed in wild-type cells (Bigge et al. 2020). Thus, we stained cells with phalloidin to visualize filamentous actin and these endocytosis-like punctate structures when cells are treated with GSK3 inhibitors. Untreated cells formed some puncta at the apex of the cell (**Fig. 4.8A**), but treatment with either LiCl, CHIR99021, 6-BIO, or Tideglusib increased the percentage of cells with dots and the number of dots per cell (**Fig. 4.8A-B**). *arpc4* mutant cells never form dots confirming that the formation of these actin puncta is Arp2/3-dependent (**Fig. 4.8B**). The increased formation of these Arp2/3 complex-dependent filamentous actin puncta suggests a burst of endocytosis triggered by inhibition of GSK3 occurring during times of rapid ciliary elongation.

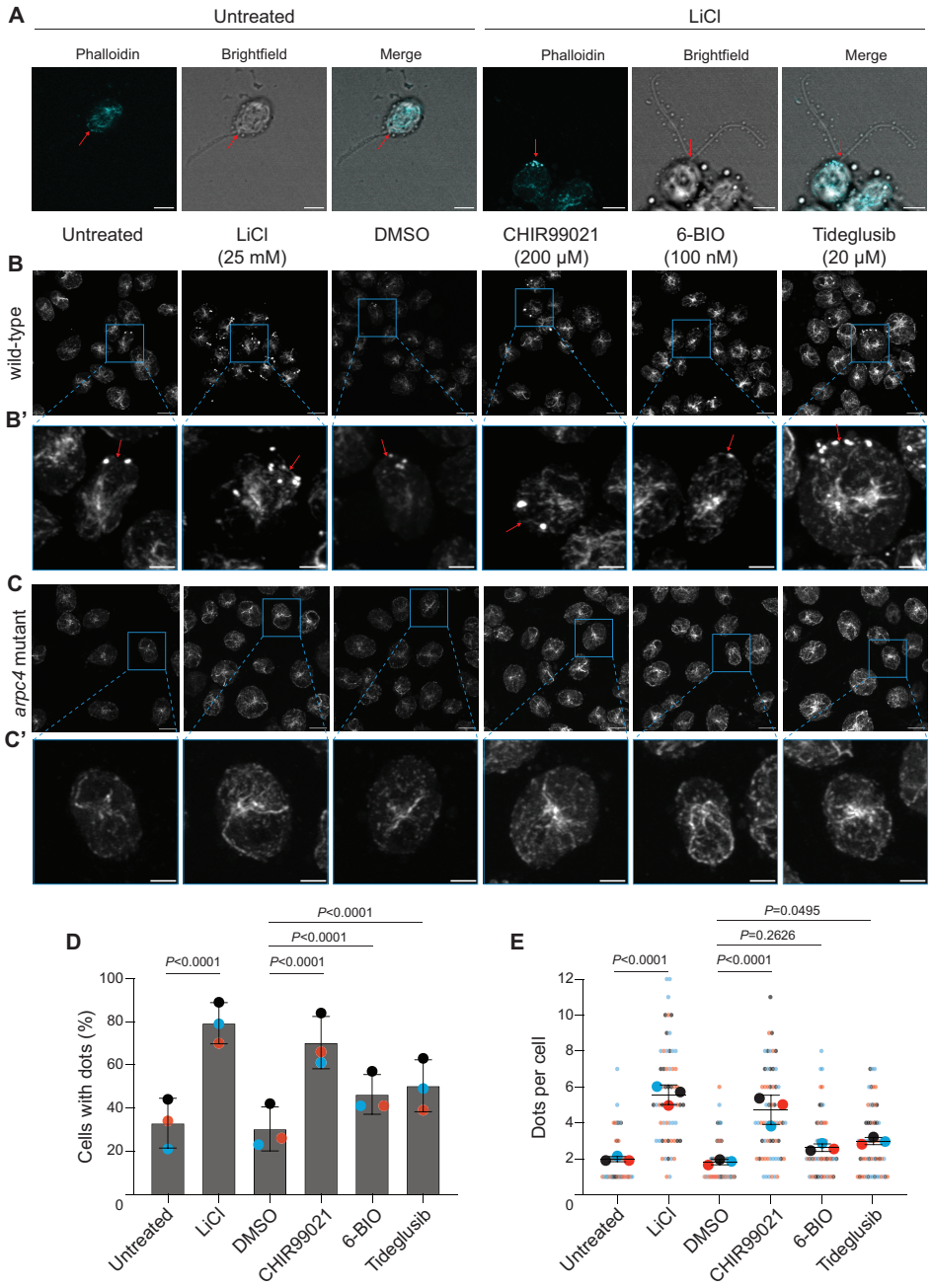

Fig. 4.8. GSK3 inhibition increases Arp2/3 complex-dependent filamentous actin puncta. A) Wild-type cells either untreated or treated with 25 mM LiCl for 30 minutes were stained with phalloidin. Red arrows point to the apex of the cell as signified by the presence of cilia in the brightfield images and the cellular actin structures. **B)** Maximum intensity projections of z stacks of wild-type cells treated with LiCl (25 mM), DMSO, CHIR99021 (200 μM), BIO (100 nM), or Tideglusib (20 μM) and stained with phalloidin. Scale bars represent 5 μm. **B')** Zoomed in images of the boxed cells in A. Red arrows point to the apex of cells. **C)** Maximum intensity projections of z stacks taken of *arpc4* mutant cells treated with LiCl (25 mM), DMSO, CHIR99021 (200 μM), BIO (100 nM), or Tideglusib (20 μM) and stained with phalloidin. Scale bars represent 5 μm. **D')** Zoomed in images of the boxed cells in B. **C)** Quantification of the percentage of cells with dots in each treatment. n=100 in 3 separate biological replicates. Significance was determined using Chi Square analysis and Fisher's exact tests. **E)** Quantification of the number of dots per cell in cells in each group. n=20 cell in 3 separate biological replicates. Significance was determined using a one-way ANOVA and a Tukey's multiple comparisons test.

To further investigate the increase in actin puncta, we employed an mNeonGreen-tagged Lifeact peptide, which labels filamentous actin populations in live cells. Using this method, we were able to visualize dynamic actin and puncta in both untreated and lithium-treated wild-type cells (**Fig. 4.9A**). Then using the ImageJ/FIJI Plugin Trackmate, we tracked the movement of filamentous actin accumulations within the cell (Ershov et al. 2021; Tinevez et al. 2017). We found that actin dynamics were significantly increased in wild-type cells treated with lithium compared with untreated cells (**Fig. 4.9B-C**). The increased actin dynamics in lithium-treated cells were particularly enriched near the membrane.

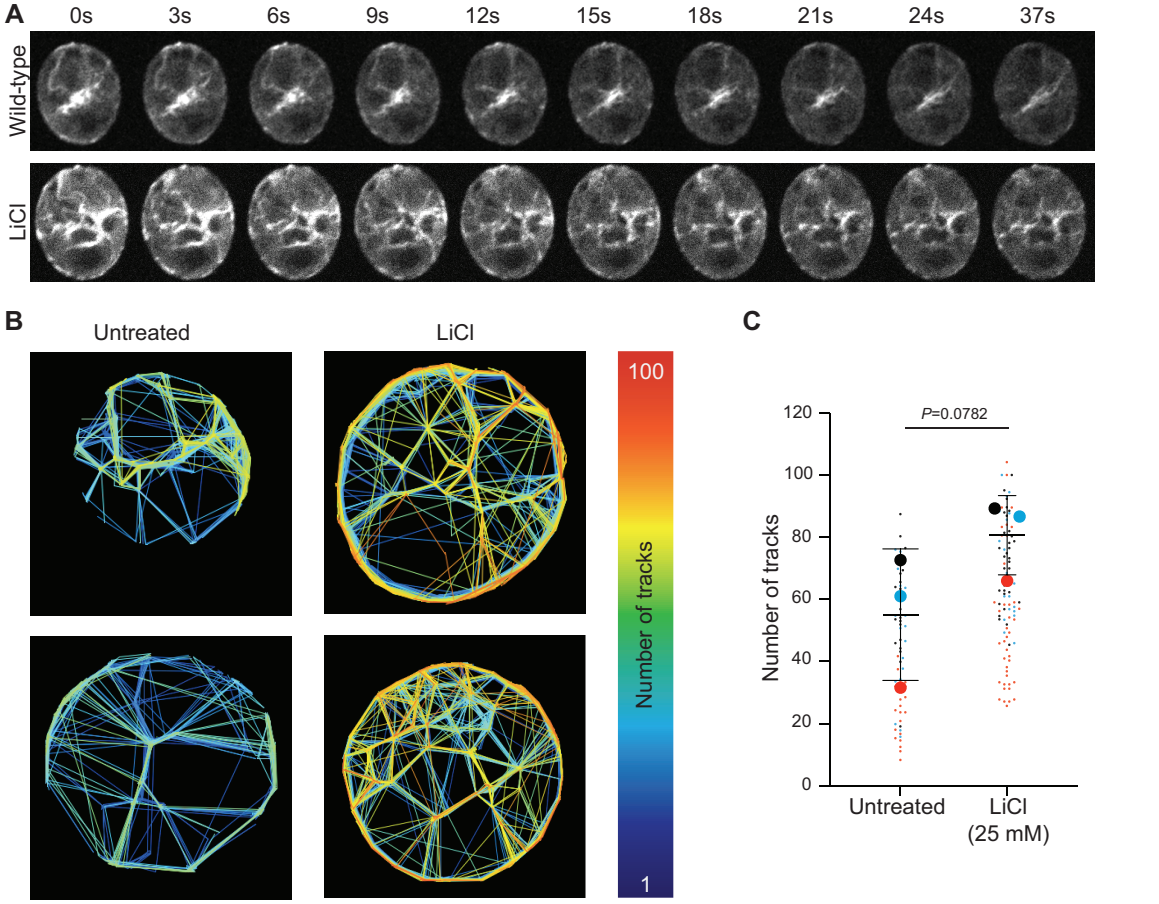

Fig. 4.9. Actin dynamics increase near the membrane during lithium-induced ciliary elongation. A) Time-lapse representation of videos taken of cells expressing Lifeact-mNeonGreen either untreated or treated with 25 mM LiCl and then immediately imaged on a Nikon Spinning Disk microscope for 30 seconds. **B)** Videos represented in (A) were analyzed using the FIJI plugin, TrackMate. This identifies spots in videos and tracks their movement allowing us to measure actin dynamics. The tracks created in TrackMate were adjusted so that cells with less tracks will have more blue tracks, but cells with more tracks will start to have tracks with more oranges and reds according to the scale. **C)** From the TrackMate data, we found the number of tracks in untreated cells and cells treated with LiCl. Each color represents one of 3 separate biological replicates. The large dots represent the means from each biological replicate with the line and error bars showing the mean and standard deviation of the means from each replicate. Two-tailed t-test was performed on the means to give the p-value on the graph.

The increase in actin dynamics led us to question whether myosin might be involved in reorganizing actin structures at the membrane and thus in ciliary elongation in lithium treated cells. *Chlamydomonas* contains 3 myosins, MYO1 and MYO3 (both type XI myosins) and MYO2 (a type VIII myosin). However, it has been suggested that all three myosins have sensitivity to the myosin II inhibitor, (-)-Blebbistatin (Avasthi et al. 2014). Therefore, we used this to test if any of the *Chlamydomonas* myosins are involved in the mechanisms that result in ciliary elongation. This is also an interesting question as many myosins have been found to be involved in endocytosis, and in particular, plant Type VIII myosins have been implicated in endocytosis (Kasprowicz et al. 2009; Sattarzadeh, Franzen, and Schmelzer 2008; Golomb et al. 2008; Samaj et al. 2005; Baluska et al. 2004; Volkmann et al. 2003). Consistent with previous results, (-)-Blebbistatin did not alter steady state ciliary length (Avasthi et al. 2014) (**Fig. 4.10**). However, cells without myosin function were able to undergo lithium-induced ciliary elongation, but not to the same degree as untreated wild-type cells or wild-type cells treated with the inactive (+)-Blebbistatin (**Fig. 4.10**), suggesting that in *Chlamydomonas,* myosins may be involved in the actin-dependent process required for ciliary elongation due to lithium.

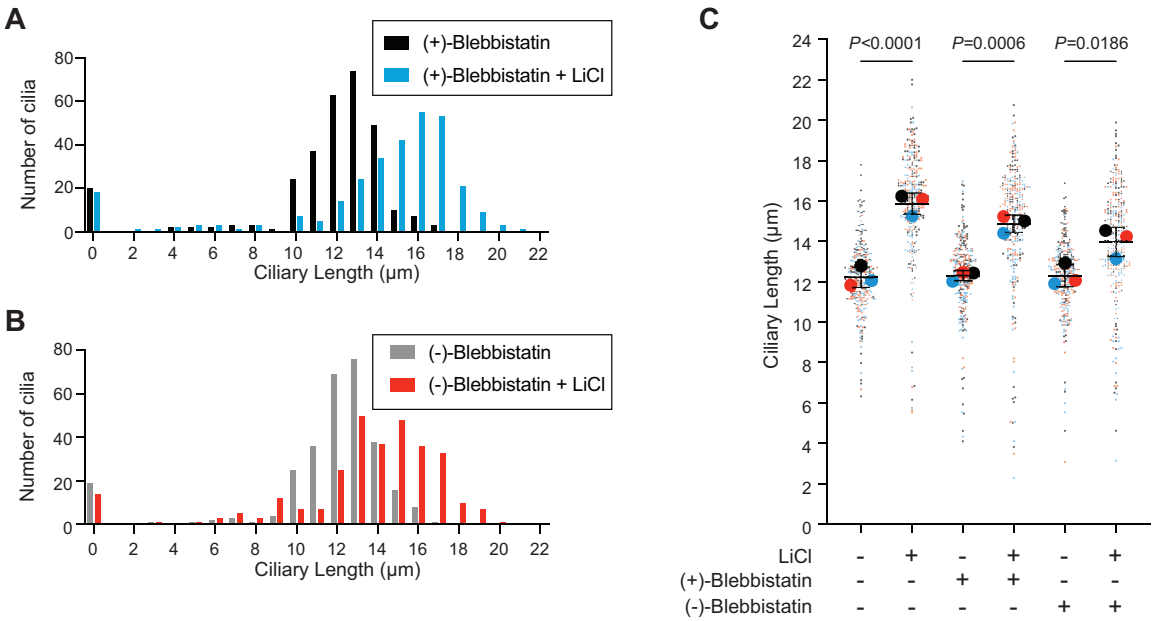

Fig. 4.10. Myosin is required for lithium-induced ciliary elongation. **A)** Cells were treated with a combination of 25 mM LiCl and 150 μM of either (+)-Blebbistatin for 90 minutes. n=100 in each of 3 separate biological replicates. **B)** Cells were treated with a combination of 25 mM LiCl and 150 μM of either (-)Blebbistatin for 90 minutes. n=100 in each of 3 separate biological replicates. **C)** Untreated cells and cells treated with a combination of 25 mM LiCl, 150 μM (+)-Blebbistatin, and 150 μM (-)-Blebbistatin were incubated for 90 minutes. n=100 in each of 3 separate biological replicates. Each replicate is represented by a different color with the large dots showing the means of each replicate. These were then used to calculate the mean (line), standard deviation (error bars), and P values. P values were calculated using a one-way ANOVA followed by a Tukey's multiple comparisons analysis. Each is significantly different.

The Arp2/3 complex is required for lithium-induced ciliary elongation

The increase in Arp2/3 complex-dependent actin puncta with lithium or GSK3 inhibition led us to question whether the Arp2/3 complex was required for ciliary elongation induced by lithium. Also, we previously showed that the Arp2/3 complex is required for rapid ciliary assembly in the initial stages of ciliogenesis (Bigge et al. 2020). Specifically, we found that the Arp2/3 complex is required for reclamation of membrane from a pool in the plasma membrane during the rapid growth that occurs during early ciliary assembly (Bigge et al. 2020). This leads us to hypothesize that the Arp2/3 complex will also be required for rapid ciliary elongation induced by lithium. Chemical inhibition of the Arp2/3 complex with the small molecule inhibitor CK-666 resulted in defective ciliary elongation induced by lithium (**Fig. 4.11A-B**). We confirmed this result with genetic inhibition of the Arp2/3 complex component ARPC4 using an *arpc4* mutant first described in (Bigge et al. 2020) (**Fig. 4.11C-E, 4.1**). This suggests the Arp2/3 complex is required for lithium-induced ciliary elongation.

To confirm that this requirement of the Arp2/3 complex is connected to the inhibition of GSK3, we also treated wild-type and *arpc4* mutant cells with CHIR99021, BIO, and Tideglusib. In all cases, wild-type cells were able to elongate while *arpc4* mutant cells either did not elongate or shortened (**Fig. 4.11G-L**). Thus, the mechanism whereby GSK3 inhibition results in ciliary elongation requires the Arp2/3 complex.

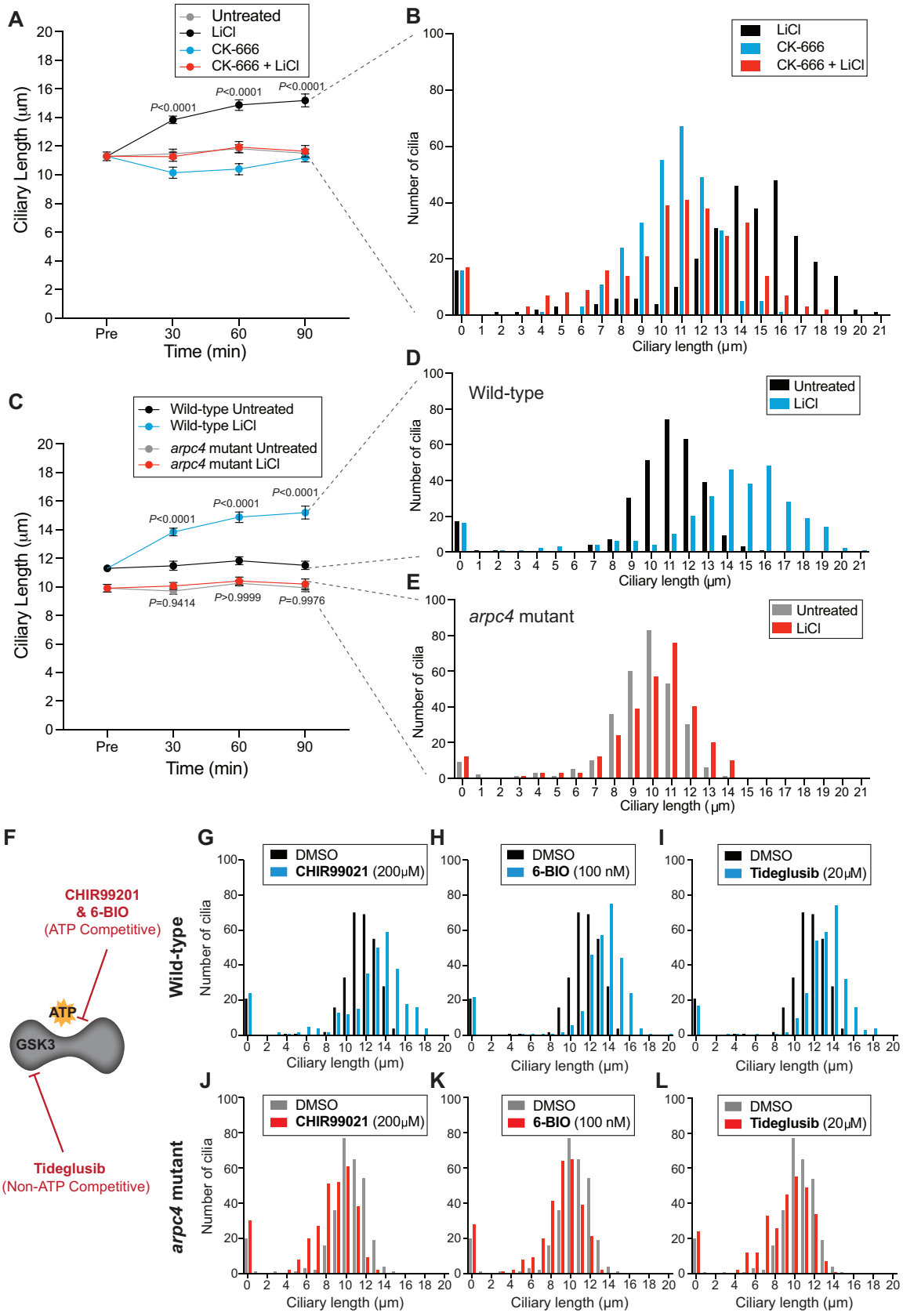
A
Untreated
LiCl
CK-666
CK-666 + LiCl
Ciliary Length (µm)
Time (min)
Pre
30
60
90
P<0.0001
P<0.0001
P<0.0001
B
LiCl
CK-666
CK-666 + LiCl
Number of cilia
Ciliary length (µm)
C
Wild-type Untreated
Wild-type LiCl
arpc4 mutant Untreated
arpc4 mutant LiCl
P<0.0001
P<0.0001
P<0.0001
P=0.9414
P>0.9999
P=0.9976
D
Wild-type
Untreated
LiCl
E
arpc4 mutant
F
CHIR99201
& 6-BIO
(ATP Competitive)
ATP
GSK3
Tideglusib
(Non-ATP Competitive)
G
H
I
J
K
L
DMSO
CHIR99021 (200µM)
6-BIO (100 nM)
Tideglusib (20µM)
Wild-type
arpc4 mutant

Fig. 4.11. The Arp2/3 complex is required for ciliary elongation induced by GSK3 inhibition. A) Wild-type cells treated with 100 μM CK-666 or 100 μM CK-666 with 25 mM LiCl. n=30 cells per time point and sample in 3 separate biological replicates. Significance was determined by one-way ANOVA and a Tukey's multiple comparisons test. The p values above the lines show the comparison between cells treated with LiCl and cells treated with LiCl and CK-666. **B)** The 90-minute time point from (A) was expanded to n=100 cells for each biological replicate. The histograms show distribution of ciliary lengths. **C)** Wild-type and *arpc4* mutant cells treated with 25 mM LiCl. n=30 cells per time point and sample in 3 separate biological replicates. Significance was determined by one-way ANOVA and a Tukey's multiple comparisons test. The p values above the lines show the comparison between wild-type cells treated with LiCl and *arpc4* mutant cells treated with LiCl. The p values below the lines show the comparison between untreated *arpc4* mutant cells and *arpc4* mutant cells treated with LiCl. At each time point, this comparison was not significant. **D-E)** The 90-minute time points from (C) were expanded to n=100 cells for each biological replicate. (D) represents wild-type cells and (E) represents *arpc4* mutant cells. The histograms show distribution of ciliary lengths. **F)** Schematic showing GSK3 inhibitory functions of the inhibitors. **G-I)** Wild-type cells were treated with either 200μM CHIR99021 (B), 100nM BIO (C), or 20μM Tideglusib (E) for 90 minutes. Histograms show distribution of ciliary lengths. n=100 cells in 3 separate biological replicates. **J-L)** *arpc4* mutant cells were treated with either 200μM CHIR99021 (E), 100nM BIO (F), or 20μM Tideglusib (G) for 90 minutes. Histograms show distribution of ciliary lengths. n=100 cells in 3 separate biological replicates.

DISCUSSION:

In this work, we investigate the mechanisms behind ciliary elongation induced by lithium treatment in an effort to better understand the factors regulating ciliary length. Cilia are primarily composed of a microtubule axoneme and a plasma membrane that contains the axoneme. Many of the studies to understand ciliary length regulation focus on the microtubule axoneme, the amount of free tubulin available for assembly, and the delivery of tubulin to and from the ciliary tip through intraflagellar transport (IFT). While these are important factors and we are interested in how our data can fit with these existing models, we focus instead on the plasma membrane that ensheathes the axoneme. Because new protein synthesis is not required for ciliary elongation induced by lithium (Wilson and Lefebvre 2004) (**Fig. 4.3**), we hypothesized that the primary source of membrane for elongation was perhaps separate from the Golgi, which is typically thought to be the primary source of membrane for ciliary assembly.

Previous work has shown that while the Golgi is required for ciliary maintenance and assembly (Dentler 2013), it is not the only source of membrane. Instead, we found that membrane reclaimed through actin and Arp2/3-complex dependent endocytosis is required for ciliary assembly or growth from zero length (Bigge et al. 2020). More specifically, we found that the Arp2/3 complex is required for normal ciliary maintenance and ciliary assembly, especially in the early stages when membrane and protein are needed quickly. The Arp2/3 complex is also required for the internalization of membrane and a specific ciliary membrane protein required for mating. Further, we show that

endocytosis-like actin puncta form immediately following deciliation in an Arp2/3 complex and clathrin-dependent manner, and that membrane from the cell body plasma membrane can be reclaimed and incorporated into cilia (Bigge et al. 2020). This led us to question whether that same mechanism might be required for ciliary elongation from steady state length induced by lithium treatment.

We found that GSK3 inhibition resulted in increased ciliary length using CHIR99021, BIO, Tideglusib, and Lithium which each target GSK3 through different mechanisms (**Fig. 4.2**). CHIR99021, BIO, and Tideglusib were designed for use in humans, but their ability to elongate cilia in *Chlamydomonas* suggests that they can target GSK3 and that this results in ciliary elongation across organisms. Next, we showed that while Golgi-derived membrane was not required for ciliary lengthening, endocytosis and dynamin function were needed to elongate cilia (**Figs. 4.4-7**). We could not however rule out other sources of membrane, such as the endosomal network. Finally, we showed that GSK3 inhibition resulted in a burst of Arp2/3-complex dependent dots and increased actin dynamics at the membrane (**Figs. 4.8-9**). These actin dots were previously observed during initial ciliary assembly when there is a high demand for membrane that can be quickly incorporated into cilia (Bigge et al. 2020). They are reminiscent of endocytic patches or pits seen in yeast where actin is required for endocytosis to overcome turgor pressure related to the presence of a cell wall, which *Chlamydomonas* also has (Aghamohammadzadeh and Ayscough 2009; Basu, Munteanu, and Chang 2014; Carlsson and Bayly 2014). While we cannot say these are *Chlamydomonas* endocytic pits with the current data, we do believe they speak to the presence of actin functioning at the membrane during these periods when membrane is in high demand. One important detail is that *Chlamydomonas* differ from mammalian cells in that they have a cell wall. The stability awarded by the cell wall means that *Chlamydomonas* does not require a cortical actin network as mammalian cells do. Thus, in *Chlamydomonas,* we are able to investigate actin dynamics and functions without the interference of the cortical actin network. This also means that some of the effects we see might be masked in mammalian cells by the presence of the cortical actin network and the effect that it has on ciliary assembly and maintenance. Finally, we show that the Arp2/3 complex is absolutely required for lithium-induced ciliary lengthening from steady state (**Fig. 4.11**), again

suggesting an actin- and Arp2/3 complex-dependent process is required for ciliary elongation. We hypothesize that this Arp2/3 complex-dependent process is linked to endocytosis, but direct endocytosis during lithium treatment has not been observed in these cells.

Based on our data, we propose a model for lithium induced ciliary elongation where lithium targets GSK3 which results in a burst of Arp2/3 complex-dependent endocytosis to reclaim membrane for ciliary lengthening (**Fig. 4.12**). While we made strides toward identifying the membrane-related targets of GSK3 that result in ciliary elongation, we do not suggest that this is the only pathway targeted by GSK3 that contributes to ciliary elongation. An interesting next step would be to further dissect the targets of GSK3 that also contribute to this elongation through both targeted approaches looking at known targets of GSK3 and how they might be involved and through a more unbiased approach doing phosphoproteomics or a UV mutagenesis screen. For example, some mechanism must be at play that increases the recruitment of proteins that compose the axoneme and the IFT machinery. Additionally, it would be interesting to determine if these phenotypes observed in *Chlamydomonas* are conserved in other organisms that elongate their cilia in lithium.

Finally, because these data are focused on the ciliary membrane instead of the ciliary axoneme, they provide new insight and lend support to the models of ciliary regulation that have already been established (Ludington et al. 2015; Avasthi and Marshall 2012; Ishikawa and Marshall 2017a; Marshall 2015). The limiting-precursor model suggests that cells make exactly enough ciliary precursor proteins to form cilia of a certain length. However, even without new protein synthesis cilia are able to grow to half length (Rosenbaum, Moulder, and Ringo 1969), and in our data, cilia are able to immediately elongate their cilia well beyond steady-state length when treated with lithium. Therefore, for our lithium data and the regeneration in cycloheximide to fit, the limiting pre-cursor model would require additional mechanisms to allow for growth, like inhibition of autophagy, sequestration, and/or degradation during lithium treatment. Alternatively, it is possible that what is limiting cilium growth is not protein, but membrane, consistent with our data. The time-of-flight model proposes that there is a degradable signal, like phosphorylation, that is incorporated into IFT trains that move

into the cilia. The longer the IFT trains with the signal are in the cilia, the more time for the signal to be degraded, thus providing a readout of ciliary length. However, no active length measurer has been identified (Ishikawa and Marshall 2017b). In lithium treated cells, where cilia are much longer than usual, the degradable signal would normally be fully degraded by the time it reached the base of the cilia, so for this model to hold, lithium treatment would have to interfere with the degradation of this signal. Another model suggests that mechanosensitive ion channels in the ciliary membrane regulate ciliary length because the longer the cilia is the more ion channels can be present in the membrane and the more ions can be imported into the cell (Besschetnova et al. 2010; Beck and Uhl 1994). This model is interesting to consider as lithium itself is an ion, Li^+. It is therefore possible that the presence of lithium interferes with ion balance, such as that of Ca^{2+},to regulate cilium length (Besschetnova et al. 2010). The swim speed feedback model proposes that the cilia grow to an optimal length for swimming and that the length therefore depends on fluid forces upon the cilia (D. Tam and Hosoi 2011; Osterman and Vilfan 2011). Lithium treated cells are unable to swim as their cilia are not only elongated but also paralyzed (Wilson and Lefebvre 2004; Dentler 2005). This could affect the sensing of fluid forces in the cilia and cause feedback that could control ciliary length, although identified paralyzed flagella mutants do not generally display elongated cilia, so should this model be relevant lithium would have a different mechanism of paralysis. Our data could also support other models of ciliary length regulation that deal more with the axoneme if lithium is simultaneously affecting both the membrane and the axoneme. These models include the tubulin diffusion-based model (Levy 1974; Craft Van De Weghe et al. 2020), the signal diffusion-based model (Ludington et al. 2015), the kinesin diffusion-based model (Hendel, Thomson, and Marshall 2018), the molecular ruler model (Marshall 2015), and finally the balance point model, which considers the constant turnover of tubulin at ciliary tips and the fact that ciliary assembly is not a linear process, but instead slows as cilia lengthen. This model suggests that there is a point where the decreasing assembly rate and the constant disassembly rate where cilia reach a steady state length (Marshall and Rosenbaum 2001; Marshall et al. 2005).

Altogether, we show that GSK3 inhibition sparks Arp2/3 complex and actin-dependent endocytosis to reclaim membrane for ciliary elongation. These data fit well

with some of the proposed models for ciliary regulation outlined above. Some interesting next steps include determining other targets of GSK3 inhibition that might contribute to ciliary elongation, investigating whether this pathway is conserved across organisms as lithium induced ciliary elongation is, and uncovering new data that might help lithium-induced ciliary lengthening and our data fit with established and possibly new models of ciliary elongation.

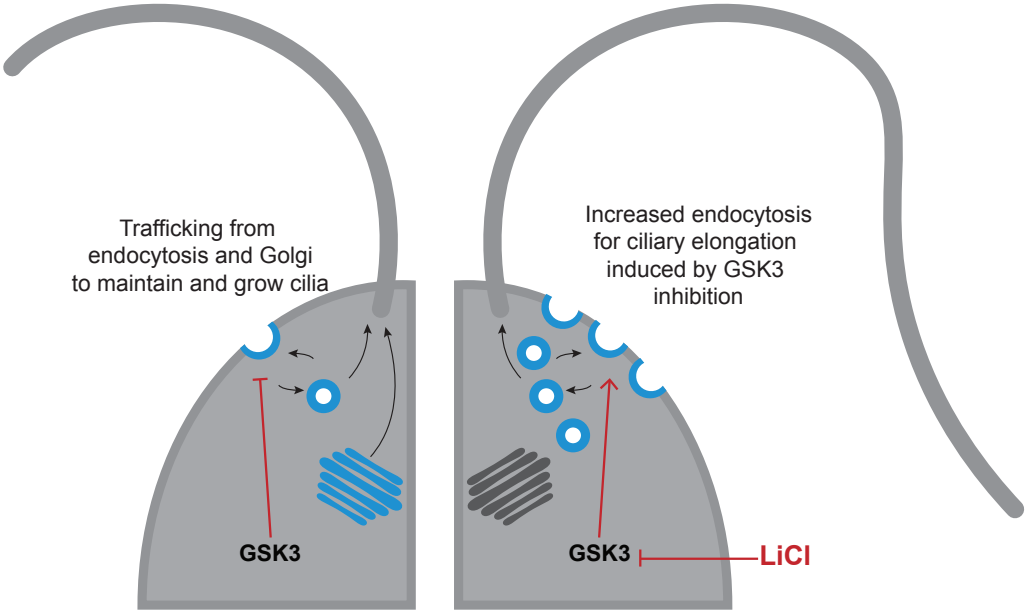

Fig. 4.12. Lithium targets GSK3 which results in a burst of endocytosis to reclaim membrane for ciliary elongation During normally ciliary maintenance and assembly, Golgi-derived membrane and some plasma membrane-derived membrane are transported to the cilium. However, during GSK3 inhibition, there is a burst of endocytic activity that is necessary to quickly grab membrane for ciliary elongation.

MATERIALS AND METHODS:

Strains:

The *arpc4* mutant (LMJ.RY0402.232713), *drp3* mutant (LMJ.RY0402.215697), and the wild-type parent strain (CC-5325) are from the *Chlamydomonas* Resource Center. The *arpc4* mutant was confirmed previously (Bigge et al. 2020). The *drp3* mutant was confirmed using 2 primer pairs. The first pair included: AGAAGGCCAGTTTCTCCTCGG and TTAAGCTCGACCTCCCTCAA. The second pair included: ATAGCCCGCCAAATCAGTCC and ACAGCAACACTGGTACACGC. Cells were grown and maintained on 1.5% Tris-Acetate Phosphate (TAP) agar plates. Prior to experiments, liquid TAP cultures were inoculated and grown overnight under constant red and blue light with agitation.

Ciliary studies:

Cells were treated with drugs at specified concentrations: 25 mM LiCl (MP Biomedicals, 194010), 200 μM CHIR99021 (Sigma, SML1046), 100 nM (2'Z,3'E)-6-Bromoindirubin-3′-oxime (Sigma, B1686), 20 μM Tideglusib (Sigma, SML0339), 10 μg/mL Cycloheximide (Sigma, C1988), 100 μM CK-666 (Sigma, 182515), 36 μM Brefeldin A (Sigma, B7651), and/or 100 μM Dynasore (Sigma, D7693). Cells were incubated with agitation under constant light for the specified times (usually 30 min, 60 min, and 90 min). Samples were taken prior to the experiment ('Pre') and at each time point by diluting 50 μl of cells 1:1 with 2% glutaraldehyde (EMS, 16220) and incubating at 4˚C to allow cells to sediment. Cells were then imaged using a Zeiss Axioscope 5 DIC microscope at 40X (0.75 numerical aperture) and Zeiss Zen 3.1 (blue edition) software. Cilia were then measured in ImageJ using the segmented line and fit spline functions. One cilium per cell was measured as the cilia of the same cell should be equivalent lengths.

Phalloidin staining:

Procedure was originally published in (Craig and Avasthi 2019). Cells were allowed to adhere to poly-lysine treated coverslips and then fixed with 4% paraformaldehyde in 1X HEPES. Cells were then permeabilized with 80% acetone followed by 100% acetone

before being allowed to dry fully. Coverslips rehydrated with PBS were then incubated with Phalloidin-Atto 488 (Sigma, 49409) for 16 minutes before being washed a final time with PBS. Coverslips were dried and then mounted with Fluoromount-G. Images were acquired using a Nikon Eclipse Ti-E microscope with a Yokogawa, two-camera CSU0W1 spinning disk system with a 100X oil-immersion objective lens (1.45 numerical aperture). Z-stacks were obtained using Nikon Elements. Then, maximum intensity projections were created in ImageJ. The number of cells with dots and the number of dots per cell were manually counted.

Live cell imaging:

The plasmid containing the Lifeact peptide tagged with mNeonGreen, pMO654, was a generous gift from Masayuki Onishi and is detailed in (Onishi et al. 2019). The plasmid was transformed into CC-5325 cells using electroporation. Briefly, cells were grown to an OD_{730} of 0.3-0.4 in liquid TAP media, pelleted, washed twice in Max Efficiency Buffer (Thermo), and finally resuspended to a volume of 250 μl Max Efficiency Buffer. This was divided into 2. To each, 1 μg of linearized plasmid was added. Cells with plasmid were incubated for 5 minutes at 4˚C. The cells were then transferred to 4mm electroporation cuvettes. Using a BioRad Gene Pulser XCell set to exponential decay at 500V, 50 μF, and 800 Ohms, cells were electroporated. Following electroporation, cells were incubated at room temperature for 15 minutes then resuspended in 7 mL of liquid TAP + 40 mM sucrose and incubated overnight in the dark with constant agitation. The following day, cells were plated on 1.5% TAP plates with the appropriate selection antibiotic (Paromomycin). Colonies were selected, grown up, and tested by visually looking for fluorescence.

For imaging, the same Nikon Spinning Disk microscope described above was used. Cells, either untreated or immediately following lithium treatment, were imaged every 100 ms for 1 minute to create time series. The time series were then analyzed in ImageJ/FIJI using the TrackMate plugin (Tinevez et al. 2017; Ershov et al. 2021). The plugin identifies spots and then tracks their movement throughout the video. Only the first 300 frames of each image were used to eliminate concerns of bleaching or cell movement.

Estimated object diameter was set to 1 μm and the quality threshold was set to 0.5. To make the colors of the track indicate how many tracks were present in each cell, they were colored by track ID with the highest track number value being set to the maximum value and the lowest track number value being set to the minimum.

Membrane stain:

Cells were incubated with 5 μg/mL FM4-64FX membrane stain (Invitrogen, F34653) in ice cold Hank's Buffered Salt Solution (HBSS) without magnesium or calcium for 1 minute on poly-lysine treated coverslips. Stain was tilted off and cells were fixed with 4% paraformaldehyde in HBSS without magnesium or calcium for 15 minutes. Cells were then washed 3 times in ice cold HBSS. Cells were imaged on the Nikon spinning disk previously described and images were analyzed in FIJI. Maximum intensity projections were created for visualization, and sum slices were used to quantify fluorescent intensity, which was then corrected for background.

ACKNOWLEDGEMENTS:

We want to express our appreciation to Masayuki Onishi for generously providing the Lifeact-mNeonGreen plasmid and the Avasthi lab for help throughout the project. We also want to thank the BioMT Core at Dartmouth College (NIH/NIGMS COBRE award P20-GM113132), the Genomics and Molecular Biology Shared Resources Core (NCI Cancer Center Support Grant 5P30CA023108-37), and Ann Lavanway for her help with microscopy. We also thank the Chlamydomonas Mutant Library Group at Princeton University, the Carnegie Institution for Science, and the Chlamydomonas Resource Center at the University of Minnesota for providing the indexed Chlamydomonas insertional mutant(s).

Finally, we thank our funding source, the NIGMS MIRA (R35GM128702).

REFERENCES:

Aghamohammadzadeh, Soheil, and Kathryn R. Ayscough. 2009. "Differential Requirements for Actin during Yeast and Mammalian Endocytosis." *Nature Cell Biology* 11 (8): 1039–42. https://doi.org/10.1038/ncb1918.

Asleson, C. M., and P. A. Lefebvre. 1998. "Genetic Analysis of Flagellar Length Control in Chlamydomonas Reinhardtii: A New Long-Flagella Locus and Extragenic Suppressor Mutations." *Genetics* 148 (2): 693–702. https://doi.org/10.1093/genetics/148.2.693.

Avasthi, Prachee, and Wallace F Marshall. 2012. "Stages of Ciliogenesis and Regulation of Ciliary Length." *Differentiation; Research in Biological Diversity* 83 (2): S30–42. https://doi.org/10.1016/j.diff.2011.11.015.

Avasthi, Prachee, Masayuki Onishi, Joel Karpiak, Ryosuke Yamamoto, Luke Mackinder, Martin C Jonikas, Winfield S Sale, Brian Shoichet, John R Pringle, and Wallace F Marshall. 2014. "Actin Is Required for IFT Regulation in Chlamydomonas Reinhardtii." *Current Biology* 24 (17): 2025–32. https://doi.org/10.1016/j.cub.2014.07.038.

Baluska, F., J. Samaj, A. Hlavacka, J. Kendrick-Jones, and D. Volkmann. 2004. "Actin-Dependent Fluid-Phase Endocytosis in Inner Cortex Cells of Maize Root Apices." *Journal of Experimental Botany* 55 (396): 463–73. https://doi.org/10.1093/jxb/erh042.

Barsel, S. E., D. E. Wexler, and P. A. Lefebvre. 1988. "Genetic Analysis of Long-Flagella Mutants of Chlamydomonas Reinhardtii." *Genetics* 118 (4): 637–48. https://doi.org/10.1093/genetics/118.4.637.

Basu, Roshni, Emilia Laura Munteanu, and Fred Chang. 2014. "Role of Turgor Pressure in Endocytosis in Fission Yeast." *Molecular Biology of the Cell* 25 (5): 679–87. https://doi.org/10.1091/mbc.E13-10-0618.

Beck, Christina, and Rainer Uhl. 1994. "On the Localization of Voltage-Sensitive Calcium Channels in the Flagella of Chlamydomonas Reinhardtii." *The Journal of Cell Biology* 125 (5): 1119–25.

Besschetnova, Tatiana Y, Elona Kolpakova-Hart, Yinghua Guan, Jing Zhou, Bjorn R Olsen, and Jagesh V Shah. 2010. "Identification of Signaling Pathways Regulating Primary Cilium Length and Flow-Mediated Adaptation." *Current Biology* 20 (2): 182–87.

Bigge, Brae M, Nicholas E Rosenthal, David Sept, Courtney M Schroeder, and Prachee Avasthi. 2020. "Initial Ciliary Assembly in Chlamydomonas</Em> Requires Arp2/3-Dependent Recruitment from a Ciliary Protein Reservoir in the Plasma Membrane." *BioRxiv*, January, 2020.11.24.396002. https://doi.org/10.1101/2020.11.24.396002.

Carlsson, Anders E., and Philip V. Bayly. 2014. "Force Generation by Endocytic Actin Patches in Budding Yeast." *Biophysical Journal* 106 (8): 1596–1606. https://doi.org/10.1016/j.bpj.2014.02.035.

Cheng, Xi, Gai Liu, Wenting Ke, Lijuan Zhao, Bo Lv, Xiaocui Ma, Nannan Xu, et al. 2017. "Building a Multipurpose Insertional Mutant Library for Forward and Reverse

Genetics in Chlamydomonas." *Plant Methods* 13 (1): 36. https://doi.org/10.1186/s13007-017-0183-5.

Craft Van De Weghe, Julie, J. Aaron Harris, Tomohiro Kubo, George B. Witman, and Karl F. Lechtreck. 2020. "Diffusion Rather than Intraflagellar Transport Likely Provides Most of the Tubulin Required for Axonemal Assembly in Chlamydomonas." *Journal of Cell Science* 133 (17). https://doi.org/10.1242/jcs.249805.

Craig, Evan W., and Prachee Avasthi. 2019. "Visualizing Filamentous Actin Using Phalloidin in Chlamydomonas Reinhardtii." *Bio-Protocol* 9 (12). https://doi.org/10.21769/BioProtoc.3274.

Dentler, William. 2005. "Intraflagellar Transport (IFT) during Assembly and Disassembly of Chlamydomonas Flagella." *The Journal of Cell Biology* 170 (4): 649–59. https://doi.org/10.1083/jcb.200412021.

Dentler, William. 2013. "A Role for the Membrane in Regulating Chlamydomonas Flagellar Length." *PLOS ONE* 8 (1): e53366. https://doi.org/10.1371/journal.pone.0053366.

Elde, Nels C, Garry Morgan, Mark Winey, Linda Sperling, and Aaron P Turkewitz. 2005. "Elucidation of Clathrin-Mediated Endocytosis in Tetrahymena Reveals an Evolutionarily Convergent Recruitment of Dynamin." *PLOS Genetics* 1 (5): e52. https://doi.org/10.1371/journal.pgen.0010052.

Ershov, Dmitry, Minh-Son Phan, Joanna W. Pylvänäinen, Stéphane U. Rigaud, Laure Le Blanc, Arthur Charles-Orszag, James R. W. Conway, et al. 2021. "Bringing TrackMate into the Era of Machine-Learning and Deep-Learning." *BioRxiv*, January, 2021.09.03.458852. https://doi.org/10.1101/2021.09.03.458852.

Golomb, Lior, Mohamad Abu-Abied, Eduard Belausov, and Einat Sadot. 2008. "Different Subcellular Localizations and Functions of Arabidopsis Myosin VIII." *BMC Plant Biology* 8 (January): 3. https://doi.org/10.1186/1471-2229-8-3.

Hendel, Nathan L., Matthew Thomson, and Wallace F. Marshall. 2018. "Diffusion as a Ruler: Modeling Kinesin Diffusion as a Length Sensor for Intraflagellar Transport." *Biophysical Journal* 114 (3): 663–74. https://doi.org/10.1016/j.bpj.2017.11.3784.

Ishikawa, Hiroaki, and Wallace F. Marshall. 2017a. "Intraflagellar Transport and Ciliary Dynamics." *Cold Spring Harbor Perspectives in Biology* 9 (3). https://doi.org/10.1101/cshperspect.a021998.

Ishikawa, Hiroaki, and Wallace F. Marshall. 2017b. "Testing the Time-of-Flight Model for Flagellar Length Sensing." *Molecular Biology of the Cell* 28 (23): 3447–56. https://doi.org/10.1091/mbc.e17-06-0384.

Jack, Brittany, and Prachee Avasthi. 2018. "Erratum to: Chemical Screening for Flagella-Associated Phenotypes in Chlamydomonas Reinhardtii." *Methods in Molecular Biology (Clifton, N.J.)* 1795: E1. https://doi.org/10.1007/978-1-4939-7874-8_19.

Jarvik, Jonathan W., Frederick D. Reinhart, Michael R. Kuchka, And Sally A. Adler. 1984. "Altered Flagellar Size-control in Shf-1 Short-flagella Mutants of Chlamydomonas Reinhardtii." *The Journal of Protozoology* 31 (2): 199–204.

Kasprowicz, Anna, Michał Michalak, Magdalena Wierzchowiecka, Michalina Maruniewicz, and Przemysław Wojtaszek. 2009. "[Endocytosis and actin-dependent transport of plant cell wall components]." *Postepy biochemii* 55 (2): 181–86.

Kong, Ji Na, Kara Hardin, Michael Dinkins, Guanghu Wang, Qian He, Tarik Mujadzic, Gu Zhu, Jacek Bielawski, Stefka Spassieva, and Erhard Bieberich. 2015. "Regulation of Chlamydomonas Flagella and Ependymal Cell Motile Cilia by Ceramide-Mediated Translocation of GSK3." *Molecular Biology of the Cell* 26 (24): 4451–65. https://doi.org/10.1091/mbc.E15-06-0371.

Laiman, Jessica, Julie Loh, Wei-Chun Tang, Mei-Chun Chuang, Hui-Kang Liu, Bi-Chang Chen, Yi-Cheng Chang, Lee-Ming Chuang, and Ya-Wen Liu. 2021. "Dynamin-2 Phosphorylation as A Critical Regulatory Target of Bin1 and GSK3α for Endocytosis in Muscle." *BioRxiv*, January, 2021.10.11.463889. https://doi.org/10.1101/2021.10.11.463889.

Lefebvre, P. A., S. A. Nordstrom, J. E. Moulder, and J. L. Rosenbaum. 1978. "Flagellar Elongation and Shortening in Chlamydomonas. IV. Effects of Flagellar Detachment, Regeneration, and Resorption on the Induction of Flagellar Protein Synthesis." *The Journal of Cell Biology* 78 (1): 8–27. https://doi.org/10.1083/jcb.78.1.8.

Lefebvre, Paul A. 1995. "Flagellar Amputation and Regeneration in Chlamydomonas." In *Methods in Cell Biology*, 47:3–7. Elsevier.

Levy, Elinor Miller. 1974. "Flagellar Elongation as a Moving Boundary Problem." *Bulletin of Mathematical Biology* 36: 265–73.

Li, Xiaobo, Weronika Patena, Friedrich Fauser, Robert E. Jinkerson, Shai Saroussi, Moritz T. Meyer, Nina Ivanova, et al. 2019. "A Genome-Wide Algal Mutant Library and Functional Screen Identifies Genes Required for Eukaryotic Photosynthesis." *Nature Genetics* 51 (4): 627–35. https://doi.org/10.1038/s41588-019-0370-6.

Ludington, William B., Hiroaki Ishikawa, Yevgeniy V. Serebrenik, Alex Ritter, Rogelio A. Hernandez-Lopez, Julia Gunzenhauser, Elisa Kannegaard, and Wallace F. Marshall. 2015. "A Systematic Comparison of Mathematical Models for Inherent Measurement of Ciliary Length: How a Cell Can Measure Length and Volume." *Biophysical Journal* 108 (6): 1361–79. https://doi.org/10.1016/j.bpj.2014.12.051.

Marshall, Wallace F. 2015. "How Cells Measure Length on Subcellular Scales." *Special Issue: Quantitative Cell Biology* 25 (12): 760–68. https://doi.org/10.1016/j.tcb.2015.08.008.

Marshall, Wallace F, Hongmin Qin, Mónica Rodrigo Brenni, and Joel L Rosenbaum. 2005. "Flagellar Length Control System: Testing a Simple Model Based on Intraflagellar Transport and Turnover." *Molecular Biology of the Cell* 16 (1): 270–78. https://doi.org/10.1091/mbc.e04-07-0586.

Marshall, Wallace F., and Joel L. Rosenbaum. 2001. "Intraflagellar Transport Balances Continuous Turnover of Outer Doublet Microtubules: Implications for Flagellar Length Control." *The Journal of Cell Biology* 155 (3): 405–14.

Miki, Daisuke, Yuki Kobayashi, Tomoya Okada, Tatuso Miyamoto, Nobuyuki Takei, Yuko Sekino, Noriko Koganezawa, Tomoaki Shirao, and Yumiko Saito. 2019. "Characterization of Functional Primary Cilia in Human Induced Pluripotent Stem Cell-Derived Neurons." *Neurochemical Research* 44 (7): 1736–44. https://doi.org/10.1007/s11064-019-02806-4.

Miyoshi, Ko, Kyosuke Kasahara, Ikuko Miyazaki, and Masato Asanuma. 2009. "Lithium Treatment Elongates Primary Cilia in the Mouse Brain and in Cultured Cells." *Biochemical and Biophysical Research Communications* 388 (4): 757–62. https://doi.org/10.1016/j.bbrc.2009.08.099.

Nachury, Maxence V., E. Scott Seeley, and Hua Jin. 2010. "Trafficking to the Ciliary Membrane: How to Get across the Periciliary Diffusion Barrier?" *Annual Review of Cell and Developmental Biology* 26: 59–87. https://doi.org/10.1146/annurev.cellbio.042308.113337.

Nakamura, Shogo, Hiroyoshi Takino, and Manabu K. Kojima. 1987. "Effect of Lithium on Flagellar Length in Chlamydomonas Reinhardtii." *Cell Structure and Function* 12 (4): 369–74. https://doi.org/10.1247/csf.12.369.

Nguyen, Rachel L., Lai-Wa Tam, and Paul A. Lefebvre. 2005. "The LF1 Gene of Chlamydomonas Reinhardtii Encodes a Novel Protein Required for Flagellar Length Control." *Genetics* 169 (3): 1415–24. https://doi.org/10.1534/genetics.104.027615.

Onishi, Masayuki, James G. Umen, Frederick R. Cross, and John R. Pringle. 2019. "Cleavage-Furrow Formation without F-Actin in Chlamydomonas</Em>." *BioRxiv*, January, 789016. https://doi.org/10.1101/789016.

Osterman, Natan, and Andrej Vilfan. 2011. "Finding the Ciliary Beating Pattern with Optimal Efficiency." *Proceedings of the National Academy of Sciences* 108 (38): 15727–32.

Ou, Young, Camila Dores, Jose-Rafael Rodriguez-Sosa, Frans A. van der Hoorn, and Ina Dobrinski. 2014. "Primary Cilia in the Developing Pig Testis." *Cell and Tissue Research* 358 (2): 597–605. https://doi.org/10.1007/s00441-014-1973-y.

Ou, Young, Yibing Ruan, Min Cheng, Joanna J Moser, Jerome B Rattner, and Frans A van der Hoorn. 2009. "Adenylate Cyclase Regulates Elongation of Mammalian Primary Cilia." *Experimental Cell Research* 315 (16): 2802–17. https://doi.org/10.1016/j.yexcr.2009.06.028.

Ou, Young, Ying Zhang, Min Cheng, Jerome B. Rattner, Ina Dobrinski, and Frans A. van der Hoorn. 2012. "Targeting of CRMP-2 to the Primary Cilium Is Modulated by GSK-3β." *PloS One* 7 (11): e48773. https://doi.org/10.1371/journal.pone.0048773.

Reiter, Jeremy F., and Michel R. Leroux. 2017. "Genes and Molecular Pathways Underpinning Ciliopathies." *Nature Reviews Molecular Cell Biology* 18 (9): 533–47. https://doi.org/10.1038/nrm.2017.60.

Rohatgi, Rajat, and William J Snell. 2010. "The Ciliary Membrane." *Current Opinion in Cell Biology* 22 (4): 541–46. https://doi.org/10.1016/j.ceb.2010.03.010.

Rosenbaum, J. L., J. E. Moulder, and D. L. Ringo. 1969. "Flagellar Elongation and Shortening in Chlamydomonas. The Use of Cycloheximide and Colchicine to Study the Synthesis and Assembly of Flagellar Proteins." *The Journal of Cell Biology* 41 (2): 600–619. https://doi.org/10.1083/jcb.41.2.600.

Samaj, Jozef, Nick D. Read, Dieter Volkmann, Diedrik Menzel, and Frantisek Baluska. 2005. "The Endocytic Network in Plants." *Trends in Cell Biology* 15 (8): 425–33. https://doi.org/10.1016/j.tcb.2005.06.006.

Sattarzadeh, Amirali, Rainer Franzen, and Elmon Schmelzer. 2008. "The Arabidopsis Class VIII Myosin ATM2 Is Involved in Endocytosis." *Cell Motility and the Cytoskeleton* 65 (6): 457–68. https://doi.org/10.1002/cm.20271.

Smillie, Karen J., and Michael A. Cousin. 2012. "Akt/PKB Controls the Activity-Dependent Bulk Endocytosis of Synaptic Vesicles." *Traffic (Copenhagen, Denmark)* 13 (7): 1004–11. https://doi.org/10.1111/j.1600-0854.2012.01365.x.

Soave, Arianna, Loraine L. Y. Chiu, Aisha Momin, and Stephen D. Waldman. 2022. "Lithium Chloride-Induced Primary Cilia Recovery Enhances Biosynthetic Response of Chondrocytes to Mechanical Stimulation." *Biomechanics and Modeling in Mechanobiology*, January. https://doi.org/10.1007/s10237-021-01551-4.

Srinivasan, Saipraveen, Christoph J. Burckhardt, Madhura Bhave, Zhiming Chen, Ping-Hung Chen, Xinxin Wang, Gaudenz Danuser, and Sandra L. Schmid. 2018. "A Noncanonical Role for Dynamin-1 in Regulating Early Stages of Clathrin-Mediated Endocytosis in Non-Neuronal Cells." *PLOS Biology* 16 (4): e2005377. https://doi.org/10.1371/journal.pbio.2005377.

Tam, Daniel, and AE Hosoi. 2011. "Optimal Feeding and Swimming Gaits of Biflagellated Organisms." *Proceedings of the National Academy of Sciences* 108 (3): 1001–6.

Tam, Lai-Wa, Nedra F. Wilson, and Paul A. Lefebvre. 2007. "A CDK-Related Kinase Regulates the Length and Assembly of Flagella in Chlamydomonas." *The Journal of Cell Biology* 176 (6): 819–29. https://doi.org/10.1083/jcb.200610022.

Thompson, Clare L., Anna Wiles, C. Anthony Poole, and Martin M. Knight. 2016. "Lithium Chloride Modulates Chondrocyte Primary Cilia and Inhibits Hedgehog Signaling." *FASEB Journal : Official Publication of the Federation of American Societies for Experimental Biology* 30 (2): 716–26. https://doi.org/10.1096/fj.15-274944.

Tinevez, Jean-Yves, Nick Perry, Johannes Schindelin, Genevieve M. Hoopes, Gregory D. Reynolds, Emmanuel Laplantine, Sebastian Y. Bednarek, Spencer L. Shorte, and Kevin W. Eliceiri. 2017. "TrackMate: An Open and Extensible Platform for Single-Particle Tracking." *Image Processing for Biologists* 115 (February): 80–90. https://doi.org/10.1016/j.ymeth.2016.09.016.

Volkmann, D., T. Mori, U. K. Tirlapur, K. König, T. Fujiwara, J. Kendrick-Jones, and F. Baluska. 2003. "Unconventional Myosins of the Plant-Specific Class VIII: Endocytosis, Cytokinesis, Plasmodesmata/Pit-Fields, and Cell-to-Cell Coupling." *Cell Biology International* 27 (3): 289–91. https://doi.org/10.1016/s1065-6995(02)00330-x.

Wilson, Nedra F, and Paul A Lefebvre. 2004. “Regulation of Flagellar Assembly by Glycogen Synthase Kinase 3 in Chlamydomonas Reinhardtii.” *Eukaryotic Cell* 3 (5): 1307–19. https://doi.org/10.1128/EC.3.5.1307-1319.2004.

CHAPTER 5:
CONCLUSIONS AND DISCUSSION

This work uses the model organism *Chlamydomonas reinhardtii* to help answer broader questions about actin biology, ciliary biology, and how these two could be related. More specifically, it provides evidence for a novel trafficking pathway for ciliary membrane and ciliary membrane proteins that is actin and Arp2/3 complex dependent and involves a previously uncharacterized endocytic process. It also provides some insight into novel actin functions and interactions and evolution of all these different processes.

Actin biology:

In the second chapter of this work, we aim to better understand aspects of actin biology including actin divergency, actin gene redundancy, and the interaction of actins with actin binding proteins (ABPs). Studies have been done to study divergent actins in isolation, but this work takes advantage of the unique actin cytoskeleton of *Chlamydomonas* to investigate the interaction of a divergent actin with ABPs in a system that has a built-in conventional actin control. We show that despite the sequence variance between IDA5 and NAP1 particularly in the region expected to bind the Arp2/3 complex, networks of either actin can be nucleated by the Arp2/3 complex for specific actin structures and functions. This suggests that we cannot predict binding based on sequence conservation or divergence alone. This is further supported by the structural similarity between IDA5 and NAP1 monomers, which suggests that structure may also be important (**Fig. 1.7**).

Another important element to consider is the divergence of the Arp2/3 complex itself. The predicted binding site used to inform this study was based on the binding of mammalian Arp2/3 complex to mammalian actin. However, the Arp2/3 complex of *Chlamydomonas* itself is not necessarily conserved in relation to mammalian actin (**Fig. 3.S1**). The core of the complex, ARPC2 and ARPC4, have 29.1% and 68% sequence similarity respectively. Arp2 and Arp3, the subunits that serve as the template for actin nucleation, have 75.1% and 61.5% sequence similarity respectively. The regulatory units, ARPC1 and ARPC3 have 44.1% and 52.6% sequence similarity. An ARPC5 subunit has not been found in *Chlamydomonas* meaning the Arp2/3 complex in this organism is perhaps a 6-membered complex or it contains a highly divergent ARPC5 subunit.

Complexes lacking ARPC5 are still able to function (Gournier et al., 2001), but there could be differences in binding. More work should be done to characterize the Arp2/3 complex in this organism. Specifically, uncovering a potential ARPC5 subunit by doing a pull down of the full complex would be useful. Further, because of the divergence of the complex, it would be useful to investigate the biochemical function of this complex. Is it able to nucleate branched or dendritic actin networks like it does in other systems?

Additionally, Arp2/3 complexes require activation. The complex binds an existing actin filament, and then, a nucleation promoting factor (NPF) binds the complex instigating a conformational change that is necessary for activation (Goley and Welch, 2006, p. 3). These NPFs include proteins such as N-WASP, WASP, WAVEs, WASH, and WHAMM (Suetsugu, 2013). In *Chlamydomonas*, none of these common NPFs have been identified based on sequence searches, and very few candidate NPFs have been identified at all. These candidate NPFs should be characterized to determine if they are required for Arp2/3 complex function in *Chlamydomonas,* but it might also be interesting to do an unbiased screen for other potential NPFs in this organism.

Beyond furthering our understanding about the Arp2/3 complex and its biochemical characteristics in this organism, additional investigation of the biochemical characteristics of the actins themselves would be an interesting next step. Purification of IDA5 and NAP1 would allow for studies regarding polymerization and binding of other ABPs. The regions of IDA5 that are responsible for polymerization are relatively well conserved. Further, IDA5 can polymerize as evidenced by it being labeled with phalloidin which only binds filamentous actin. However, the polymerization of NAP1 might be less straightforward. The residues important for polymerization are less conserved in NAP1 (**Fig. 5.1**). Studies using a tagged NAP1 have shown that it exists primarily in a monomeric state (Kato-Minoura, 2011), but our work also suggests that NAP1 can form filamentous actin rings, which we can label with phalloidin (Craig et al., 2019) (**Fig. 2.3 and Appendix I**). Further, in many studies of divergent actins, differences in polymerization kinetics have been found. In the parasites *Plasmodium* and *Toxoplasma,* whose sequences share only about 80% of their sequences with mammalian actin, the sequence differences allow for faster assembly and disassembly kinetics that allow the parasites to move more quickly during invasion (Kumpula et al., 2017;

Skillman et al., 2013). Finally, we wonder whether IDA5 and NAP1 can copolymerize or form heterologous filaments containing both actin isoforms. There is some evidence for this as the tagged NAP1 did seem to colocalize with IDA5 (Kato-Minoura, 2011), but more studies are needed to fully answer this question.

Additional work studying IDA5 and NAP1 could also provide novel information about ABPs and their interaction with divergent and conventional actins. Some organisms, like *Plasmodium* and *Toxoplasma,* that contain divergent actins contain conventional ABPs (Baum et al., 2006; Schüler and Matuschewski, 2006). The single cell parasite *Giardia* on the other hand, which contains only one highly divergent actin gene with only 58% sequence identity when compared to mammalian actin (Paredez et al., 2011), encodes almost no canonical ABPs. The organism lacks Arp2/3, formin, myosin, and other typically ubiquitously expressed ABPs (Morrison et al., 2007). However, *Giardia* is still able to perform many essential actin functions including maintaining cell morphogenesis, membrane trafficking, and cytokinesis without the assistance of the usual ABPs (Paredez et al., 2011). *Chlamydomonas* contains several conventional ABPs, including formins, profilin, myosins, and the Arp2/3 complex (**Table 1.1)**, but further studies of how these proteins interact with the conventional and the divergent actins in this organism could provide insight into evolution of the actin cytoskeleton. Further, an unbiased screen to identify novel binding partners could uncover new actin binding partners.

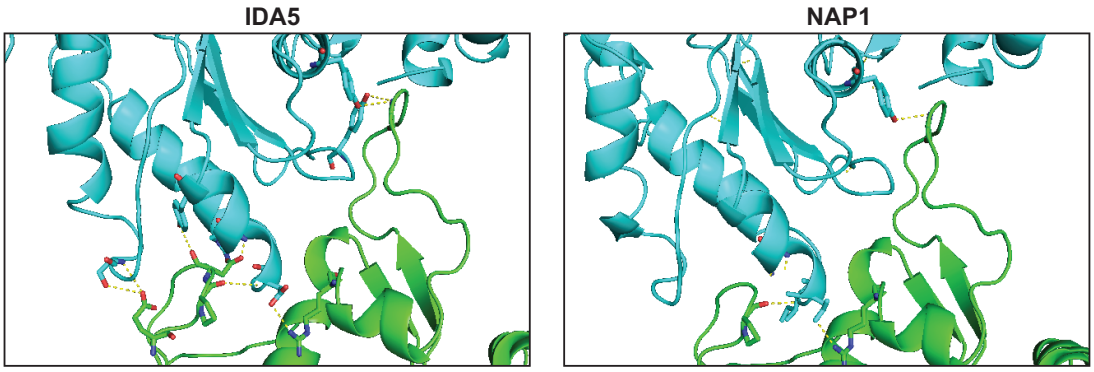

Fig. 5.1. Residues involved in polymerization are not well conserved in NAP1. Two monomers of IDA5 (left) or NAP1 (right) based on homology models. One monomer is cyan, the other is green . Interacting residues are highlighted in red and yellow. Note that NAP1 has less interactions present than IDA5.

In this work, we also found specific roles for Arp2/3 complex-mediated actin networks. We found that the Arp2/3 complex is required for forming a NAP1 ring around the nucleus when IDA5 is depolymerized with LatB. These rings are a novel structure that is not well understood. We hypothesize that these rings are responsible for either nuclear protection (Khatau et al., 2009), nuclear positioning (Gundersen and Worman, 2013), or nuclear rupture (Hatch and Hetzer, 2016; Wesolowska et al., 2018). Alternatively rings like these have been seen in mammalian cells undergoing the novel cell death pathway, ferroptosis (Dangol et al., 2019; Distéfano et al., 2017). Better understanding the proteins involved in ring formation and various treatments that trigger ring formation could help unlock the mystery around these rings.

Finally, we found that Arp2/3 complex-mediated IDA5 and NAP1 are involved in ciliary maintenance (**Fig. 2.4**). This is investigated thoroughly in the additional chapters, but further characterization of the other ABPs involved in ciliary assembly and maintenance would help inform the proposed mechanism.

Ciliary biology:

Ciliary maintenance and assembly are tightly regulated through a well-studied but still not well-known set of mechanisms. Much of what we do know about regulation of cilia comes from work focused on the availability, trafficking, and incorporation of the tubulin that make up the axoneme of the cilia or the other soluble proteins involved in intraflagellar transport (IFT) (Avasthi and Marshall, 2012; Hendel et al., 2018; Ishikawa and Marshall, 2017; Levy, 1974; Ludington et al., 2015; Marshall, 2015; Marshall and Rosenbaum, 2001; Rosenbaum et al., 1969). Models exist that consider the availability of protein, the trafficking or movement of protein to and from the cilia, and the dynamics of protein movement. These include models like the limiting precursor model that postulates there is a particular ciliary protein present in only enough quantity to make cilia of a specified length (Rosenbaum et al., 1969), diffusion-based models that focus on either tubulin or some other protein (Craft Van De Weghe et al., 2020; Hendel et al., 2018; Levy, 1974; Ludington et al., 2015), the balance point model which considers the assembly and disassembly rates of the cilium and the axoneme and how these dynamics are related (Marshall et al., 2005; Marshall and Rosenbaum, 2001), and others. However,

in this work, we focus instead on the membrane required for ciliary maintenance and assembly as the ciliary axoneme is ensheathed in a ciliary membrane that is contiguous with the cell body plasma membrane but separated by a septin-based diffusion barrier (Hu Qicong et al., 2010). We propose a new model based on membrane availability and dynamics that could work in concert with previous models of ciliary assembly and length maintenance that are more focused on protein availability and dynamics.

Traditionally, the Golgi is thought to be the primary source of membrane, proteins, and membrane proteins for cilia (Dentler, 2013; Nachury et al., 2010; Rohatgi and Snell, 2010). This is best illustrated in the case of Brefeldin A (BFA) treatment, which induces Golgi collapse by blocking traffic between the endoplasmic reticulum and the Golgi (Helms and Rothman, 1992; Hutchinson et al., 1983). When *Chlamydomonas* cells are treated with this drug, cilia shorten significantly (Dentler, 2013), suggesting that ciliary materials do come from the Golgi. Other work also shows that soluble proteins can "piggy-back" on post-Golgi vesicles bound for the cilia (Wood and Rosenbaum, 2014).

However, there is also data supporting the presence of membrane proteins in the cilia that originate from the cell body plasma membrane. In one experiment first done in Dentler, 2013 and repeated by us in Chapter 3 (**Fig. 3.8)**, all surface proteins are biotinylated. Cilia are then removed via pH shock and allowed to synchronously regrow. The new cilia are isolated and probed for biotinylated proteins. Any biotinylated proteins present in new cilia must have come from the plasma membrane, and in fact, we do see biotinylated proteins present in the new cilia (Bigge et al., 2020; Dentler, 2013). This confirms that cell body plasma membrane proteins can be transported from the cell body plasma membrane to the cilia, but it does not necessarily tell us how. It could be occurring through internalization and internal trafficking or through lateral diffusion through the diffusion barrier. One example of a protein that uses the first potential path is the specific ciliary membrane protein SAG1, which is relocalized from the cell body plasma membrane to cilia through internalization and trafficking on microtubules (Belzile et al., 2013; Ranjan et al., 2019). The data presented in Chapter 3 of this thesis further supports the presence of a path where ciliary materials exist in the plasma membrane and are reclaimed through some sort of internalization, like endocytosis, before being

trafficked to cilia. We find that this pathway is particularly important in the early stages of ciliary assembly when ciliary protein is readily available and cilia need to assemble rapidly. Thus, we hypothesize that during early assembly, membrane availability could be a limiting factor for ciliary growth, but upon new protein synthesis and further assembly, some other ciliary material could become limiting.

In Chapter 4 of this thesis, we also show that internalization or endocytosis is required for growth of cilia beyond full-length, again suggesting that membrane could be limiting when cilia are rapidly elongating and when they have plenty of protein present to assemble further. When *Chlamydomonas* cells are treated with lithium, cilia elongate to about 1.5 times their original length (Nakamura et al., 1987; Wilson and Lefebvre, 2004). This elongation in lithium is not specific to *Chlamydomonas* cells and occurs in organisms and cell types across the tree of life (Kong et al., 2015; Miki et al., 2019; Miyoshi et al., 2009; Ou et al., 2014, 2012; Soave et al., 2022; Thompson et al., 2016). Elongation in lithium does not require new protein synthesis, suggesting that the material for elongation past full-length is already present in the cell (Wilson and Lefebvre, 2004). In this work, we find that elongation requires membrane from endocytosis but not from the Golgi (**Fig. 4.2-4.3**), supporting a model where ciliary material can come from the cell body plasma membrane, and because this elongation in lithium occurs across cell types and organisms, this model could be applicable beyond *Chlamydomonas*.

Overall, we know that ciliary membrane proteins can and do come from the cell body plasma membrane (Bigge et al., 2020; Dentler, 2013). We know that for a specific ciliary membrane protein required for mating, relocalization from the cell body plasma membrane to the cilia occurs through internalization through an endocytosis-like process. Finally, we know that endocytosis is required for the elongation of cilia past full-length when cells are treated with LiCl (Bigge and Avasthi, 2022). Thus, we propose that an endocytic mechanism at play that might be involved in ciliary maintenance, assembly, and elongation.

This work has implications in studies of ciliary maintenance of length regulation, ciliary assembly, and ciliary elongation. The reliance of each of these processes on endocytosis suggests that perhaps membrane for cilia could be the limiting factor in length regulation and growth. Further studies would need to be done to determine if this

were the case, but an interesting path forward would be to determine if ciliary membrane was indeed limiting. To further investigate this, we turned to the actin cytoskeleton and the Arp2/3 complex.

Actin-based regulation of every step of ciliary assembly:

Most of the work in this thesis is aimed at understanding how actin is involved in ciliary growth and maintenance. In previous sections, we discussed that ciliary assembly is a complex process involving many subprocesses including protein synthesis, protein trafficking to cilia, protein trafficking within cilia (IFT), incorporation into cilia, recruitment and incorporation of membrane, and basal body docking. Researchers have been focused on understanding proteins involved in each individual step of assembly, but we find that actin is involved in regulating and driving every sub-process required for assembly.

Previous work from our lab found that filamentous actin is involved in incorporation of existing protein and organizing the transition zone, synthesis of new protein, and trafficking of that new protein through the Golgi to cilia (Jack et al., 2019). There are also defects in IFT train injection without actin (Avasthi et al., 2014). In this thesis, by focusing on actin networks mediated only by the Arp2/3 complex, we find additional roles for actin in ciliary maintenance and growth. Because the Arp2/3 complex is often involved in membrane remodeling functions in other systems, including the formation of lamellipodia and endocytosis (Aghamohammadzadeh and Ayscough, 2009; Basu et al., 2014; Carlsson and Bayly, 2014), and because the availability, recruitment, and incorporation of membrane into cilia are generally understudied, we focused our work on these topics.

We found that a Golgi-independent, Arp2/3 complex-dependent mechanism is at play in early ciliary assembly, ciliary maintenance, and ciliary elongation past steady-state length. We propose an endocytic mechanism where ciliary material is reclaimed from the cell body plasma membrane in an Arp2/3-complex dependent manner for ciliary assembly, maintenance, and elongation. This model is based on our findings that the Arp2/3 complex is required for the formation of actin puncta that resemble endocytic pits,

the internalization of a membrane dye, and the internalization of the specific ciliary protein.

While we propose an endocytic pathway for the delivery of ciliary material to the cilia for various functions, we do not claim that this is the only pathway available to the cilia. Which pathway a particular cargo takes is likely time- and cargo-dependent. For example, our proposed pathway is essential in early ciliary assembly when enough protein exists to assemble at least half-length cilia and when assembly must occur rapidly. This suggests that membrane could be a limiting factor early on in assembly or during periods of rapid assembly, but another ciliary component could be limiting later on. Thus, one important next step would be determining specific ciliary components or proteins that take the different pathways to cilia. This would allow for tagging and live cell tracking of different pathways to cilia during different processes including maintenance and assembly. This could answer questions about which pathway is taken, but it could also allow for further dissection of specific pathways. For example, we might discover if this cargo is trafficked on microtubule tracks or actin tracks.

Additionally, further characterization of endocytosis in this organism should be performed. Based on comparative genomics, we hypothesize that clathrin mediated endocytosis is occurring in this organism, but to confirm this, experiments should be done to identify other proteins involved in this process, to establish a timeline for the formation and dynamics of the endocytosis-like actin puncta, and to characterize endocytic structures using electron microscopy. The higher implications of such a project would include not only lending support to the model proposed in this thesis but also helping us understand how and why plant and animal endocytosis differ.

Finally, it is important to look at how conserved this pathway is in relation to other ciliated cells, including mammalian cells. There are several differences between *Chlamydomonas* and mammalian cells related to this pathway. The first is the presence or absence of a cell wall. *Chlamydomonas* cells contain a cell wall, while mammalian cells do not. This means that mammalian cells have an actin cortex that could alter the availability of the membrane for ciliary assembly, while *Chlamydomonas* cells are not complicated by the presence of this actin cortex. This also means that there could be differences in endocytosis in these cells. The Arp2/3 complex is involved in endocytosis

in yeast to overcome turgor pressure associated with the cell wall (Aghamohammadzadeh and Ayscough, 2009; Basu et al., 2014). Because mammalian cells do not have a cell wall, the Arp2/3 complex may not be involved. However, the finding that this pathway occurs not just for ciliary assembly but also for ciliary elongation in the presence of lithium, which occurs across cell types and organisms, suggests that a similar pathway does likely exist in those cells and organisms. Thus, despite the differences between *Chlamydomonas* and other organisms, these findings could provide potential new avenues of investigation into human ciliary diseases, termed ciliopathies. Understanding how cilia assemble and are maintained is important for understanding the underlying issues that result in these diseases.

Bringing it all together:

Here, we investigate the actin-dependent processes involved in ciliary assembly. We add to previous work from the lab that showed actin is involved in protein synthesis, protein trafficking from the Golgi, protein incorporation into cilia, and IFT (Jack et al., 2019; Avasthi et al, 2014). We show that actin networks composed of either IDA5 or NAP1 and mediated by the Arp2/3 complex are also required for the endocytic recruitment of membrane and membrane proteins from the cell body plasma membrane for ciliary assembly, maintenance, and elongation in lithium. So, despite cilia being primarily composed of microtubules, the mechanisms governing the sub-processes required for ciliary growth and maintenance seem to be primarily actin-based.

The work in this thesis will inform future studies on ciliary assembly and maintenance across organisms and cell types. It also provides insight into *Chlamydomonas* cell functions as prior to this work actin was relatively understudied in this organism and endocytosis had not yet been described. Finally, this work provides some insight into actin evolution as we study a case of gene redundancy where one gene is conventional and one is divergent.

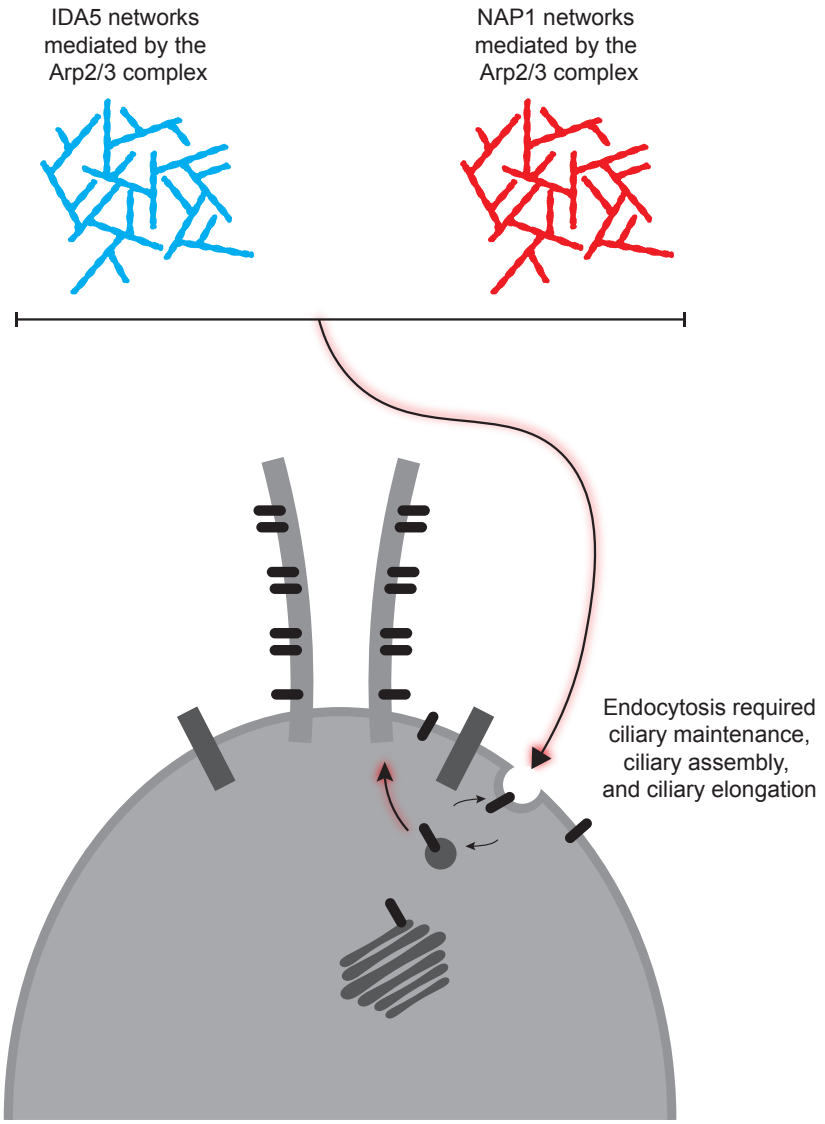

Fig. 5.2. Actin networks mediated by the Arp2/3 complex are required for endocytosis to reclaim membrane for ciliary assembly, ciliary length maintenance, and ciliary elongation.

References:

Aghamohammadzadeh, S., Ayscough, K.R., 2009. Differential requirements for actin during yeast and mammalian endocytosis. Nat. Cell Biol. 11, 1039–1042. https://doi.org/10.1038/ncb1918

Avasthi, P., Marshall, W.F., 2012. Stages of ciliogenesis and regulation of ciliary length. Differ. Res. Biol. Divers. 83, S30–S42. https://doi.org/10.1016/j.diff.2011.11.015

Avasthi, P., Onishi, M., Karpiak, J., Yamamoto, R., Mackinder, L., Jonikas, M.C., Sale, W.S., Shoichet, B., Pringle, J.R., Marshall, W.F., 2014. Actin Is Required for IFT Regulation in Chlamydomonas reinhardtii. Curr. Biol. 24, 2025–2032. https://doi.org/10.1016/j.cub.2014.07.038

Basu, R., Munteanu, E.L., Chang, F., 2014. Role of turgor pressure in endocytosis in fission yeast. Mol. Biol. Cell 25, 679–687. https://doi.org/10.1091/mbc.E13-10-0618

Baum, J., Papenfuss, A.T., Baum, B., Speed, T.P., Cowman, A.F., 2006. Regulation of apicomplexan actin-based motility. Nat. Rev. Microbiol. 4, 621–628. https://doi.org/10.1038/nrmicro1465

Belzile, O., Hernandez-Lara, C.I., Wang, Q., Snell, W.J., 2013. Regulated membrane protein entry into flagella is facilitated by cytoplasmic microtubules and does not require IFT. Curr. Biol. CB 23, 1460–1465. https://doi.org/10.1016/j.cub.2013.06.025

Bigge, B.M., Avasthi, P., 2022. Lithium-induced ciliary lengthening sparks Arp2/3 complex-dependent endocytosis. bioRxiv 2022.04.18.488674. https://doi.org/10.1101/2022.04.18.488674

Bigge, B.M., Rosenthal, N.E., Sept, D., Schroeder, C.M., Avasthi, P., 2020. Initial ciliary assembly in Chlamydomonas requires Arp2/3-dependent recruitment from a ciliary protein reservoir in the plasma membrane. bioRxiv 2020.11.24.396002. https://doi.org/10.1101/2020.11.24.396002

Carlsson, A.E., Bayly, P.V., 2014. Force generation by endocytic actin patches in budding yeast. Biophys. J. 106, 1596–1606. https://doi.org/10.1016/j.bpj.2014.02.035

Craft Van De Weghe, J., Harris, J.A., Kubo, T., Witman, G.B., Lechtreck, K.F., 2020. Diffusion rather than intraflagellar transport likely provides most of the tubulin required for axonemal assembly in Chlamydomonas. J. Cell Sci. 133. https://doi.org/10.1242/jcs.249805

Craig, E.W., Mueller, D.M., Bigge, B.M., Schaffer, M., Engel, B.D., Avasthi, P., 2019. The elusive actin cytoskeleton of a green alga expressing both conventional and divergent actins. Mol. Biol. Cell mbc.E19-03-0141. https://doi.org/10.1091/mbc.E19-03-0141

Dangol, S., Chen, Y., Hwang, B.K., Jwa, N.-S., 2019. Iron- and Reactive Oxygen Species-Dependent Ferroptotic Cell Death in Rice-Magnaporthe oryzae Interactions. Plant Cell 31, 189–209. https://doi.org/10.1105/tpc.18.00535

Dentler, W., 2013. A Role for the Membrane in Regulating Chlamydomonas Flagellar Length. PLOS ONE 8, e53366. https://doi.org/10.1371/journal.pone.0053366

Distéfano, A.M., Martin, M.V., Córdoba, J.P., Bellido, A.M., D'Ippólito, S., Colman, S.L., Soto, D., Roldán, J.A., Bartoli, C.G., Zabaleta, E.J., Fiol, D.F., Stockwell, B.R., Dixon, S.J., Pagnussat, G.C., 2017. Heat stress induces ferroptosis-like cell death in plants. J. Cell Biol. 216, 463–476. https://doi.org/10.1083/jcb.201605110

Goley, E.D., Welch, M.D., 2006. The ARP2/3 complex: an actin nucleator comes of age. Nat. Rev. Mol. Cell Biol. 7, 713–726. https://doi.org/10.1038/nrm2026

Gournier, H., Goley, E.D., Niederstrasser, H., Trinh, T., Welch, M.D., 2001. Reconstitution of Human Arp2/3 Complex Reveals Critical Roles of Individual Subunits in Complex Structure and Activity. Mol. Cell 8, 1041–1052. https://doi.org/10.1016/S1097-2765(01)00393-8

Gundersen, G.G., Worman, H.J., 2013. Nuclear positioning. Cell 152, 1376–1389. https://doi.org/10.1016/j.cell.2013.02.031

Hatch, E.M., Hetzer, M.W., 2016. Nuclear envelope rupture is induced by actin-based nucleus confinement. J. Cell Biol. 215, 27–36. https://doi.org/10.1083/jcb.201603053

Helms, J.B., Rothman, J.E., 1992. Inhibition by brefeldin A of a Golgi membrane enzyme that catalyses exchange of guanine nucleotide bound to ARF. Nature 360, 352–354. https://doi.org/10.1038/360352a0

Hendel, N.L., Thomson, M., Marshall, W.F., 2018. Diffusion as a Ruler: Modeling Kinesin Diffusion as a Length Sensor for Intraflagellar Transport. Biophys. J. 114, 663–674. https://doi.org/10.1016/j.bpj.2017.11.3784

Hu Qicong, Milenkovic Ljiljana, Jin Hua, Scott Matthew P., Nachury Maxence V., Spiliotis Elias T., Nelson W. James, 2010. A Septin Diffusion Barrier at the Base of the Primary Cilium Maintains Ciliary Membrane Protein Distribution. Science 329, 436–439. https://doi.org/10.1126/science.1191054

Hutchinson, C.R., Shu-Wen, L., McInnes, A.G., Walter, J.A., 1983. Comparative biochemistry of fatty acid and macrolide antibiotic (brefeldin a). Formation in penicillium brefeldianum. Tetrahedron 39, 3507–3513. https://doi.org/10.1016/S0040-4020(01)88660-9

Ishikawa, H., Marshall, W.F., 2017. Testing the time-of-flight model for flagellar length sensing. Mol. Biol. Cell 28, 3447–3456. https://doi.org/10.1091/mbc.e17-06-0384

Jack, B., Mueller, D.M., Fee, A.C., Tetlow, A.L., Avasthi, P., 2019. Partially Redundant Actin Genes in Chlamydomonas Control Transition Zone Organization and Flagellum-Directed Traffic. Cell Rep. 27, 2459-2467.e3. https://doi.org/10.1016/j.celrep.2019.04.087

Kato-Minoura, T., 2011. Extremely low polymerizability of a highly-divergent Chlamydomonas actin (NAP). Biochem. Biophys. Res. Commun. 412, 723–727. https://doi.org/10.1016/j.bbrc.2011.08.040

Khatau, S.B., Hale, C.M., Stewart-Hutchinson, P.J., Patel, M.S., Stewart, C.L., Searson, P.C., Hodzic, D., Wirtz, D., 2009. A perinuclear actin cap regulates nuclear shape. Proc. Natl. Acad. Sci. U. S. A. 106, 19017–19022. https://doi.org/10.1073/pnas.0908686106

Kong, J.N., Hardin, K., Dinkins, M., Wang, G., He, Q., Mujadzic, T., Zhu, G., Bielawski, J., Spassieva, S., Bieberich, E., 2015. Regulation of Chlamydomonas flagella and ependymal cell motile cilia by ceramide-mediated translocation of GSK3. Mol. Biol. Cell 26, 4451–4465. https://doi.org/10.1091/mbc.E15-06-0371

Kumpula, E.-P., Pires, I., Lasiwa, D., Piirainen, H., Bergmann, U., Vahokoski, J., Kursula, I., 2017. Apicomplexan actin polymerization depends on nucleation. Sci. Rep. 7, 12137. https://doi.org/10.1038/s41598-017-11330-w

Levy, E.M., 1974. Flagellar elongation as a moving boundary problem. Bull. Math. Biol. 36, 265–273.

Ludington, W.B., Ishikawa, H., Serebrenik, Y.V., Ritter, A., Hernandez-Lopez, R.A., Gunzenhauser, J., Kannegaard, E., Marshall, W.F., 2015. A Systematic Comparison of Mathematical Models for Inherent Measurement of Ciliary Length: How a Cell Can Measure Length and Volume. Biophys. J. 108, 1361–1379. https://doi.org/10.1016/j.bpj.2014.12.051

Marshall, W.F., 2015. How Cells Measure Length on Subcellular Scales. Spec. Issue Quant. Cell Biol. 25, 760–768. https://doi.org/10.1016/j.tcb.2015.08.008

Marshall, W.F., Qin, H., Rodrigo Brenni, M., Rosenbaum, J.L., 2005. Flagellar length control system: testing a simple model based on intraflagellar transport and turnover. Mol. Biol. Cell 16, 270–278. https://doi.org/10.1091/mbc.e04-07-0586

Marshall, W.F., Rosenbaum, J.L., 2001. Intraflagellar transport balances continuous turnover of outer doublet microtubules: implications for flagellar length control. J. Cell Biol. 155, 405–414.

Miki, D., Kobayashi, Y., Okada, T., Miyamoto, T., Takei, N., Sekino, Y., Koganezawa, N., Shirao, T., Saito, Y., 2019. Characterization of Functional Primary Cilia in Human Induced Pluripotent Stem Cell-Derived Neurons. Neurochem. Res. 44, 1736–1744. https://doi.org/10.1007/s11064-019-02806-4

Miyoshi, K., Kasahara, K., Miyazaki, I., Asanuma, M., 2009. Lithium treatment elongates primary cilia in the mouse brain and in cultured cells. Biochem. Biophys. Res. Commun. 388, 757–762. https://doi.org/10.1016/j.bbrc.2009.08.099

Morrison, H.G., McArthur, A.G., Gillin, F.D., Aley, S.B., Adam, R.D., Olsen, G.J., Best, A.A., Cande, W.Z., Chen, F., Cipriano, M.J., Davids, B.J., Dawson, S.C., Elmendorf, H.G., Hehl, A.B., Holder, M.E., Huse, S.M., Kim, U.U., Lasek-Nesselquist, E., Manning, G., Nigam, A., Nixon, J.E.J., Palm, D., Passamaneck, N.E., Prabhu, A., Reich, C.I., Reiner, D.S., Samuelson, J., Svard, S.G., Sogin, M.L., 2007. Genomic Minimalism in the Early Diverging Intestinal Parasite Giardia lamblia. Science 317, 1921. https://doi.org/10.1126/science.1143837

Nachury, M.V., Seeley, E.S., Jin, H., 2010. Trafficking to the ciliary membrane: how to get across the periciliary diffusion barrier? Annu. Rev. Cell Dev. Biol. 26, 59–87. https://doi.org/10.1146/annurev.cellbio.042308.113337

Nakamura, S., Takino, H., Kojima, M.K., 1987. Effect of Lithium on Flagellar Length in Chlamydomonas reinhardtii. Cell Struct. Funct. 12, 369–374. https://doi.org/10.1247/csf.12.369

Ou, Y., Dores, C., Rodriguez-Sosa, J.-R., van der Hoorn, F.A., Dobrinski, I., 2014. Primary cilia in the developing pig testis. Cell Tissue Res. 358, 597–605. https://doi.org/10.1007/s00441-014-1973-y

Ou, Y., Zhang, Y., Cheng, M., Rattner, J.B., Dobrinski, I., van der Hoorn, F.A., 2012. Targeting of CRMP-2 to the primary cilium is modulated by GSK-3β. PloS One 7, e48773. https://doi.org/10.1371/journal.pone.0048773

Paredez, A.R., Assaf, Z.J., Sept, D., Timofejeva, L., Dawson, S.C., Wang, C.J., Cande, W.Z., 2011. An actin cytoskeleton with evolutionarily conserved functions in the absence of canonical actin-binding proteins. Proc Natl Acad Sci U A 108, 6151–6. https://doi.org/10.1073/pnas.1018593108

Ranjan, P., Awasthi, M., Snell, W.J., 2019. Transient Internalization and Microtubule-Dependent Trafficking of a Ciliary Signaling Receptor from the Plasma Membrane to the Cilium. Curr. Biol. 29, 2942-2947.e2. https://doi.org/10.1016/j.cub.2019.07.022

Rohatgi, R., Snell, W.J., 2010. The ciliary membrane. Curr. Opin. Cell Biol. 22, 541–546. https://doi.org/10.1016/j.ceb.2010.03.010

Rosenbaum, J.L., Moulder, J.E., Ringo, D.L., 1969. Flagellar elongation and shortening in Chlamydomonas. The use of cycloheximide and colchicine to study the synthesis and assembly of flagellar proteins. J. Cell Biol. 41, 600–619. https://doi.org/10.1083/jcb.41.2.600

Schüler, H., Matuschewski, K., 2006. Regulation of Apicomplexan Microfilament Dynamics by a Minimal Set of Actin-Binding Proteins. Traffic 7, 1433–1439. https://doi.org/10.1111/j.1600-0854.2006.00484.x

Skillman, K.M., Ma, C.I., Fremont, D.H., Diraviyam, K., Cooper, J.A., Sept, D., Sibley, L.D., 2013. The unusual dynamics of parasite actin result from isodesmic polymerization. Nat. Commun. 4, 2285. https://doi.org/10.1038/ncomms3285

Soave, A., Chiu, L.L.Y., Momin, A., Waldman, S.D., 2022. Lithium chloride-induced primary cilia recovery enhances biosynthetic response of chondrocytes to mechanical stimulation. Biomech. Model. Mechanobiol. https://doi.org/10.1007/s10237-021-01551-4

Suetsugu, S., 2013. Activation of nucleation promoting factors for directional actin filament elongation: allosteric regulation and multimerization on the membrane. Semin. Cell Dev. Biol. 24, 267–271. https://doi.org/10.1016/j.semcdb.2013.01.006

Thompson, C.L., Wiles, A., Poole, C.A., Knight, M.M., 2016. Lithium chloride modulates chondrocyte primary cilia and inhibits Hedgehog signaling. FASEB J. Off. Publ. Fed. Am. Soc. Exp. Biol. 30, 716–726. https://doi.org/10.1096/fj.15-274944

Wesolowska, N., Machado, P., Geiss, C., Kondo, H., Mori, M., Schwab, Y., Lénárt, P., 2018. An F-actin shell ruptures the nuclear envelope by sorting pore-dense and pore-free membranes in meiosis of starfish oocytes. bioRxiv 480434. https://doi.org/10.1101/480434

Wilson, N.F., Lefebvre, P.A., 2004. Regulation of flagellar assembly by glycogen synthase kinase 3 in Chlamydomonas reinhardtii. Eukaryot. Cell 3, 1307–1319. https://doi.org/10.1128/EC.3.5.1307-1319.2004

Wood, C.R., Rosenbaum, J.L., 2014. Proteins of the Ciliary Axoneme Are Found on Cytoplasmic Membrane Vesicles during Growth of Cilia. Curr. Biol. 24, 1114–1120. https://doi.org/10.1016/j.cub.2014.03.047

APPENDIX I:

The elusive actin cytoskeleton of a green alga expressing both conventional and divergent actins

Craig EC[1], Mueller DM[1], Bigge BM[1], Schaffer M[2], Engel BD[2], Avasthi, P[1]

Published in: Mol Biol Cell. 2019 Oct 15; 30(22): 2827–2837

[1]Department of Anatomy and Cell Biology, University of Kansas Medical Center, Kansas City, KS 66160

[2]Department of Molecular and Structural Biology, Max Planck Institute of Biochemistry, 82152 Martinsried, Germany

Published in: Mol Biol Cell. 2019 Oct 15; 30(22): 2827–2837. doi: 10.1091/mbc.E19-03-0141.

Contributions by BM Bigge: Fig. s 5, 7, 8 (experiments, analysis, data visualization), formatting other figs, writing and editing the manuscript

Introduction:

Actin is a highly conserved protein that is essential for survival in most eukaryotic cells (Pollard et al., 2000a). In yeast, the only actin isoform makes distinct structures such as actin patches, cables, and cytokinetic rings (Kilmartin and Adams, 1984; Warren et al., 2002). These structures function in endocytosis, organelle and protein transport, and cell division, respectively. Unlike yeast, mammalian cells have six different actin isoforms encoded by six separate genes. These function collectively to regulate cell morphology, motility, mechanotransduction, membrane dynamics, and intracellular trafficking. Some of these functions require complex interactions between actin isoforms, and single actin knockout studies in mice revealed that loss of one gene causes a compensatory up-regulation of a subset of the remaining actin isoforms (Benjamin J Perrin and Ervasti, 2010).

The genome of the unicellular green alga *Chlamydomonas reinhardtii* contains two actin genes that vary significantly in sequence. Inner dynein arm 5 (IDA5) is a highly conserved conventional actin, whereas novel actin-like protein 1 (NAP1) is a divergent actin that only shares ~65% sequence identity with mammalian actin (Takako Kato-Minoura et al., 1997; M. Onishi et al., 2016). Genetic loss of IDA5, a condition in which NAP1 is expressed at low levels, results in slow swimming (Ohara et al., 1998a) and early ciliary growth defects due to reduced ciliary protein accumulation and entry (Avasthi et al., 2014a). Ciliary growth ultimately proceeds and can reach normal length. However, when both actins are disrupted acutely, *Chlamydomonas* cells show dramatic defects in ciliary protein synthesis, vesicular trafficking, and organization of a key gating region dictating ciliary protein composition (Jack et al., 2019a). Given that *ida5* mutants expressing NAP1 alone do not show these defects, it appears NAP1 can largely perform the actin-dependent functions needed for ciliary assembly despite its sequence divergence with IDA5. Although we have been able to genetically and chemically dissect the functions of the individual actin isoforms, detailed visual characterization of filamentous actin networks has eluded the field.

Although actin filaments are readily visualized by traditional phallotoxin staining in mammalian systems, a variety of protein and cellular differences complicate actin visualization in protists and highlight the need for labeling optimization in different

cellular systems. In the parasite Toxoplasma gondii, the actin gene ACT1 shares 83% sequence identity with mammalian actin and is required for cell motility, yet filamentous actin is undetectable by phalloidin staining (Dobrowolski et al., 1997). Other conventional filamentous actin labeling techniques such as LifeAct and SiR-actin also fail to label filamentous actin in this parasite (Periz et al., 2017a). This may be due to the highly dynamic filament turnover and distinct actin polymerization kinetics (Miraldi et al., 2008) found in T. gondii and closely related Plasmodium falciparum. Biochemical assays also show that 97% of the parasites' actin exists in globular form (Dobrowolski et al., 1997; Skillman et al., 2011; Wetzel et al., 2003), creating unfavorable conditions for filamentous actin staining. As in parasitic protists, *Chlamydomonas* actin visualization with conventional strategies has been challenging. Actin antibodies do not discriminate between filamentous and monomeric actin, and previous attempts to visualize the filamentous actin cytoskeleton using fluorescent phallotoxins resulted in a diffuse signal throughout the cytoplasm in vegetative *Chlamydomonas* cells (J D Harper et al., 1992), leading some to conclude that these cells made few, if any, filaments (J D Harper et al., 1992). The only condition where phallotoxins have been shown to clearly label filamentous actin in *Chlamydomonas* is in gametes, where filamentous actin-rich tubules can be seen at the apical surface between the flagella upon mating or artificial induction (Patricia A. Detmers et al., 1985).

Advancements in vegetative *Chlamydomonas* actin filament visualization came from live-cell imaging using strains expressing the fluorescently tagged filament binding peptide, LifeAct (Avasthi et al., 2014a; M. Onishi et al., 2016). This method identified linear structures at the posterior of the nucleus and less frequently at the base of the flagella. Acute treatment with the actin-depolymerizing agent latrunculin B (Lat B) eliminated this labeling (Avasthi et al., 2014a; M. Onishi et al., 2016), demonstrating the specificity of the fluorescent LifeAct for actin filaments.

However, longer incubation with Lat B restored a partial signal with a slightly different distribution (M. Onishi et al., 2016). This new signal likely represents the Lat B–induced up-regulation of a second *Chlamydomonas* actin normally expressed at low levels, the novel actin-like protein NAP1 (T Kato-Minoura et al., 1998; M. Onishi et al., 2016). Despite the identification of a clear filamentous actin-based perinuclear structure

using fluorescent LifeAct, technical challenges to maintaining LifeAct expression and the inability to preserve labeled structures in fixed cells for colocalization with cellular organelles required a different method of actin visualization.

We reasoned that *Chlamydomonas* actin, IDA5, which shares 90% sequence identity with mammalian actins, is inherently capable of binding fluorescent phallotoxins due to the intense staining of fertilization tubules in gametes. For this study, we developed an optimized protocol for phalloidin staining that recapitulated LifeAct labeling (Evan W. Craig and Avasthi, 2019). Using this method, and corroborating with live-cell visualization and cryo-electron tomography (cryo-ET), we can now show for the first time how actin filaments are localized and dynamically redistributed in vegetative and gametic *Chlamydomonas* cells. In addition, we applied this staining method to mutants of each actin isotype to reveal new insights into isoform-specific organization and function.

Results:

Filamentous actin visualization in vegetative Chlamydomonas *achieved by an optimized phalloidin staining protocol*

To optimize phalloidin labeling, which previously produced only a weak, diffuse, seemingly nonspecific signal in vegetative cells (**Fig. AI.1A, C, and E**; and Harper et al., 1992), we used a combination of bright and photostable Atto fluorophores and reduced incubation times to limit background fluorescence. Specifically, reducing incubation to 16 min was crucial to successful staining. We also improved the imaging by employing deconvolution microscopy to remove out-of-focus light. Using this optimized protocol (Evan W. Craig and Avasthi, 2019), we found that the pattern of phalloidin staining matched what was seen for LifeAct–Venus fluorescence, with a tangle of linear filaments at the posterior of the nucleus (**Fig. AI.1B, D, and F**), providing further support that the previously identified midcell LifeAct signal (Avasthi et al., 2014a; M. Onishi et al., 2016) represents the filamentous actin population. Phalloidin-labeled structures were disrupted when treated with the actin-depolymerizing drug, Lat B (**Fig. AI.2**).

With a newly developed method for actin labeling *Chlamydomonas* cells, we tested the ability of Atto 488 phalloidin to costain with probes for other cytoskeletal

proteins (**Fig. AI.3**). Filamentous actin was observed in the midcell region (**Fig. AI.3A**), and costaining with 4′,6-diamidino-2-phenylindole (DAPI), a DNA label, we observed localization posterior to the nucleus with occasional threads linking to a region near the apical flagellar base (**Fig. AI.3B**). Atto 488 phalloidin costained efficiently with centrin antibodies, which mark the basal bodies and fibers connecting to the nucleus (**Fig. AI.3C**), as well as α-tubulin antibodies, which stain microtubules in the cilia, basal bodies, and cell body (**Fig. AI.3D**).

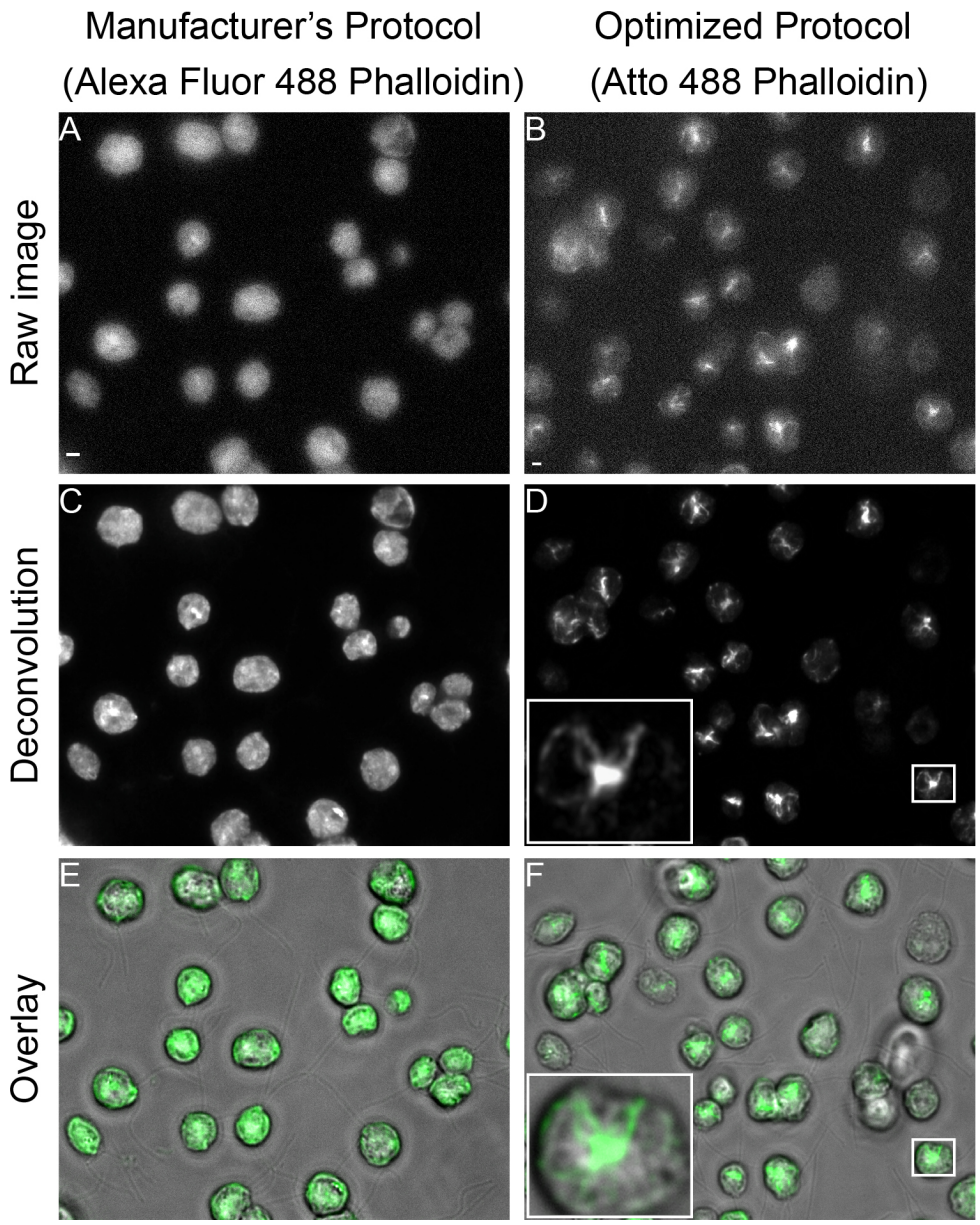

Fig. AI.1. Filamentous actin staining optimization using phalloidin in *Chlamydomonas reinhardtii*. (A) Raw fluorescence image of phalloidin-stained vegetative *Chlamydomonas* cells using the manufacturer's recommended protocol and Alexa Fluor 488 phalloidin. Signal is generally bright with hazy fluorescence throughout the cell, similar to previous reports. (B) Raw fluorescence image using our optimized phalloidin protocol and Atto 488 phalloidin (49409; Sigma) reagent. Signal from filamentous actin is clearly present. (C) Deconvolution of the image in A does not reveal much actin signal that can be easily distinguished from the high background fluorescence. (D) Deconvolution of B shows filamentous actin posterior of the nucleus and filaments spanning across the cell body. (E) Overlay of C and the brightfield image with phalloidin signal in green. (F) Overlay of D and the brightfield image shows that in vegetative cells, the brightness and staining consistency were greatly enhanced by using the Atto 488 conjugate instead of Alexa Fluor 488. Scale bar is 5 μm. **From (Craig et al., 2019).**

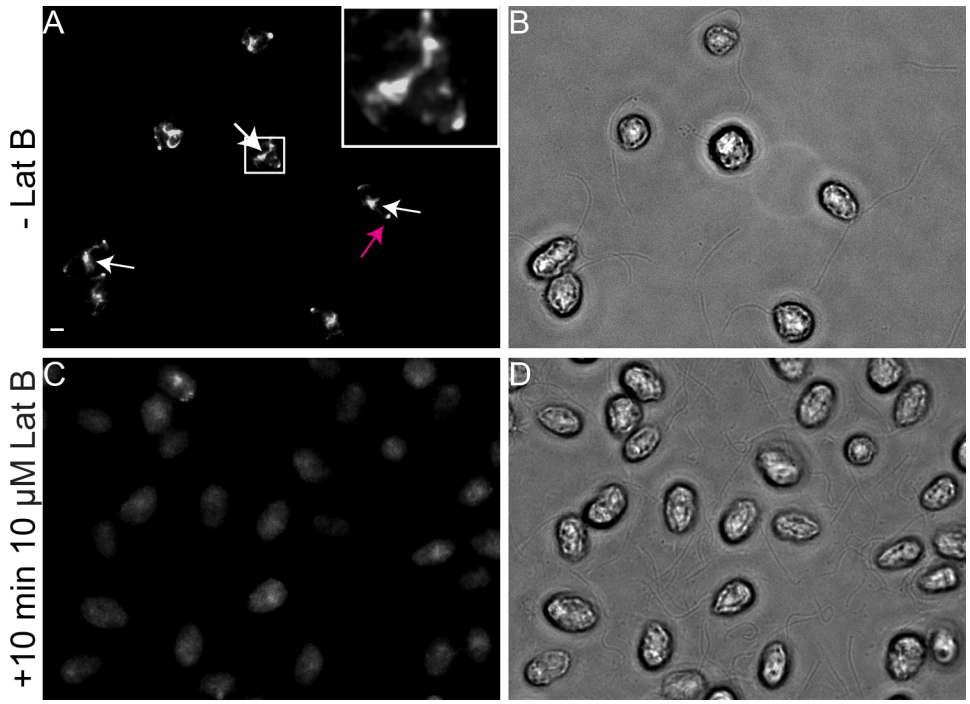

Fig. AI.2. Phalloidin-labeled filamentous actin depolymerizes upon Lat B treatment in wild-type CC-125 cells. (A) Gametic CC-125 cells stained with Atto 488 phalloidin, showing midcell actin staining (white arrows) and apical actin fluorescence (magenta arrow). (B) Brightfield image of the cells in A showing filamentous actin signal. (C) Atto 488 phalloidin–stained gametic CC-125 cells after 10 min of treatment with 10 μM Lat B. Filamentous actin signal dramatically decreases. (D) Brightfield image of cells in C show filamentous actin signal in relation to the cell body and flagella. Scale bar is5 μm. **From (Craig et al., 2019).**

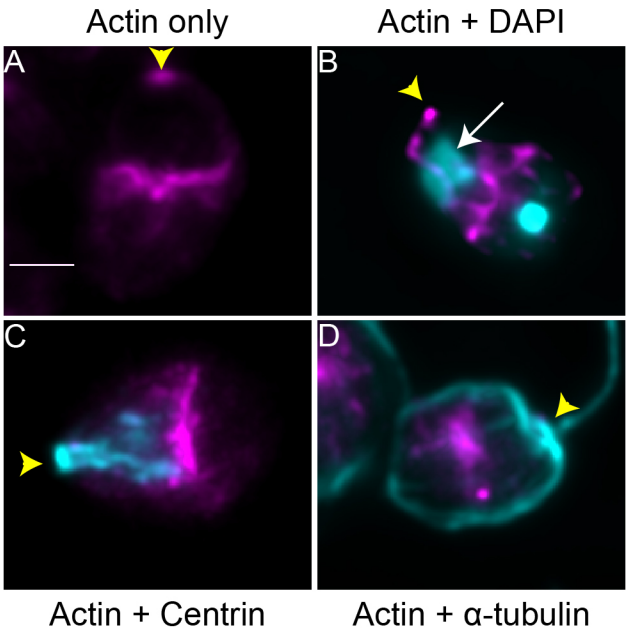

Fig. AI.3. Actin colabeling with cellular structures. (A) Representative image of filamentous actin localization (magenta) in a *Chlamydomonas* cell stained with Atto 488 phalloidin. (B) Atto phalloidin and DAPI costaining, showing filamentous actin (magenta) in relation to the *Chlamydomonas* nucleus (cyan). The intense punctate DAPI staining toward the cell's basal side labels chloroplast DNA packed within DNA–protein structures called nucleoids. The nucleus is marked with an arrow and has broader and less intense DAPI staining. (C) Cell costained with phalloidin (magenta) and anti-centrin antibody (cyan). (D) Cell costained with phalloidin (magenta) and anti–α-tubulin antibody, which marks axonemal and cytoplasmic microtubules (cyan). Yellow arrowheads specify the apical end of the cell. Scale bar is 5 μm.

In situ cryo-electron tomography of actin filaments

To directly visualize actin filaments within the native cellular environment, we rapidly froze vegetative *Chlamydomonas* cells in vitreous ice, thinned these cells by focused ion beam milling, and then imaged them by cryo-ET (Asano et al., 2016). Helical filaments with a diameter of ~7 nm (consistent with filamentous actin) were observed in the cytosol at the posterior side of the nucleus, near the nuclear envelope, endoplasmic reticulum, and Golgi (**Fig. AI.4**). In addition to relatively straight individual actin filaments (**Fig. AI.4A and B**), we also observed loosely tangled bundles of filaments with increased local curvature (**Fig. AI.4C**).

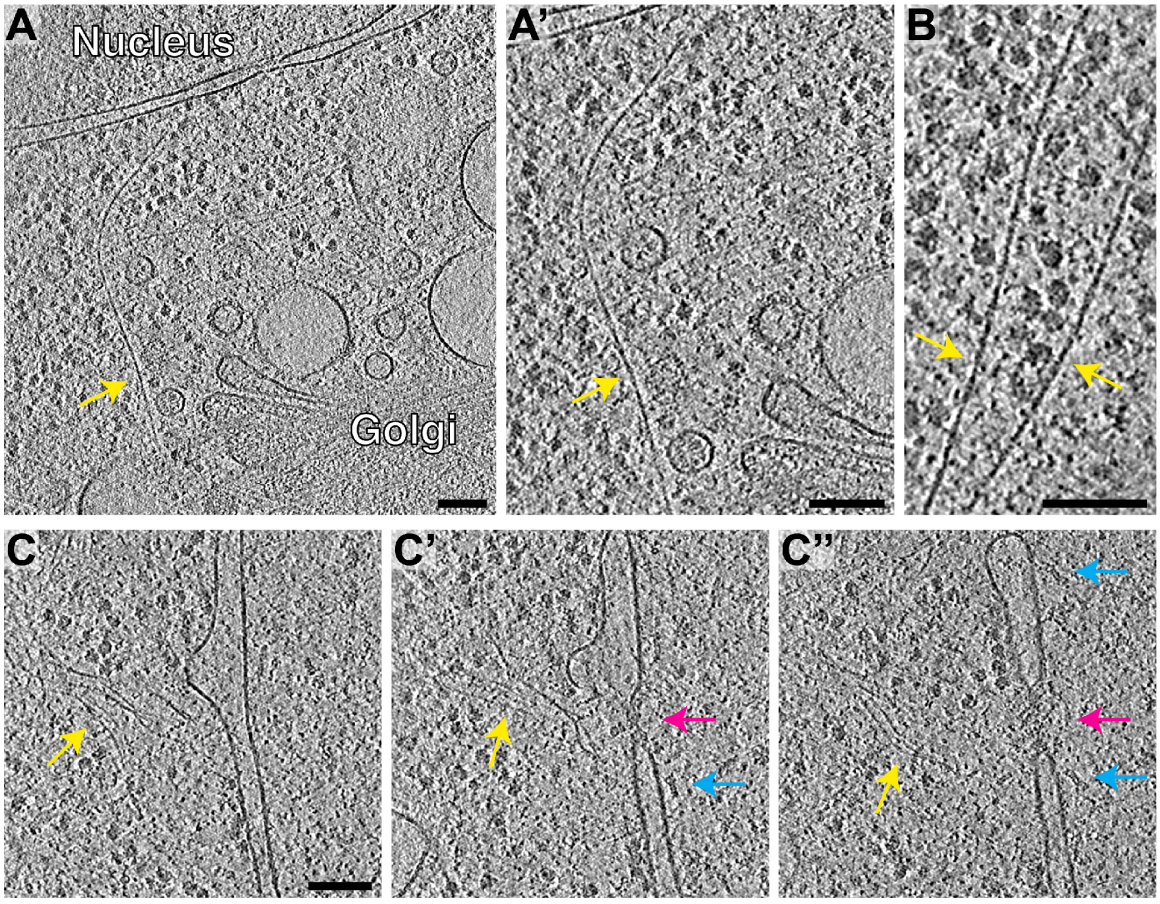

Fig. AI.4. Direct visualization of actin filaments inside native *Chlamydomonas* cells by in situ cryo-ET. (A, B) Slices through tomographic volumes. Yellow arrows indicate individual actin filaments near the nuclear envelope and Golgi apparatus. A′ is an enlarged view of the filament from A. The helical structure of the actin filaments is apparent in B. (C) A loose bundle of actin filaments (yellow arrow) in close proximity to a nuclear pore complex (magenta arrow). Clearly resolved nuclear proteasomes tethered to the nuclear pore complex (blue arrows, previously described in Albert et al., 2017 blue right-pointing triangle) illustrate the molecular clarity of this tomogram. C, C′, and C″ show three different slices through one tomographic volume. Scale bars are 100 nm in all panels.

Reorganization of filaments during gamete induction

Our optimized staining protocol allowed us to compare actin filament localization across *Chlamydomonas* cell states. Vegetative and gametic cells displayed similar perinuclear actin localization. Interestingly, gametic cells often showed a single apical fluorescent spot between the two flagella (**Fig. AI.5B, inset**). In the case of vegetative cells, this apical fluorescence was observed much less frequently and formed one, two, three, or four spots. Even in synchronous cultures, no consistent apical staining pattern was observed. The apical filamentous actin foci in gametes may mark the location of eventual fertilization tubule formation before induction in mating type plus CC-125 cells. To test this hypothesis, we asked whether mating type minus CC-124 cells, which do not make fertilization tubules, have filamentous actin foci at their apex. We observed that the foci persisted in CC-124, suggesting that this apical staining may mark the formation of the mating type minus actin structure (**Fig. AI.5E, inset**), which is a small membrane protrusion (Misamore et al., 2003a).

During artificial induction of gametes, fertilization tubules form after the addition of papavarine and dibutyryl cAMP in mating type plus cells. This actin-rich fusion organelle protrudes from the apex of the cell, the same location where we observed apical actin accumulation in uninduced gametes (**Fig. AI.5C, inset**). During tubule induction, the midcell filamentous actin population disappeared (**Fig. AI.5C**). However, this loss of midcell actin was not seen in mating type minus CC-124 cells, which do not form tubules (**Fig. AI.5F**). This led to the hypothesis that midcell filamentous actin rearranges to form the tubules. To test this hypothesis, gametes were induced in the presence of cycloheximide (**Fig. AI.5G–I**), a drug that blocks translation (Supplemental Fig. 2) and thus the up-regulation of actin expression that occurs during induction (Ning et al., 2013). Strikingly, treatment with cycloheximide did not prevent tubule formation, and the number of tubules formed in the presence of cycloheximide was comparable to the number of tubules formed under control conditions (**Fig. AI.5G–I**). This result indicates that fertilization tubules do not require newly synthesized actin and instead can be formed by the redistribution of existing actin to the cell apex.

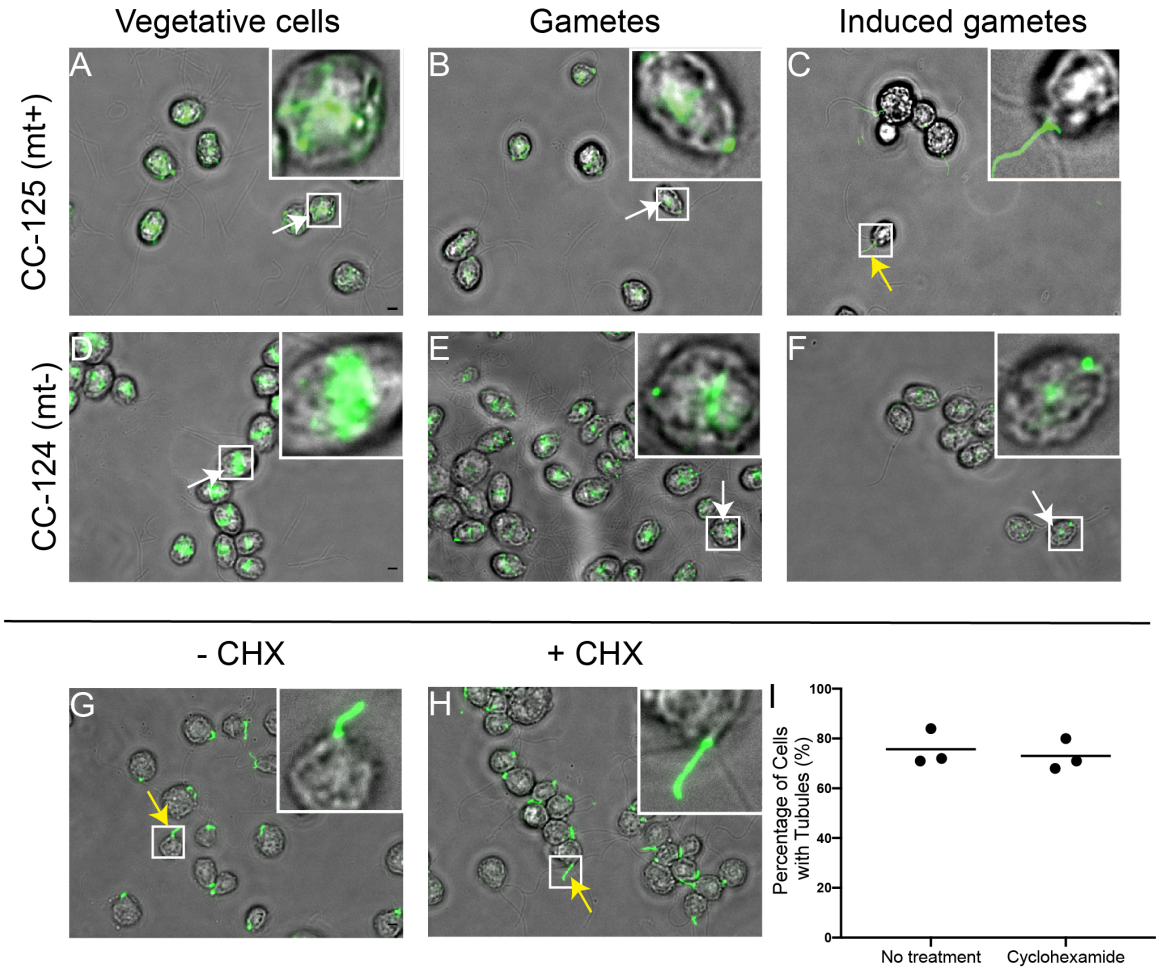

Fig. AI.5. Expression-independent reorganization of actin filaments during gamete induction. All cells stained with Atto 488 phalloidin. Actin in green. (A) Vegetative CC-125 cells of the mating type plus background show perinuclear actin signal. (B) Gametic CC-125 cells often display a single apical actin pool near the site of eventual fertilization tubule formation. (C) Inducing gametic CC-125 cells with papavarine and dibutyryl cAMP causes cells to form actin-rich fertilization tubules. (D) Vegetative CC-124 cells of the mating type minus background have comparable actin signal to vegetative CC-125. (E) Gametic CC-124 also show frequent apical actin signal. (F) Induced CC-124 cells retain the midcell actin population and do not form long fertilization tubules observed in CC-125 cells, but a small actin pool does accumulate near the apical surface in these cells. (G) CC-125 cells induced under control conditions form fertilization tubules. (H) CC-125 cells induced in the presence of 10 μM cycloheximide still form a comparable number of fertilization tubules, suggesting that the increased actin expression caused by gametic induction is not required for tubule formation. Scale bars are 5 μm. (I) Quantification of the percentage of cells that form fertilization tubules in the presence of 10 μM cycloheximide. Dots represent means from three separate experiments where n = 100 cells in each experiment. The mean of these three experiments is represented by a line. **From (Craig et al., 2019).**

Actin dynamics throughout the Chlamydomonas *cell cycle*

Previously, Harper et al. (1992) investigated total actin dynamics in *Chlamydomonas* using actin antibodies. With our newly established ability to specifically monitor the filamentous actin population, we synchronized cells using a light/dark regime to track filamentous actin through the cell cycle. The *Chlamydomonas* nucleus positioning and morphology, visualized by costaining with DAPI, acted as an indicator for cell cycle events. For interphase cells, which are recognizable by the nucleus's central position, Harper and colleagues (1992) reported diffuse actin localization surrounding the nucleus. Our data suggest actin filament localization is strictly perinuclear, and the Atto 488 phalloidin signal often revealed more linear structures compared with diffuse total actin staining (**Fig. AI.6A**). Additionally, we see punctate apical actin signal in some cells, but we have not been able to observe a cell cycle–-dependent pattern to these puncta. In preprophase, we observe that actin forms an angular shape around part of the nucleus (**Fig. AI.6B**). In prophase, there is a dense epicenter of filamentous actin signal near the nucleus, but a few actin threads remain that stretch across the cell (**Fig. AI.6A**). Metaphase and anaphase are recognizable by the flattening of the DAPI signal, indicating that condensed chromosomes are aligning for segregation. During this stage of the cell cycle, filamentous actin creates a linear arrangement behind the nucleus (**Fig. AI.6C**). We observe filamentous actin localization during early telophase, where filaments localize to both sides of the nucleus to help initiate cleavage furrow formation, similar to total actin dynamics seen by Harper et al. (1992) (**Fig. AI.6D**). Previously, total actin was shown to return to its state of diffuse localization around the reformed daughter nuclei. We did not observe actin filaments completely surrounding nuclei, regardless of cell cycle stage. This suggests that the diffuse population is exclusively monomeric. Cytokinetic actin filaments are present at the cleavage furrow (**Fig. AI.6E**), consistent with the pattern previously seen with total actin staining. Throughout mitosis, a population of actin filaments can be seen near the cell cortex, which is typically not present in interphase cells.

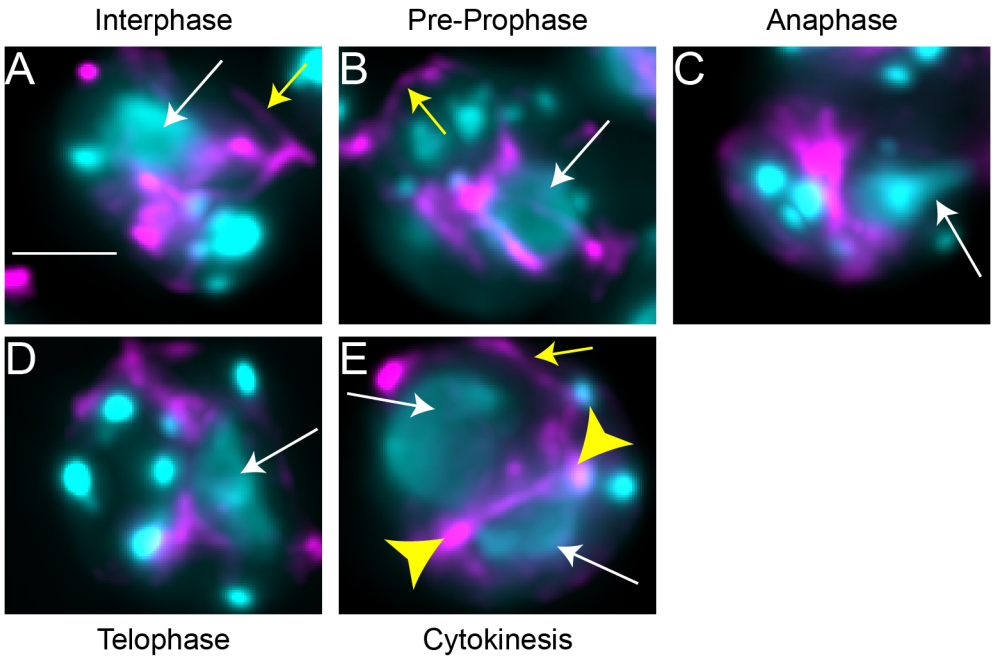

Fig. AI.6. Filamentous actin localization across the cell cycle. Atto 488 phalloidin (magenta) and DAPI (cyan) costaining. The intense smaller DAPI puncta are chloroplast nucleoids. The nuclei (white arrows) have larger and less intense DAPI staining. (A) Filamentous actin is found posterior to the nucleus in interphase cells. (B) In early prophase, filamentous actin forms additional bands connecting the midcell actin to the apical side of the cell. (C) During anaphase, filamentous actin appears orthogonal to the elongating nucleus. (D) In early stages of telophase, filamentous actin pinches on both sides of the nucleus. (E) During cytokinesis, linear actin filaments are present in the cleavage furrow (yellow arrowheads). Throughout the mitotic stages, additional actin filaments appear around the cell cortex. Scale bar is 5 μm.

Visualization of conventional and non-conventional actins

After localizing IDA5 filaments in gametic and cycling cells, we wondered whether NAP1 could form distinct structures. Treating wild-type cells with the actin-depolymerizing drug Lat B for 10 min eliminated the specific midcell filamentous actin staining (**Fig. AI.7B**). Lat B incubation for longer times, which is known to up-regulate NAP1 expression (M. Onishi et al., 2016), resulted in the formation of transient actin ring structures (**Fig. AI.7C**). Costaining cells with phalloidin and DAPI after 45 min of Lat B treatment showed that filamentous actin rings assemble around the nucleus (**Fig. AI.7D**). The prevalence of these rings in the cell population peaked at 60 min and then decreased until 150 min, at which point the rings had almost completely disassembled (**Fig. AI.7F**). Live-cell imaging using a LifeAct–Venus transformant revealed a similar ring phenotype, often accompanied by an additional linear or dot-like signal rarely observed in phalloidin-stained cells (**Fig. AI.7E**). Another difference between the LifeAct–-Venus and phalloidin-stained cells is the onset of ring formation, as ring structures do not begin to form until around 2 h of Lat B treatment in LifeAct–Venus cells. The variable timing of ring onset may be due to the differences in strain background between the LifeAct-expressing strain and the CC-125 wild-type strain. Alternatively, LifeAct binding may interfere with ring formation in live cells due to its documented effects on altering endogenous actin networks (Courtemanche et al., 2016a; Luis R Flores et al., 2019).

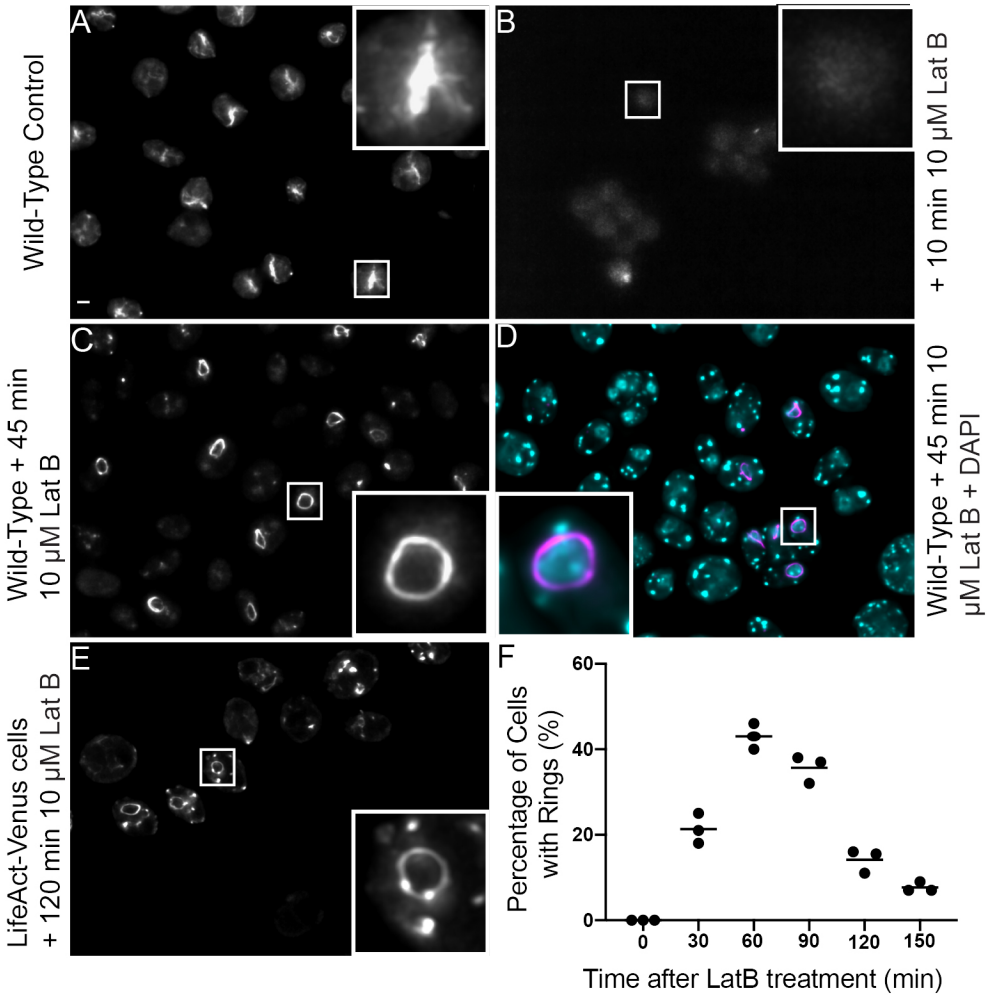

Fig. AI.7. Ring-like actin structures in CC-125 cells are induced by prolonged Lat B treatment. (A) Vegetative wild-type CC-125 cells stained with Atto 488 phalloidin. (B) The filamentous actin signal disappears after 10 min of treatment with 10 μM Lat B. Cells stained with Atto 488 phalloidin. (C) Filamentous actin ring structures form in many CC-125 cells after 45 min of treatment with 10 μM Lat B. Cells stained with Atto 488 phalloidin. (D) Actin ring structures colocalize around the nucleus under identical treatment conditions in wild-type cells. Actin in magenta; DAPI in cyan. (E) Live LifeAct–Venus cells treated with 10 μM Lat B for 120 min also show the actin ring phenotype. Scale bar is 5 μm. (F) Bar graph depicting ring frequency in populations of Lat B–treated wild-type cells stained with Atto 488 phalloidin. Dots represent means from three separate experiments where n = 200 cells in each experiment. The mean of these three experiments is represented by a line.

On the basis of the Lat B–induced up-regulation of NAP1 expression and the insensitivity of NAP1 to Lat B (M. Onishi et al., 2016), we hypothesized that this ring structure is composed of NAP1 filaments. We first attempted to visualize the two *Chlamydomonas* actins independently by staining *nap1* mutants (expressing only IDA5) and *ida5* mutants (expressing only NAP1) with Atto 488 phalloidin. Atto 488 phalloidin staining in *nap1* vegetative cells displayed a wild-type-like midcell actin signal (**Fig. AI.8A and C**), and a single apical spot was often present (**Fig. AI.8C**). However, in *ida5* mutants, the signal remained weak and hazy (**Fig. AI.8E**). This may be due to low NAP1 abundance or slight sequence differences in the phalloidin binding sites of IDA5 and NAP1. Actin has two methionine residues that are critical for phalloidin binding, which are conserved in the IDA5 sequence. However, NAP1 contains mutations at both methionine sites, which could reduce phalloidin's ability to label NAP1 filaments (Joel Vandekerckhove et al., 1985).

Despite poor efficiency of labeling low endogenous levels of NAP1, we reasoned that increases in NAP1 expression upon Lat B treatment (M. Onishi et al., 2018) and increased local filament concentration may still allow for phalloidin-labeling of rings composed of NAP1. To test whether rings require NAP1, we treated the *nap1* mutant with Lat B for 45 min. In the absence of drug, Atto 488 phalloidin–stained *nap1* cells displayed similar wild-type-like midcell actin signal (**Fig. AI.8C**). However, Lat B treatment did not result in the formation of filamentous ring structures in *nap1* cells (**Fig. AI.8D**), suggesting that ring assembly is NAP1-dependent. Furthermore, Lat B–treated *ida5* cells that express only NAP1 are capable of forming these ring structures, albeit at a much lower frequency (**Fig. AI.8F**). These results demonstrate that NAP1 is necessary and sufficient for ring formation.

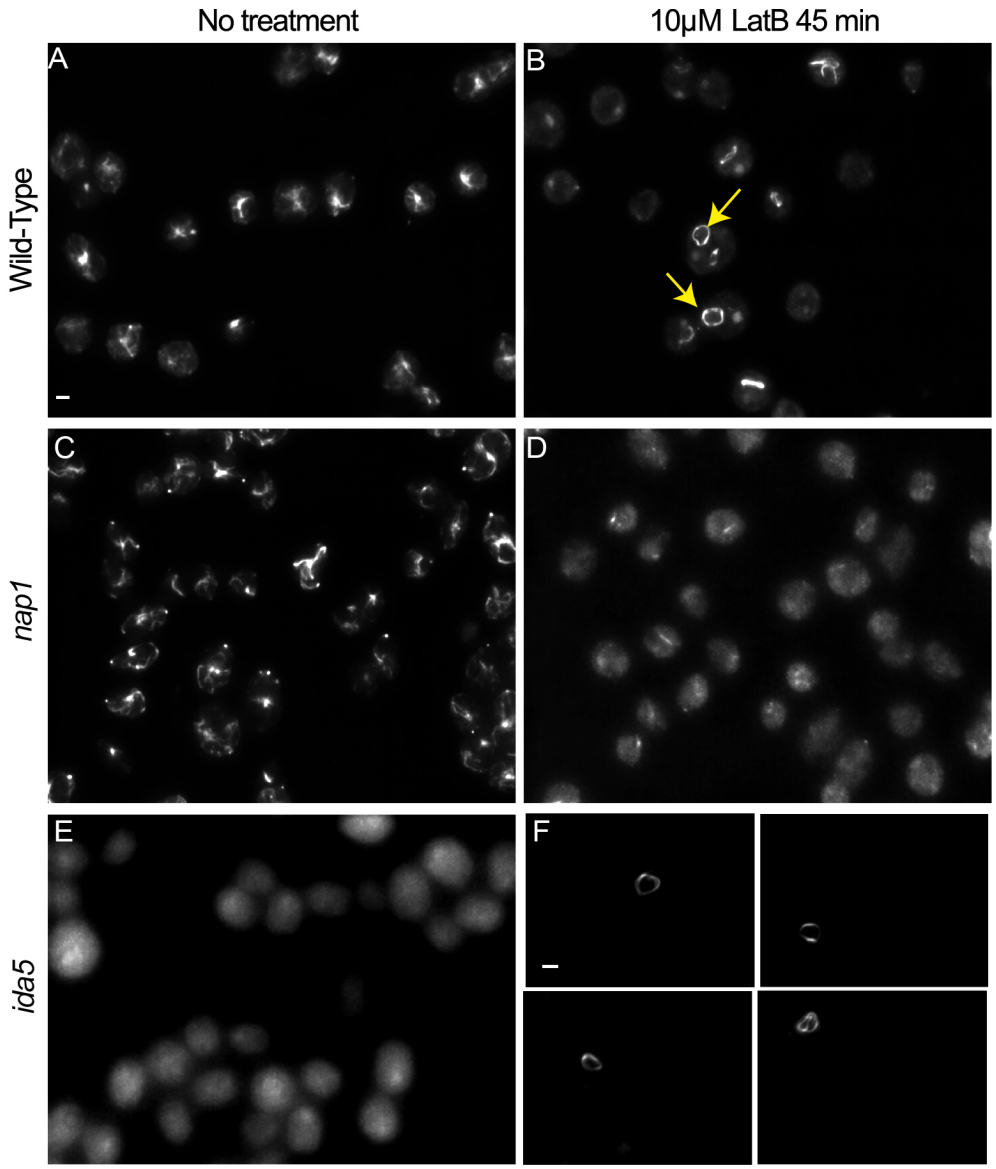

Fig. AI.8. NAP1 is necessary and sufficient for assembly of the ring-like filamentous structure in Lat B–treated cells. (A) Vegetative wild-type CC-125 cells stained with Atto 488 phalloidin. (B) Lat B–treated wild-type cells displaying actin rings. (C) Vegetative *nap1* cells stained with Atto 488 phalloidin display similar actin signal to wild-type cells. (D) Rings do not form in *nap1* cells treated with 10 μM Lat B for 45 min. (E) Atto 488 phalloidin labeling does not detect filaments in *ida5* stained cells. (F) Very few (<3%) *ida5* cells form actin rings under Lat B treatment conditions. Scale bars are 5 μm.

Discussion:

The coordinated expression and polymerization of two actins that share ~65% sequence identity within the same cell can provide broader insight into mechanisms of actin regulation and segregation of actin-dependent functions in vivo. The two *Chlamydomonas* actin genes are poorly characterized. One reason for this is that the *ida5* null mutant appears to have a mild, wild-type-like phenotype. We now believe this is due to compensation by the up-regulation of NAP1 in *ida5* mutants (Kato-Minoura, 2005a; M. Onishi et al., 2018, 2016). Loss of both actins is lethal (M. Onishi et al., 2016), and our recent studies demonstrate partially redundant functions for the two actins at multiple stages of ciliary assembly (Jack et al., 2019a).

Outside of the compensatory functions, the requirement for dual expression is not clear because NAP1 expression is undetectable under normal conditions and only up-regulated slightly in the absence of IDA5 or strongly upon flagellar reassembly following deflagellation (Hirono et al., 2003a). Despite the up-regulation of NAP1 upon flagellar regeneration, we previously found that *nap1* null mutants have no flagellar assembly defect outside of the inability to buffer perturbations to IDA5 (Jack et al., 2019a). NAP1 can largely perform the functions of filamentous IDA5, as *ida5* mutants show only slow swimming. This is likely due to the loss of four axonemal inner dynein arm subspecies within flagella (Takako Kato-Minoura et al., 1997) slow initial phases of flagellar assembly (Avasthi et al., 2014a). NAP1 cannot replace IDA5 in all cases, however. Despite localization of NAP1 to actin-rich fertilization tubules (Hirono et al., 2003a), *nap1* mutant cells assemble normal fertilization tubules (Jenna R Christensen et al., 2019) and *ida5* mutants expressing NAP1 alone form structurally defective fertilization tubules, resulting in a drastically reduced mating efficiency (Takako Kato-Minoura et al., 1997).

To complement our functional studies of IDA5 and NAP1, we wanted to understand whether the two proteins exhibit similar localization and dynamics. However, actins in *Chlamydomonas* have been difficult to visualize by fluorescence microscopy and traditional electron microscopy. Actin mutant phenotypes suggest actin localization in flagella, fertilization tubules, and the cleavage furrow. Indeed, this has been visualized using phalloidin in fertilization tubules (Wilson et al., 1997) and actin antibodies (which cannot discriminate between actin monomers and filaments) in the cleavage furrow

(Linda L. Ehler and Dutcher, 1998; T Kato-Minoura et al., 1998). It was reported that phalloidin did not clearly label filamentous structures in vegetative *Chlamydomonas* cells after 2 h of staining; instead, only bright fluorescence throughout the cell body could be observed (J D Harper et al., 1992). Recently, it was shown that *Chlamydomonas* cells deficient in peptidylglycine α-amidating monooxygenase (PAM) displayed altered actin organization. PAM knockdown cells displayed patches of filamentous actin via bodipy-phalloidin staining, whereas control cells exhibited only diffuse cytoplasmic signal, a common result when using a non-*Chlamydomona*s optimized phalloidin protocol (Kumar et al., 2018). We initially encountered similar results, even when using a much shorter incubation time of 30 min. However, reducing the staining time to 16 min resulted in optimal signal to noise and clear labeling of filamentous structures. Despite this improvement, many phalloidin trials using this 16-min incubation time resulted in a bright and diffuse signal in the cell body, and cells were susceptible to rapid photobleaching during imaging. These inconsistencies were alleviated after switching to a different phalloidin conjugate, Atto 488 phalloidin, which produced a clear and consistent photostable signal (**Fig. AI.S1**).

The addition of this reagent to our optimized actin staining protocol led to a powerful and reproducible method for visualizing filamentous actin in fixed vegetative *Chlamydomonas* cells (Evan W. Craig and Avasthi, 2019). Combining three independent visualization methods (live-cell LifeAct labeling, fixed-cell phalloidin labeling, and direct imaging of filaments inside native cells by cryo-ET) with analysis of Lat B sensitivity, our study confirms that *Chlamydomonas* cells have a bona fide actin filament network at the posterior of the nucleus that occasionally extends to the flagellar base at the apex of the cell (**Fig. AI.9**).

Our study reveals previously unreported filamentous structures in C*hlamydomonas*. Most obvious is the array of filamentous actin localized posterior of the nucleus in vegetative and gametic cell types. The actin-binding and nucleating proteins responsible for coordinating this actin population are not known, but recent findings in our lab strongly suggest a role for actin in trafficking vesicles from the Golgi (Jack et al., 2019a). This midcell actin revealed by Atto phalloidin along with cryo-ET showing distinct actin filaments near the Golgi (**Fig. AI.4A**) steers us to investigate the functional

role of actin in ciliary protein transport (Avasthi et al., 2014a; Jack et al., 2019a). The midcell actin is likely composed of IDA5 filaments, as we see similar actin localization when labeling *nap1* mutant cells and no filamentous signal in this region when labeling *ida5* mutants. NAP1 expression is undetectable in unperturbed vegetative cells, but increased in *ida5* mutant cells (Ohara et al., 1998a) and additionally increased to a small degree in Lat B–treated *ida5* mutants (M. Onishi et al., 2018). This increased expression and concentration of NAP1 may contribute to the ability to visualize infrequent rings in Lat B–treated *ida5* mutants. Although we have struggled to visualize the normal population of filamentous NAP1 with phalloidin staining, we are pursuing improved stability LifeAct probes and alternative strategies.

We provide the first report of filamentous actin dynamics across the *Chlamydomonas* cell cycle, and find several new labeling patterns compared with the total actin localization initially reported by Harper et al. (1992). Filamentous actin is dynamic throughout the cell cycle and redistributes most dramatically in telophase and cytokinesis (**Fig. AI.6D-E).** Total actin staining shows diffuse localization around the entire nucleus, whereas filamentous actin remains strictly linear and posterior to the nucleus until early telophase. Although filaments can be seen in the cleavage furrow in telophase and between the two daughter nuclei during cytokinesis, no ring structure is seen during ingression. *Chlamydomonas* cells instead use a microtubule-dependent structure called the phycoplast for cytokinesis (Gaffal and el-Gammal, 1990; Holmes and Dutcher, 1989; Johnson and Porter, 1968; Schibler and Huang, 1991). Our data show that mitotic cells also appear to have additional actin filaments near the cell cortex (**Fig. AI.6A, B, and E**). As *Chlamydomonas* cells divide several times before breaking out of the mother cell wall, the cell wall is not immediately adjacent to the plasma membrane of daughter cells during division. Actin filaments adjacent to the cortex may provide structural support during this stage. Further characterizing this filament population and observing the effects of actin inhibitors on daughter cell morphology will help determine the role of these filaments.

We consistently observed apical accumulation of filamentous actin between the flagella in gametic cells, and more variable apical signal in vegetative cells. We believe this filamentous actin population in gametes serves as an actin recruitment site, perhaps

supplying a pool of actin monomers for building the highly filamentous fertilization tubule formed in mating type plus gametic cells. It is thought that fertilization tubules may assemble from newly synthesized actin, as actin expression is known to increase during gamete activation and mating (Hirono et al., 2003a). However, treatment with cycloheximide to block transcription during induction did not significantly reduce the percentage of cells that formed fertilization tubules (**Fig. AI.5I**). Thus, tubule formation can occur without increased expression, suggesting that there is a common pool of monomers that can either form the network of midcell actin filaments or remodel to form other actin structures like fertilization tubules. This implies that the fertilization tubule serves as a sink for monomers that causes the concentration of the monomers in the middle of the cell to drop below the critical concentration for polymerization, resulting in the loss of the midcell actin filaments. This hypothesis is further supported by our observation that induction of mating type minus cells, where fertilization tubules do not form, does not result in a loss of filamentous actin.

We rarely observed actin mislocalization from the subflagellar region or multiple spots of apical accumulation in gametes. A well-conserved function of actin is in endocytosis. It is possible that the variable spots we see at the cell periphery in vegetative cells are analogous to endocytic patches or pits. Although there is little evidence for endocytosis in *Chlamydomonas*, studies of cell adhesion during mating show that activity-dependent redistribution of signaling proteins from the cell body plasma membrane into cilia seems to occur in a microtubule-dependent manner but is independent of ciliary motors (Belzile et al., 2013a). This leaves open the possibility that the redistribution of the membrane proteins may involve actin-dependent endocytosis and intracellular trafficking using cytoplasmic microtubule motors.

We found that NAP1 is both necessary and sufficient for formation of phalloidin-stained perinuclear rings induced by Lat B. However, given the low frequency of ring formation in *ida5* mutant cells, we cannot rule out the possibility that the Lat B rings in wild-type cells are made of IDA5/NAP1 copolymers. These ring structures appeared after ~30 min of Lat B treatment, became most frequent at 1 h, and dissipated by 2 h (**Fig. AI.7F**). This timing is consistent with findings from Onishi et al. (2016) and Onishi et al. (2018), where Lat B–induced NAP1 expression was measured by RT-PCR, RNAseq, and

Western blot. NAP1 expression levels dramatically increased at 30 min after the addition of 10 μM Lat B. Although the onset of ring formation is coincident with an up-regulation of actin, ring frequency declines while levels of actin expression remain elevated. Given the transient nature of the actin rings, it is possible that these rings acutely compensate for actin-dependent functions to protect the nucleus. These functions may include regulating nuclear shape (Khatau et al., 2009), nuclear positioning (Gundersen and Worman, 2013), or connecting with the nucleoskeleton to transduce mechanical signals (Tapley and Starr, 2013). The ring may interact with nuclear pore complexes (Mosalaganti et al., 2018), as we observed a cluster of filaments gather near one of these sites before Lat B disruption (**Fig. AI.4C**). Another possibility is that ring formation may be involved in nuclear rupture (Hatch and Hetzer, 2016; Wesolowska et al., 2018). Although actin--dependent nuclear envelope rupture does not kill cells in all circumstances, a decrease in frequency of rings at the population level after 2 h may be due to the death of ring-containing cells. Live-cell microscopy following individual cells or analysis of synchronized populations will likely discriminate between these possibilities.

A seemingly universal function of actin is directing mitotic and meiotic events by localizing vesicles and the cytokinetic machinery in plant, fungi, and animal cells. Filamentous actin-rich ring structures have been associated with cytokinesis in animal cells (Wang, 2005) and yeast (Arai and Mabuchi, 2002). Many of these rings undergo a constriction that is mediated by a contractile class II myosin. Given that *Chlamydomonas* cells lack this type of myosin, we believe the NAP1-dependent ring structures are unlikely to be an analogue to contractile actin rings used for cell division.

The coexpression of a conventional and divergent actin within a single cell establishes *Chlamydomonas* as an excellent new system to identify fundamental principles of actin biology. Robust visualization of the filamentous actin network in these cells may reveal novel modes of actin-dependent regulation for major cellular processes, such as ciliary biology and photosynthesis, for which *Chlamydomonas* is already a leading model organism.

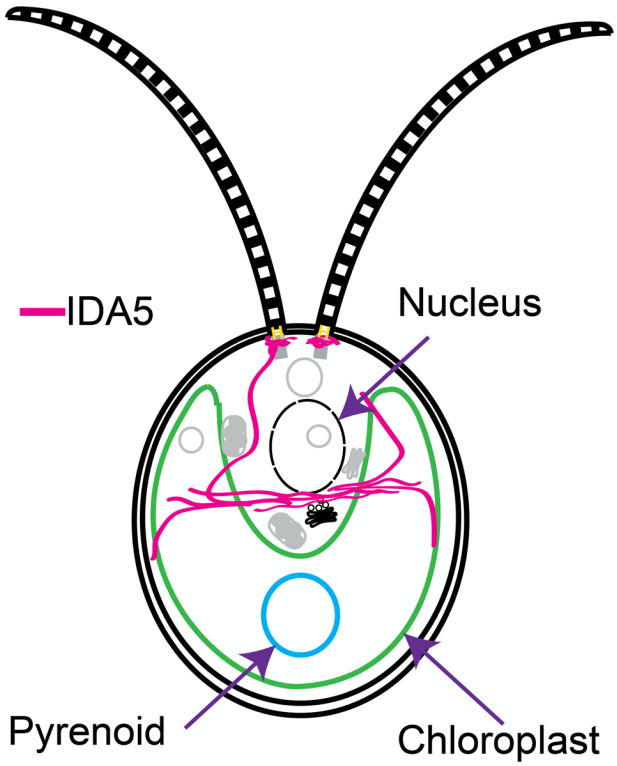

Fig. AI.9. Distribution of filamentous actin in *Chlamydomonas*. Diagram depicting IDA5 filaments (pink) relative to landmark *Chlamydomonas* organelles. Actin filaments are predominantly localized basal of the nucleus, near the Golgi, but strands also extend throughout the cell to locations including the flagellar base.

Methods:

Chlamydomonas strains

The wild-type strains CC-125 mt +, CC-124 mt –, and mat3-4 strain CC-3994 mt + were obtained from the *Chlamydomonas* Resource Center (University of Minnesota). The *nap1* mutant was a generous gift from Fred Cross (The Rockefeller University), Masayuki Onishi (Stanford University), and John Pringle (Stanford University). The LifeAct–Venus wild-type transformant was gifted by Masayuki Onishi, Stanford University.

Phalloidin staining

Cells were grown in 2 ml of TAP (Tris acetate phosphate) liquid media on a roller drum for 17 h (overnight). It is essential to select healthy cells by centrifuging 1 ml of cell culture at 1800 rpm for 1.5 min. The supernatant was discarded and cells were resuspended in 600 μl fresh TAP. Resuspended cells (200 µl) were adhered on poly-l-lysine–coated coverslips for 5 min and covered. The liquid was tilted off the coverslips and replaced with 4% fresh paraformaldehyde (PFA) in 7.5 mM HEPES, pH 7.24. The PFA is prepared from a 16% fresh ampoule of PFA. See Farhat (2013) for a detailed protocol for making this fixative solution. The pattern of staining changes (producing a bright pyrenoid signal) and nonspecific cytoplasmic fluorescence increases if using PFA that is not fresh. Coverslips were washed with 1X phosphate-buffered saline (PBS) for 3 min. For cell permeabilization, coverslips were submerged in a coplin jar containing 80% precooled acetone and then incubated for 5 min at –20°C. Coverslips were quickly transferred to a second coplin jar containing 100% precooled acetone and incubated again for 5 min at –20°C. Coverslips were allowed to air dry for a minimum of 2 min, and for longer if needed. Next, cells were rehydrated by transferring coverslips to a coplin jar containing 1X PBS for 5 min. Coverslips were then stained with Atto 488 phalloidin (49409; Sigma) for 16 min in the dark, significantly reducing background and increasing the signal-to-noise ratio. The Atto 488 phalloidin reagent greatly enhanced photostability and brightness compared with Alexa Fluor 488 phalloidin (Supplemental Fig. 1), which allowed for more uniform and reproducible filament labeling. Phalloidin incubation was followed by a wash in 1X PBS for 5 min. Finally, coverslips were mounted on slides as

quickly as possible with self-sealing Fluoromount-G (Invitrogen). We have published a more detailed protocol (Evan W. Craig and Avasthi, 2019).

Cell synchronization

For experiments requiring synchronous cultures, cells were grown in HS media (Sueoka, 1960) and followed a 14 h light, 10 h dark growth regime. To initiate the dark period, culture tubes were wrapped in tin foil to prevent light exposure. Cells were immediately fixed following transition to the dark period and stained according to the phalloidin protocol above. For nucleic acid labeling, 200 µl of 1:3000 10 mg/ml DAPI solution in 1X PBS was added to the phalloidin staining solution for the final 10 min of phalloidin incubation. Cell cycle events were identified by nuclear morphology and localization in light–dark synchronized cultures.

Immunofluorescence for colocalization microscopy

Wild-type cells were grown overnight in TAP media. Cells were treated following the general phalloidin staining protocol up to the rehydration step. After cells had been rehydrated in 1X PBS for 5 min, cells were incubated in 100% block solution (5% bovine serum albumin, 1% cold water fish gelatin in 1X PBS) for 30 min, followed by a secondary blocking step containing 10% normal goat serum in block solution for another 30 min. Cells were incubated in either 1:500 anti-centrin or 1:500 anti–α-tubulin overnight in a humidified chamber. The next morning, cells were washed three times (10 min each) with 1X PBS. Cells were stained with anti-mouse594 diluted 1:500 for 1 h, and stained with Atto 488 phalloidin for the final 16 min of the stain. Cells were then washed three times (10 min each) in 1X PBS, mounted on slides with Fluoromount-G, and imaged on a Nikon TiS microscope.

Cell vitrification and FIB milling

Chlamydomonas cells were grown and prepared for cryo-ET as previously described (Albert et al., 2017; Bykov et al., 2017). We used the mat3-4 strain (Umen and Goodenough, 2001), which has smaller cells that improve vitrification by plunge-freezing. Cells were grown with constant light (~90 µmol photons m–2 s–1) in TAP

medium, bubbling with normal air. Liquid culture (5 µl, ~1000 cells/µl) was blotted onto carbon-coated 200-mesh copper grids (Quantifoil Micro Tools), which were then plunged into a liquid ethane–propane mixture using a Vitrobot Mark 4 (FEI Thermo Fisher). Frozen grids were mounted into modified autogrids (FEI Thermo Fisher) and loaded into either a Scios (FEI Thermo Fisher) or a Quanta 3D FEG (FEI Thermo Fisher) FIB/SEM microscope. The grids were coated with a thin layer of organometallic platinum using the gas injection system (FEI Thermo Fisher), and then the Ga+ beam was used to mill thin lamellae (100–200 nm thick), following the protocols detailed in (Schaffer et al., 2017, 2015).

Cryo-electron tomography

Tomography was performed on a 300 kV Titan Krios (FEI Thermo Fisher) equipped with a quantum postcolumn energy filter (Gatan) and a K2 Summit direct electron detector (Gatan) operated in movie mode at 12 frames per second. Using SerialEM software (Mastronarde, 2005), tilt series were acquired over an angular range of approximately –60° to +60°, using a bidirectional tilt scheme with 2° increments. Cumulative electron dose was ~100 e–/Å2, the object pixel size was 3.42 Å, and defocus ranged from –4 to –6 µm. Raw image frames were aligned with MotionCorr2 software (Zheng et al., 2017), and tomograms were reconstructed in IMOD software (Kremer et al, 1996) using patch tracking and back projection. The images displayed in this article were binned twice. To enhance the contrast, we used the tom_deconv deconvolution filter (https://github.com/dtegunov/tom_deconv).

Fertilization tubule induction

To induce gametogenesis, cells were grown in M-N (M1 minimal media without nitrogen) overnight under growth lighting. Gametes were mixed with dibutyryl cAMP (13.5 mM) and papaverine (135 μM) for 45 min to induce fertilization tubule formation (modified from Wilson et al., 1997). Cells were then stained in accordance with our phalloidin protocol (see above).

Latrunculin B treatment

Lat B was purchased from Sigma and used with the specified concentrations and incubation times. Typically, depolymerizing treatment was performed for 10 min, and cells were treated for 45 min to induce NAP1 up-regulation and ring formation.

Acknowledgements:

We thank Masayuki Onishi, John Pringle, and Fred Cross for providing the *nap1* mutant. Thank you to members of the Avasthi lab for troubleshooting and manuscript feedback. We acknowledge Wolfgang Baumeister and Jurgen Plitzko for enabling the cryo-ET work by providing support and instrumentation. This work was funded through National Institutes of Health grants P20GM104936 and P20GM103418 (to P.A.), Deutsche Forschungsgemeinschaft Grant no. EN 1194/1-1 as part of research unit FOR2092 (to B.D.E.), and The Max Planck Society.

References:

Albert, S., Schaffer, M., Beck, F., Mosalaganti, S., Asano, S., Thomas, H.F., Plitzko, J.M., Beck, M., Baumeister, W., Engel, B.D., 2017. Proteasomes tether to two distinct sites at the nuclear pore complex. Proc. Natl. Acad. Sci. U. S. A. 114, 13726–13731. https://doi.org/10.1073/pnas.1716305114

Arai, R., Mabuchi, I., 2002. F-actin ring formation and the role of F-actin cables in the fission yeast Schizosaccharomyces pombe. J. Cell Sci. 115, 887–898. https://doi.org/10.1242/jcs.115.5.887

Asano, S., Engel, B.D., Baumeister, W., 2016. In Situ Cryo-Electron Tomography: A Post-Reductionist Approach to Structural Biology. J. Mol. Biol. 428, 332–343. https://doi.org/10.1016/j.jmb.2015.09.030

Avasthi, P., Onishi, M., Karpiak, J., Yamamoto, R., Mackinder, L., Jonikas, M.C., Sale, W.S., Shoichet, B., Pringle, J.R., Marshall, W.F., 2014b. Actin is required for IFT regulation in Chlamydomonas reinhardtii. Curr. Biol. CB 24, 2025–2032. https://doi.org/10.1016/j.cub.2014.07.038

Belzile, O., Hernandez-Lara, C.I., Wang, Q., Snell, W.J., 2013b. Regulated membrane protein entry into flagella is facilitated by cytoplasmic microtubules and does not require IFT. Curr. Biol. CB 23, 1460–1465. https://doi.org/10.1016/j.cub.2013.06.025

Bykov, Y.S., Schaffer, M., Dodonova, S.O., Albert, S., Plitzko, J.M., Baumeister, W., Engel, B.D., Briggs, J.A., 2017. The structure of the COPI coat determined within the cell. eLife 6. https://doi.org/10.7554/eLife.32493

Christensen, Jenna R., Craig, E.W., Glista, M.J., Mueller, D.M., Li, Y., Sees, J.A., Huang, S., Suarez, C., Mets, L.J., Kovar, D.R., Avasthi, P., 2019. Chlamydomonas reinhardtii formin FOR1 and profilin PRF1 are optimized for acute rapid actin filament assembly. Mol. Biol. Cell 30, 3123–3135. https://doi.org/10.1091/mbc.E19-08-0463

Courtemanche, N., Pollard, T.D., Chen, Q., 2016b. Avoiding artefacts when counting polymerized actin in live cells with LifeAct fused to fluorescent proteins. Nat. Cell Biol. 18, 676–683. https://doi.org/10.1038/ncb3351

Craig, Evan W, Avasthi, P., 2019. Visualizing Filamentous Actin Using Phalloidin in Chlamydomonas reinhardtii. Bio-Protoc. 9, e3274. https://doi.org/10.21769/BioProtoc.3274

Detmers, P. A., Carboni, J.M., Condeelis, J., 1985. Localization of actin in Chlamydomonas using antiactin and NBD-phallacidin. Cell Motil. 5, 415–430. https://doi.org/10.1002/cm.970050505

Dobrowolski, J.M., Niesman, I.R., Sibley, L.D., 1997. Actin in the parasite Toxoplasma gondii is encoded by a single copy gene, ACT1 and exists primarily in a globular form. Cell Motil. Cytoskeleton 37, 253–262. https://doi.org/10.1002/(SICI)1097-0169(1997)37:3<253::AID-CM7>3.0.CO;2-7

Ehler, L. L., Dutcher, S.K., 1998. Pharmacological and genetic evidence for a role of rootlet and phycoplast microtubules in the positioning and assembly of cleavage furrows

in Chlamydomonas reinhardtii. Cell Motil. Cytoskeleton 40, 193–207. https://doi.org/10.1002/(SICI)1097-0169(1998)40:2<193::AID-CM8>3.0.CO;2-G

Flores, Luis R., Keeling, M.C., Zhang, X., Sliogeryte, K., Gavara, N., 2019. Lifeact-GFP alters F-actin organization, cellular morphology and biophysical behaviour. Sci. Rep. 9, 3241. https://doi.org/10.1038/s41598-019-40092-w

Gaffal, K.P., el-Gammal, S., 1990. Elucidation of the enigma of the "metaphase band" ofChlamydomonas reinhardtii. Protoplasma 156, 139–148. https://doi.org/10.1007/BF01560652

Gundersen, G.G., Worman, H.J., 2013. Nuclear positioning. Cell 152, 1376–1389. https://doi.org/10.1016/j.cell.2013.02.031

Harper, J. D., McCurdy, D.W., Sanders, M.A., Salisbury, J.L., John, P.C., 1992. Actin dynamics during the cell cycle in Chlamydomonas reinhardtii. Cell Motil. Cytoskeleton 22, 117–126. https://doi.org/10.1002/cm.970220205

Hatch, E.M., Hetzer, M.W., 2016. Nuclear envelope rupture is induced by actin-based nucleus confinement. J. Cell Biol. 215, 27–36. https://doi.org/10.1083/jcb.201603053

Hirono, M., Uryu, S., Ohara, A., Kato-Minoura, T., Kamiya, R., 2003b. Expression of conventional and unconventional actins in Chlamydomonas reinhardtii upon deflagellation and sexual adhesion. Eukaryot. Cell 2, 486–493. https://doi.org/10.1128/EC.2.3.486-493.2003

Holmes, J.A., Dutcher, S.K., 1989. Cellular asymmetry in Chlamydomonas reinhardtii. J. Cell Sci. 94 (Pt 2), 273–285. https://doi.org/10.1242/jcs.94.2.273

Jack, B., Mueller, D.M., Fee, A.C., Tetlow, A.L., Avasthi, P., 2019b. Partially Redundant Actin Genes in Chlamydomonas Control Transition Zone Organization and Flagellum-Directed Traffic. Cell Rep. 27, 2459-2467.e3. https://doi.org/10.1016/j.celrep.2019.04.087

Johnson, U.G., Porter, K.R., 1968. Fine structure of cell division in Chlamydomonas reinhardi. Basal bodies and microtubules. J. Cell Biol. 38, 403–425. https://doi.org/10.1083/jcb.38.2.403

Kato-Minoura, T., 2005b. Impaired flagellar regeneration due to uncoordinated expression of two divergent actin genes in Chlamydomonas. Zoolog. Sci. 22, 571–577. https://doi.org/10.2108/zsj.22.571

Kato-Minoura, T., Hirono, M., Kamiya, R., 1997. Chlamydomonas inner-arm dynein mutant, ida5, has a mutation in an actin-encoding gene. J. Cell Biol. 137, 649–656. https://doi.org/10.1083/jcb.137.3.649

Kato-Minoura, T., Uryu, S., Hirono, M., Kamiya, R., 1998. Highly divergent actin expressed in a Chlamydomonas mutant lacking the conventional actin gene. Biochem. Biophys. Res. Commun. 251, 71–76. https://doi.org/10.1006/bbrc.1998.9373

Khatau, S.B., Hale, C.M., Stewart-Hutchinson, P.J., Patel, M.S., Stewart, C.L., Searson, P.C., Hodzic, D., Wirtz, D., 2009. A perinuclear actin cap regulates nuclear shape. Proc. Natl. Acad. Sci. U. S. A. 106, 19017–19022. https://doi.org/10.1073/pnas.0908686106

Kilmartin, J.V., Adams, A.E., 1984. Structural rearrangements of tubulin and actin during the cell cycle of the yeast Saccharomyces. J. Cell Biol. 98, 922–933. https://doi.org/10.1083/jcb.98.3.922

Kremer, J.R., Mastronarde, D.N., McIntosh, J.R., 1996. Computer visualization of three-dimensional image data using IMOD. J. Struct. Biol. 116, 71–76. https://doi.org/10.1006/jsbi.1996.0013

Kumar, D., Thomason, R.T., Yankova, M., Gitlin, J.D., Mains, R.E., Eipper, B.A., King, S.M., 2018. Microvillar and ciliary defects in zebrafish lacking an actin-binding bioactive peptide amidating enzyme. Sci. Rep. 8, 4547. https://doi.org/10.1038/s41598-018-22732-9

Mastronarde, D.N., 2005. Automated electron microscope tomography using robust prediction of specimen movements. J. Struct. Biol. 152, 36–51. https://doi.org/10.1016/j.jsb.2005.07.007

Miraldi, E.R., Thomas, P.J., Romberg, L., 2008. Allosteric models for cooperative polymerization of linear polymers. Biophys. J. 95, 2470–2486. https://doi.org/10.1529/biophysj.107.126219

Misamore, M.J., Gupta, S., Snell, W.J., 2003b. The Chlamydomonas Fus1 protein is present on the mating type plus fusion organelle and required for a critical membrane adhesion event during fusion with minus gametes. Mol. Biol. Cell 14, 2530–2542. https://doi.org/10.1091/mbc.e02-12-0790

Mosalaganti, S., Kosinski, J., Albert, S., Schaffer, M., Strenkert, D., Salomé, P.A., Merchant, S.S., Plitzko, J.M., Baumeister, W., Engel, B.D., Beck, M., 2018. In situ architecture of the algal nuclear pore complex. Nat. Commun. 9, 2361. https://doi.org/10.1038/s41467-018-04739-y

Ning, J., Otto, T.D., Pfander, C., Schwach, F., Brochet, M., Bushell, E., Goulding, D., Sanders, M., Lefebvre, P.A., Pei, J., Grishin, N.V., Vanderlaan, G., Billker, O., Snell, W.J., 2013. Comparative genomics in Chlamydomonas and Plasmodium identifies an ancient nuclear envelope protein family essential for sexual reproduction in protists, fungi, plants, and vertebrates. Genes Dev. 27, 1198–1215. https://doi.org/10.1101/gad.212746.112

Ohara, A., Kato-Minoura, T., Kamiya, R., Hirono, M., 1998b. Recovery of flagellar inner-arm dynein and the fertilization tubule in Chlamydomonas ida5 mutant by transformation with actin genes. Cell Struct. Funct. 23, 273–281. https://doi.org/10.1247/csf.23.273

Onishi, Masayuki, Pecani, K., Jones, T. 4th, Pringle, J.R., Cross, F.R., 2018a. F-actin homeostasis through transcriptional regulation and proteasome-mediated proteolysis. Proc. Natl. Acad. Sci. U. S. A. 115, E6487–E6496. https://doi.org/10.1073/pnas.1721935115

Onishi, Masayuki, Pringle, J.R., Cross, F.R., 2016. Evidence That an Unconventional Actin Can Provide Essential F-Actin Function and That a Surveillance System Monitors F-Actin Integrity in Chlamydomonas. Genetics 202, 977–996. https://doi.org/10.1534/genetics.115.184663

Periz, J., Whitelaw, J., Harding, C., Gras, S., Del Rosario Minina, M.I., Latorre-Barragan, F., Lemgruber, L., Reimer, M.A., Insall, R., Heaslip, A., Meissner, M., 2017b. Toxoplasma gondii F-actin forms an extensive filamentous network required for material exchange and parasite maturation. eLife 6, e24119. https://doi.org/10.7554/eLife.24119

Perrin, Benjamin J., Ervasti, J.M., 2010. The actin gene family: function follows isoform. Cytoskelet. Hoboken NJ 67, 630–634. https://doi.org/10.1002/cm.20475

Pollard, T.D., Blanchoin, L., Mullins, R.D., 2000b. Molecular mechanisms controlling actin filament dynamics in nonmuscle cells. Annu. Rev. Biophys. Biomol. Struct. 29, 545–576. https://doi.org/10.1146/annurev.biophys.29.1.545

Schaffer, M., Engel, B.D., Laugks, T., Mahamid, J., Plitzko, J.M., Baumeister, W., 2015. Cryo-focused Ion Beam Sample Preparation for Imaging Vitreous Cells by Cryo-electron Tomography. Bio-Protoc. 5, e1575. https://doi.org/10.21769/bioprotoc.1575

Schaffer, M., Mahamid, J., Engel, B.D., Laugks, T., Baumeister, W., Plitzko, J.M., 2017. Optimized cryo-focused ion beam sample preparation aimed at in situ structural studies of membrane proteins. J. Struct. Biol. 197, 73–82. https://doi.org/10.1016/j.jsb.2016.07.010

Schibler, M.J., Huang, B., 1991. The colR4 and colR15 beta-tubulin mutations in Chlamydomonas reinhardtii confer altered sensitivities to microtubule inhibitors and herbicides by enhancing microtubule stability. J. Cell Biol. 113, 605–614. https://doi.org/10.1083/jcb.113.3.605

Skillman, K.M., Diraviyam, K., Khan, A., Tang, K., Sept, D., Sibley, L.D., 2011. Evolutionarily divergent, unstable filamentous actin is essential for gliding motility in apicomplexan parasites. PLoS Pathog. 7, e1002280. https://doi.org/10.1371/journal.ppat.1002280

Sueoka, N., 1960. MITOTIC REPLICATION OF DEOXYRIBONUCLEIC ACID IN CHLAMYDOMONAS REINHARDI. Proc. Natl. Acad. Sci. U. S. A. 46, 83–91. https://doi.org/10.1073/pnas.46.1.83

Tapley, E.C., Starr, D.A., 2013. Connecting the nucleus to the cytoskeleton by SUN-KASH bridges across the nuclear envelope. Curr. Opin. Cell Biol. 25, 57–62. https://doi.org/10.1016/j.ceb.2012.10.014

Umen, J.G., Goodenough, U.W., 2001. Control of cell division by a retinoblastoma protein homolog in Chlamydomonas. Genes Dev. 15, 1652–1661. https://doi.org/10.1101/gad.892101

Vandekerckhove, J., Deboben, A., Nassal, M., Wieland, T., 1985. The phalloidin binding site of F-actin. EMBO J. 4, 2815–2818. https://doi.org/10.1002/j.1460-2075.1985.tb04008.x

Wang, Y., 2005. The mechanism of cortical ingression during early cytokinesis: thinking beyond the contractile ring hypothesis. Trends Cell Biol. 15, 581–588. https://doi.org/10.1016/j.tcb.2005.09.006

Warren, D.T., Andrews, P.D., Gourlay, C.W., Ayscough, K.R., 2002. Sla1p couples the yeast endocytic machinery to proteins regulating actin dynamics. J. Cell Sci. 115, 1703–1715. https://doi.org/10.1242/jcs.115.8.1703

Wesolowska, N., Machado, P., Geiss, C., Kondo, H., Mori, M., Schwab, Y., Lénárt, P., 2018. An F-actin shell ruptures the nuclear envelope by sorting pore-dense and pore-free membranes in meiosis of starfish oocytes. bioRxiv 480434. https://doi.org/10.1101/480434

Wetzel, D.M., Håkansson, S., Hu, K., Roos, D., Sibley, L.D., 2003. Actin filament polymerization regulates gliding motility by apicomplexan parasites. Mol. Biol. Cell 14, 396–406. https://doi.org/10.1091/mbc.e02-08-0458

Wilson, N.F., Foglesong, M.J., Snell, W.J., 1997. The Chlamydomonas mating type plus fertilization tubule, a prototypic cell fusion organelle: isolation, characterization, and in vitro adhesion to mating type minus gametes. J. Cell Biol. 137, 1537–1553. https://doi.org/10.1083/jcb.137.7.1537

Zheng, S.Q., Palovcak, E., Armache, J.-P., Verba, K.A., Cheng, Y., Agard, D.A., 2017. MotionCor2: anisotropic correction of beam-induced motion for improved cryo-electron microscopy. Nat. Methods 14, 331–332. https://doi.org/10.1038/nmeth.4193

Supplemental material:

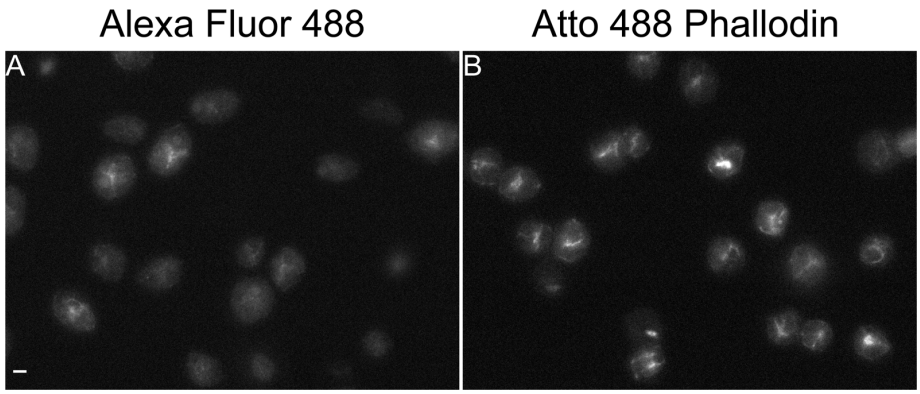

Fig. AI.S1. Atto 488 Phalloidin displays superior performance versus Alexa Fluor 488 Phalloidin in labeling *Chlamydomonas* actin under optimized conditions. Representative raw images comparing Alexa Fluor 488 Phalloidin (**A**) to Atto 488 Phalloidin (**B**) in vegetative cells stained following our optimized actin labeling protocol. Atto 488 Phalloidin-stained cells show increased staining efficiency and brighter signal compared to Alexa Fluor 488 Phalloidin-stained cells. Scale bar is 5 μm.

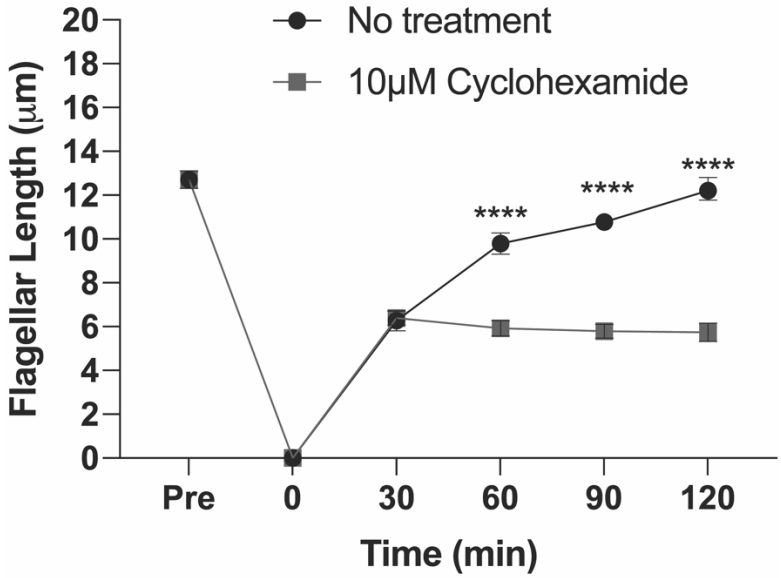

Fig. AI.S2. Cycloheximide does not allow flagellar growth beyond half length. A control experiment confirming the efficacy of cycloheximide used in the fertilization tubule experiments shown in Fig. 5. As previously reported (Rosenbaum et al., 1969), we observe that flagella regrow to half-length following deflagellation in cycloheximide.

APPENDIX II:

Comparative Phenotyping of Two Commonly Used *Chlamydomonas reinhardtii* Background Strains: CC-1690 (21gr) and CC-5325 (The CLiP Mutant Library Background)

Ningning Zhang[1] , Leila Pazouki[1] , Huong Nguyen[1] , Sigrid Jacobshagen[2] , Brae M Bigge[3] , Ming Xia[1] , Erin M Mattoon[1,4] , Anastasiya Klebanovych[1] , Maria Sorkin[1,4] , Dmitri A Nusinow[1] , Prachee Avasthi[3] , Kirk J Czymmek[1] , Ru Zhang[1]

[1]Donald Danforth Plant Science Center, St. Louis, MO 63132, USA.
[2]Department of Biology, Western Kentucky University, Bowling Green, KY 42101, USA.
[3]Department of Biochemistry and Cell Biology, Geisel School of Medicine at Dartmouth, Hanover, NH 03755, USA.
[4]Plant and Microbial Biosciences Program, Division of Biology and Biomedical Sciences, Washington University in Saint Louis, St. Louis, MO 63130, USA.

Published in: Plants. 2022 Feb 22;11(5):585. doi: 10.3390/plants11050585.

Contributions of BM Bigge: Fig. 10 (experiments, analysis, data visualization), manuscript writing and revision

Introduction:

Chlamydomonas cells are an excellent model to study ciliary assembly and maintenance, photosynthesis, cell cycle, lipid accumulation, stress responses, and biofuel production. Two commonly used "wild-type" *Chlamydomonas* strains are CC-1690 and CC-5325. CC-1690 is mating type plus and has been used to create most of the genetic libraries and the *Chlamydomonas* Genome Project (Pröschold et al., 2005; Sager, 1955; Shrager et al., 2003). CC-5325 is the parent strain for the *Chlamydomonas* mutant library and is typically used a parent strain or a wild-type control for mutant studies (Cheng et al., 2017; Li et al., 2019; Zhang et al., 2014). CC-5325 is mating type minus. It is the result of a cross between the 4A- strain and the D66+ strain. D66+ is a cell-wall deficient strain, leading to questions regarding the cell wall of CC-5325. CC-5325 does however have high electroporation and mating efficiencies, it can grow in several conditions, it swims relatively normally, and does not adhere to glass, making it an ideal strain for mutant studies. However, questions remain regarding CC-5325 as it has not been fully characterized.

Here, we answer questions regarding photosynthesis, the cell wall, and circadian rhythms of CC-5325 in relation to that of the more established wild-type strain CC-1690. We found that CC-5325 has lower photosynthetic efficiency than CC-1690, but it grew better than CC-1690 in dark conditions. We also found that CC-5325 was more heat-sensitive than CC-1690. We found that CC-5325 had an intact cell wall despite being the progeny of a cell wall-less strain. We found that CC-5325 was unable to maintain a robust circadian rhythm. Finally, we found that CC-5325 had longer cilia, but slower swimming speed.

Results:

Because cilia affect phototaxis, we further investigated cilia morphology and swimming speed. Cells were grown in either TAP (with acetate) or M-N (without acetate and nitrogen) medium with constant agitation and light. The M-N condition induces gamete formation and eliminates the effect of the cell cycle on percent ciliation and ciliary length. The percent of cells with cilia was comparable between CC-1690 and CC-5325 in both TAP and M-N medium (**Fig. AII.1A-B**). However, CC-5325 had significantly longer cilia than CC-1690 in TAP medium; this trend might be also true for cells in M-N medium, but the differences were not significant (**Fig. AII.1C-D**). We quantified swimming speed by creating traces of how far the cells moved during a 1 s exposure using a darkfield microscopy (**Fig. AII.1E-F**). CC-1690 and CC-5325 had a similar swimming speed when grown in TAP. When grown in M-N, CC-1690 swam faster than CC-5325 (**Fig. AII.1G-H).**

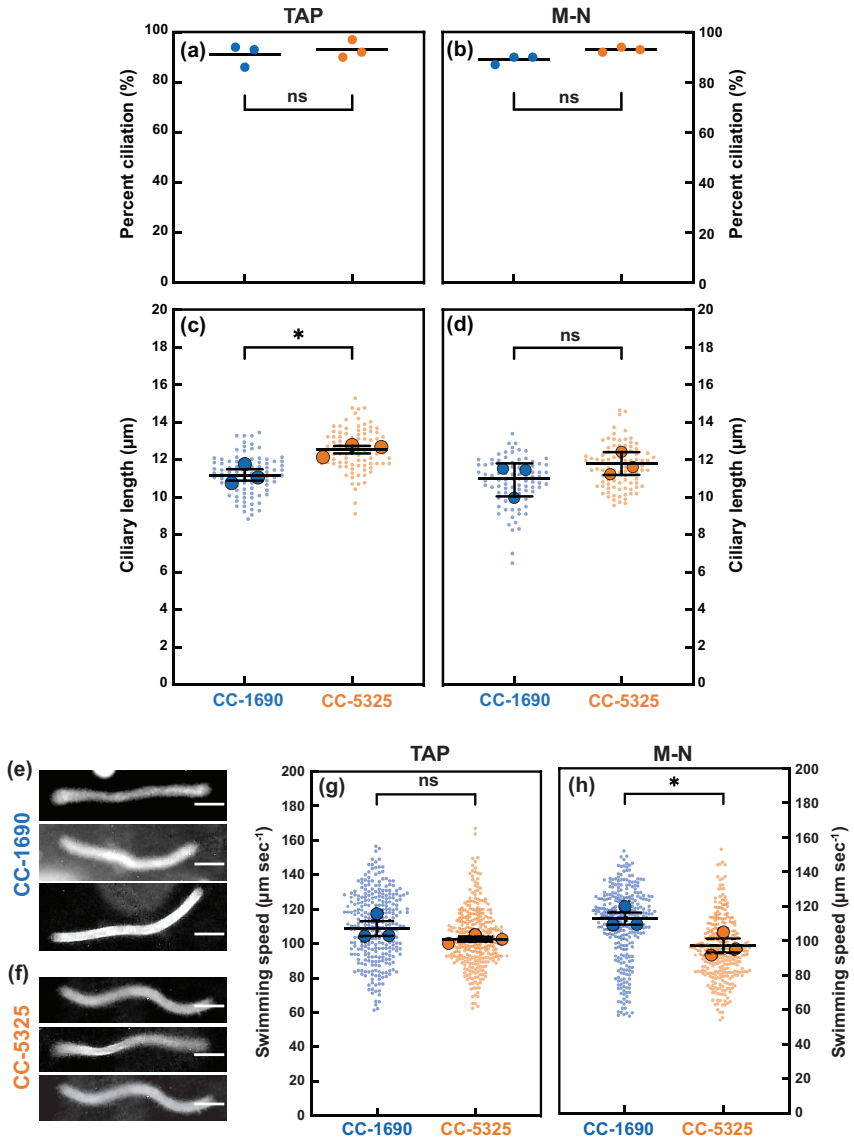

Fig. AII.1. In comparison to CC-1690, CC-5325 had longer cilia in TAP but slower swimming speed in M-N medium. CC-1690 and CC-5325 cells were grown in TAP (a,c,g) or in M-N (b,d,h) with constant agitation and light. (a,b) The percentage of cells with cilia was counted. Center (horizontal lines) represents the mean of 3 biological replicates where n=100. The three dots represent the mean of each biological replicate. Significance was determined by Chi-square analysis, p=0.4521 for (a), p=0.1159 for (b); ns, not significant. (c,d) Ciliary length was measured using ImageJ. Superplots were created by measuring the mean (the larger dots) of 3 biological replicates. Mean represents the center of the 3 biological replicates (n=30), and error bars show standard error. Significance was determined by using a two-tailed t-test assuming unequal variance, (c) p = 0.0265 and (d) p = 0.2877, ns, not significant. (e,f) Representative images of the traces created by swimming cells in TAP. CC-1690 and CC-5325 cells were allowed to swim on a microscope slide during darkfield microscopy with the camera exposure set to 1 sec. The resulting images contain traces that represent the path the cells travelled during the 1 sec exposure. The length of these traces was measured in ImageJ to estimate swimming speed. The scale bars represent 25 µm. (g,h) The swimming speed of CC-1690 and CC-5325 cells grown in TAP (g) or M-N (h). Superplots were created by measuring the mean (the larger dots) of 3 biological replicates where n=100. The mean represents the center of 3 biological replicates, and error bars are standard error. Significance was determined by using a two-tailed t-test assuming unequal variance. (g) p = 0.2422, ns, not significant. (h) p = 0.0438. **From Zhang, et al. 2022.**

Discussion:

Here, we show that CC-5325, the *Chlamydomonas* mutant library background strain is larger than CC-1690 cells, while their cell cycles and growth are similar. CC-5325 cells had lower photosynthetic efficiency but could grow faster in the dark. Both strains could grow in mixotrophic and photoautotrophic growth conditions. CC-5325 cells were more resistant to heat stress than CC-1690 cells. Both strains had similar freezing tolerance and detergence tolerance all suggesting that both had similar cell wall integrity despite the cell wall-less parent of the CC-5325 cells. CC-5325 cells were incapable of maintaining a circadian rhythm like CC-1690 cells can. Finally, both CC-1690 and CC-5325 cells had similar percentage of cells with cilia, but there were differences in both ciliary length and swimming speed.

CC-1690 and CC-5325 also had some differences in cilia length and swimming speed (**Fig. AII.1**). CC-5325 had longer cilia in TAP medium than CC-1690, consistent with the increased cell volume of CC-5325 in TAP as compared to CC-1690, as ciliary length scales with cell size (Bauer et al., 2021). CC-5325 had slower swimming speed in M-N medium than CC-1690, which may be related to additional influences by positive gravitaxis (downward swimming in response to gravity), as we observed that CC-5325 gravitaxed and settled faster than CC-1690 in both TAP and M-N medium. This may be due to shape-based mechanical orientation of cells (Roberts, 2006) rather than due to the large size of CC-5325 as another large-size strain, CC-125, does not exhibit positive gravitaxis. Additionally, the tendency to swim downward did not lead to increased clumping in CC-5325 in our algal cultivation in flasks or algal photobioreactors.

Materials and Methods:

CC-5325 and CC-1690 cells were grown overnight with constant agitation and light at 100 μmol photons m−2 s−1 light in either liquid TAP or M-N (minimal medium without acetate and nitrogen) to induce gamete formation and eliminate the effects of the cell cycle on cilia length. A sample of each strain was fixed by mixing 1:1 with 2% glutaraldehyde for a final concentration of 1% glutaraldehyde. After fixation, cells were imaged with a DIC microscope. Images were analyzed in ImageJ/FIJI using the segmented line tool. Each cell has two cilia with the same length. One cilium per cell was traced from base to tip, then fit using the "Fit Spline" function (Jack and Avasthi, 2018). The length of the line was then measured and converted to micrometers. Cells were only included in the measurement if both cilia were visible. The ciliation percentage was obtained by counting the number of cells with at least 1 visible cilium out of 100 cells.

For swimming speed assay, cells were allowed to settle for 15 min so that swimmers could be selected. The swimmers taken from the top of the cultures were diluted 1:10 in the same media they were grown in (either TAP or M-N). To give the cells appropriate room to swim between the slide and coverslip, a chamber was created on the slides using double stick tape. Cells were placed in the chamber and a coverslip was placed on top. Samples were imaged using a darkfield microscope set to a 1-s exposure. The resulting images show traces representing where and how far the cells swam during the 1-s exposure (Mitchell and Rosenbaum, 1985). To estimate the swimming speed, the traces were measured in ImageJ/FIJI using the segmented line tool and the "Fit Spline" function. Superplots for ciliary length and swimming speed were created by measuring the mean of 3 biological replicates (Lord et al., 2020).

References:

Bauer, D., Ishikawa, H., Wemmer, K.A., Hendel, N.L., Kondev, J., Marshall, W.F., 2021. Analysis of biological noise in the flagellar length control system. iScience 24, 102354. https://doi.org/10.1016/j.isci.2021.102354

Cheng, X., Liu, G., Ke, W., Zhao, L., Lv, B., Ma, X., Xu, N., Xia, X., Deng, X., Zheng, C., Huang, K., 2017. Building a multipurpose insertional mutant library for forward and reverse genetics in Chlamydomonas. Plant Methods 13, 36. https://doi.org/10.1186/s13007-017-0183-5

Jack, B., Avasthi, P., 2018. Erratum to: Chemical Screening for Flagella-Associated Phenotypes in Chlamydomonas reinhardtii. Methods Mol. Biol. Clifton NJ 1795, E1. https://doi.org/10.1007/978-1-4939-7874-8_19

Li, X., Patena, W., Fauser, F., Jinkerson, R.E., Saroussi, S., Meyer, M.T., Ivanova, N., Robertson, J.M., Yue, R., Zhang, R., Vilarrasa-Blasi, J., Wittkopp, T.M., Ramundo, S., Blum, S.R., Goh, A., Laudon, M., Srikumar, T., Lefebvre, P.A., Grossman, A.R., Jonikas, M.C., 2019. A genome-wide algal mutant library and functional screen identifies genes required for eukaryotic photosynthesis. Nat. Genet. 51, 627–635. https://doi.org/10.1038/s41588-019-0370-6

Lord, S.J., Velle, K.B., Mullins, R.D., Fritz-Laylin, L.K., 2020. SuperPlots: Communicating reproducibility and variability in cell biology. J. Cell Biol. 219. https://doi.org/10.1083/jcb.202001064

Mitchell, D.R., Rosenbaum, J.L., 1985. A motile Chlamydomonas flagellar mutant that lacks outer dynein arms. J. Cell Biol. 100, 1228–1234. https://doi.org/10.1083/jcb.100.4.1228

Pröschold, T., Harris, E.H., Coleman, A.W., 2005. Portrait of a species: Chlamydomonas reinhardtii. Genetics 170, 1601–1610.

Roberts, A., 2006. Mechanisms of gravitaxis in Chlamydomonas. Biol. Bull. 210, 78–80.

Sager, R., 1955. Inheritance in the green alga Chlamydomonas reinhardi. Genetics 40, 476.

Shrager, J., Hauser, C., Chang, C.-W., Harris, E.H., Davies, J., McDermott, J., Tamse, R., Zhang, Z., Grossman, A.R., 2003. Chlamydomonas reinhardtii genome project. A guide to the generation and use of the cDNA information. Plant Physiol. 131, 401–408.